MSc thesis

The dynamics of foredune restoration measures

Author: A.J. Bruijns (5781930)
MSc Thesis Physical Geography

Supervisors:
1st: Prof. Dr. Gerben Ruessink
2nd: Dr. Christian Schwarz

Department of Physical Geography
Faculty of Geosciences, Utrecht University
The Netherlands

Utrecht University

December 2018

MSc thesis

The dynamics of foredune restoration measures

Author: A.J. Bruijns (5781930)
Part of MSc Thesis Physical Geography

Supervisors:
1st: Prof. Dr. Gerben Ruessink
2nd: Dr. Christian Schwarz

Department of Physical Geography
Faculty of Geosciences, Utrecht University
The Netherlands

December 2018

Utrecht University

Abstract

This thesis focusses on the development of dune vegetation and dune morphology in two coastal areas in the Netherlands. The dunes on the northern coast of Terschelling and west of Heemskerk, that are under the influence of blowouts. These blowouts occurred as dynamic coastal management was implemented to increase flood protection by the dunes, this was done by a learn-by-doing concept. These measures have increased flood protection, as dune crest height increased. But now, after more than 30 years of developing, the question arises whether the blowouts have benefited the coastal morphology and ecology, and if there is a relationship between the two. Therefore, two blowout systems were analysed over longer periods of time: the artificial blowout area on the northern coastline of Wadden Island Terschelling (1997-2016) and a single naturally developed blowout west of Heemskerk (2007-2016). The blowouts have different origins, as Terschelling was artificially created by digging eight notches into the dunes and removing vegetation. Whereas the blowout in Heemskerk initiated and developed naturally by letting the area develop freely. These study areas were analysed based on the development of both morphology and vegetation using airborne LIDAR elevation data and Landsat satellite imagery. Overall, the dune volume of both areas increased: 54% for the hinterland of Terschelling and 7% for the area behind the much smaller blowout near Heemskerk.

The mapping of vegetation using NDVI resulted in maps, which indicate the amount vegetation cover of the blowouts with bare soil for Terschelling; hinterland initially decreased (to 0,3 in 2003) but is now increasing (to 0,4 from 2004 to present). As annual volume change decreased in the blowout area, from 5.700m^3/year to 1.500m^3/year (from 1997 LIDAR). Depositing sand both in front and behind of the blowout; resulting in the disappearance of original foredunes from pre-1996 and growth of the secondary dunes. For Heemskerk, the NDVI is high and is decreasing (from 0,4 in 2004 to 0,2 in 2016 in the blowout area), as the blowout is still progressing landward; a large lobe is forming behind the blowout. The blowout still had an annual volume change of 1.900 m^3/year in 2015. The results of both locations substantiate the fact that blowouts increase throughput of sand from the beach further into the dune system. The seasonality of this phenomena could be analysed more accurately with other imagery, such as aerial photography or newer satellite imagery (ESA's Sentinel 2). As Sentinel has more images available (one every eight days) and the resolution is higher (10 by 10 versus 30 by 30 of Landsat).

Acknowledgements

I hereby present my master thesis “The dynamics of foredune restoration measures”, the final product of my Master of Science in Earth Surface and Water. This thesis was made in cooperation with the department of Physical Geography of Utrecht University during the period between January 2018 and July 2018.

While working on my master thesis I’ve expanded my knowledge of coastal dynamics and dune systems. I learned how the Dutch sandy coasts developed (both physically as in policies) over the last decades. I even read some of the first coastal policy documents of the Netherlands. The acquired knowledge of coastal systems will help me during my further career.

I would like to thank everyone that contributed to the completion of this thesis. First of all, I would like to thank my supervisors Christian and Gerben helping me whenever I needed them. Next, I would like to thank my roommate Max de Groot for the evenings filled with discussions about this thesis and the results involved. Also, my girlfriend Jalina Jannink, who helped me while writing by supporting me throughout. Finally, I would like to thank my parents for supporting me during some of the stressful periods while writing this.

I hope this thesis will contribute to the knowledge and research of coastal areas around the world!

Now, nothing else lasts me than wishing you a lot of pleasure reading!

Andy Bruijns

Utrecht, December 07, 2018

Table of Contents

List of Figures

List of Tables

List of Equations

1. Introduction

The Netherlands is a low-lying country in which 9 million people live below sea level. The majority of the coastline is a wave-dominated sandy coast with aeolian sand dunes and some minor stretches being reinforced with hard sea-defence structures (Mulder, Hommes, & Horstman, 2011a). Traditionally, the Dutch coastal water defence policy was primarily focused on flood protection. This changed after primary coastal defence was established in the second half of the 20th century and structural coastal erosion problems emerged along the Dutch coast (Mulder, Hommes & Horstman, 2011). From the mid 70's, the coastal policy was gradually expanded, as other functions and themes (e.g. ecology, leisure) became more important and were included in future decision-making (Koningsveld et al., 2007). Counteractions were needed to ensure the sustainability of all coastal functions (e.g. safety, ecology, leisure) that was threatened by coastal erosion (before 1990, ca. 20 ha of dunes disappeared because of coastal retreat). And as the primary function of the aeolian sand dunes is to protect the hinterland from flooding, large scale coastal erosion management became necessary. Therefore, the Dutch Government adopted the national coastal policy of 'Dynamic Preservation' with the strategic objective: sustainable preservation of safety against flooding and of values and functions in the dune area (de Ruig, 1998; Koningsveld & Mulder, 2004). In 1990 the Dutch Government decided that preservation could be guaranteed by maintaining the 1990's coastline in the future, hence the introduction of the Dutch basal coastline (BCL). The preservation would be maintained through coastal sand nourishments wherever (and whenever) necessary (MIN V&W, 1990; Mulder et al., 2007). More importantly, the introduction of the BCL opened new opportunities for dynamic coastal management. New types of measures could be implemented at the coastal foredune without jeopardizing its protective function of the coast: rejuvenation of dune systems through additional sand transport with blowouts (Van der Valk et al., 2013).

Figure 1-1 - Sand passing the foredune through a blowout on Terschelling (B. Van der Valk et al., 2013).

Initially, this type of management strategy (was used until the mid-90s) did not lead to the desired effect; the growth of foredunes through aeolian transport from the adjacent beach. Mainly because a line of vegetation retained sand on the seaward side of the foredunes. This hindered sand transport further into the dune system; growth of the dune system and ultimately it prohibited further dune growth (e.g. increase in crest height) to improve flood protection (Löffler, van der Spek & van Gelder-Maas, 2011). In fact, the measures that were taken, (e.g. nourishments on the foredune, establishing a high vegetated foredune, decoupling the beach and the hinterland, sand fences) even led to an increase in seaward sand transport and therefore a decrease in coastal protection by dunes (Damsma, 2009). In the 1990's, the coastal management policy of several dune areas (e.g. dunes of Terschelling and Heemskerk) changed again to create a more dynamic system (e.g. Arens et al., 2013; Van der Valk et al., 2013). These policies can be characterized as learn-by-doing as they developed over time. Instead of extensive modelling beforehand, management was changed in several areas to find out whether it would work (or not) later on. This newer version of dynamic coastal management focused on linking aeolian transport on the beach, foredunes and the rest of the dune system using blowouts. These were meant to increase (aeolian) transport from the beach into (and over) the foredunes, resulting in a more natural development and growth of dunes (MIN V&W, 2000).

The new strategies had positive outcomes; the exceedance rate of the BCL decreased: from 32% in 1992 to 7% in 2015 (MIN V&W, 2016) . More positive results of these developments can be found near Heemskerk (Arens et al., 2013). After implementing this new strategy (in 2006/2007) in the dunes nearby, in this case by removing sand fences and vegetation, blowouts started to form naturally in the

dune system and transport into the dune system increased. This can be derived from the formation of depositional lobes of sand, which became visible on aerial photography (actual elevation measurements of Heemskerk are not available yet). Elsewhere, in a section of dunes on the Wadden Island Terschelling, nature was helped by digging eight notches and removing vegetation in the first row of dunes to form a corridor for the wind-blown beach sand to be transported into the dune system, these notches turned into (artificial) blowouts over time with positive results; e.g. an average deposition of 0.3m 300m downwind of the foredune in a period of 14 years (Arens et al., 2013; Van der Valk et al., 2013).

It seems that the formation of blowouts are good measures to reactivate, but there is still a need to understand the development over time. Therefore, after more than 20 years of dynamic coastal management, these areas (e.g. Heemskerk and Terschelling) along Dutch coast changed considerably in terms of morphology and dune vegetation (e.g. Arens & Overdiep, 2008; Arens, Loffler & Nuijen, 2006; Löffler, van der Spek & van Gelder-Maas, 2011; Van der Valk et al., 2013). And the question arises if the behaviour of blowouts can be derived through long-term datasets (e.g. satellite imagery and LIDAR elevation data) and what the consequences of blowout initiation are for the dune morphology and vegetation. For example, if they can be linked to each other; if dune vegetation changes (increase/decrease in coverage) accordingly to morphological change (or the other way around) and if the interaction amplifies dune growth.

This MSc thesis aims to quantify the relationship between blowout morphology and dune vegetation by generating and its development over time. This will be done by analysing and interpreting data on large spatial and temporal scales. So far, there is still a research gap in this thesis's aimed spatial scale and temporal scale. As this thesis aim will be to describe complete blowout systems over periods such as seasonal, annual or decadal. Therefore, using newly available material (Landsat satellite imagery and LIDAR elevation maps) to increase understanding of the blowout dynamics and their evolution over a longer timescale, this research could make a valuable addition to current knowledge of sandy coasts and in particular the evolution of blowout systems.

2. Literature review

This chapter contains an overview of the current state of research and knowledge of sandy coastal systems, focusing on dune vegetation and blowouts. This chapter describes the inner workings of this these systems and the terminology that is used in the further thesis. Following the literature is the definition of the research gap and the research questions focus area(s) for this thesis and a hypothesis.

2.1. Aeolian transport

The definition of aeolian transport can be described as the transportation of sandy particles using the uplifting force of wind (Bauer & Davidson-Arnott, 2003). Aeolian sand transport on a beach is dependable of the interaction between beach geometry (e.g. beach length, slope), surface conditions (e.g. soil moisture, grain size) and wind attributes (e.g. speed, fetch length) (Bauer et al., 2009).

Equation 2-1 - Aeolian sand transport by Nickling & Davidson-Arnott (1990)

$$Q_D = C\,\rho_a/g\,(d/D)^{0.5} \sum_{i=1}^{n} \cos\alpha_i\,(U_i - U_t)^3\,F_i\,.\,3600$$

Q_D = total sand transport from the beach over the time period considered (kg/m width of beach)
C = empirical coefficient
ρ_a = density of air (kg m^{-3})
g = acceleration due to gravity (m sec^{-1})
d = grain diameter of beach sand (m)
D = standard grain diameter (2.5×10^{-3}m)
N = total hours with wind speeds U_t
α_i = wind angle to shore perpendicular
U_i = average wind speed for hour i (m sec^{-1})
U_t = threshold wind speed associated with d (m sec^{-1})
F_i = dimensionless proportionality term relating sediment flux associated with beach fetch for hour i to transport limited flux for U_i.

Wind driven sand transport is the second largest transport mechanism after sea-level rise. Drivers of the aeolian transport mechanism are divided into three categories: air, ground and sediment (Table 2-1; Nickling & Davidson-Arnott, 1990)). In this research, factors from Table 2-1 such as vegetation cover and local topography (e.g. morphology, blowout locations) will be studied more closely. These are combined in Equation 2-1. Surface roughness, in this case dune vegetation (e.g. marram grass) in foredunes, increases threshold velocity (U_t) for sand transport and decreases local erosion, which can hinder aeolian transport further into dune systems. The current state of research about the interaction between aeolian transport and vegetation will be explained in paragraph 2.4.

Table 2-1 - Wind erosion factors by Nickling and Davidson-Arnott (1990)

Air	Ground	Sediment
Velocity profile	**Roughness elements**	**Texture**
- Fetch length (beach width)	- Height	- Height
- Surface character	- Spacing	- Size
Turbulence	**Vegetation cover**	- Packing
Density	**Obstructions**	**Specific gravity**
- Temperature	**Temperature**	**Moisture content**
- Pressure	**Beach slope**	**Bonding agents**
- Humidity	**Topography**	**Crust development**
Viscosity		**Soluble salts**
		Algae
		Silts and clays

2.2. Dune morphology and development (including parabolic dunes)

2.2.1. Dunes

Coastal dunes can be classified as shadow dunes, embryo dunes, dune ridges, transgressive dune fields and parabolic dunes (Johnson & Martin, 2016). This research will focus on parabolic dunes Figure 2-1 shows a schematic overview of the terms that are used in this review. In general, dune formation requires: an onshore wind above the sand transport threshold wind velocity; an obstacle to reduce wind velocity and capture sand; a steady supply of sand. This can come from river discharge, cliff and coastal erosion and from sediment input from the sea itself (Hesp, 2011). The captured sand forms a small lump of sand; an incipient dune. As the embryo dune continues to grow, an embryo dune will form. If there is enough supply of sand, a foredune can grow. A summary of the terminology used in this thesis is presented in Figure 2-1.

Parabolic dunes, also described as U-dunes, upsiloidal dunes and hairpin dunes have a typical V- or U-shape. They are characterized by Hesp (2011) to have a short to elongate trailing ridge, which terminates downwind into either U- or V-shaped depositional lobes. A parabolic dune typically forms from a blowout in the dune system. They can be distinguished by (sometimes vegetated) trailing ridges, blowouts do not have these (Figure 2-2).

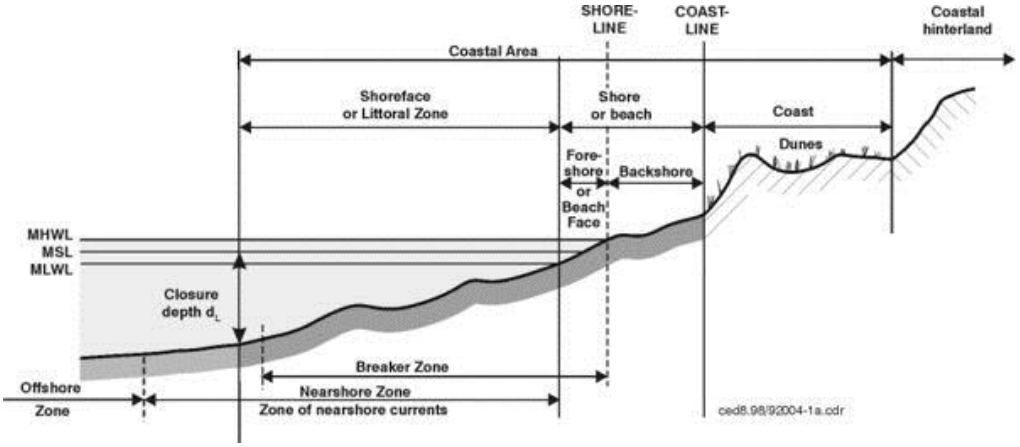

Figure 2-1 - Definition of relevant coastal terms (Mangor, 2018).

Incipient dune morphology

Hesp (2011) describes incipient foredune as a new/developing foredune that forms by aeolian sand deposition within pioneer plan communities. Three types of incipient foredunes can be derived: ramps, terraces and ridges. These types form under their own specific circumstances.

- Ramps form on locations were seedling germinate on a seaward slope. These plants grow further from a landward source towards the sea and gradually trap sand on the seaward slope. Plants that germinate on steep slopes cause gradual accretion (Hesp, 2011);
- Terraces will form on locations were rapid plant growth takes place in combination with an accreting beach. It will occur when seaward plant growth roughly matches the accretion rate. And plants will grow on a shore with little accretion, due to a low energy environment (because of a moderate plant density or low plant height) (Hesp, 2011);
- Ridges form on locations where accretion rates are high, and sand is deposited primarily in the seaward portion of a plant canopy. They will also form when plant density and height is high. Thirdly, the will form on locations were seaward growth rates are slow compared with accretion. And on location were waves scarp the foredune (Hesp, 2002, 2011).

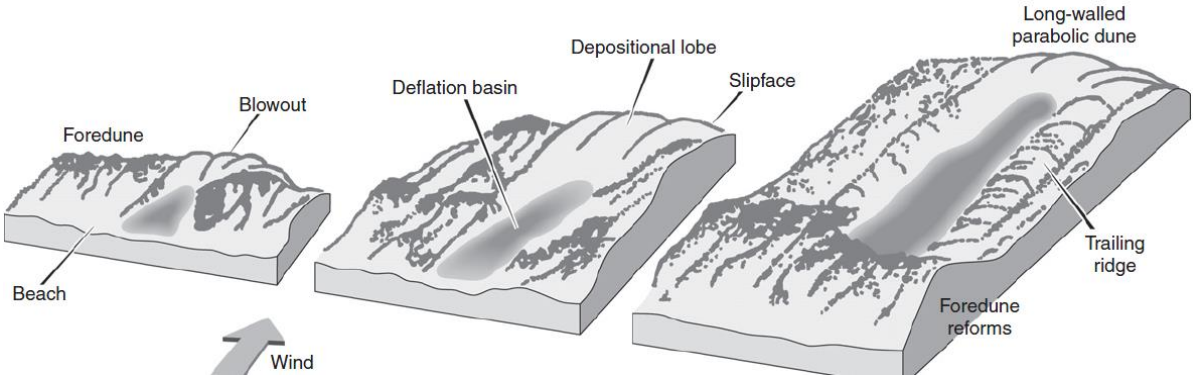

Figure 2-2 - Evolution of a blowout into a parabolic shaped foredune (Hesp, 2011).

The development of dunes starts with incipient dunes (terraces, ramps or ridges), then embryo dunes and then foredunes. Shadow/incipient dunes are shore-parallel ridges, formed on the back shore by aeolian sand deposition. The type of dune that forms then is highly dependent on the ability of pioneer plant to colonize the backshore and embryo dunes. Generally, the dominance of plants and low impact of extreme events lead to the development of foredunes (paragraph 2.2.3) and foredune plains.

Disturbance of the coast will lead to the formation of blowouts (paragraph2.3) and parabolic dunes (paragraph 2.2.2). And in some case, an high sediment supply, combined with restricted plant cover and high wave/wind energy lead to the development of dune fields (Hesp, 2011).

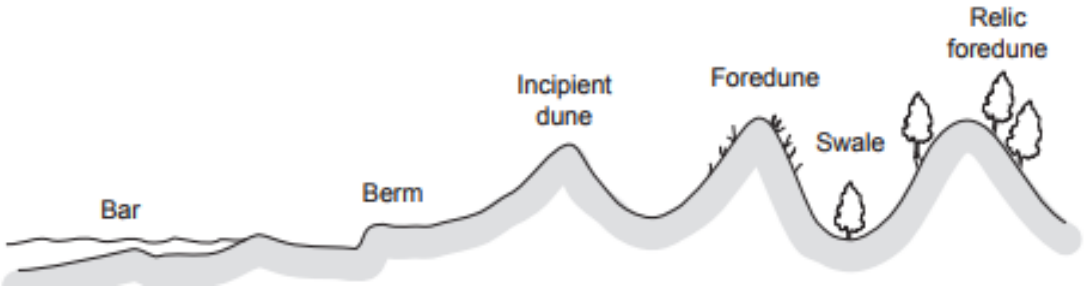

Figure 2-3 - Schematic overview of a beach system and terms used (Johnson & Martin, 2016).

Dune hinterland: dune slack area

This area is located behind the primary row of dunes. It is named swale (Figure 2-3), dune hinterland or dune slack area. If there is no human interference (e.g. boardwalks, roads, buildings) here, the area is covered in low vegetation, such as grass, shrubs, plants (NJSGC, 2016). This dune slack area provides space for depositional lobes to form from the sediment, transported through blowout areas (e.g. Arens, Geelen, Van der Hagen, & Slings, n.d.; P. Hesp, 2011). A dune slack is damp or wet hollow in between dunes, where the water table reaches or approaches the surface. There are also dry slacks, areas that were created by wind deflation. The presence of a slack can mean that there is e.g. seaward development of a new foredune (Hesp, 2011).

2.3. Blowouts

Blowouts can be found in three general shapes along a coast and are common in dune environments with either occasional erosion accretion in combination with high wind and wave energy. They can form in a saucer-, cup- or trough-shape and are naturally formed by wind erosion. Despite the wide range of types in aeolian environments, many blowouts can be classified in 2 primary types: saucer and trough blowouts, as shown in Figure 2-3 and in Figure 2-4 (Hesp, 2002). Another classification is made by Barchyn & Hugenholtz (2013): dividing blowouts into two types based on behaviour: depth-limited and morphology-limited. The first describe blowouts where the bottom reaches a non-erodible substrate and can host higher sand deposition rates. And the latter describes the behaviour of a blow-out that digs deep into the sediment and creates a large, slow deposition aprons. Hesp (2012) gives an overview of 7 ways in which a blowout can be initiated:

1. Wave erosion
2. Topographic acceleration of airflow
3. Climate change
4. Vegetation variation (spatially and/or temporally)
5. Water erosion
6. High velocity wind erosion
7. Human activities

For this research, type 4 and 7 are most relevant. The degree of vegetation density cover or species can vary alongshore. Areas with low density or cover can be eroded in more easily. Therefore, many studies consider that a low (or reduction) in vegetation cover is a critical factor in the initiation of blowouts (e.g., Melton, 1940; Jennings, 1957; Steers, 1964; Bird, 1984; Tinley, 1985; Carter et al., 1990). Type 7, the human interference, is present at a few locations along the Dutch coast were artificial blowouts have been made, such as in Terschelling (Arens, 2011). Moreover blowout incision was found to be dependent on presence of weak spots with damaged the vegetation cover (Crawford, 2009).

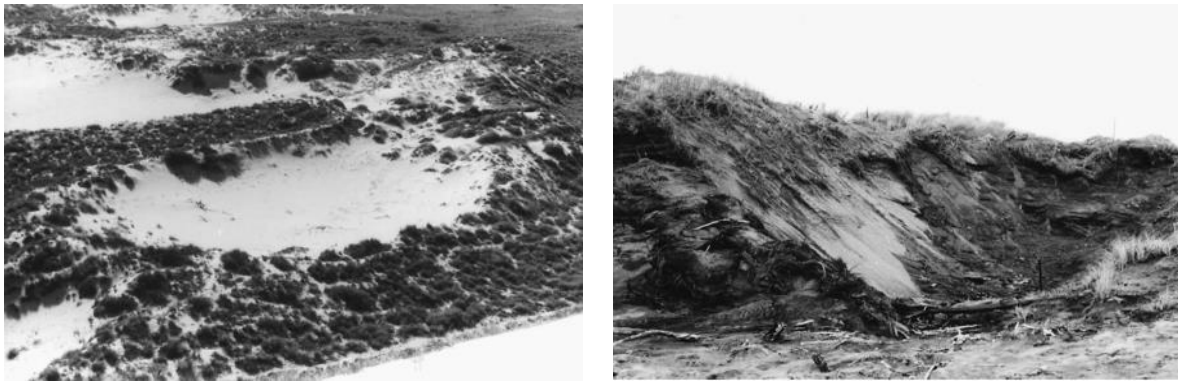

Figure 2-4 - An example of a saucer blowout (left) and a narrow, trough shaped blowout (right) (Hesp, 2002)

Including initiation there are 3 stages of blowout development: initiation of deflation (1), continued deflation (2) and stabilization (3). The initiation of a blowout starts with deflation patches of a few meters in diameter and where the sandy soil is exposed, as stated by Jungerius and van der Meulen (1989). Most of these disappear within a year, but others gradually become deeper and develop into a blowout. Stage 2 includes slumping and erosion of side walls and sand movement to the leeward side. Whereas stabilization (3) is triggered by re-vegetation and lead to infilling of the blowout (Carter et al., 1990). Trough blowouts close after they are stabilized (e.g. by decreasing wind energy or vegetation growth). A parabolic dune will arise with a long deflation basin with coarser sand; an eroding windward crest will develop; elongated vegetated side ridges and an actively depositing lee slope. The blowout cycle continues with further dune retreat from the coast; this decreases wind velocity and (transport) energy, as the fetch length increase. This reduces burial of plants on the leeward side and allows for vegetation to recolonize on bare areas, leading to more and more stabilization on both sides of the dune. Eventually, more woody-species will re-establish themselves on the leeward side. On the seaward side, grasses will start to grow first, followed by the growth of shrubs and trees.

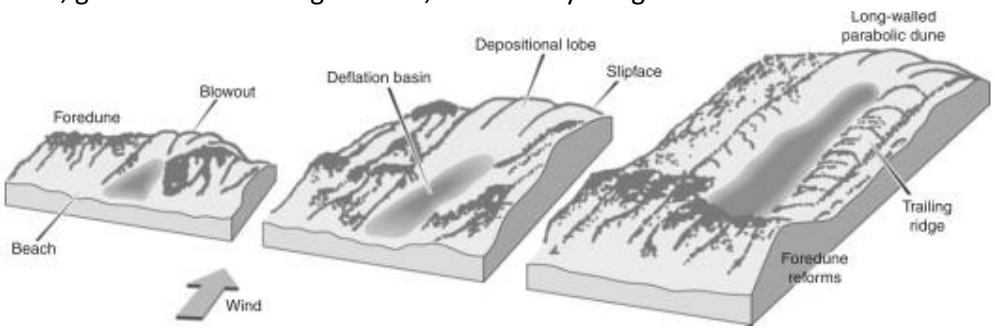

Figure 2-5 - Development of a blowout (Hesp, 2011).

The three stages occur in a cyclic manner. The blowouts undergo a cyclic behaviour of opening (1,2), closing (3) and re-opening (1, 2) of 10-20 years. It was further proposed that cyclic behaviour can be disturbed by three factors: changes in the feedback between landform, wind and vegetation cover; variations in wave climate and of course, human interaction. However which combination factors lead to cyclic or closing blowouts remains unclear. In which stage 3 takes about 5-10 years to deposit sediment in the throat, re-establish vegetation and round of the topography. (Gares & Nordstrom, 1995).

General flow dynamics of blowouts

The internal and external flow dynamics are important characteristics of blowouts, as they determine the further development of the site. The first study of wind flow in blowouts dates back to 1943. Landsberg & Riley concluded that wind speeds are topographically accelerated over higher dune terrain, flows are separated by obstacles, such as lee slopes and jet flow may occur. After this study, the separation is made between saucer and trough blowout research (Hesp, 2002).

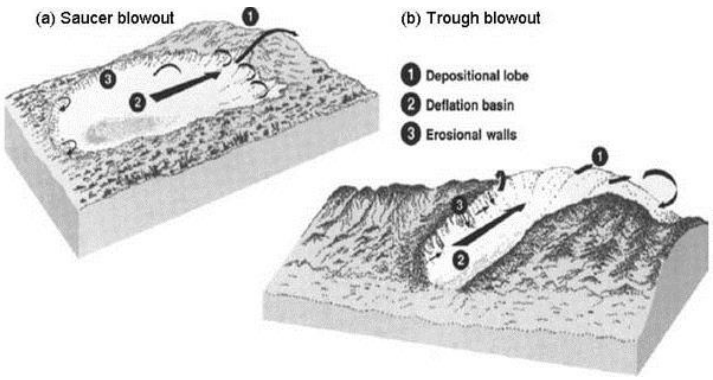

Figure 2-6 - Blowout expressions and wind flow patterns of a saucer (left) and trough (right) blowout (Hesp & Hyde, 1996; Hesp 2002).

Saucer blowout

Saucer shaped blowouts (Figure 2-4) are more common on low-gradient slopes on the windward side of large foredunes or on low rolling topography from which vegetation has been denuded. In general, the shape is shallow, ovoid, and dish-shaped. There is a depositional lobe present at the down-wind side and the lateral walls are steep (Carter et al., 1990; Maun, 2009). The flow pattern in a saucer blowout is largely dependent on the wind direction. If wind approaches the saucer in the right angle, flow in the saucer itself forms a rotor shape. If winds are oblique, maximum wind speeds occur on the deflation floor and steering of the flow will be present because of the blowout topography (Bennet & Halls, 1980). Most erosion and deposition takes place on the depositional lobes(crest) and the blowout throats, while less erosion/deposition occurred in the blowout centre (Lancaster, as cited in Hesp, 2002). Pluis (1992) found that less erosion occurs in winter (windiest period) and more in the summer. This is due to the higher soil moister levels in winter. Also, deflation rates were higher than surrounding surface areas, due to the rain-washed sand supply.

Trough blowout

In general, beach sediment is transported landward and towards the trough blowout (Figure 2-4) by onshore winds. It then passes through the blowout while picking up more sediment from the erosion of the lateral blowout walls. The sediment then accumulates on depositional fans landward of the blowout (Gares & Nordstrom, 1995) This type of blowout are more common in relatively high dune ridges and evolve into U-shaped or parabolic dunes (Crawford, 2009).

Internal flow dynamics and sand transport

Previous studies on the development of wind velocities throughout a trough blowout showed maximum wind speeds to be aligned with the blowout axis (Hesp, 1996; Hesp & Hyde 1996). They found that the highest wind speeds occur along the axis in the deflation basin and along the lateral erosional walls. Corkscrew vortices are present near the erosional walls' crests and the flow over the crest of the depositional lobe experiences rapid deceleration and flow separation (Figure 2-6). Flow structure is highly variable due to the presence of vegetation. Sand is deposited within 30 m of a blowout. But this depends heavily on the size of the blowout and the local topography (van Boxel et al., 1997). Other blowout locations, on Terschelling, showed a deposition of 1m, more than 100m away from the blowout (van der Meulen et al., 1996). The seasonality of sand transport patterns in a trough shaped blowout were more closely studied by Byrne (1997). The link is researched between increased erosion in winter and fall with the absence of plants (dead or dormant). Accretion of the dune occurred during spring and summer. However, no evidence was found for the relation between sediment transport and presence of vegetation. A bulk of the transport happens in winter/fall, which results into an overall seaward transport. The seasonal variability could also be concluded from the differences in grain sizes

on the dune crest; finer in spring/summer and coarser in winter. Eventually, most sand is deposited near the blowout.

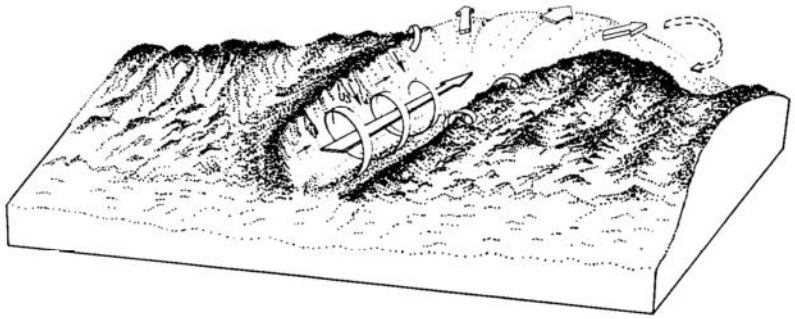

Figure 2-7 - Generalized flow in a trough shaped blowout (Hesp & Hyde, 1996).

Influence of wind direction

Hesp and Pringle (2001) found that wind direction is eventually steered into the blowout by the erosional walls (Figure 2-4). Hesp and Pringle (2001) even state that even alongshore winds can get sucked into the trough blowouts and can transport sediment up to 100 degrees opposite to the approach wind. Earlier, Hesp and Hyde (1996) stated that this kind of steering results in the prevailing of corkscrew vortexes and that the maximum transport is relocated from the centre axis to an erosional wall. This effect causes the trough shaped blowout to get a skewed form, since the oblique (or even alongshore) wind result into more preferential erosion on one side of the trough (Byrne, 1997). The approaching wind direction does have a large influence on the wind velocities within a blowout. For instance, if the wind direction is in accordance with the orientation of the blowout, wind speeds are accelerated in the throat. This is called a "jet effect". After that the wind decelerates over the rim at the landward side (Carter et al., 1990). A study by Gares and Nordstrom (1987) found that perpendicular winds produce a 70 to 90% lower wind velocity in the throat than on the highest part of the foredune ridge. In comparison, when winds did come in at the same angle as the blowout axis, the wind velocities were only 10-30% lower than on the surrounding ridges.

Influence of wind speed

Wind speed has a large influence on the formation of blowouts. Jungerius, Witter and Boxel (1991) state that blowout changes correlate best with wind velocities between 6.25 and 12.5 m/s, which is also the critical wind velocity for moving particles off 0,15 to 0,42 mm. These winds typically blow from the southwest. The blowouts along the Dutch coast elongate in the same direction because of this. Jungerius, Witter and Boxel (1991) state that extreme wind events during storms have little effect on the blowouts related sand transport compared with higher frequency, lower magnitude events. Only the combination of increase in wind speed and wind direction will alter the blowout form whereas a change in wind speed will only change the blowout morphology itself (e.g. depth, lobe formation).

Figure 2-8 – Dunes and vegetation of around km 15-20 on Terschelling (Arens et al., 2006)

2.4. Dune ecology: influence of vegetation on blowouts

The cover of dune vegetation is one the characteristics that controls aeolian sand transport in coastal areas, it is important to blowouts (e.g. Jungerius & Schoonderbeek, 1992; Nickling & Davidson-Arnott, 1990). More specifically, the impact of vegetation on wind flow and sand transport in coastal areas depends on the interaction of: plant species, plant density, distribution, plant height and morphology (P. Hesp, 2002; Maun, 2009). The interaction between wind and vegetation has a large influence on the morphology of (incipient) foredunes. As plant density and distribution vary seasonally, the growth rates (low/absent in winter and high in spring) strongly influence patterns of sand transport and depositions on foredunes (Hesp, 2002). Removing vegetation from the area in front of the parabolic dune, increases the supply of sand to the upwind slope. On the other side, removal of vegetation from the crest results in a lowering of the crest (of several m) and transfer of sand over the lee slop farther downwind. Consequently, the parabolic crest disintegrates partially (Arens et al., 2013).

The planting of vegetation has been used to increase height and sand volume of dunes in the past Aeolian dune fields, as is the case in most of the Dutch coast, can be divided into stable (vegetated) and active (non-vegetated) states. The reactivation can be initiated by wind speed increase, fire, biogenic disturbance, human interference (vegetation removal) or a combination of these. In the case of the Dutch dunes, removing vegetation was used to try reactivated dune fields. This was only successful if vegetation was removed completely, including roots. These block transport when they surface because of deepening (Arens et al., 2013; Barchyn & Hugenholtz, 2013). Vegetation might also disappear after enough accumulation of sand, but this is not the case for all species. Shrubs and marram grass for instance, does not suffer from burring at all. Whereas sea buckthorn and moss will disappear when the accumulation exceeds a few centimetres per year (van Boxel et al., 1997). Vegetation in blowout areas can be described in two categories: a protective skin and a blowout suppression (Barchyn & Hugenholtz, 2013). The protective skin responds slowly to changing boundary conditions and is susceptible to disturbance. A blowout suppressing vegetation contains vegetation with the ability to arrest blowouts and hinder them from growing further. As the blowout continues to grow, it will reach a stable state. Vegetation will have a chance to grow. (Nordstrom & Arens, 1998). The dune becomes immobilized once they reach this stable state and get covered with dune vegetation, such as helm grass (Barchyn & Hugenholtz, 2013).

2.5. Research objective and main research question

The aim of this thesis will be to increase understanding of blowouts, acting mechanisms (morphological and vegetational) and the combined functioning of these mechanisms over long time and large temporal scales using a remote sensing approach with extensive datasets: satellite imagery to indicate vegetation cover and Lidar elevation data for morphological change of two areas along the Dutch coast. This will increase knowledge about blowouts in sandy coasts and their development over time (focussing on vegetational and morphological changes and their interaction). The presence of both natural (dynamic dune management) and artificial (foredune restoration measures) blowouts in the Netherlands also raises the question what their differences/similarities are and if they can be derived from vegetational and/or morphological changes. This, in combination with the literature review, has led to a set of research questions. With the main research question:

What are the effects of foredune restoration measures on dune-, and more specifically, blowout development in the dunes of Heemskerk and Terschelling?

The main research question is divided in four sub questions, each with their own theme: changes in dune morphology (1); changes in dune vegetation (2,3); the interaction between dune morphology and dune vegetation (4) and the comparison of artificial/natural blowouts (5). Resulting in the following sub questions:

1. What is the annual morphological development in the morphological areas in/around the blowouts of Terschelling and Heemskerk (i.e. sediment eroded/deposited in front of/behind the dunes; in the blowout and behind blowout), derived from annually required airborne LIDAR imagery (between 1997/2007 to 2016?
2. How does the dune vegetation develop, annually averaged, in terms of average vegetation coverage of blowouts and the morphological units around them at Heemskerk and Terschelling based on vegetation index (NDVI), derived from Landsat satellite imagery?
3. What is the seasonal cycle of vegetation, based on vegetation index derived from Landsat satellite imagery, and how does this cycle develop by comparing the first year (Heemskerk;2006 and Terschelling; 1997) to the last year (both 2016) with Landsat imagery of blowout development in the blowouts of Terschelling and Heemskerk?
4. Can vegetation presence, measured in annual percentage of vegetation cover in the blowout, be linked to the annual accretion/erosion (in m^3) of the blowout and its surroundings?
5. What are the differences and similarities in artificial/manmade and natural blowouts, in terms of morphology (annual change of volume within morphological units) and vegetation (annual NDVI and seasonal cycle of NDVI, based on the blowouts of Terschelling and Heemskerk?

2.6. Hypotheses

This research will combine (and compare) datasets of elevation and vegetation on large temporal and spatial scales, as this has not been done before. The change in morphology has been linked with presence of vegetation in several researches (e.g. Barchyn & Hugenholtz, 2013; Gares & Nordstrom, 1987; Hesp, 2002; Hesp & Pringle, 2001; Pluis & Winder, 1989), generally these studies prove that lack of vegetation is linked to the initiation of blowouts and the initiation of plants can stabilize blowouts and eventually close them (Crawford, 2009). Hesp (2011) has shown that blowouts undergo development cycles, without reaching a steady state. These cycles are driven by changing boundary conditions (e.g. growth of vegetation patches, decreasing of average wind speed). Therefor vegetation cover can be used as an indicator of blowout development and, which can now be monitored on large time and spatial scale through satellite imagery than in previous research. Secondly, as boundary conditions change over time, sediment transport trough blowouts develop. This changes the surrounding morphology. These changes could be measured by using LIDAR elevation data to determine annual

sediment volume of morphological units of areas in/around the blowout (Hesp & Hyde, 1996; Ruessink et al., 2018). At the end of a blowout cycle, vegetation will grow, and sand will be deposited, as the threshold velocity for transport increases due to the resistance by vegetation. Eventually the blowout will close by sedimentation, and more dense vegetation will grow. The discrepancy between these observations is still uncertain to date.

This study tries to investigate the development of these cycles in the light of vegetation and morphology, as there is still a research gap present in their combined development. The origin of vegetation and the development can therefore be seen as indicators of blowout development (or closure) after its initiation. All of these vegetational changes are measurable using NDVI of satellite imagery and the morphological development should be visible in the LIDAR elevation data. The development of vegetation cover and morphology can be tracked using pre-defined areas in the dune system (e.g. foredune, beach, hinterland).

As blowout areas in the Netherlands have generally been instigated by either man-made excavations and vegetation removal or one incising naturally, two research areas will be defined: the dunes of Terschelling and Heemskerk. The distinction between artificial (Terschelling) and natural (Heemskerk) developed blowouts could be made by the rate of accretion/erosion in the initial years of development. As an artificial blowout has steeper walls, which will collapse and will increase erosion rates of the dune area (Ruessink et al., 2018). Whereas a natural blowout should have lower transport rates in the starting years, since vegetation will have to disappear before more sand will erode (Hesp, 2011).

3. Datasets and data analysis

3.1. Data sets

The evolution of the dunes since the change in management strategy will be researched using two types of datasets: Lidar elevation data and Landsat satellite imagery. The Lidar elevation data will be used to analyse annual change in morphology, whereas seasonal NDVI-vegetation index will be used to find annual and seasonal changes in dune vegetation. Two or three research locations in the Netherlands will be used as case studies: the dunes of Heemskerk and Terschelling. Each research area will be split in two parts: a blowout, evolving since the 90's and a nearby area where no change of dune management was made. Annual change in morphology and seasonal change in vegetation of both areas can be compared to monitor change and the influence of blowouts. These locations are interesting since they have different types of blowout systems. Terschelling has a system of multiple, smaller blowouts, whereas Heemskerk has a large, singular blowout. The use of vegetation indices will help developing an understanding of the possible relation between dune vegetation development and dune morphology (blowouts). A low vegetation density increases sand transport (Hesp, 2002, 2011; Loffler et al., 2011). The relation between vegetation and sand transport will be researched by making vegetation, contour maps with satellite images from Google Earth Engine. This information will be combined with changes in dune morphology (annual) to see if there might be a relation between them. Eventually, it will be possible to evaluate the change in coastal management and assess whether dune protection was improved by increasing overall dune height and sand transport into the dune system in a more natural way.

3.1.1. Landsat satellite imagery

The Landsat Satellite Program started in 1972 and provides a continuous set of satellite imagery around the globe (Figure 3-10. Landsat provides high-resolution, multispectral data and it is currently the only long-term (1972 to present) source of global, calibrated and high spatial resolution measurements of the earth surface. The satellites are equipped with multiple remote sensors and data relay systems with altitude-control and orbit-adjust systems, power supply and on-ground station commands and transmitters (NASA, 2009; USGS, 2016). Due to its spatial resolution (30mx30m for Landsat 5, 7 and 8), has been used for large observations (e.g. land cover change for an entire bay area). The use for smaller regions, such as blowouts, will have to take in account an error margin because of the pixel size (Klemas, 2011; Ozkan, Mert & Gülsoy, 2010).

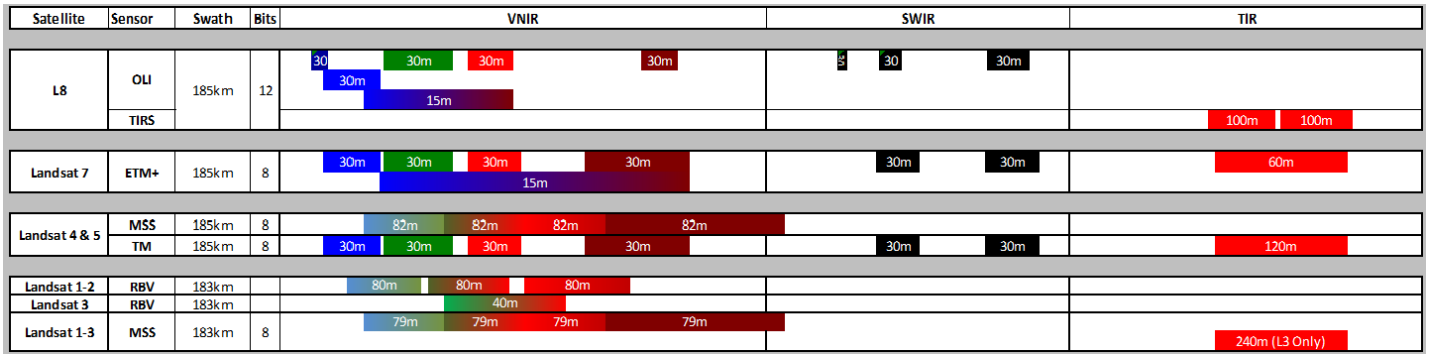

Figure 3-1 - Continuity of Landsat Data (USGS, 2016).

Landsat 5

Landsat 5 was launched in 1984 as a duplicate of Landsat 4. It was still retrieving useful data in 2010. This was 26 years after its launch and well over its 5-year design cycle (NASA, 2009). Landsat 5 imagery was collected using two scanners: Multispectral Scanner (MSS) and Thematic Mapper (TM). Both scanners have different characteristics: whereas the MSS has a resolution of 60 by 60 m, the TM has a resolution of 30 by 30 m. The MMS's resolution originally was 79 by 57, but this was resampled. Both

scanners have a scene size of approximately 170 by 183 kilometres; more than enough to fit the relatively small research areas (see Table 3-4 for details).

Table 3-1 - Band widths of the Landsat 5 scanners: MSS and TM (USGS, 2018a).

Multispectral Scanner (MSS)		Thematic Mapper (TM)	
Band	**Range**	**Band**	**Range**
B1	Blue (0,5 - 0,9 µm)	**B1**	Green (0,5 - 0,9 µm)
B2	Green (0,6 - 0,7 µm)	**B2**	Red (0,6 - 0,7 µm)
B3	Red (0,7 - 0,8 µm)	**B3**	Near Infrared (0,7 - 0,8 µm)
B4	Near Infrared (0,76 – 0,9 µm)	**B4**	Near Infrared (0,8 - 1,1 µm)
B5	Shortwave Infrared 1 (1,55 – 1,75 µm)		
B6	Thermal (10,40-12,50 µm)		
B7	Shortwave Infrared 2 (2,08-2,35 µm)		

Landsat 5 images could be used to measure vegetation indices in the 90's. The imagery made with the TM should be used, as it has a higher resolution (Barsi et al., 2014). From the Landsat 5 mission the dataset 'Landsat 5 TM Collection 1 Tier 1 calibrated top-of-atmosphere (TOA) reflectance' will be used. This set has data availability from 01-01-1984 to 05-05-2012, a large range compared with the Landsat 7 and 8, but the data is also less accurate since it has a lower resolution (as mentioned before). Tier 1 data contains the most accurate data available: it is filtered by USGS and has a tolerance of a root mean square error (RMSE) of 12m (USGS, 2017).

Landsat 7

The Landsat 7 satellite was launched in 1999 and used to it full potential until 2003, when its Scan Line Corrector (SCL) failed in May 2003. Landsat 7 carried a more advanced scanner than its predecessor. Landsat 7 orbits around the whole planet in 16 days. The Enhanced Thematic Mapper Plus (ETM+) can collect up to 8 different spectral bands and has a higher resolution. A failure in the SLC in 2003 is the cause of gaps between scan lines in imagery, as the SLC is used to correct for orbital motion to create a rectilinear scan pattern instead of a zigzag pattern (see Figure 3-11 and Figure 3-12).

Figure 3-2 - Malfunction of the SLC causes scan lines to appear: left shows SLC-off and right is with the SLC-on (USGS, 2018b).

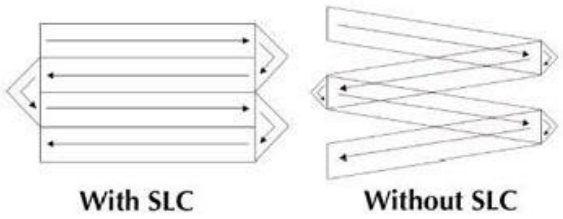

Figure 3-3 - Difference of scanning with the SCL and without (USGS, 2018b).

Table 3-2 - Landsat 7 data bands (NASA, 2009).

Band	Range	Band	Range
B1	Blue (0,45 - 0,52 µm)	**B5**	Shortwave infrared 1(1,55 – 1,75 µm)
B2	Green (0,52 - 0,60 µm)	**B6**	Thermal (10,40 – 12,50 µm)
B3	Red (0,64 - 0,69 µm)	**B7**	Shortwave infrared 2 (2,09 – 2,35 µm)
B4	Near Infrared (0,77 - 0,90 µm)	**B8**	Panchromatic (0,52 – 0,90 µm)

However, the satellite still collects data with the SLC-mode turned off with the same radiometric and geometric quality as before. The scan lines are corrected by NASA after retrieving data from the satellite (NASA, 2009; Barsi et al., 2014). The satellite produces imagery with a resolution of 30 by 30 m, which can be used in further research. The dataset that will be used for this research is the 'USGS Landsat 7 Raw Scenes (Orthorectified)' imagery. This image collection contains scaled, calibrated at-sensor radiance, orthorectified scenes.

Landsat 8

The first images of Landsat 8's scanners date back to February 2013. It orbits and scans the entire Earth in 16 days with an offset of 8 days from the Landsat 7 satellite. Landsat 8 scans 12 bands, including a band which assesses data quality in terms of cloudiness, this helps selecting the best quality imagery. Table 3-6 gives an overview of Landsat 8´s data bands. GEE provides multiple sets of imagery from Landsat 8. In this study ´USGS Landsat 8 Raw Scenes (Orthorectified) ´ will be used to calculate vegetation indices in the research areas. This data set contains scaled, calibrated at-sensor radiance, orthorectified scenes only. These images have a resolution of 30 by 30 m per pixel, except for the panchromatic (15m) and thermal bands (100m).

Table 3-3 - Landsat 8 data bands (USGS, 2016).

Band	Range	Band	Range
B1	Coastal aerosol (0,43 - 0,45 µm)	**B7**	Short-wave infrared 2 (2,11 - 2,29 µm)
B2	Blue (0,45 - 0,51 µm)	**B8**	Panchromatic (0,50 - 0,68 µm)
B3	Green (0,53 - 0,59 µm)	**B9**	Cirrus (1,36 - 1,38 µm)
B4	Red (0,64 - 0,67 µm)	**B10**	Thermal infrared 1 (10,60 - 11,19 µm)
B5	Near infrared (0,85 - 0,88 µm)	**B11**	Thermal infrared 2 (11,50 - 12,51 µm)
B6	Short-wave infrared 1 (1,57 - 1,65 µm)	**BQA**	Data quality assessment band

3.1.2. LIDAR: surface elevation data.

The change in dune morphology since the 1990's can be analysed through annual airborne Lidar elevation data, acquired from Rijkswaterstaat. Utrecht University (UU) has an annual surface elevation data available for both research areas (Figure 3-9 and Table 3-3). The datasets of UU are available for different periods: 1997-2016 for Terschelling and 2007 - 2016 for Heemskerk. The latter does not interfere with the results, as the blowout near Heemskerk became active after suppletions in 2006 (MIN I&W, 2017). The elevation is measured with respect to the mean sea level (MSL). These datasets are stored in both MATLAB and .asc-raster files. The surface elevation data of Terschelling has been modified to a local coordinate system: it has been moved, with beach pole 14 as origin, and rotated with 18 degrees to form a horizontal cross-shore image. The data of Heemskerk was not moved and/or rotated. The LIDAR-data of Terschelling originally had a pixel size of 2 by 2 meter, whereas Heemskerk has a grid size of 1 x 1. The Terschelling LIDAR-dataset was manipulated to increase accuracy: each original annual dataset was interpolated to increase point density (to 1x1m resolution) using linear interpolation (MathWorks, 2018). This increased grid size to 2100m by 8.000m and pixel size to 1x1 meter. A large region of this contains NaN's (Not-a-Number), which have no value in further analysis. These were removed be clipping each data set to the region of x=1.500-6.500 and y= 1.250-1.800. These manipulations decreased calculation times enormously. The grids size of the Terschelling LIDAR data that was used in further calculations became 551m by 5001m. The elevation is measured in m mean sea level in both datasets. The datasets of Heemskerk have an average point density of 0,81 per m^2, whereas the Terschelling Lidar data has a point density of 0,45 per m^2 for the whole image. This is relatively low compared to Heemskerk, but still a good point density. This is caused by the initial resolution.

Table 3-4 - Available Lidar elevation datasets from UU and characteristics

Datasets	Available years	Grid size	Pixel size (m)	X Coordinates	Y Coordinates
Terschelling	1997 to 2000, 2002, 2004, 2006 to 2016	1051 x 4001	2 x 2	0 – 8002	-100 –1000
Heemskerk	2007 to 2016	501 x 501	1 x 1	300 - 800	0 –1000

3.2. Data analysis

3.2.1. Google Earth Engine

Google Earth Engine (GEE) was used to research the development of vegetation in and around the blowout areas of Heemskerk and Terschelling. GEE is a software package which allows users to explore and manipulate satellite data in a cloud environment. All data has been released by Google and is approved to be used in educational and scientific manners. GEE contains all sorts of diverse data, such as Landsat and MODIS satellite imagery. GEE can be excessed through the internet and can be used with coding languages Python and JavaScript. Java is used to build scripts which can import imagery, make calculations with image bands (e.g. calculate NDVI), choose the most cloud free image; make time-series charts and among many other options. GEE can also be used in research to create local NDVI maps at the research locations. These maps can be generated from satellite imagery that goes back several decades: Landsat 4 starts in 1982. There are two main types of satellite datasets available: MODIS and Landsat. Of which Landsat contains the most accurate imagery: up to 30 by 30-meter resolution. The different Landsat missions are discussed in paragraph 3.2.3 (Fawcett et al., 2017; Sidhu, Pebesma, & Câmaraa, 2018). The script used for this MSc research can be accessed through the following link: https://code.earthengine.google.com/0bf5506d94e3ed7d2259192f14f39235.

NDVI

The Normalized Difference Vegetation Index (NDVI) can be used to display greenness (relative biomass) on aerial photographs and satellite imagery. The foundation of NDVI is based on the fact that vegetation has a high reflectivity of the near-infrared (NIR) band and absorbs chlorophyll pigment in the red band width. This means that healthy vegetation reflects more near infrared and absorbs more visible light than non-healthy vegetation (Figure 3-8). NDVI calculations (Equation 3-1) result in a value between -1 and 1 for each pixel in an image. All values below 0 are considered non-vegetation (e.g. water, sand and rock) and values near +1 indicate very dense, healthy vegetation (high density of green leaves). NDVI currently is used worldwide to monitor agriculture, drought, forest fire risk and more (Weier & Herring, 2000). For the use in this research classes have to determine to indicate the presence of vegetation: most commonly the NDVI-value of 0.2 is used as a boundary. Values above 0.2 will be considered vegetation (Table 3-5).

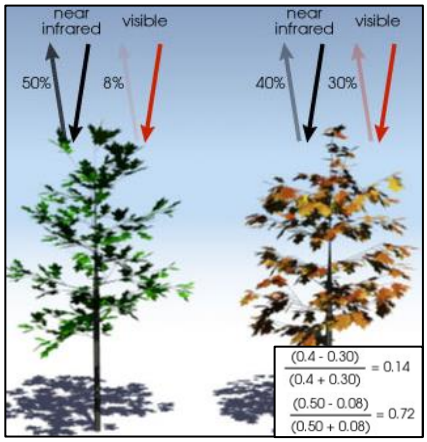

Figure 3-4 - Explanation of NDVI (Weier & Herring, 2000).

Table 3-5 - Classification of NDVI-values(Weier & Herring, 2000).

NDVI-value	Definition
<0.1	Barren area: water, sand, rock, snow etc.
0.2 – 0.3	Shrub areas and grassland
0.6 – 0.8	Tropical rainforest

$$NDVI = \frac{NIR-RED}{NIR+RED},$$

Equation 3-1 – NDVI with: NIR = near infrared band and RED = red band (Weier & Herring, 2000).

3.2.2. Analysing vegetation with Google Earth Engine (GEE), LANDSAT and NDVI

GEE was used to calculate NDVI for satellite imagery, covering three decades of vegetational changes. The use of GEE in this thesis is presented in Figure 3-16 and can be summarized in the following three steps: Importing and filtering data based on: dates, locally calculated cloud cover and region by user-specified geometry (1); Calculations: using all bands of satellite imagery, such as: optical bands (e.g. red, blue), but also thermal (2); Analyses and display: creating maps and charts with both temporal

(time series analysis) and regional changes (3).Information about the initiation and filtering of imagery (steps 1 and 2) are added to the appendix (page 62). The complete GEE is added to the appendix (page 65). The satellite imagery that was used is classified as Tier 1 Top-of-Atmosphere (TOA) Reflectance by USGS.

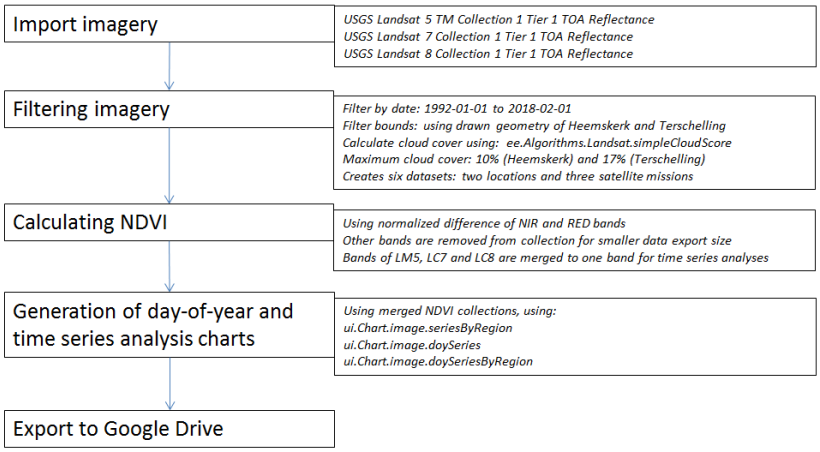

Figure 3-5 - Flowchart with the NDVI calculations using GEE. The boxes on the right show the data input and the functions used.

Step 3: NDVI analysis

The analysis of the vegetation index is done locally by using geometry of that roughly represent the morphological units, as derived from the Lidar datasets. It is important to well define these regions as the size and shape of these areas have an influence on the outcome of the analysis. This allows for computations within relatively small regions of interest, for example inside a blowout or the lobe behind it. It will provide insight in local vegetation changes over time. The geometries, for both Terschelling and Heemskerk are shown in Figure 3-20. A larger version of these maps is added to the appendix (page 67). The time series analysis is divided into two types: one focussing on seasonal changes of vegetation and one focussing on the vegetational changes over multiple years. The main goals of this analysis will be:

1. Analysing change seasonal variation of vegetation of three period: pre-blowout (1), active blowout (2) and closing blowout (3) within the mentioned time spans for Heemskerk and Terschelling. This will be done by calculating the seasonal average NDVI for each season over all datasets.
2. Analysing seasonal vegetation development in specific areas: e.g. in and around blowouts.
3. Comparing overall dune vegetation development of blowouts with a nearby reference dune area.

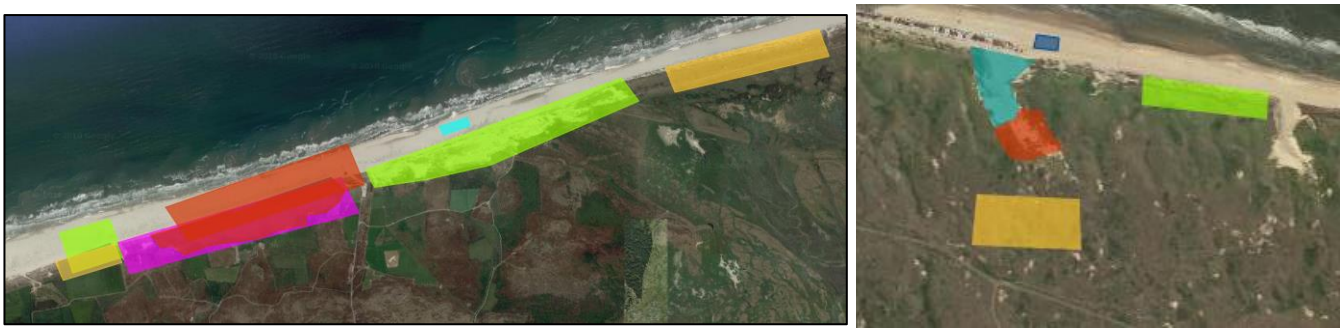

Figure 3-6 – ROIs around the blowout area on Terschelling (left) and Heemskerk (right; rotated 90 degrees eastward).

The seasonal changes are analysed by creating day-of-year (DOY) charts (Figure 4-14). Basically, the DOY analysis calculates the mean NDVI of each day of the year over all images or full period. The result is a graph that shows the seasonality of the vegetation (high in spring/summer and low in fall/winter). A DOY analysis is made for all regions of interest in both Terschelling as Heemskerk. To gain insight in the development of vegetation since the initiation of a blowout, the vegetation in the study areas is

studied over a larger temporal scale; from 1994 to 2017 (Figure 4-17). The figure shows deviations around dates such as: 03-01-1993, 19-02-2017 and 13-08-2013.
The seasonal change of NDVI on Terschelling was analysed using a Day-Of-Year analysis (DOY) from GEE. GEE calculates the average NDVI of each day of the year for the whole period (1997-2016) and per ROI. The NDVI was determined for five locations: the blowout areas (left and right), two reference dunes and an area on the beach.

3.2.1. Analysing morphology using annual LIDAR elevation datasets

The LIDAR data for Heemskerk and Terschelling is analysed using MATLAB. As described before, the datasets are from different measuring periods (Table 3-3). The elevation (Z) is displayed in m above average sea level.

Cross-shore and alongshore profiles

The profiles (paragraph 4.1.2) are made for two reasons: determining the annual morphological change and to accurately determine the locations of the blowouts using profiles of 1997. The locations of the profiles are presented in Figure 0-8. Annual cross-shore and alongshore profiles were made to analyse the morphological development. The cross-shore profiles have been made along specific cross-shore coordinates (e.g. blowout, reference dune) for each data set to determine local volume changes and morphological movement (landward/seaward). The profiles focus on the first dune row (0> Z<20). The profiles measure up to 725 m land inward from -250 m. Table 3-7 shows the cross-shore location of the elevation profiles. Also, alongshore profiles were produced from the LIDAR elevation data to look more closely at landward/seaward movement of the dunes. The alongshore profiles were made along multiple y-coordinates for both research areas, as neither LIDAR dataset is perfectly shore normal. Figure 3-13 shows the locations of the alongshore profiles at Terschelling. The alongshore profiles the coordinates presented in Table 3-6. The profiles of Heemskerk are combined in the overview in Figure 4-3. The alongshore profiles show elevation in m above sea level.

Table 3-6 – Locations of alongshore and cross-shore profile lines.

Line	Onshore distance (m)	Cross-shore distance (m)
ycoord1	430	1940
ycoord2	440	2530
ycoord3	450	2957
ycoord4	456	3956
ycoord5	470	5150
ycoord6	474	6450

Table 3-7 – Location of cross-shore profiles.

Line	Cross-shore distance (m)
xcoord1	1000
xcoord2	2500
xcoord3	3500
xcoord4	4000
xcoord5	5000
xcoord6	6500

Determining blowout locations on Terschelling using standard deviation

The literature review indicated the presence of artificial blowouts on Terschelling, but nothing was found about the exact location. Therefore, a method was developed to determine the locations from the Lidar Elevation data. The locations of the blowouts on Terschelling were determined by creating six alongshore profiles (Figure 4-4 and Figure 4-5). The distinction was made in the elevation map between a cross-shore distance of 1800 to 3500(left) and 3500 to 6800 (right) as the dune are still not perfectly aligned in cross-shore direction: the left side is slightly more seaward. The alongshore profiles were analysed for the LIDAR data of 1997, determining the standard deviation (SD) per 5 datapoints along each line. SD was calculated within a moving window of 10m wide along the lines as presented in Table 3-8. More window sizes were used (2, 10, 20), but a width of 10m proved to be the best fit to find the blowout locations. Spikes in SD are an indication of a steep profile, which is the case for the artificial blowouts on Terschelling. The area was divided in two parts: left and right of the beach entrance around x=3500m. The calculated standard deviation for the left side of Terschelling shows spikes at an alongshore distance of 1800, 2000, 2200, 2500, 2600, 2700, 2900 and 3290 m in Figure 0-6A, in the appendix. Figure 0-6B shows the alongshore profile and its standard deviation for east of

the beach entrance. Here, blowouts are less easy to locate due to interference of the beach entrance with the elevation profile. Therefore, the spikes in standard deviation around x=3750 are ignored. Other spikes are present roughly around x= 4500, 5200 and 5800. All these peaks add up to the amount of 8 blowout locations, these locations will be used as indicators for blowout locations in the volume calculations.

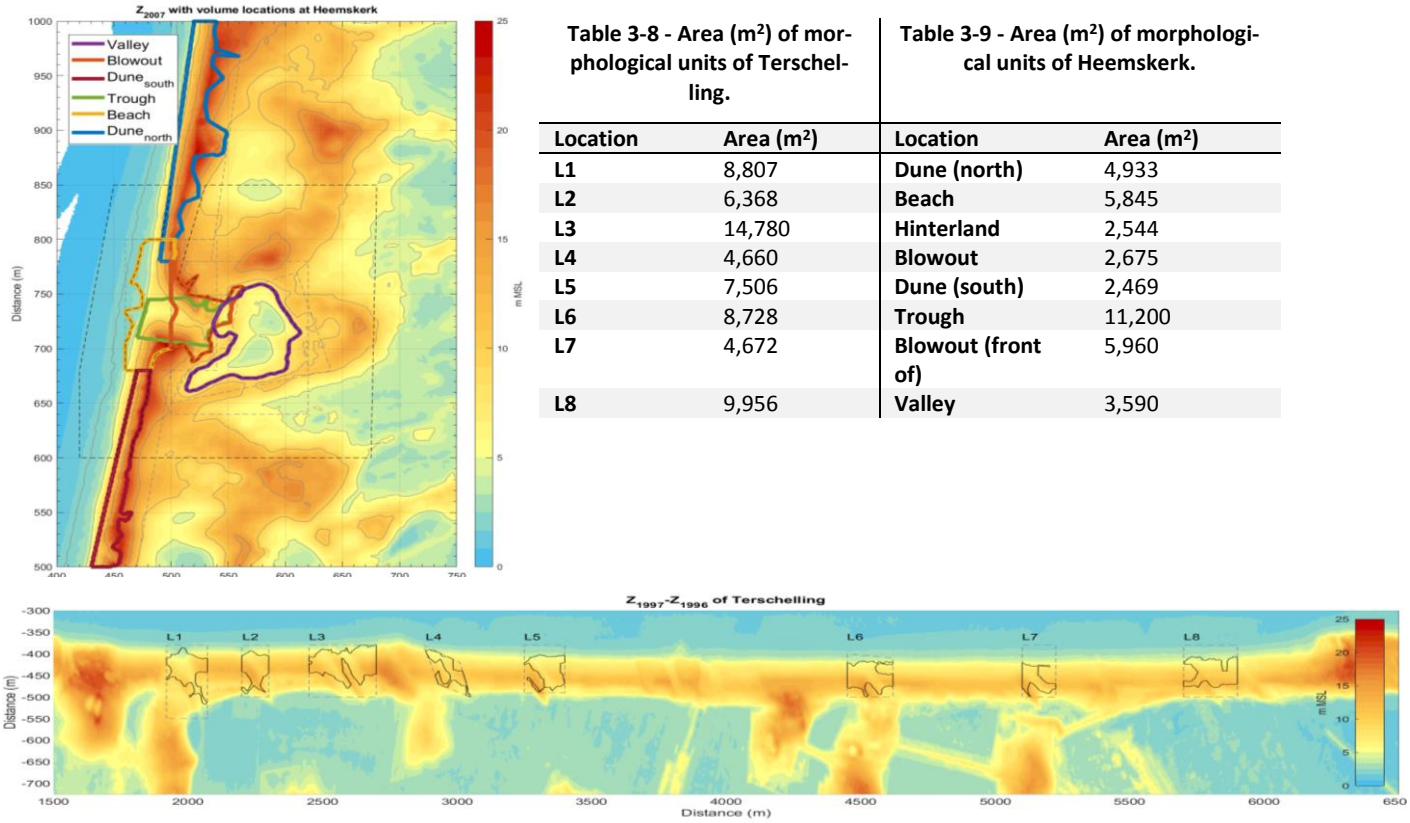

Table 3-8 - Area (m²) of morphological units of Terschelling.

Location	Area (m²)
L1	8,807
L2	6,368
L3	14,780
L4	4,660
L5	7,506
L6	8,728
L7	4,672
L8	9,956

Table 3-9 - Area (m²) of morphological units of Heemskerk.

Location	Area (m²)
Dune (north)	4,933
Beach	5,845
Hinterland	2,544
Blowout	2,675
Dune (south)	2,469
Trough	11,200
Blowout (front of)	5,960
Valley	3,590

Figure 3-7 - Locations of morphological units (e.g. blowouts) used for volumetric analysis in Terschelling (below) and Heemskerk (above), as defined from the 1997(Terschelling) and 2007 (Heemskerk) Lidar elevation data.

Volumetric change of blowouts and lobes

The volumetric change (ΔV) of the dunes was determined for each yearly dataset. The volume was determined for specific areas within the elevation maps. The calculated volume will be used to determine amounts of annual growth/degradation of the first dune row; in blowouts; lobes etc. Table 3-9 contains the area of the locations near Heemskerk. The area of the locations on Terschelling are presented in Table 3-8. The created MATLAB script works with a user-specified area of interest. Within this area a minimum elevation (or elevation change) must be specified. For a blowout for instance, a decrease of elevation of more than 2 m per year can be specified. The contours of this elevation change will be used as morphological unit 'blowout' to calculate annual volume (and volume change). These areas will be used to determine the change of volume over time within the initial morphological unit. Examples of other used morphological units are: nearby reference dune, foreland/beach and hinterland (in the appendix; Figure 0-7). The volume of this area is calculated for each annual dataset. The annual volumes are presented in a graph for comparison between morphological areas. The annual volume change is calculated by subtracting the volume (and volume change) within these areas can give an indication of the amounts of sand transported through the blowouts each year, as an increase in hinterland (behind blowout and first dune row) will mainly be caused by this phenomenon. These same morphological units (or areas of interest) will also be analysed based on vegetation (NDVI) using GEE.

3.2.1. Combining morphological and vegetational data

The interaction of morphology and vegetation during blowout development is analysed by combining the LIDAR and Landsat (NDVI) data. This was done in two steps: visual (with GIS-software) and analytical (with MATLAB).

The visual combination of annual elevation data and NDVI imagery was made in Qgis. The LIDAR imagery was imported and the annual change in elevation was calculated by subtracting subsequent years of data. The NDVI imagery was imported and converted to contour maps with steps of 0.025, which can adequately represent four types of locations: water (NDVI<0), bare soil (NDVI 0<1), so vegetation (0.1>NDVI<0.2) and vegetated (NDVI<0.2). This data was overlaid and visually inspected for a correlation between the type of vegetated area and the amount of decrease/increase of elevation (erosion or sedimentation).

From the LIDAR elevation maps, the annual change in volume is calculated to indicate the level of activity of the blowout. With the Landsat imagery, the annual percentage of sand cover for each ROI is calculated. This is done by combining Landsat imagery into annual NDVI-maps by taking the mean value over each pixel within the study areas. These annual images are exported and further analysed using MATLAB. The percentage of pixels with bare soil or sand cover within the ROIs is calculated based on the threshold NDVI-value of 0,2. Every value above 0,2 will be considered vegetated (or partly vegetated). Hereafter, the annual percentage of sand cover is plotted against the annual volume change within the morphological areas, as defined in Figure 3-7.

3.3. Field site descriptions

The Dutch coast has a length of 451 km and consists out of several coast types: island heads/tails, wide and narrow dunes, accreting coasts, coastal towns, dams and dikes and connecting constructions (Koningsveld et al., 2007; Löffler et al., 2011). More than 15 dune restoration projects were performed to restore aeolian dynamics, landscape building processes and improve ecological characteristics in dune areas along the Dutch coast. These projects started in the 1990's in combination with the new management strategy (MIN V&W, 1990). The projects were aiming to reactivate smaller scale blow-outs; mobilize (parabolic dunes or restoring landscapes by removing or adapting artificial landscapes). Figure 3-1 contains an overview of these projects along the Dutch coast (Arens et al., 2013). The location of the projects is indicated with beach poles (bp), which are were placed every kilometre along the Dutch coast. The dunes near Heemskerk are presented as a location where 'Dynamic foredune management' was implemented, whereas the dunes near Terschelling are referred to as 'restoration of foredune dynamics'. There is a difference in the two projects. At Heemskerk, the dynamics of the dunes are restored by change in management: more natural development of dunes. The location at Terschelling was actively restored by human intervention (e.g. with artificial blowouts). Two of these sites were chosen as study areas for this research: the dunes near Heemskerk (bp 47-50) and the beach of Terschelling (bp 16-22).

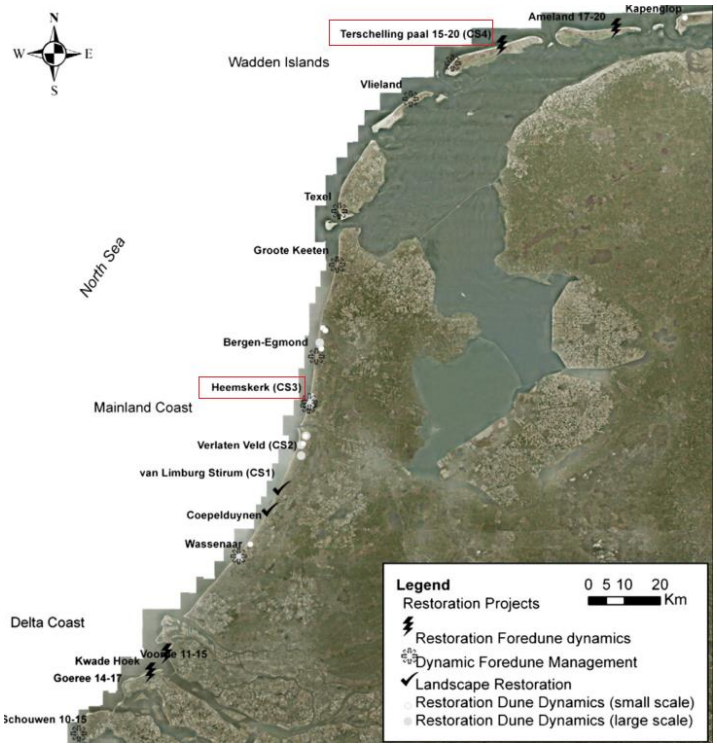

Figure 3-8 - Dune restoration projects aiming at aeolian processes (modified from Arens et al., 2013).

3.3.1. Heemskerk

The beach and parabolic dunes near Heemskerk (The Netherlands) cover a stretch of 3,7 kilometres within the border of the municipality. The dune system has a size of 11.20 ha and is part of nature park Noordhollands Duinreservaat (with an area of 5.300 ha). The coast has many different functions here. First, it provides safety against coastal flooding, through its dune system. It also has a recreational use: there are paths in the dune valleys and nearby forest. The dunes are located in a transitional area of chalk rich and poor soil. This has an impact on the ecology. The northern part, near Bergen aan Zee, lacks chalk. Whereas the dunes more south are richer in chalk. This can also be derived from the present plant species: more north crowberry, creeping willow and grey hairgrass are present; whereas more south the soil is covered with Syntrichia ruraliformi and humus or 'zeedorp vegetation' (Alterra, 2017). It also houses a drinking water basin, which is in the dune area and is visible on satellite imagery (Figure 3-3). The dune area is maintained PWN. It is also recognized as a Natura2000 area, because of

its ecological values (PWN, 2018). More recently in 2017, a beach nourishment was completed between bp 48 and 51, because the BCL was exceeded too frequently. 1.000.000 m^3 of sand was deposited over a length of five kilometres to ensure enough sediment would be available on the beach to be transported into (and over) the dunes (MIN I&M, 2017).

Wind conditions

The general boundary conditions of both locations contain characteristics such as sea-level rise (SLR) and wind. The wind conditions, speed and direction, were required from the Royal Netherlands Meteorological Institute (KNMI, 2018). The measuring station of Ijmuiden was used for the Heemskerk dune area. This station is located approximately five kilometres south of Heemskerk. The wind directions prove to be similar for both locations: both locations are dominated by wind from south-west/west direction. The original wind speed data from the KNMI was the average wind speed per day. High wind speeds (>10 m/s) were measured more frequently (19.5% of measurements) near Heemskerk than on Terschelling (10.3%). As for the average wind speed, this was measured at 6.3 m/s over all wind directions and 7.3 m/s for the prevailing south-west wind.

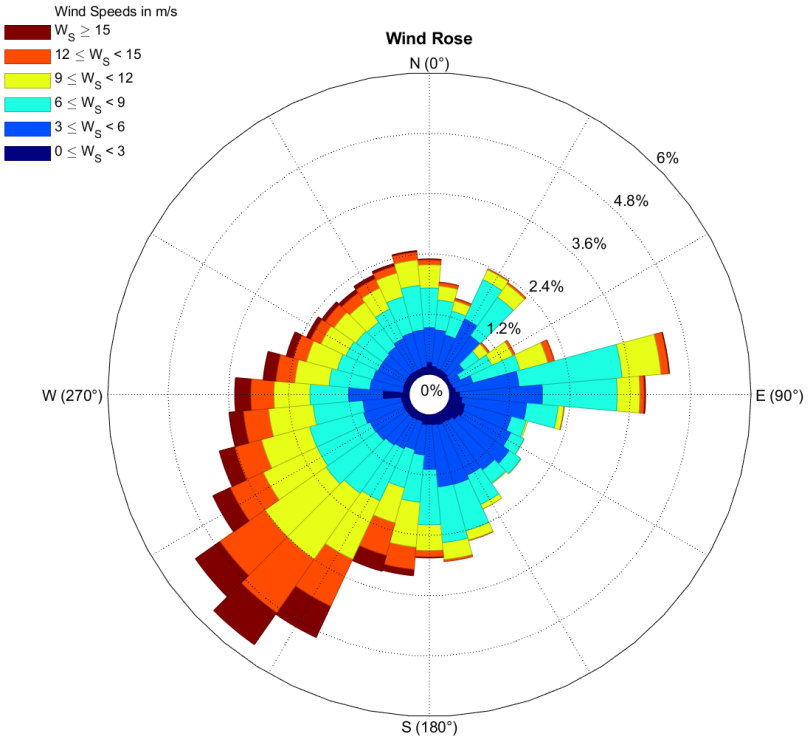

Figure 3-9 - Wind rose from station 225 (IJmuiden) of the KNMI from 01-01-1997 to 01-01-2016. Average wind speeds are presented in m/s and are converted from hourly averaged wind speeds (KNMI, 2018).

Blowouts near Heemskerk

Several blowouts initiated recently after beach nourishments in 2005-2006 and 2011 near Heemskerk (near bp 48 and 49), the Netherlands. Objectives of the specific local dune management includes rejuvenation of vegetation in the dunes and valleys behind, therefore a dynamic foredune management being applied. The blowout formation in Figure 3-3 has led to the formation a depositional lobe 130 m behind the dune (Löffler et al., 2016; Van der Valk et al., 2013). This type of management recently led to the development and growth of blowouts and carves (Figure 3-4). The figure shows a domination of marram vegetation and use of sand fences in 1996. The new dynamics developed into active parabolic dunes with local amounts of erosion exceeding 10 m and sand burial of below 10m (Figure 3-4). This movement is great enough to prevent colonization of vegetation. This al led to an increase of landward moving sand to the dunes behind, the amounts of sand are not specified, since there are no actual measurements available yet (Arens et al., 2013). However, initial blowouts are visible from satellite imagery starting in 2006. From then on blowouts formed pronounced deflation basins and

depositional lobes. For an in-depth investigation of the natural blowout development in this area, the southern blowout has been chosen as a reference site. The southern blowout of Figure 3-4 will be researched more closely with the use of LIDAR elevation data (paragraph 3.2.2). Figure 3-4 clearly shows the erosion of the foredune and, in combination with the aerial photography, the development of the blowouts land inward. The development is characterized by the withdrawal of vegetation, the deepening of the blowout and the lobe forming behind it in the form of a parabolic dune.

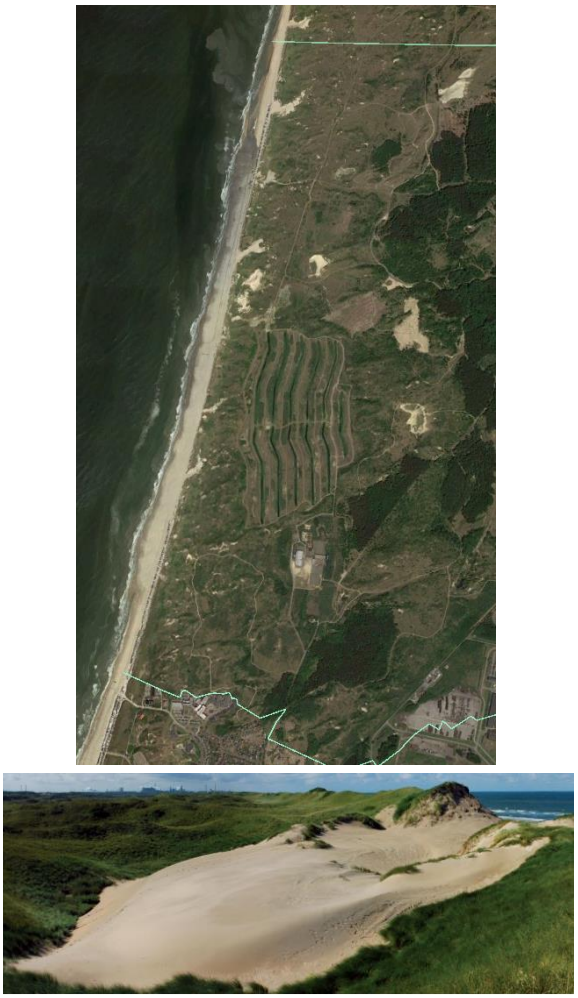

Figure 3-10 – Satellite imagery of the coast near Heemskerk, the Netherlands (Google Earth, 2018) and a large blowout in the area called 'Gat van Heemskerk' (Löffler et al., 2016).

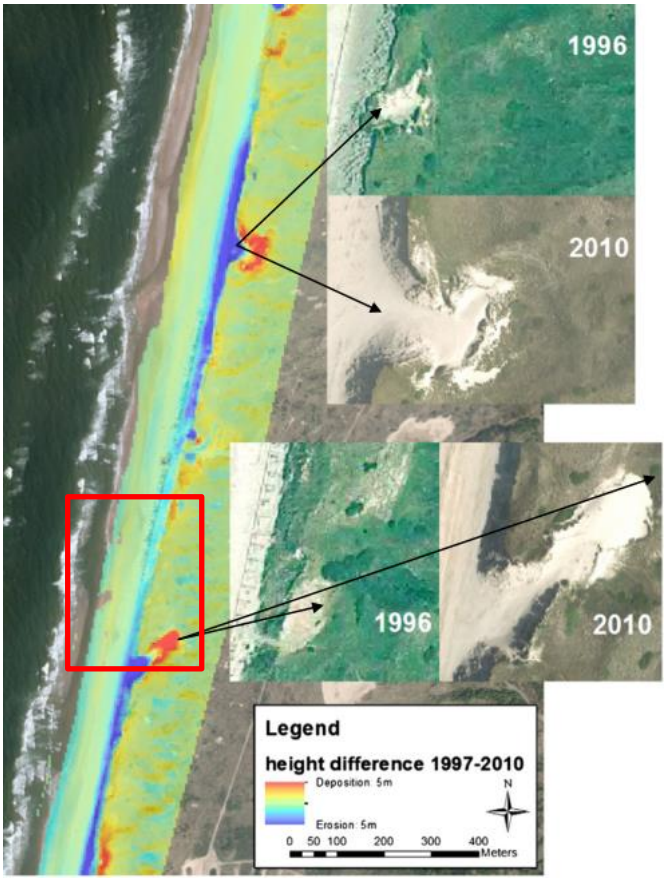

Figure 3-11 - Origin and growth of 2 blowouts near Heemskerk and the research area in red (Arens et al., 2013).

3.3.2. Terschelling

The research location on Terschelling is located on the northern side of the Wadden Island and the region of interest (ROI) consists of a stretch of coast which is approximately 4.500 m wide (Figure 1-1 and Figure 3-12). At the blowout location on Terschelling, a new management strategy was chosen in 1995 to restore the foredune dynamics. The goal was to adjust the relatively high and steep foredune to fit better with the landscape, while increasing natural values (e.g. ecology) of the area. The foredune dynamics were attempted to restore by digging eight artificial blowouts (or notches) between bp 16 and bp 20 into the foredune. These cuts were made in WNW – EZE direction; the prevailing wind direction. Also, sand fences were removed from the foredune and vegetation was kept to a minimal for five years, starting in 1997. After doing this the system on Terschelling developed in a more natural manner, as human interference was minimized. The result is a unique (in terms of morphology and vegetation) and dynamic dune area of 100 ha. A fresh water bubble formed after blowout initiation, which improved local ecology as it attracted new plant species (Löffler et al., 2016; Van der Valk et al., 2013).

Figure 3-12 - Terschelling and the blowout region in red (bp 15-bp 20) from Google earth (2018)

Wind conditions

Terschelling has its own meteorological measuring station in the municipality Hoorn, which is less than two kilometres south from the blowout area. The prevailing wind direction is west/south-west. The highest wind speeds also come from these directions (7.2 m/s on average from south-west). The averaged for all directions near the research area of Terschelling was 6.3 m/s. The average wind speeds on Terschelling are lower than the wind speeds measured nearby Heemskerk. The derived wind direction and wind speed data is presented in the wind rose in Figure 3-13.

Morphological changes of the blowout area on Terschelling in the last three decades

The appendix includes several maps which display the change in dune morphology since this change of management. Figure 3-14 shows the erosion/deposition in the blowout area of Terschelling between bp 16 and bp 20 is shown. The foredunes in the blowout area have eroded almost completely and this material is deposited landward of the initial first dune row. Figure 3-14 shows this erosion(blue)/deposition(red) in the blowout area of Terschelling between bp 16 and bp 20. It shows the initial cuts that resulted into the trough shaped blowouts over time (black circles). Only 7 are clearly visible from this map, whilst there are 8 notches. The lowering of the initial foredunes (blue); the growth of the blowouts; the widening of the whole dune system (landward growth/accretion in red) and the growth of the dune row behind the foredune are al present in Figure 3-14 (Arens et al., 2013). The crest height of the second dune row is increasing since 2008. This is supported by the measured growth of overall sand volume in the dune area; it increased from 2.9000.000 m^3 to almost 3.500.000 m^3 in 2013 (Rijkswaterstaat, 2014). Also, the system of blowouts transported sand 300 m land inward, increasing the average height of the dune valley with 0,3 m. Nearby dunes (without blowouts) transported sand only 80 m land inward (Arens et al., 2013). The downside of the blowout and aeolian sand

transport is the sand covering roads nearby. This is countered by placing fences and marram grass nearby (Arens, 2007). Some areas were found to be too dynamic; too much sand was transported into the hinterland. Around area around bp 18 for instance, sand fences were placed to reduce aeolian transport and a sandbar formed them in seaward, although this is not visible in the map of Arens (2013) (MIN I&M & STOWA, 2013).

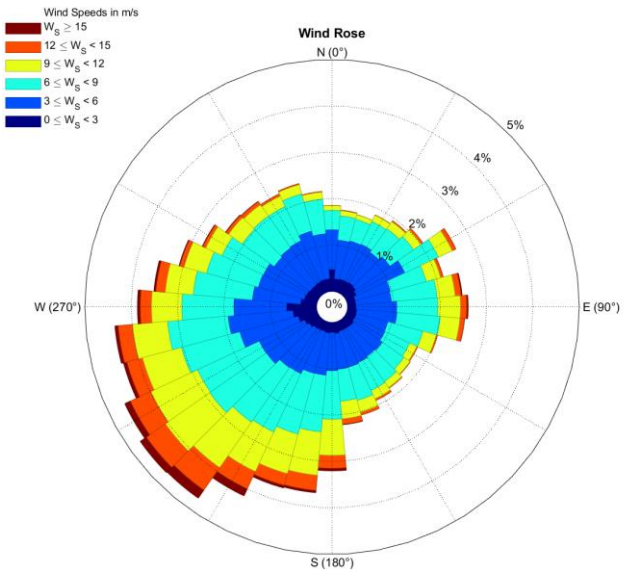

Figure 3-13 - Wind rose from station 251 (Hoorn Terschelling) of the KNMI from 01-01-1997 to 01-01-2016. Average wind speeds are presented in m/s and are converted from hourly averaged wind speeds (KNMI, 2018).

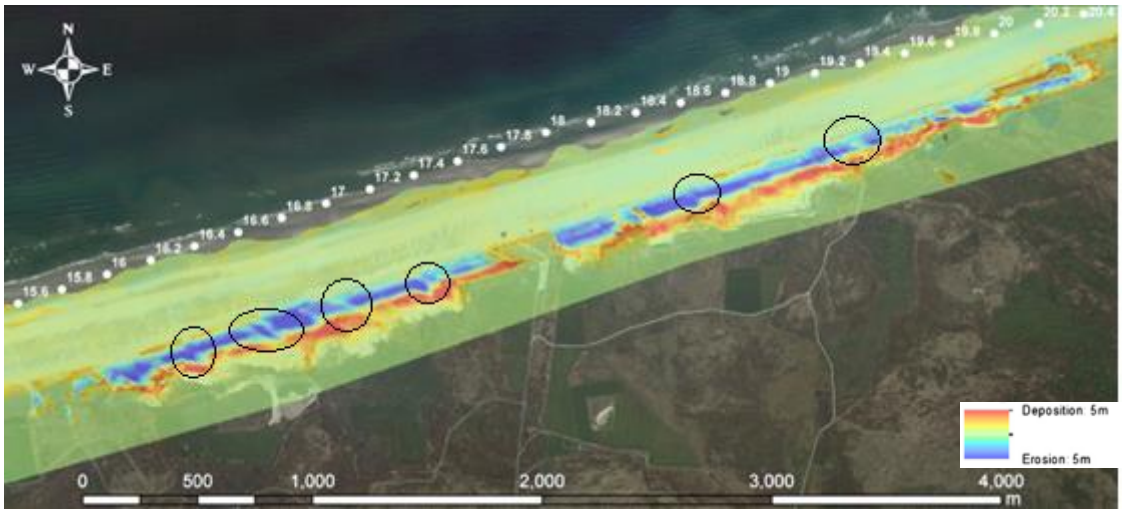

Figure 3-14 - Foredune remobilization after human interference, captured in an elevation difference map from airborne Lidar data (1997-2010) in Terschelling. Seven of eight blowout locations can be derived (black circles). Distance between white dots at the coastline is 200 m (Arens et al., 2013).

4. Results

4.1. Morphology of Terschelling

Sediment deposition occurred around y=-350; sediment erosion between y=-450 to y=-400 (pre-1996 first dune row; up to 10 m of erosion) and sediment deposition between y=-450 to y=-650. A decrease in crest height of the original foredune (Lidar 1997) of 4-5 meters can also be derived. Figure 4-1 shows the total change in elevation in Terschelling during the period of 1997 to 2016. The Contour lines shown are from Z_{1996}= 0,2m above MSL (dune foot) and 10m above MSL (dunes notches). Overview maps containing the annual change in elevation are added to the appendix (page 84).

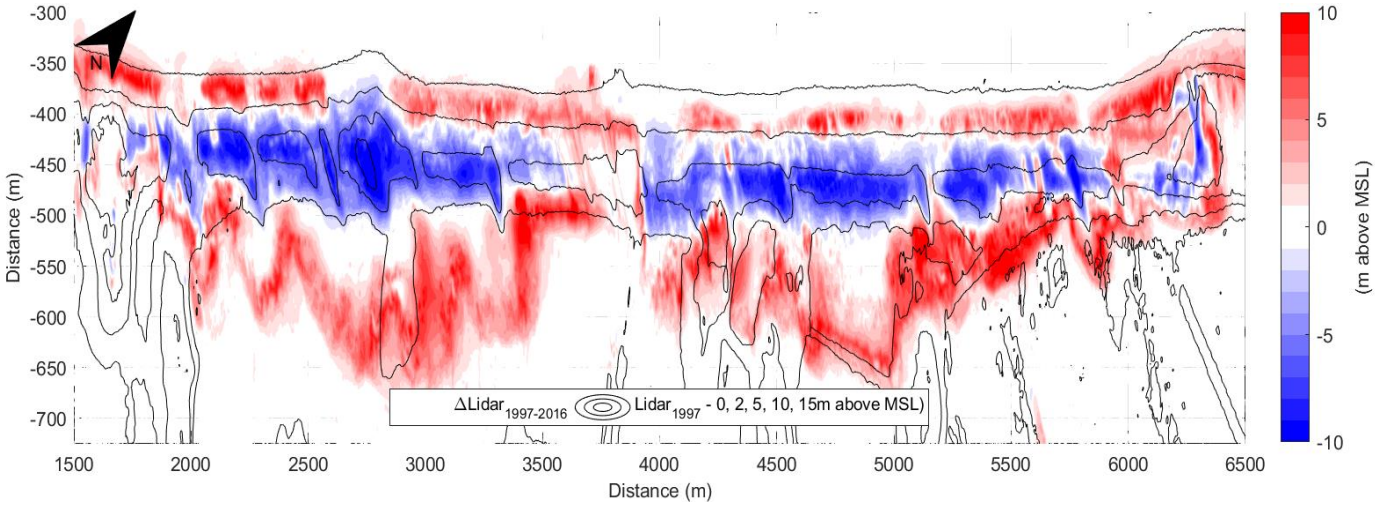

Figure 4-1 - Change in elevation (ΔZ), scaling from -10m (blue) to +10m (red) in the period 1997-2016 at Terschelling. A larger version of this map is added to the appendix (page 73).

4.1.1. Alongshore profile: Terschelling

A selection of the annual alongshore profiles is presented in Figure 4-3 and Figure 4-4. The figures contain profiles along four y-coordinates: -400 (Figure 4-3A), -420(Figure 4-3B), -480(Figure 4-4A) and -500(Figure 4-4B), as shown in the map of Figure 0-8 and Figure 4-2. These coordinates differ from the coordinates as mentioned in 3.1.2, as they are chosen to provide insight in dune development (Figure 4-3A and C) and development of the hinterland (Figure 4-4A and B). A distinction was made between right and left side of the blowout area, as the dunes are located more landward between x=3500m and x=6500m. Figure 4-3A and Figure 4-3B show the disappearance of the original foredune over the years. It also shows the landward extension of the blowouts, near x=2050m for instance in Figure 4-4B.

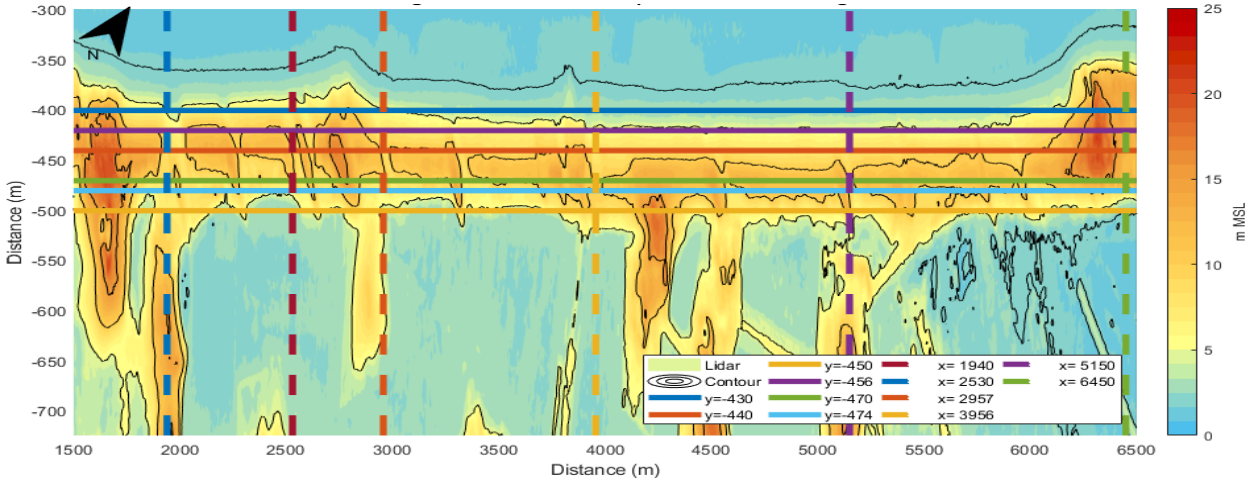

Figure 4-2 - Locations of profiles for Terschelling.

The blowout are visible in 1997 on Figure 4-4A, but the notch shows up later more landward, around 2002 and onward deepening of the blowout is visible, from +8 m above MSL in 1999 to only 4m above MSL in 2016. Figure 4-3A and Figure 4-3B show the same phenomenon at the blowout locations. It also shows erosion landward (y=-480) between x=4300m and x=5300m: from 12m above MSL to just

above 2m above MSL. This morphological change is not visible on the seaward profile of Figure 4-4A. The large amounts of erosion indicate a large influence of blowouts more landward.

The formation of new (embryo) dunes are visible on the seaward profiles (Figure 4-3A and Figure 4-4A). Around x=2500m in Figure 4-4A and around x=5600 in Figure 4-4A. Where the highest points are reached in 2016, respectively 10 and 12 m above MSL. The fact that the highest points are reached in the most recent profile indicate that the dunes are still actively growing.

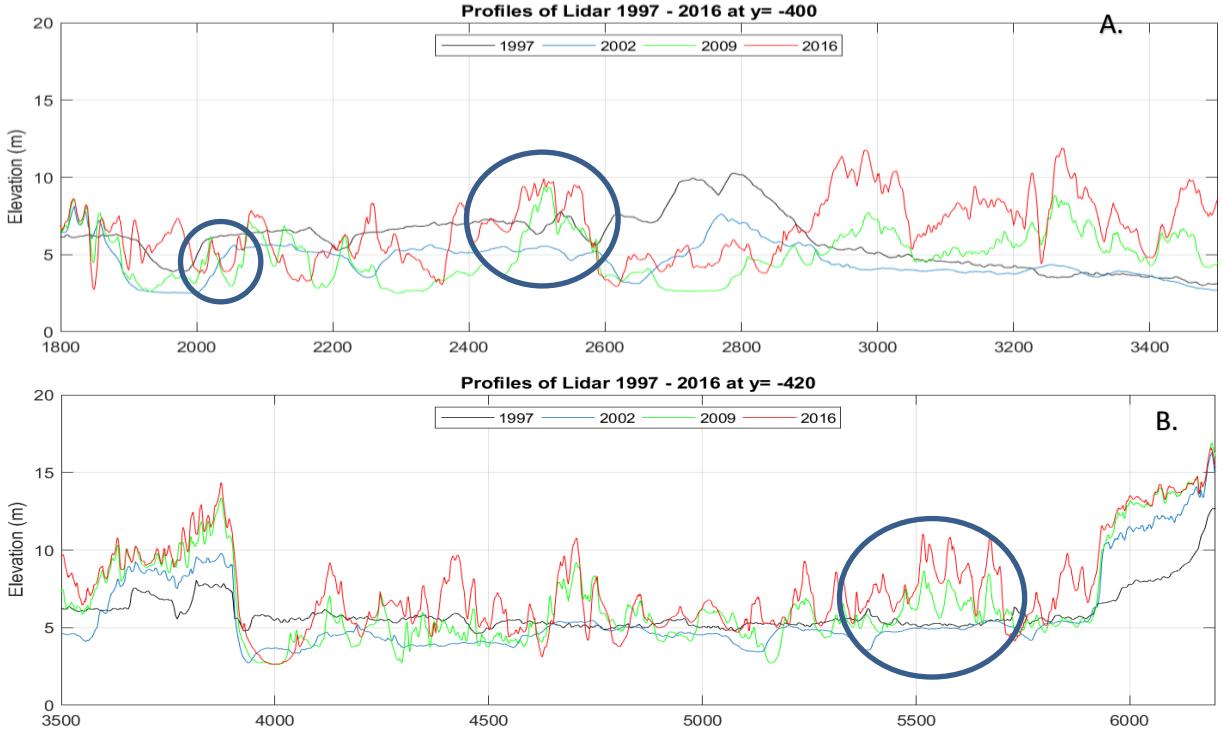

Figure 4-3 - Alongshore elevation profiles of Terschelling at y= -400m(A) and -420(B) with alongshore distance (m) on the x-axis and elevation (m) above MSL on y-axis (1997 - 2016). The location of the profile (Figure 4-1 and Figure 0-8).

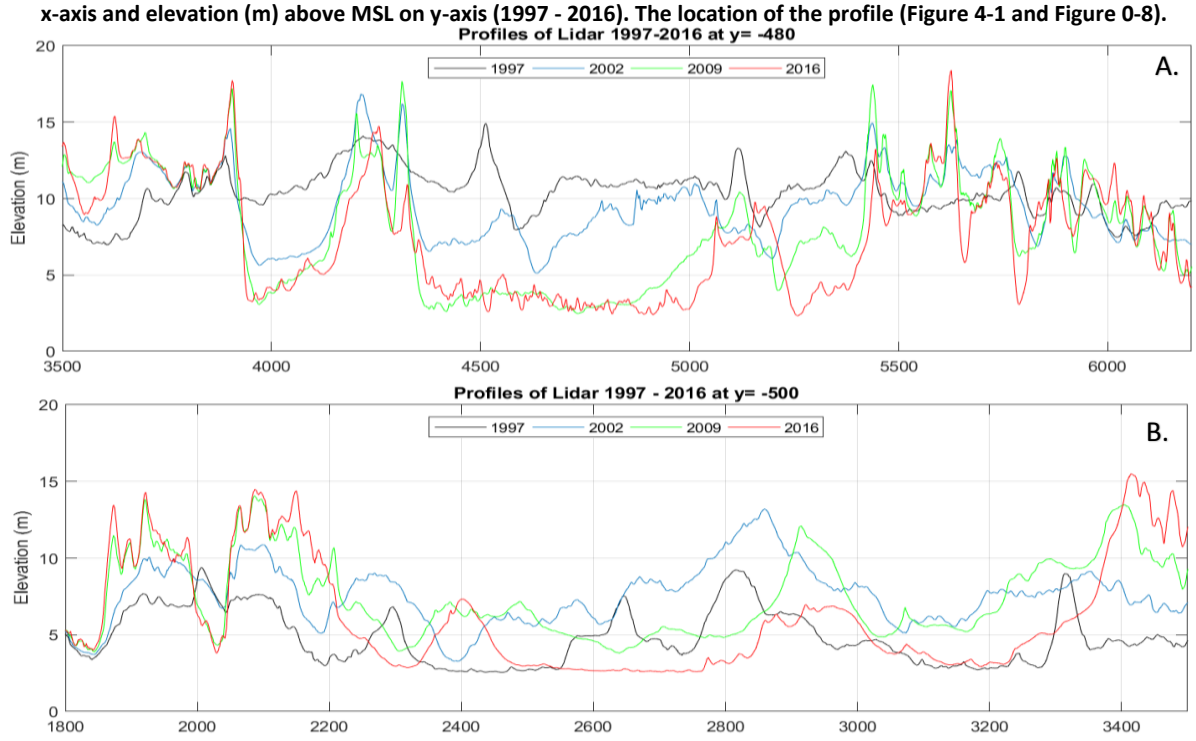

Figure 4-4 - Alongshore elevation profiles of Terschelling at y= -480m(A) and-500m(B) with alongshore distance (m) on the x-axis and elevation (m) above MSL on y-axis (1997 - 2016). The location of the profile (Figure 4-1 and Figure 0-8).

4.1.2. Cross-shore: Terschelling

The cross-shore profiles (Figure 4-5) show a landward growth of the dunes. This can be derived from the cross-shore profiles at the positions x=1940(A), x=2530(B) and x=2957(C). All positions show the formation of an embryo dune seaward of the original dune around y=-400. The dunes initially show a landward growth in the period of 1997 to 2002, as the original foredune (located around y=475) moves landward (left). In the period after that a seaward movement is visible on all three locations, as a new foredune forms; for example around y=-375 in Figure 4-5B. Figure 4-5B and C also indicate the formation of a lobe or foredune behind the blowouts (around y=-505), as the elevation rises from nearly sea level to 7.5 (B) and 12.5 m above MSL at a new landward location (between y= -550 and y=-500). The initial dune row seems to be divided in two separate dunes at the locations where blowouts are present. Figure 4-5 also shows cross-shore profiles east of the beach entrance, at x=3956m(D), 5150m(E) and 6450m(F). Profiles D and E are near blowouts, whereas F is a reference dune profile. Figure 4-5A is a location where the crest elevation lowered over time and moved seaward. The maximum crest elevation changed from 9.9 m to 6.9m above MSL. At the refence dune (F) the maximum dune crest elevation increases from 14.3m to 21.3m above MSL in 2016. The dune also moved seaward with ca. 30 m.

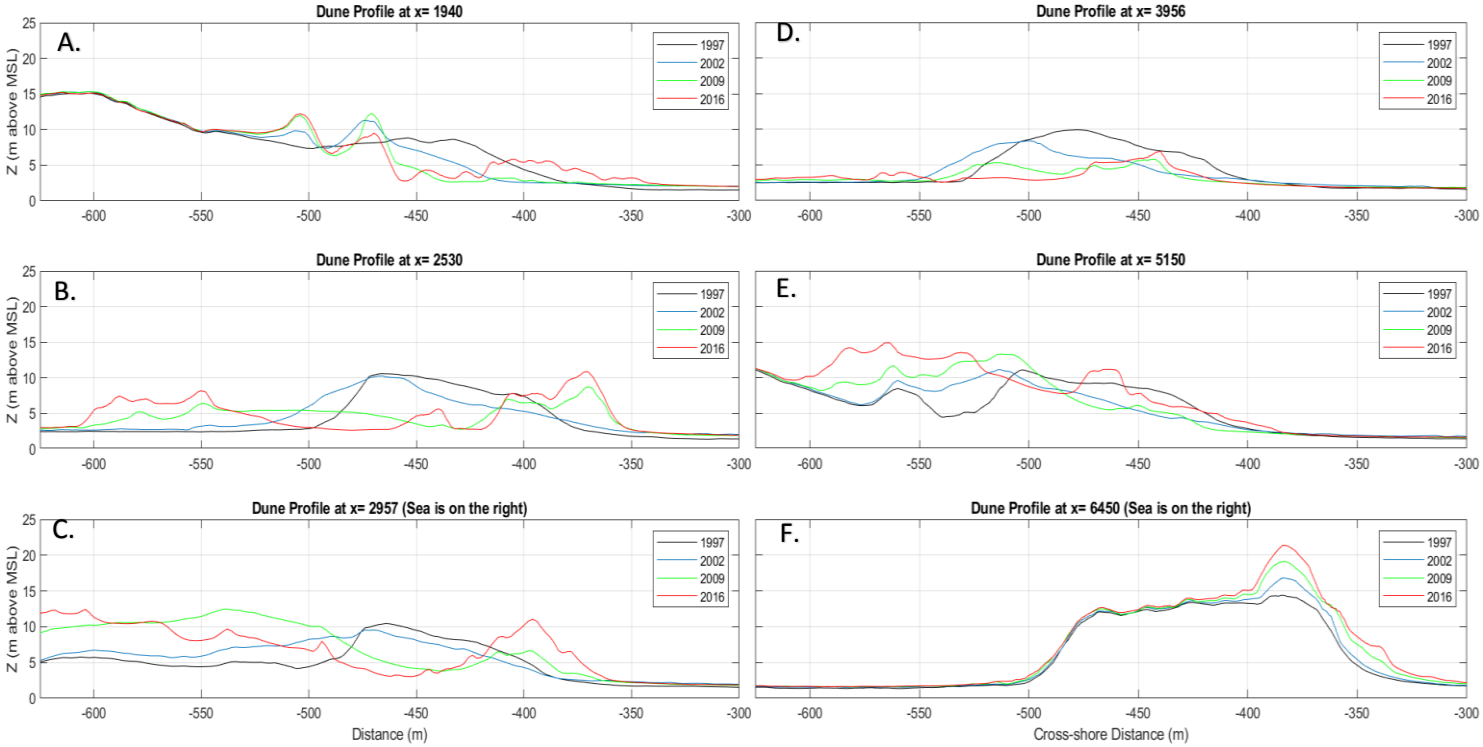

Figure 4-5 - Cross-shore profiles of Terschelling at x=1940 (A), 2530 (B), 2597 (C), x=3956m(D), 5150m(E) and 6450m(F), the North Sea is on the right. Overview of exact locations is shown in Figure 3-13.

4.1.3. Annual dune and blowout volume

The annual dune volume of the blowout areas in Terschelling are shown in Figure 4-7. In total the volume within the blowout locations decreases with 4,1x10^3 m^3 in the period from 1997 to 2016. Most of this decrease occurs in the first years after the notches were dug in the dunes. From 1997 to 2002 the volume in the ROIs decreases with 3.3x10^3 m^3. After this the annual change in volume decreases to about 400 m^3 of erosion annually. The largest amount of erosion takes place in 1998. Here the ROIs erode by 8,1x10^3 m^3 on average. Whereas the largest amount of accretion took place more recently in 2011, by 2,2x10^3 m^3 on average. The figure shows a relatively large decrease in beach volume at L3; from approximately 1,75x10^5 m^3 in 1997 to less than 1x10^5 m^3 in 2016.Figure 4-7 presents the annual change in volume within the blowout areas and Figure 4-9 shows the annual change in dune volume(ΔV). ΔV develops from relatively large amounts of erosion (up to 15.000m^3 at L3 in 1997-1998) to smaller amounts of accretion at all location more recently (from 2014 to 2016). The absolute annual change decreases over time (Figure 4-9); from 17.267 m^3 at L3 in 1998-1999 to a maximum of 3.022m^3 in 2015-2016. This is an indication that the dune dynamics decreased over time. The most active location remains L3 with a total change in volume of 108.686 m^3 from 1997-2016.

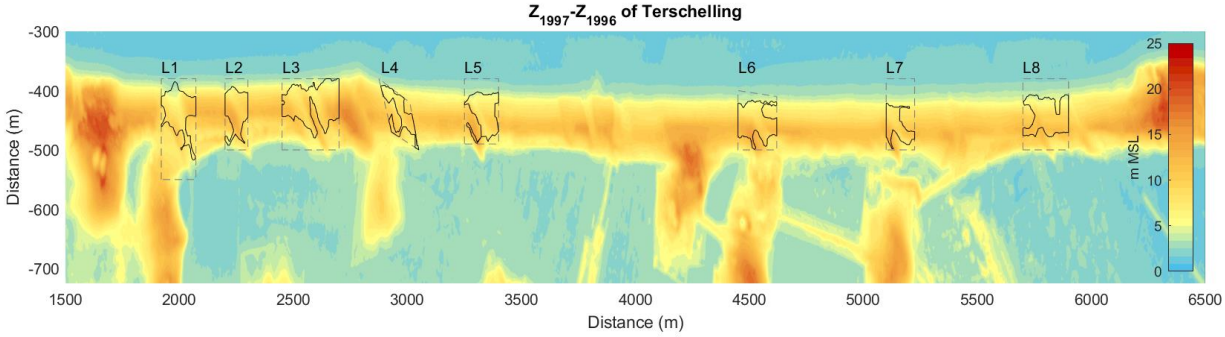

Figure 4-6 - Locations of morphological units of blowouts on Terschelling. Determined using 1997-1998 Lidar data.

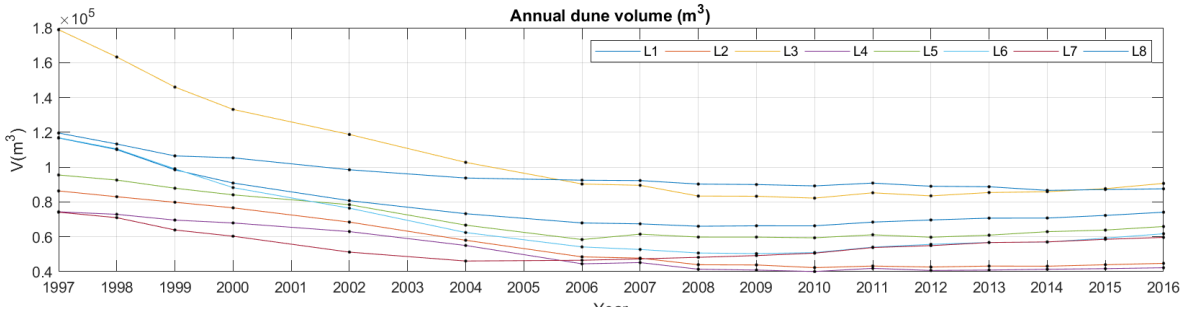

Figure 4-7 – Annual dune volume (m³) of the morphological units of blowouts on Terschelling. An overview of the locations is shown in Figure 4-8.

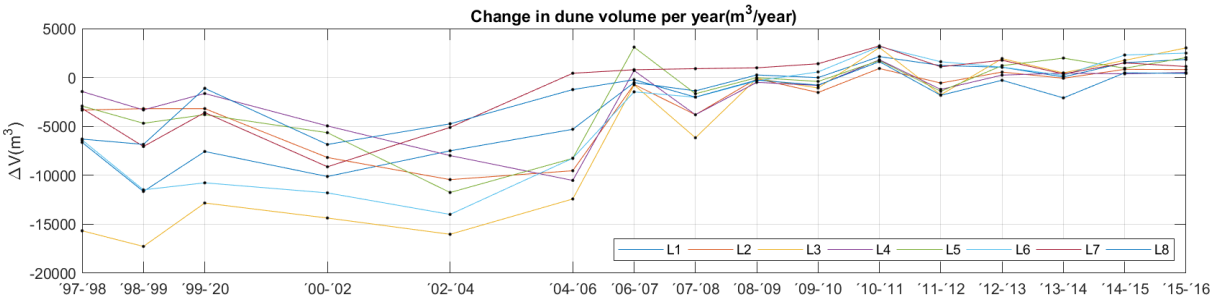

Figure 4-9 – Annual change in volume (m³/year) from 1997 – 2016 of the blowouts on Terschelling. An overview of the locations is shown in in Figure 4-10.

Beach and hinterland

The beach (in front of the blowout) and hinterland (behind the blowout) elevation data was also analysed, as they are influenced by blowout related transport; the sand will be transported from the beach to the hinterland through the blowouts. Figure 4-11 shows the total annual volume (above) and the change in volume (below) of these areas on Terschelling. The regions have an area of 64 ha (beach) and 112 ha (hinterland). The volume the beach increases with 13% or 3,09E+05 m^3 from 1997 to 2016. The largest changes can be found in 1998-1999: -4% or -9,39*10^4 m^3 of erosion; 2004-2006: +5% or 1,13*$10^5$$m^3$ accretion and in 2010-2011: +4% or 1,01*10^5 m^3 accretion. The hinterland increased with 17% or 1,09*10^6 m^3 between 1997-2016. In the hinterland the largest changes can be found in 2000: +5% or +3,25*10^5 m^3 (accretion) and an increase of 4% or 2,66*10^5 m^3. The largest amount of erosion measured is -5,43*10^4 m^3 or -1%, considerably less than the measured amounts of accretion. The absolute change of both beach and hinterland vary over the years, with a maximum for both areas in 2006. After that the change decreases. The change in beach decrease to 1%/2% and in the hinterland the relative change decreases below 1% after 2012.

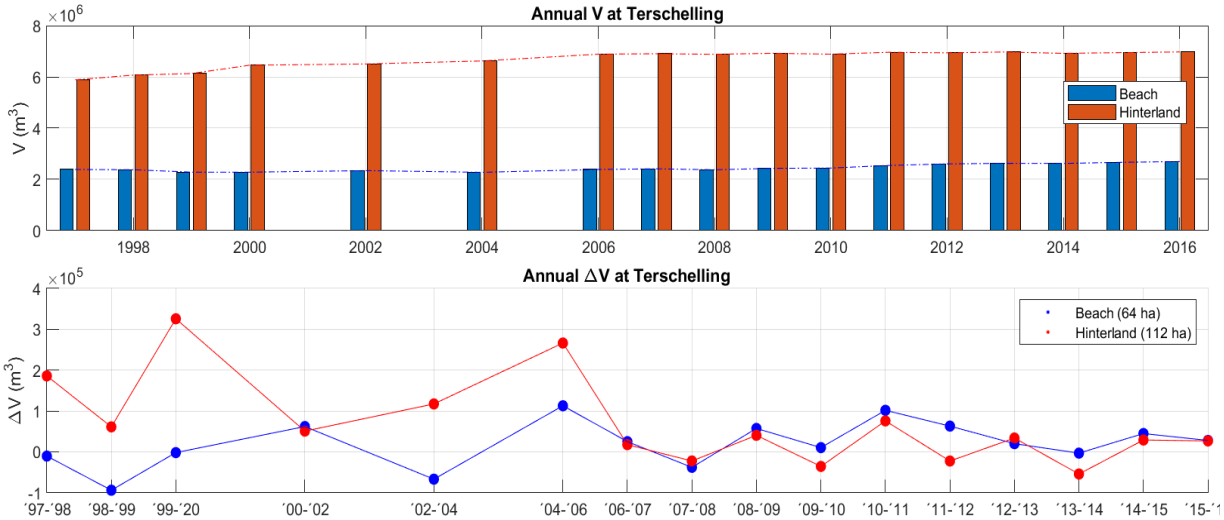

Figure 4-11 - Volumetric change in front of/behind the blowout in Heemskerk. The exact areas are shown in Figure 0-7.

4.1. Morphology of Heemskerk

At the blowout location of Heemskerk, the original blowout grew, eroded the initial foredune and caused the formation of a lobe behind it. Over the timespan of 15 years, most erosion is found around the blowout entrance (up to 10 m) and the formation of a lobe (or new foredune) behind the blowout, as the elevation increased up to 10 m behind the trough. The map also shows an increase in elevation on the beach, in front of the dune crests north and south of the blowout of approximately 4-5 m. A decrease in dune elevation of approximately 4-5 m in the crests can also be derived. The total change in elevation in/around the blowout near Heemskerk is shown in Figure 4-1B.

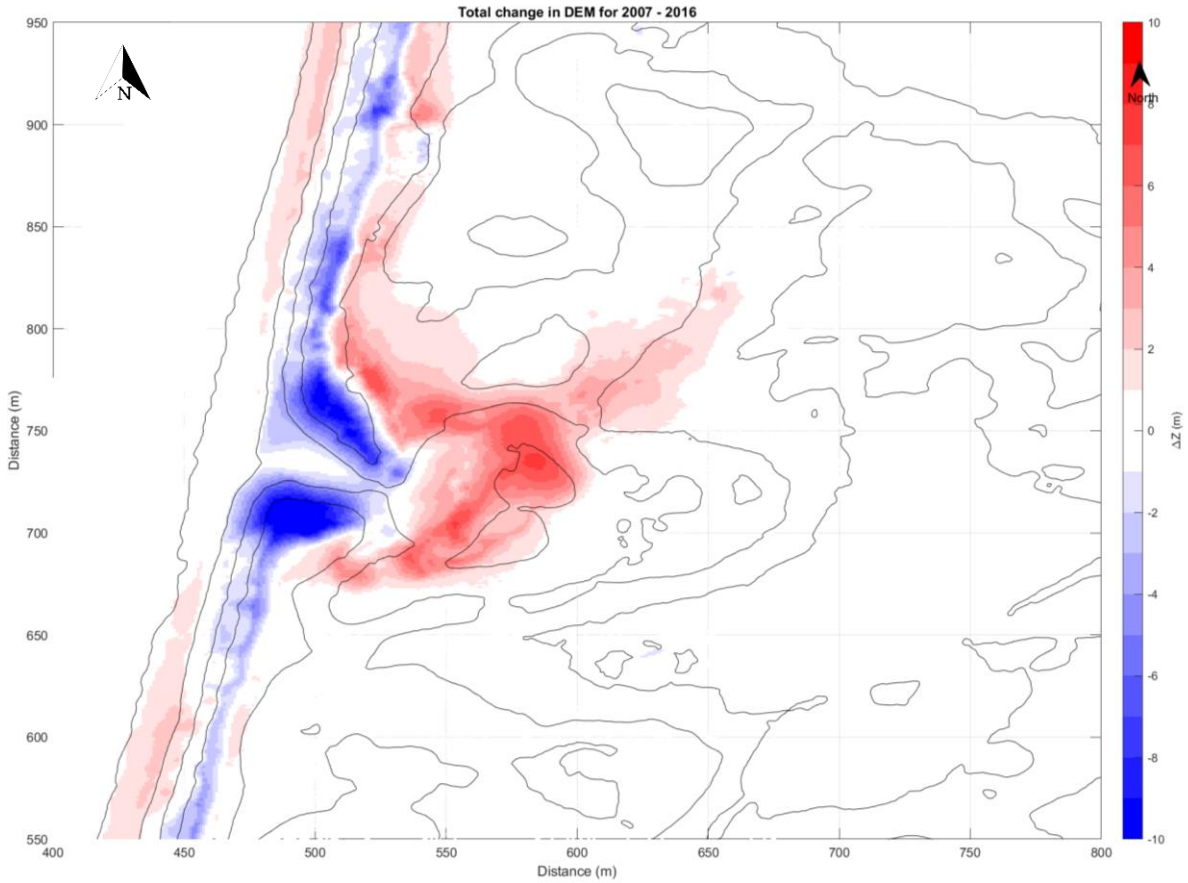

Figure 4-12 - Change in elevation (ΔZ), scaling from -10m (blue) to +10m (red) for the period of 2007 to 2016 near Heemskerk. A larger version of this map is added to the appendix (page 89).

4.1.1. Alongshore profiles: Heemskerk

The blowout entrance width (Figure 4-13B) expands over time: the blowout walls move from respectively y=702 (south) and y=765 (north) in 2007 to y=691 and y=780 in 2016. Which means the entrance width increases with 26m, from 63m to 89m, over the whole period. Both profiles are located in the blowout area to show the annual change in elevation within the blowout. The depth of the blowout entrance (Figure 4-13B; x500) decreases until 2009 and increases again between 2011 and 2016, but it has change a lot between these years; the elevation increased ca. 2 m to 8.2m above MSL in 2009 and 2011 and then decreased again to its original level around 6,5 m above MSL from 2011 to 2016. Further in the blowout, in the deflation basin (Figure 4-13C), a change in elevation occurs: it deepens in 2009; from 6.4 to 5.3 m above MSL in the lowest point (around x=735 for both alongshore profiles). After, the elevation rises to approximately 9.1 m above MSL. The elevation of the walls (and crests) in the blowout (Figure 4-13C) increase to 15m (south) and 14.9m (north) above MSL. The alongshore profiles near Heemskerk are presented in Figure 4-13.

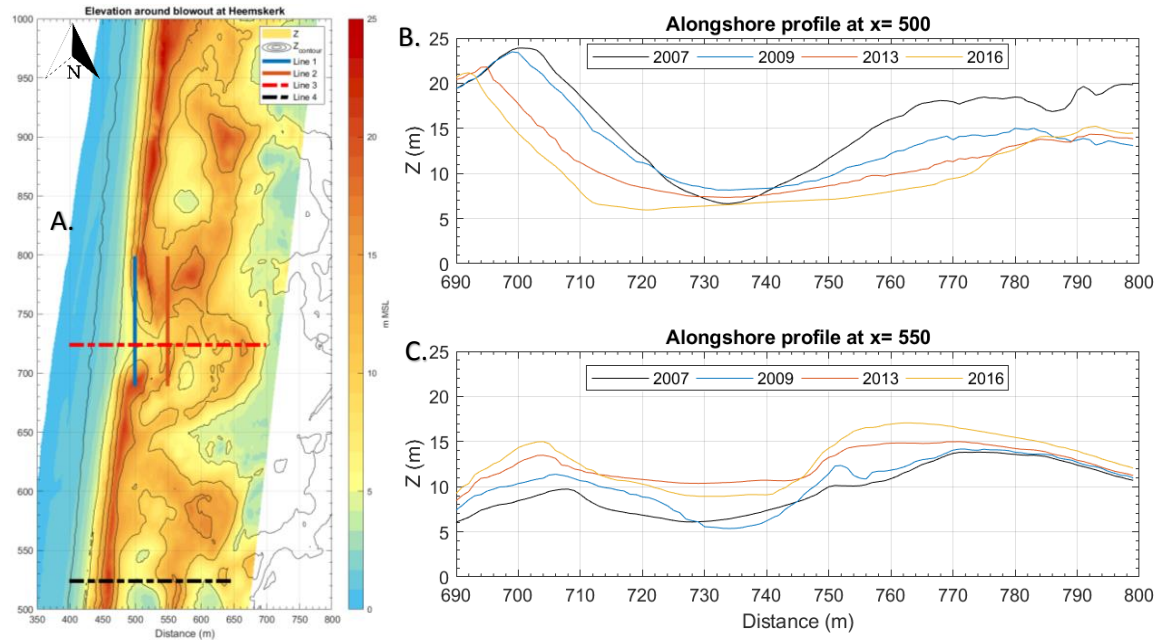

Figure 4-13 - Alongshore profiles of Heemskerk at x=500(B; blowout opening) and x=550(C; trough). Larger version in appendix at page 90. The North Sea is located on the left.

4.1.2. Cross-shore: Heemskerk

The reference dune moved seaward, as the dune crest moves from y=459 to y=456. The dune at the blowout location (Figure 4-14B) shows a lot more movement. The initial dune crest at y=487 disappeared over time, as the blowout was present. The sand moved landward into the valley behind the first dune row, which was filled up almost completely in 2016. The presence of the blowout does not seem to influence the dune area further than y=612, as the elevation profile here remained similar over time. The cross-shore evolution of the blowout near Heemskerk is shown in Figure 4-14. Figure 4-14A. depicts a reference dune location to compare the blowout development with.

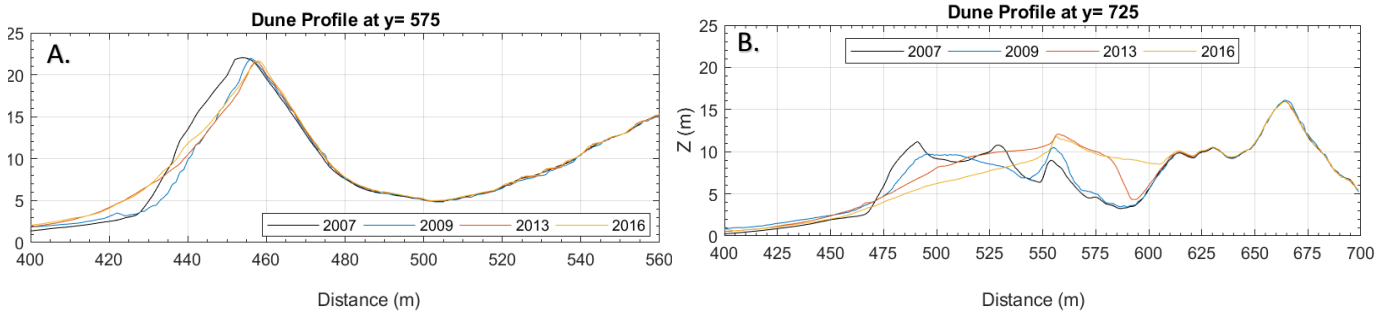

Figure 4-14 - Cross-shore profiles at y=575 (A; reference dune) and 725 (B; blowout) at Heemskerk. The exact locations are presented in Figure 4-3. Larger version is added to the appendix (page 90). The North Sea is located on the left.

4.1.3. Annual dune and blowout volume

The annual dune volume within the areas near Heemskerk is shown in Figure 4-15. The bar plot indicates that the dune volume in all regions stayed relatively similar. On average the dune volume decreased by 4% (2.459 m^3) over the period of 2007-2016. The volume inside de blowout area decreased by 7% from 5,97*10^4 m^3 to 5,53*10^4 m^3 in 2016. The dune valley behind the blowouts increases in volume over time; an accretion of 54% is measured (3.02*10^4 m^3 in 2007 to 4.66*10^4 m^3 in 2016). The annual change of volume in de ROIs near Heemskerk (Figure 4-17 and Figure 4-11) is high initially in 2007-2008: 3.663 m^3/year on average for all locations. After that it decreases and stays more stable around 1.200 m^3/year for all locations.

The blowout is most active in the first year, as the change in volume inside the blowout is the largest here (7.668 m^3/year). The annual volume change in the blowout decreases after 2007-2008. However, in front of the blowout (Blowout front) and behind the blowout (Valley), there is still a lot of sand transport; the blowout front increases in volume with 1.881 m^3/year on average. Whereas the valley

behind the blowout fills up as sand is transported towards it through the blowout. The valley's sand volume increases with 1826 m^3/year on average and the total change from 2007-2016 is an accretion of 1,64*10^4 $m^3$of sand. Both reference dunes (north and south) show a high initial erosion of sand, 6.953 m^3/year and 971 m^3/year. This indicates that the initial erosion levels are not only present in the blowout, but also in other locations around it.

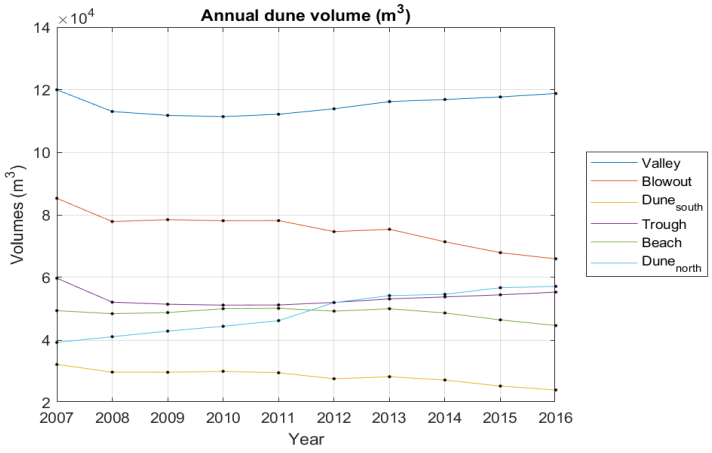

Figure 4-15 - Annual dune volume (m^3) at the locations of Heemskerk. An overview of the locations is shown in Figure 3-7.

Figure 4-16 - Annual change of volume within the blowout related ROIs: blowout, Trough, blowout front and valley behind.

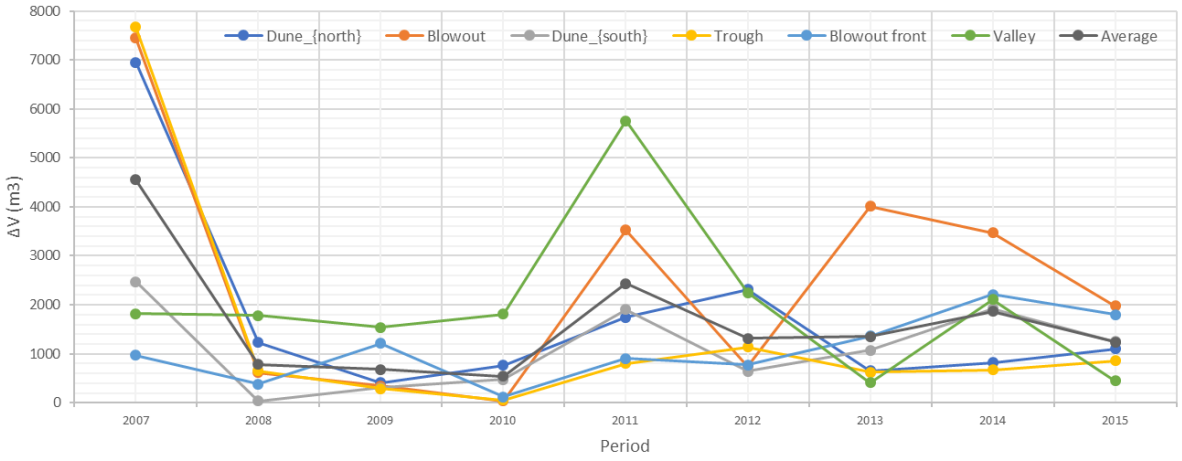

Figure 4-17 – Absolut annual change of dune volume (m^3) at the locations of Heemskerk. An overview of locations is shown in Figure 3-7. The dashed line represents the average change in volume of all mentioned locations.

Beach and hinterland

The volume change of the beach (beach) and hinterland (landward dune system) around the blowout near Heemskerk are also closely examined (Figure 4-18). The area of the beach is 1 ha. The hinterland area is 4 ha. The beach increases from 2,64*10^4 m^3 with 22% to 3,03*10^4 m^3. The beach of this blowout undergoes more dramatic changes than the same area on Terschelling; the average change is 12% with extremes in 2007-2008, 2008-2009 and 2011-2012 of respectively -3,38*10^3 m^3(-13%), +7,69*10^3

m^3(+33%) and-4,71*$10^3 m^3$ (-13%). Within the hinterland, the change is a lot less. The overall volume increases from 2007 (3,87*$10^5 m^3$), with 7% or 2,72*10^4 m^3 to 4,14*10^4 m^3 in 2016. The average annual change is 1% or 3.392 m^3. Therefore, the hinterland seems stable, compared with the large amounts of change in the beach. The peaks in change occur in 2012-2013 and 2014-2015: +6,18*10^3 m^3 or 2% and +6,99*10^3 m^3 or 2%.

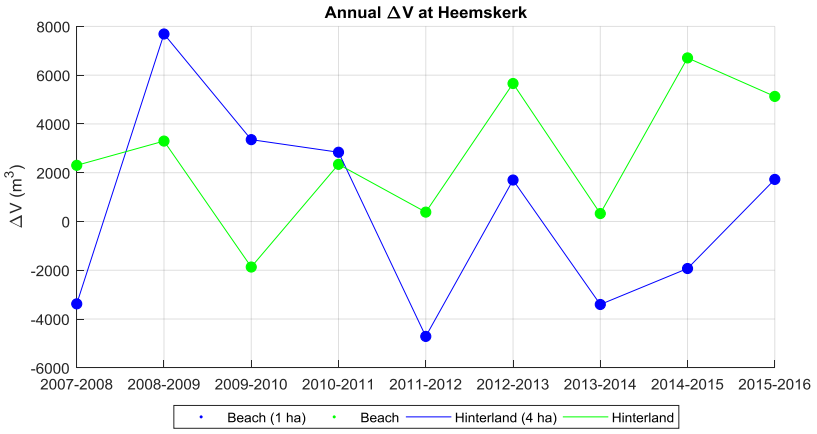

Figure 4-18 - Volumetric change in front of/behind the blowout in Heemskerk. The exact areas can be found in Figure 0-7.

4.2. Vegetation of Terschelling

4.2.1. Annual variation of NDVI

Overall, the NDVI in the blowouts decreased; more bare soil appeared within the blowout regions (Figure 4-19). The red areas indicate the decrease in NDVI and therefore the decrease in vegetation. The blowouts grew into/over these areas over time. Figure 4-19 shows the annual change of vegetation (NDVI) over the period of 1997-2016. This was calculated from the average NDVI per year and within the ROIs There was no satellite imagery available of the year 1998, hence the absence of data/maps. The 0,2-contour of 1997 was added as reference, this represents the dune foot. This is the boundary of vegetation in the first year. The image clearly shows the decrease of NDVI (relative to the NDVI of 1996), thus presence of vegetation, landward of this boundary. Indication an increase of sand covered area and therefor the growth of the blowout area since 1997. The annual change was also mapped and is added to the appendix (page 100). The average NDVI was also determined for four regions of interest (ROIs): the whole blowout area, left blowout area (x=420 - x=700), right blowout area (x=800 - x=1100) and a vegetated area landward of the blowouts (reference area). The result of this analysis is shown in Figure 4-21. A threshold NDVI of 0,2 (NDVI of bare ground) is added to the scatter plot to give an indication of the presence of vegetation. The two blowout areas clearly show that most soil is bare (sand) within the ROI, as the average NDVI is always in/around 0,2. The NDVI values of 2003 and 2011 are relatively low, this is caused by faulty satellite imagery. The annual NDVI maps are added to the appendix for more details (page 93).

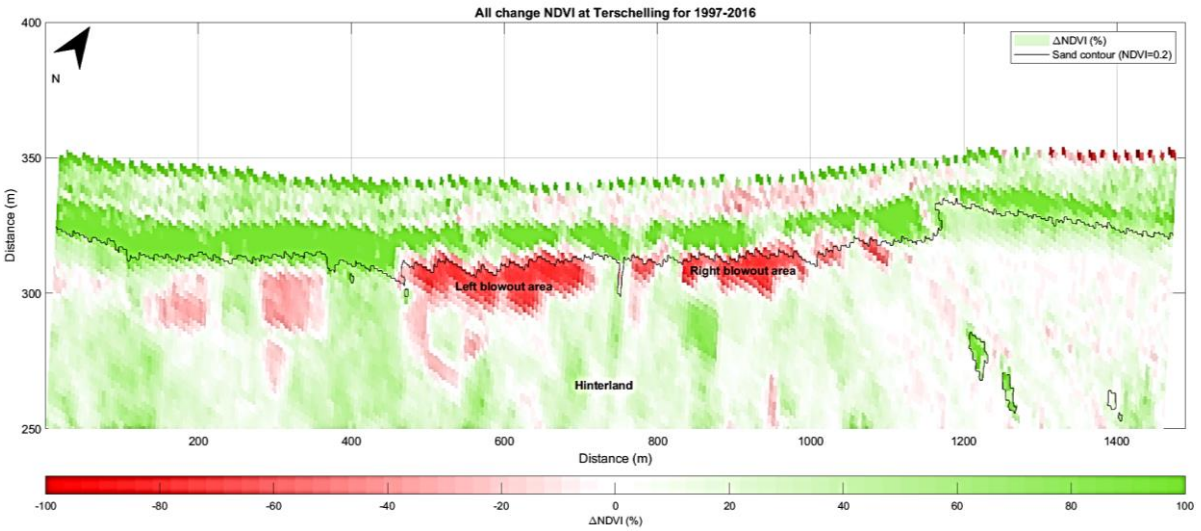

Figure 4-19 - Change in NDVI (%) between 1997 and 2016 at the dune area on Terschelling.

4.2.2. Soil coverage in the ROIs

The growth of the blowouts is monitored by determining the percentage of coverage of the ROIs with bare soil. The distinction is made between three areas: blowout area (whole area from bp 16 to 22) and left/right blowout areas. This distinction is made to compare both sites to each other and the average of the combined ROIs. Using the previously mentioned threshold NDVI score of 0,2. Figure 4-20 shows the coverage rates of sands within the ROIs on Terschelling (the exact locations and sizes of the ROIs are visible on the map in the appendix). The graph shows a total increase of bare soil within the ROIs between 1997-2016: 13% in the both blowout areas; 11% in the left blowout area and 19% in the right blowout area. The maximum coverage with sand is reached in 2003: left blowout 79%, right blowout 83%, whole area 85% and 8% in the reference area. The least amount of coverage of sand appeared in 1997, respectively: 61% (blowout), 53% (left blowout), 60% (right blowout) and no bare soil in the landward area (Ref. Area). The reference area only appears to have a noticeable bare soil in the years 2001(0,3%) and 2002 (8%).

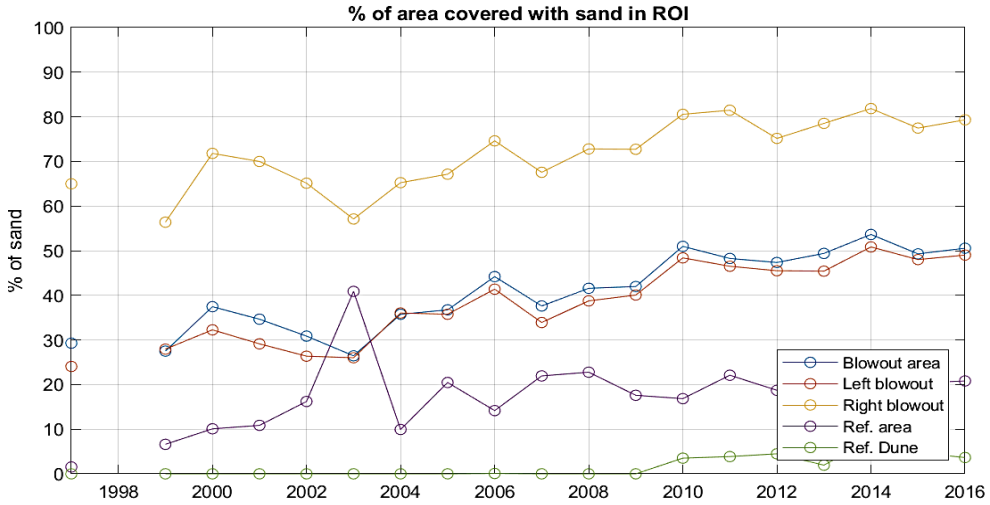

Figure 4-20 - Percentage of area within ROIs covered with sand on Terschelling. ROIs are visible on map on page 92.

The annual change in coverage can be an indication of the amount of dynamicness of a blowout area. Average annual change in coverage is: 4% (for the whole area), 5% (for each blowout areas) and 0,9% for the hinterland. The absolute annual change is higher in the initial years of monitoring than the last years (2011-2016): 3.6% versus 1,3% for the blowout areas. The amount of bare soil decreases heavily in the years 2003-2004, respectively: -14%, -20%, -18% and -8% (Figure 4-20).

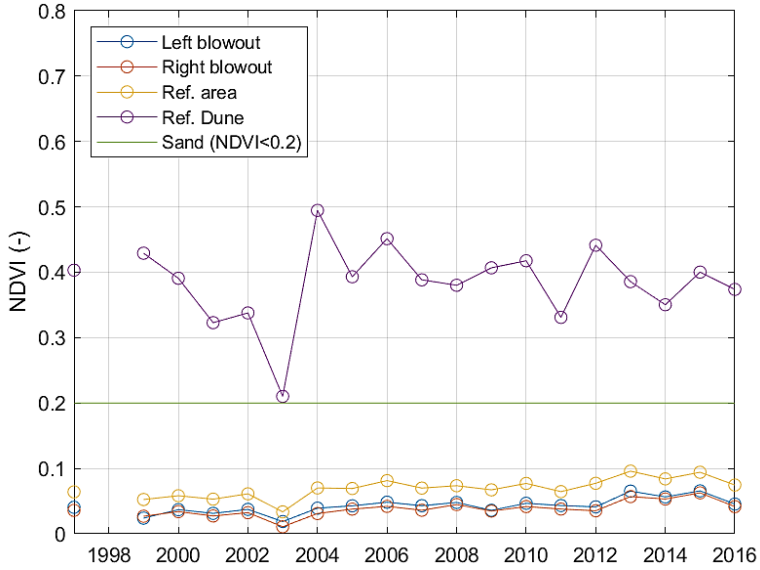

Figure 4-21 - Average NDVI within ROIs for Terschelling. Exact locations of ROIs are presented in map on page 92.

4.2.3. Seasonal change in NDVI

Figure 4-22). The reference dune areas have an NDVI of 0,15, whereas the blowouts have an average NDVI of 0,08 and 0,09, indicating the absence of vegetation here. More interesting is the seasonality of NDVI within the different locations. All areas show some form of seasonality, even the beach area. Which should be stable as it should be covered with sand all year long. The difference between the reference dunes and the blowout areas is present on all datapoints but is largest is summer: the reference dunes have a higher NDVI of respectively 0,11 (left) and 0,09 (right) than the blowout areas in the months May, June, July and August. Whereas the difference in NDVI winter is only +0,03 on average.

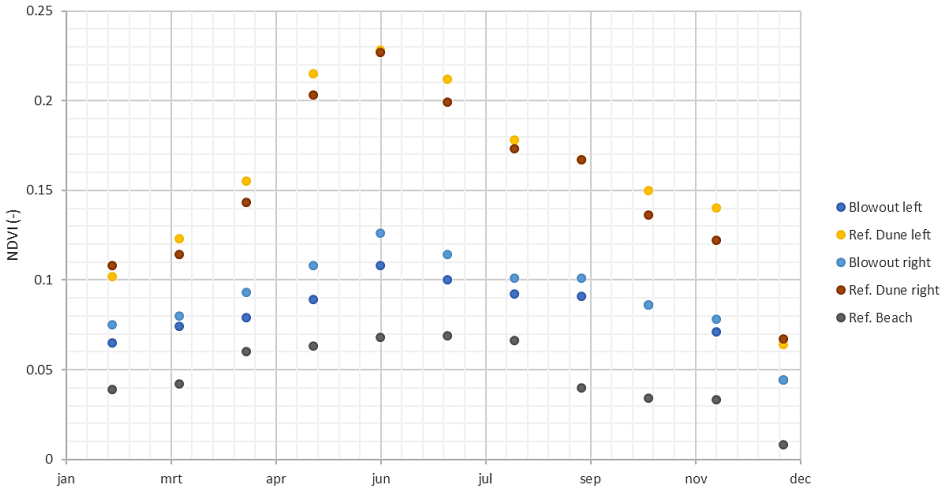

Figure 4-22 - DOY of the blowout area on Terschelling (1997-2016).

A decrease in average NDVI of the blowout are of Terschelling can be found from the seasonal behaviour of vegetation (Figure 4-23). Initially, there is a large decrease in overall NDVI score (1994-1999 vs 2000-2010), but the period 2011-2018 actually shows an increase of 0.06 (0.28 on average) versus the original situation. Figure 4-23 shows the trends in seasonal behaviour of the whole blowout area on Terschelling. The spikiness of the 1994-1999 is caused by a lack of data/images, these were filtered out in previous steps.

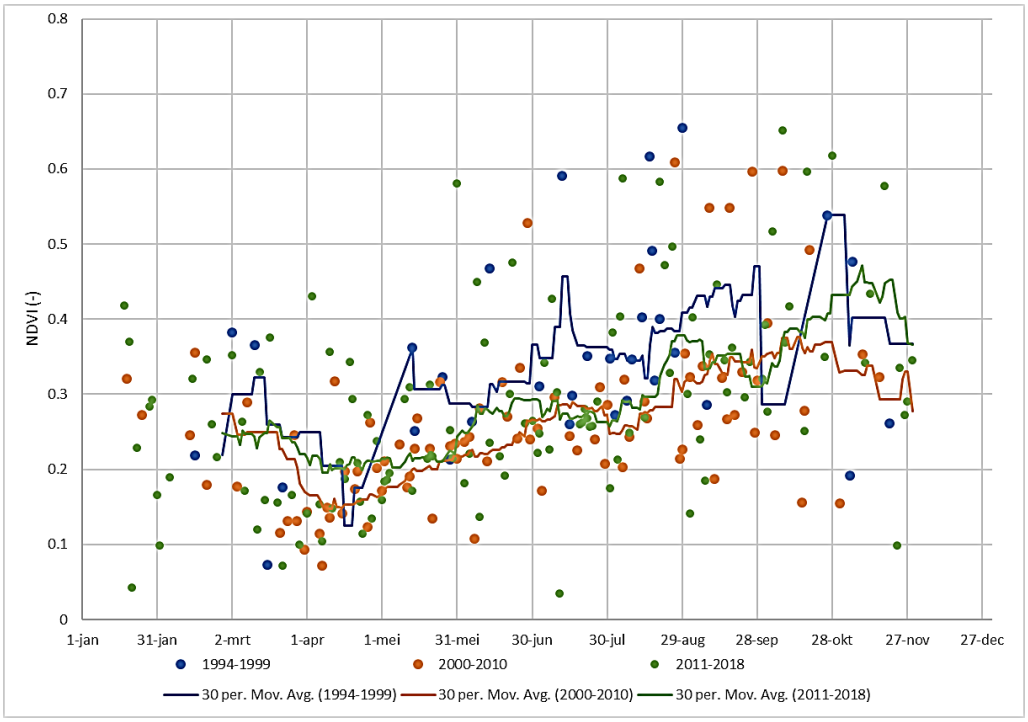

Figure 4-23 - Seasonal behaviour of the research location at Terschelling.

Table 4-1 - Seasonality of NDVI of Terschelling: whole area on the left, blowout on the right.

	All Areas				*Blowout*		
	1994-1999	2000-2010	2011-2018		1994-1999	2000-2010	2011-2018
Min	-0.09	0.07	-0.09	**Min**	-0.10	0.03	0.03
Max	0.66	0.65	0.75	**Max**	0.62	0.18	0.41
Average	0.34	0.26	0.28	**Average**	0.20	0.08	0.10

4.3. Vegetation of Heemskerk

4.3.1. Annual variation of NDVI

he average NDVI of the areas is consistent with the mentioned threshold values (Table 3-5): 0,26 for the blowout; 0,44 for the lobe; 0,54 for the reference dune; 0,08 for the beach and 0,52 for the ROI in the hinterland. Interestingly, the blowout and the lobe regions show the largest decrease rate of NDVI. This indicated the increase of bare soil in the regions and therefore the growth of the blowout. The average NDVI of the blowout lobe is similar to the reference dune up until 2013. The difference increases from 0.06 to 0.14. This is consistent with aerial photography, as the lobe formation only present after 2013 (Figure 4-25). Figure 4-24 shows decreasing trends for the NDVI value of all regions, except the beach, which is stable. The calculation of NDVI for Landsat imagery of Heemskerk resulted in the annual NDVI chart presented in Figure 4-24. The average NDVI for each pixel (within each ROI) and per year was calculated in GEE and exported for further analysis. T

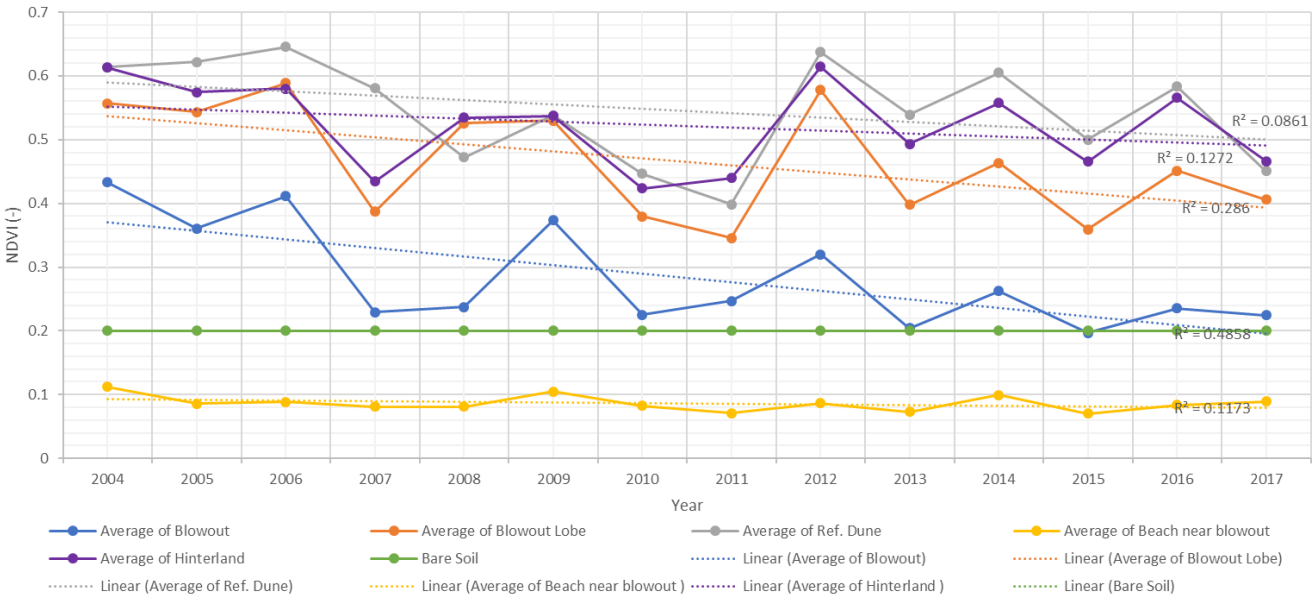

Figure 4-24 - Annual NDVI of the ROIs for 2004-2017 near Heemskerk, including trendlines and their R^2 value.

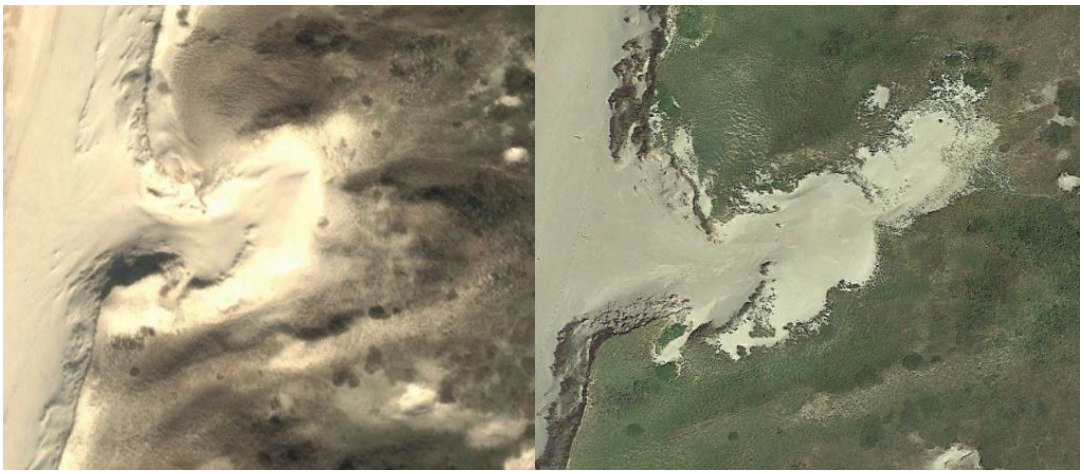

Figure 4-25 - Aerial photography of the blowout near Heemskerk from 23-3-2012 and 30-6-2015 (Google, 2018).

4.3.2. Soil coverage in the ROIs

The average coverage for the blowout area is 25%, with peaks in 2007, 2010, 2011 and 2015-2017. The coverage is largest in 2017 (37%). The annual soil coverage of the regions is shown in Figure 4-26. The coverage was only determined for the blowout. As the pixel size was too coarse to distinct the blowout from the lobe behind. Also, the NDVI value of bare soil appeared to be higher in this area, around 0.3.

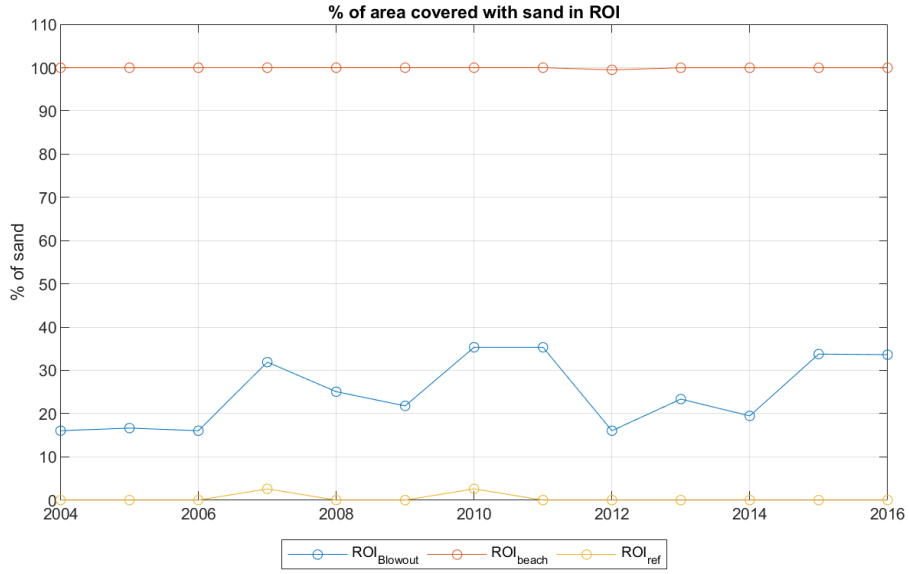

Figure 4-26 - Annual averaged soil cover of the ROIs near Heemskerk. The locations of the ROIs are added to the map in the appendix (page 106).

4.3.3. Seasonal change in NDVI

The difference in NDVI between the blowout and the reference dune is larger in spring/summer (0.2 vs 0.4). The beach area does not show seasonality as has almost a constant value throughout the year. The other ROIs show the same trend: a higher NDVI value in spring/summer and a lower NDVI value in autumn/winter. The difference between the blowout and reference dune indicates that there is a lot more vegetation present in the reference dune in the summer than in winter periods. The NDVI of the lobe is, again, lower than the NDVI of the reference areas. This is caused by the overall decrease in NDVI within the research period. Figure 4-27 shows the monthly averaged NDVI values of the ROIs.

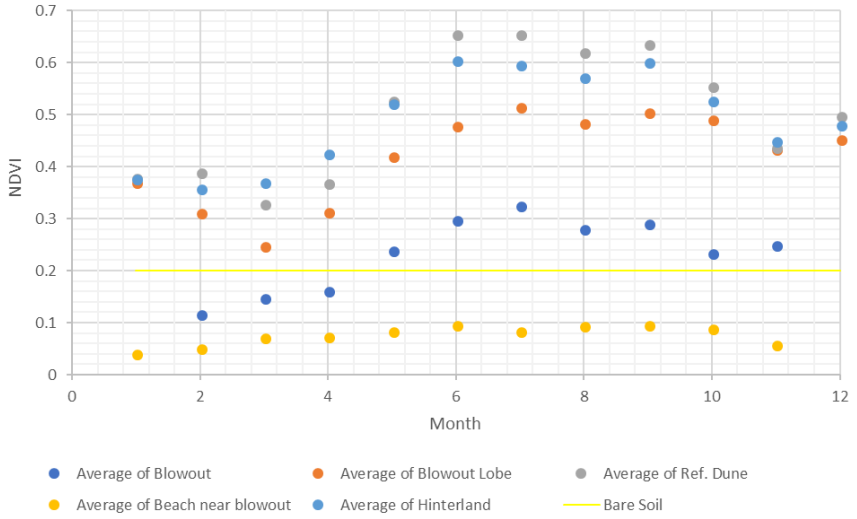

Figure 4-27 - Monthly averaged NDVI (2004-2018) of the ROIs near Heemskerk, with the bare soil threshold in yellow (NDVI=0,2).

Change in seasonality over time

The seasonal signal of NDVI in the blowout area decreased over time (Table 4-2 and Figure 4-28). The moving average (30 days) shows that NDVI decreased in spring/summer between the periods 2004-2008 and 2014-2018, proving that vegetation decreased/disappeared over the years. This can also be concluded from the average NDVI (Table 4-2). The amount of days where the NDVI succeeds the threshold of vegetation (NDVI = 0.3) also decrease: from 76% to 55%.

Table 4-2 - Change in seasonal behaviour of NDVI in the blowout near Heemskerk.

	2004-2008	2009-2013	2014-2018
Min	0.09	0.07	0.09
Max	0.56	0.44	0.46
Average	0.29	0.23	0.21
NDVI>0.3 (%)	76%	63%	55%

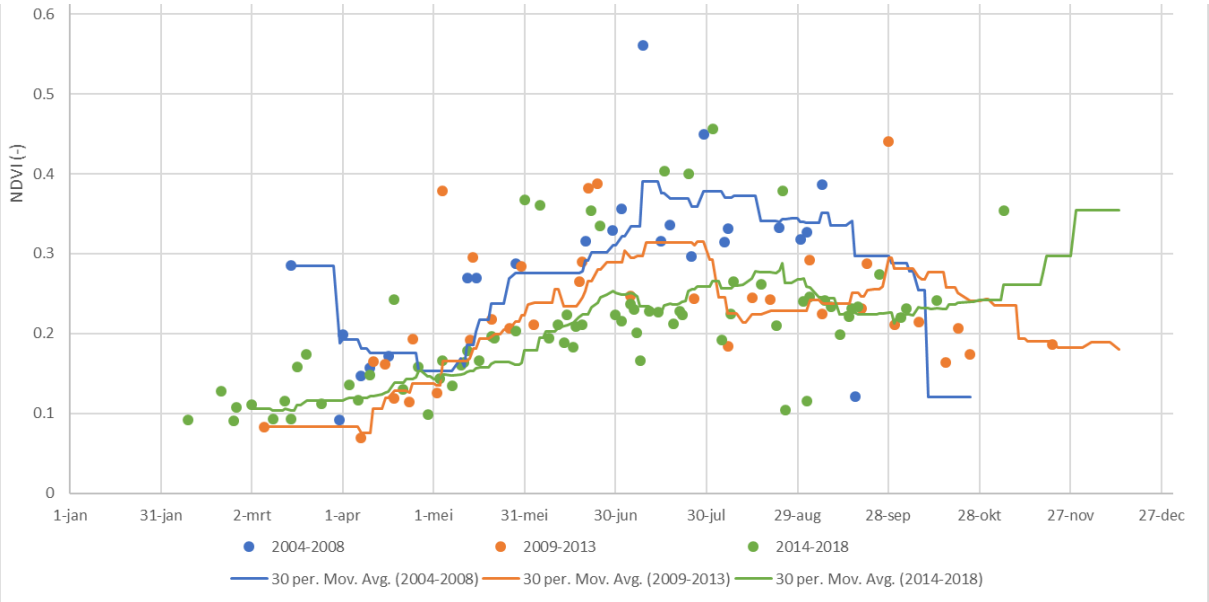

Figure 4-28 – Change in seasonal behaviour of the inner-blowout area near Heemskerk

4.4. Sentinel NDVI imagery

The resolution of imagery produced by the Landsat satellite missions proved to be very coarse for the research area near Heemskerk. The area has a size of approximately 50.000 m^2, whereas the pixel resolution is 30m x 30m (or 900 m^2), resulting in around 55 pixels within the blowout area. The blowout area could not be determined precisely enough from these coarse images, as Figure 4-29 shows. Therefore, another satellite mission was also used to analyse the annual change of NDVI; the Sentinel 2. Sentinel 2 imagery is produced by the European Space Agency (ESA). This satellite has much higher resolution (up to 10m x 10m), but contains a lot less data: imagery is from the period Jun 23, 2015 - Jul 19, 2018 (ESA, 2018). Only the data 2015 and 2016 were used for NDVI calculation since the used LIDAR elevation data only overlaps with these two years.

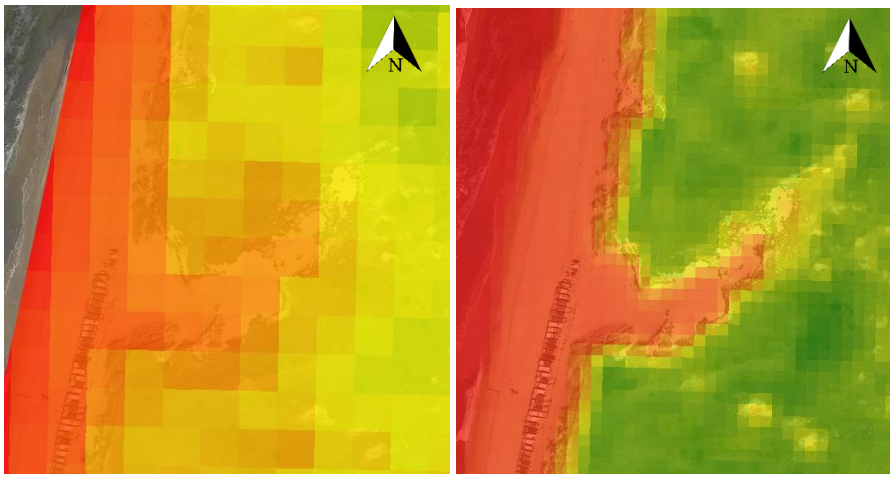

Figure 4-29 – Average NDVI of 2016 made with Landsat imagery (left) and Sentinel imagery (right) of the blowout near Heemskerk. The resolution of Landsat proved to be too coarse for further calculations (Google, 2018).

4.4.1. Annual variation of NDVI

The relative change of NDVI between 2015 and 2016 is displayed in Figure 4-30. The 0,2-contour of NDVI is plotted for reference. The map shows a decrease in NDVI north of the blowout and a small increase on/around the southern border of the blowout. This indicates that the blowout is progressing northward, as vegetation starting to grow in the southern area of the blowout. The average NDVI within the blowout decreases with almost 30% from 0,36 to 0,28. Indicating the decrease of vegetation presence within the blowout.

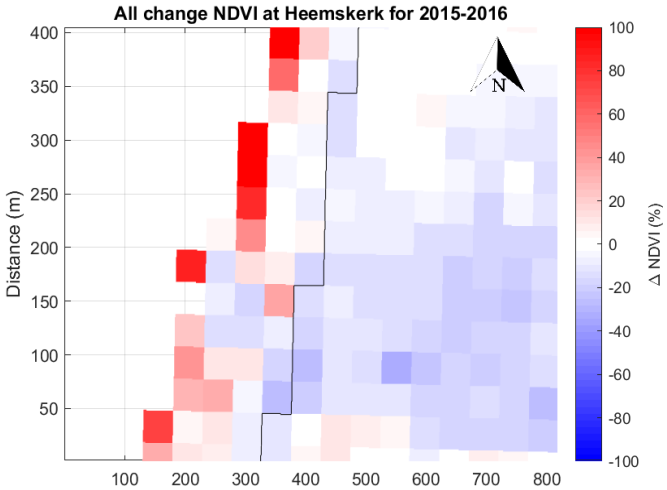

Figure 4-30 – Relative change of NDVI at Heemskerk between 2015-2016.

4.4.2. Soil coverage of dune area

The soil coverage is also calculated for this location. This was done within the ROIs, as defined in the map in the appendix (page 106). The soil coverage turned out to be mostly vegetation within the ROI,

as the average soil coverage of bare soil (NDVI<0,2) were 22,7% (2015) and 30,5% (2016) within the blowout. Again, an increase in bare soil is indicated by these percentages; the blowout seems to have grown between 2015 and 2016.

4.4.3. Seasonal change in NDVI

The blowout and the reference dune show a similar trend in seasonal NDVI: the value is low during winter (December to March); increases during spring (April to June) and peaks in July and August. The similarity between the two regions can be linked to the coarse imagery, which makes it hard to calculated NDVI for distinct areas. The blowout starts with a lower NDVI in winter, but as vegetation grows, the NDVI is like the nearby reference area. Figure 4-31 shows the result of a Day-Of-Year analysis: the average NDVI for each day of the year was calculated for the period of 2015-2016 using the Sentinel imagery. This was done for three regions: beach, the blowout and a similar sized reference dune area north of the blowout. The beach area does not show seasonality, which is logical as it only consists out of bare soil or occasionally, water (NDVI<0) if an image was made during a period of high water. The difference between the two area is relatively small: 0,03 during spring and -0,01 during summer.

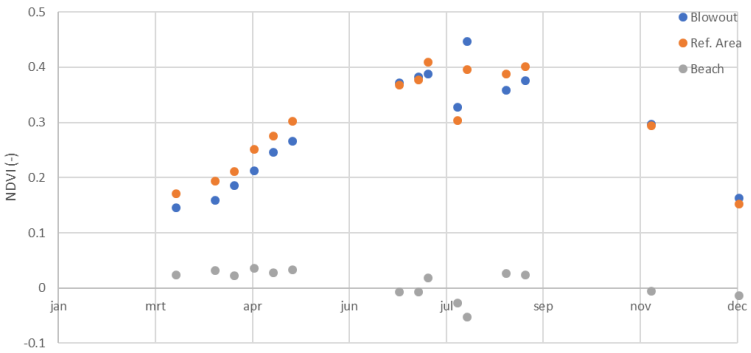

Figure 4-31 - Monthly NDVI of the blowout area near Heemskerk.

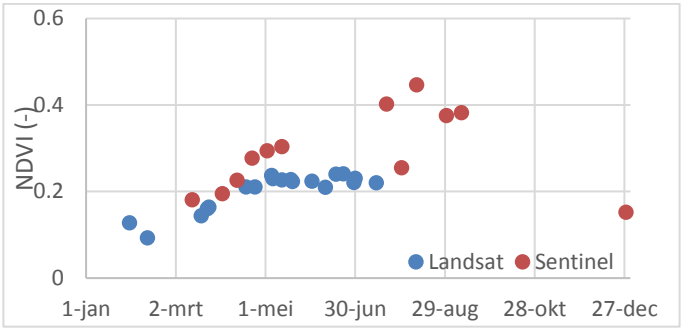

Figure 4-32 Differences between Landsat and Sentinel imagery in seasonal behaviour of the vegetation near Heemskerk.

Data from the Sentinel mission gives more detailed information on, for example, seasonal behaviour of vegetation (Figure 4-32). For 2016, the Sentinel mission provides 12 data points (or images), whereas the Landsat mission provides 19 pictures. But the extra detail from the Sentinel images (Figure 4-29) will give a better representation of the situation, with more and higher NDVI scores in the summer period. In the summer, the NDVI of the Landsat images remains around 0.25 (no vegetations/sand) because there are limited pixels present, which are averaged over the whole dune area, resulting in a similar NDVI score throughout the summer.

4.5. Combination of NDVI and LIDAR for Terschelling

Three types of interaction were found to be present in the dunes of Terschelling between the vegetation and the accretion/erosion of sand. First, the presence of vegetation causes sedimentation of the sand that is transported to the secondary row of dunes.

Sediment piles up seaward of vegetated areas (NDVI >0.2), see Figure 4-33. An increase in dune elevation is also measured in areas with lower NDVI scores (0>NDVI<0.2). This could be related to the fact that the NDVI imagery is averaged over a year. It could be possible that these areas were vegetated during some parts of the year, or that there was only very small vegetation present, which the satellite did not capture. As chapter 4.4 describes, the NDVI imagery of Heemskerk is to coarse for indept analysis. Therefore, only the data of Terschelling was analysed further by overlaying data of vegetation (NDVI) and change in elevation (LIDAR).

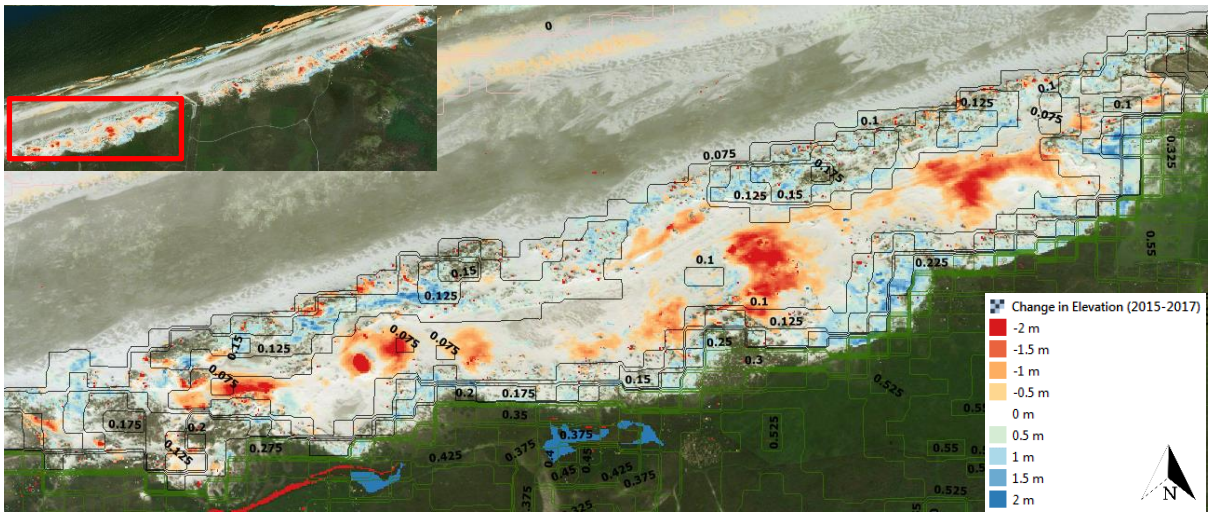

Figure 4-34 - A map of combination of change in elevation (LIDAR 2015-2017) and NDVI contours (2015) for the left blowout area of Terschelling.

The second type of interaction is with areas of high erosion rates (>1m/year), here NDVI seems to decrease (red circles in Figure 4-33). The NDVI decreases (vegetation disappears) in these locations after a year of erosion, making it less suitable for deposition the next year and more likely to become more eroded. The vegetation responds to the increase in elevation; if sediment is deposited in areas with vegetation, the NDVI will be lower in the next year (vegetation disappears). Figure 4-33 shows that vegetated areas (around red arrow), will decrease in size (contour lines disappear and areas with lower NDVI grow). This could be related to the fact that vegetation gets buried under deposited sand.

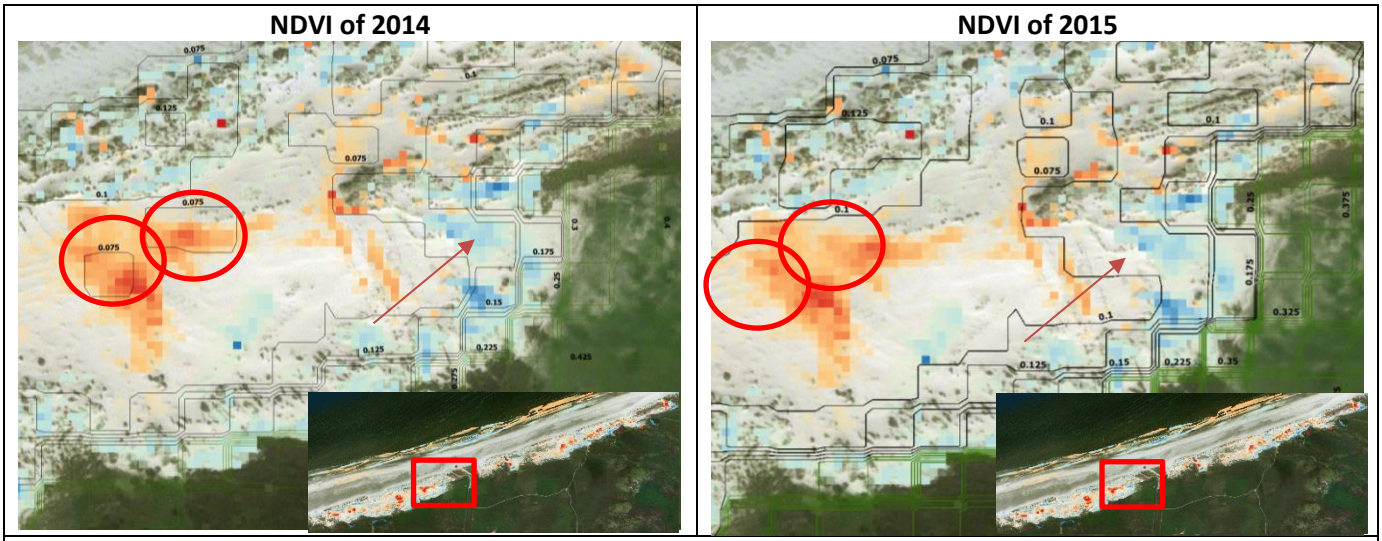

Figure 4-33 – Terschelling: Change in elevation (2014-2015) and NDVI (left;2014 and right;2015). The red circles depict locations where erosion took place and vegetation disapeared (NDVI decreased). The area around the arow shows the decrease in vegeation from deposition

5. Discussion

During this research data has been analysed to gain insight in the development of morphology and vegetation in and around blowouts in similar periods at two locations along the Dutch coast. Specifically after the change in coastal management to a more dynamic system (Arens et al., 2013; MIN V&W, 1990; Van der Valk et al., 2013). The restoration measures, in this case creating and developing blowouts seem to have a large impact on the development of the dune areas researched.

First of all, the blowout locations seem to be most active in the years after their initiation. This was found by analysing annual sets of airborne LIDAR elevation data have been analysed with alongshore profiles, cross-shore profiles and volume changes has been determined for regions in/around the blowouts. These analyses showed that the blowouts are most active, right after their initiation.

In the blowouts on Terschelling for example, the annual change of volume in the first five years, after the notches were dug, is five times higher than the annual change in the last five years of data (2010-2015). This does not happen within the blowout of Heemskerk. Here the range of annual change in volume is smaller, except for 2007: it ranges between +750 (2012) and $-7*10^3$ m^3 (2007). But this could also be linked to the fact that the data does not cover the full development. The blowout is visible on Google Earth images since 1997, but the used LIDAR data covers elevation since 2007. The initiation of blowouts led to a growth of the depositional love by 19% or $1{,}09*10^3$ m^3 for Terschelling. which directly increases the flood protection of Terschelling. In Heemskerk the hinterland volume also increases, but less, by 7%. Here most of the sand got trapped in the blowout itself; the blowout filled up with sediment, as the volume of the ROI called valley increased by 54%, compared to 7% increase in the hinterland. For Heemskerk the sediment seems to get trapped within the blowout itself and less material reaches the hinterland. As the profiles, alongshore and cross-shore, of the blowouts flattened, a steady state was reached for the blowouts in both Terschelling and Heemskerk. Decreasing sand transport within the blowout. For Heemskerk however, this does not decrease the throughput to the hinterland, as this area keeps growing in the later years after initiation. This is a difference with the blowout area in Terschelling, here the throughput decreases after 10 years. This can also be linked to the formation of an embryo dune in front of the blowout and the increase in crest height behind it in that period, blocking sand transport further into the system.

The vegetation has been analysed through a locally calculated vegetation index (NDVI) from Landsat satellite imagery of the same periods. First of all, the presence and size of (larger) blowout areas (Terschelling) can be determined well using satellite imagery (Figure 4-19). Especially the change in NDVI over longer time periods, such as decades, are great for locating. For Terschelling, the growth of the blowout areas over time was shown well in the NDVI imagery. As the average NDVI decreased within the blowout region and therefore, the amount of bare soil increased, which then increased sand transport, as the threshold transport velocity decreases.

The increase of bare soil, especially in Terschelling, seems to be in sync with the annual change in volume. In general, the coverage with bare soil (NDVI<0,2) is larger in the years after initiation. The amount of bare soil decreases over time, as the blowout reaches its steady state (Figure 4-20). The fact that transport decreases, increases the chance for vegetation to occur. Therefore, it seems that vegetation and sand transport are cooperating mechanisms. In Heemskerk however, there seems to be a lag in this mechanism. The change in volume is high, if the previous year had more coverage with bare soil. Behind the blowout, in the hinterland, the average NDVI increased. This could be linked to the fact that the increased sediment transport of blowouts can mitigate the loss of biodiversity (Ruessink et al., 2018) .

In terms of seasonality, all ROI's of Terschelling show similar trends in monthly NDVI values as reference dunes and the hinterland. There is a difference between blowouts and reference locations in NDVI throughout the year, but this difference is larger in spring/summer. This is an indication that vegetation is less likely to grow (and bloom) inside blowouts and blowout areas. During the development of blowouts, the seasonality of the NDVI signal remains, but the overall NDVI decreases (Figure 4-23 and Figure 4-28). Later in the lifespan of the blowout on Terschelling, the average annual NDVI increases, as reaches its steady state and starts to overgrow. This could not be measured in Heemskerk as the blowout there is still active. A side note to this analysis is that there was not enough imagery to plot a full year of seasonality; the images in fall/winter were heavily influenced by clouds and were filtered out beforehand, leaving gaps in the analysis of these periods.

When comparing the blowouts between the research locations, there is a difference in development of the areas. The research location on Terschelling, with artificial blowouts, show high values of erosion/deposition (sand transport) in the initial years after the trenches in the dunes were made. Average erosion rate of -10.000m3/year for the first 5 years, after there is a balance between erosion and accretion; trend is around 0m3/year (Figure 4-9). Whereas the blowout area of Heemskerk shows similar annual values in erosion/accretion; between +4000m3/year and -4000m3/year (Figure 4-16). This is related to the form of the blowouts; the artificial blowouts have steeper walls (Figure 4-3 and Figure 4-4), which will collapse more easily, making them vulnerable for erosion.

5.1. Research limitations

Limitations of this research are present the satellite imagery and its analysis. In terms of vegetation, the Landsat satellite imagery is not accurate enough to precisely analyse smaller areas, such as single blowouts. The use of higher resolution imagery, for example drone images, can give more insight in development of vegetation these smaller regions. However, this will limit the spatial band, as such imagery is only present from more recent periods. Another limitation is the fact that LIDAR elevation data was not available for every year within the blowout development period, such as for Terschelling where 2003 and 2004 where combined for example.

The goal of the filtering of the satellite imagery was to be able to work with cloud-free images. Visual inspection of the used satellite imagery in GEE reveals that clouds are still present after filtering; these interfere with the NDVI calculations. Unfortunately, it was not possible to remove these images manually and were used in further analyses, resulting in a lower average NDVI index per region in some areas. These results were removed manually in Excel. After filtering, the calculated NDVI values are under influence by two factors the change of angle of the sun and/or the growth of small vegetation (e.g. initiation of embryo dunes). The day of year analysis results a similar signal when displayed over time (see Figure 4-22 and Figure 4-27). Both figures prove that all ROI's have a form of seasonality; high NDVI in spring/summer and low NDVI in fall/winter. Even the beach (bare soil) area shows this signal. The analysis of vegetation could be extended with pixel by pixel comparison of elevation and vegetation data. This could give more examples of the interaction between plants and sand transport, for now only visual inspection has been done by overlaying images.

6. Conclusion

The foredune restoration measures taken in the dunes of Terschelling and Heemskerk, seem to have benefited the coastal protection by the dunes. As the average elevation and total dune volume of these areas, especially behind the blowouts, has increased since the decision was taken to implement dynamic coastal management. In the case of Terschelling, it even increased dune volume both seaward and landward of the initial blowout region. The measured growth of the dune system implicates that blowouts could be used often to increase coastal protection in sandy coast areas.

In terms of vegetation, the satellite images reveal that plants disappear inside blowout areas. For Terschelling, the NDVI decreased inside these areas to the value of bare soil (NDVI<0.2), which is also visible on aerial photography. The same occurred at Heemskerk, where a lobe formed behind the blowout and covered vegetation, as the accretion rate here was higher than the growth rate of the dune plants. The ecology has benefited as the NDVI of the hinterland areas increased over the years. In Terschelling for example, the average NDVI of the areas landward of the blowouts has increased, indicating the growth of more vegetation and an increase in biodiversity. Therefore, blowouts could be used to increase vegetation/biodiversity in coastal regions.

For both locations, the satellite imagery was divided in three periods and a close look to the changes in the seasonality of dune vegetation revealed that initially average NDVI decreases, but in later cycles this increases again (Figure 4-23 and Figure 4-28). However, the seasonal signal remains, as NDVI is high in spring/summer and lower in fall/winter.

Vegetation is large factor in the deposition of sand, the combination of satellite imagery and elevation data showed this; sand erodes from areas without vegetation and is deposited in front/seaward of vegetated areas. On the other side, NDVI decreases if sand is deposited, as the plants are covered by sand. Making the area more susceptible to erosion in following years, as they help controlling the sand transport and the amount of dynamicness of the dunes. In future research, the role of vegetation in dune development should always be taken into consideration. The presence of vegetation could be steered to control the erosion/accretion to, for example, stop landward growth of dune areas.

The dune areas of Heemskerk and Terschelling show differences in the development of the blowouts, as the annual change in elevation is much higher for Terschelling than Heemskerk. This is related to the steep shape of blowouts on Terschelling, whereas Heemskerk has less steep blowout walls. However, examples of these blowout types should be compared in future research, to find more possible differences and similarities. If artificial blowout will be implemented, it is important to keep in mind that these high initial erosion levels occur and will influence the surrounding foredunes.

Recommendations

More accurate imagery could be used for the analysis of vegetation in dune areas. The use of aerial photography is already common, but the use of more precise satellite imagery (Sentinel missions) could give more insight throughout the year. For instance, to research seasonal behaviour of coastal areas and/or blowouts. In this research, there was not enough good-quality imagery to analyse the NDVIs seasonal signal for each year. With new technology, or even manual selection of images (which will be very time consuming), more images could be used to make a more precise analysis of the seasonal behaviour of vegetation in blowout areas.

Further analysing overlaying data of vegetation and elevation maps in GIS-software could provide more insight in the influence of each development on each other. Only a brief comparison was made in this thesis, but annual overlap of data could provide more insight in the relation between blowout morphology and vegetation. For example, by overlaying a classified vegetation map with the contours of annual change in elevation. The overlap of these areas could explain the interworking of these mechanisms. For this, a classification of types of dune vegetation should be made, based on NDVI values.

For Heemskerk, the timeline of Lidar data could be expended. Google Earth imagery reveals that the blowout has been present since 1997 (and maybe even longer). Currently, the elevation data only covers the period from 2006 to 2016.

Bibliography

Literature

Alterra. (2017). Beschermde natuur in Nederland: Noordhollands Duinreservaat. Retrieved 29 November 2018, from https://www.synbiosys.alterra.nl/natura2000/gebiedendatabase.aspx?subj=n2k&groep=2&id=n2k87

Arens, S. M. (2007). *Naar een natuurlijke zee-land overgang op Oost-Ameland. Advies voor het stimuleren van doorstuiving.*

Arens, S. M., Geelen, L., Van der Hagen, H., & Slings, R. (2012). Is zandaanvoer door de zeereep de sleutel tot succes ? *Landschap : Tijdschrift Voor Landschapsecologie En Milieukunde*, 131–139.

Arens, S. M., Loffler, M. A. M., & Nuijen, E. M. (2006). Evaluatie dynamisch kustbeheer Friese Waddeneilanden.

Arens, S. M., Mulder, J. P. M., Slings, Q. L., Geelen, L. H. W. T., & Damsma, P. (2013). Dynamic dune management, integrating objectives of nature development and coastal safety: Examples from the Netherlands. *Geomorphology*, *199*, 205–213. https://doi.org/10.1016/j.geomorph.2012.10.034

Arens, S. M., & Overdiep, T. (2008). Vijftien jaar dynamisch zeereepbeheer op de Waddeneilanden. *Duin*, *31*(3/4).

Barchyn, T. E., & Hugenholtz, C. H. (2013). Reactivation of supply-limited dune fields from blowouts: A conceptual framework for state characterization. *Geomorphology*, *201*, 172–182. https://doi.org/10.1016/j.geomorph.2013.06.019

Barsi, J., Lee, K., Kvaran, G., Markham, B., & Pedelty, J. (2014). The Spectral Response of the Landsat-8 Operational Land Imager. *Remote Sensing*, *6*(12), 10232–10251. https://doi.org/10.3390/rs61010232

Bauer, B. O., & Davidson-Arnott, R. G. D. (2003). A general framework for modeling sediment supply to coastal dunes including wind angle, beach geometry, and fetch effects. *Geomorphology*, *49*(1), 89–108. https://doi.org/10.1016/S0169-555X(02)00165-4

Bauer, B. O., Davidson-Arnott, R. G. D., Hesp, P. A., Namikas, S. L., Ollerhead, J., & Walker, I. J. (2009). Aeolian sediment transport on a beach: Surface moisture, wind fetch, and mean transport. *Geomorphology*, *105*(1–2), 106–116. https://doi.org/10.1016/j.geomorph.2008.02.016

Bennet, J., & Halls, J. (1980). Wind and sediment movement in coastal dune areas. *Coastal Engineering*, *17*.

Byrne, M. L. (1997). Seasonal sand transport through a trough blowout at Pinery Provincial Park, Ontario. *Canadian Journal of Earth Sciences*, *34*, 1460–1466. https://doi.org/10.1139/e17-118

Carter, R. W. G., Hesp, P. A., & Nordstrom, K. F. (1990). Erosional landforms in coastal dunes. In *Coastal Dunes: Form and Process* (pp. 217–249).

Crawford, R. M. M. (2009). *The biology of coastal sand dunes*. *Oxford Biology* (Vol. 104). Oxford. https://doi.org/10.1093/aob/mcp136

Damsma, T. (2009). Dune growth on natural and nourished beaches: 'A new perspective', (April), 83.

de Ruig, J. H. M. (1998). Coastline management in The Netherlands : human use versus natural dynamics. *Journal of Coastal Conservation*, *4*(1998), 127–134.

European Space Agency (ESA). (2018). Sentinel-2 description. Retrieved 23 July 2018, from https://sentinel.esa.int/web/sentinel/missions/sentinel-2

Fawcett, D., Leiterer, R., Heisig, H., Wulf, H., Kellenberger, T., & Joerg, P. C. (2017). *Google Earth Engine Guide*. Zürich. https://doi.org/10.13140/RG.2.2.34655.25763

Foga, S., Scaramuzza, P. L., Guo, S., Zhu, Z., Dilley, R. D., Beckmann, T., … Laue, B. (2017). Cloud detection algorithm comparison and validation for operational Landsat data products. *Remote Sensing of Environment*, *194*, 379–390. https://doi.org/10.1016/j.rse.2017.03.026

Gares, P. A., & Nordstrom, K. F. (1987). Dynamics of a Coastal Foredune Blowout at Island Beach State Park, NJ. In *Coastal Sediments 87. Proceeding of a Conference on Advances in Understanding Coastal Sediment Processes* (Vol. 87, pp. 213–221). New York: American Society of Civil Engineers.

Gares, P. A., & Nordstrom, K. F. (1995). A Cyclic Model of Foredune Blowout Evolution for a Leeward Coast: Island Beach, New Jersey. *Annals of the Association of American Geographers*, *85*(1), 1–

20. https://doi.org/10.1111/j.1467-8306.1995.tb01792.x
Google. (2018). Google Earth Engine. Retrieved 28 March 2018, from https://earthengine.google.com/
Hesp, P. A. (1996). Flow dynamics in a trough blowout. *Boundary-Layer Meteorology*, *77*, 305–330. https://doi.org/10.1007/BF00123530
Hesp, P. A. (2002). Foredunes and blowouts: initiation, geomorphology and dynamics. *Geomorphology*, *48*(1–3), 245–268. https://doi.org/10.1016/S0169-555X(02)00184-8
Hesp, P. A. (2011). Dune Coasts. In *Treatise on Estuarine and Coastal Science* (Vol. 3, pp. 193–221). Baton Rouge: Elsevier Inc. https://doi.org/10.1016/B978-0-12-374711-2.00310-7
Hesp, P. A., & Hyde, R. (1996). Flow dynamics and geomorphology of a trough blowout. *Sedimentology*, *43*(3), 505–525. https://doi.org/10.1046/j.1365-3091.1996.d01-22.x
Hesp, P. A., & Pringle, A. (2001). Wind flow and topographic steering within a trough blowout at Wind Flow and Topographic Steering within a Trough Blowout. *Journal of Coastal Research*, (March), 597–601.
Johnson, E. A., & Martin, Y. E. (2016). Coastal Dunes and Vegetation Dynamics. *A Biogeoscience Approach to Ecosystems*, 435–455.
Jungerius, P. D., & Schoonderbeek, D. (1992). The use of Leica Quantimet 970 for scanning blowout development on sequential air photos of the 'Dunes de Slack', NW France. *Catena Supplement*, *23*, 59–73.
Jungerius, P. D., & van der Meulen, F. (1989). The development of dune blowouts, as measured with erosion pins and sequential air photos. *CATENA*, *16*, 369–376.
Jungerius, P. D., Witter, 1 J.V., & Boxel, J. H. van. (1991). The effects of changing wind regimes on the development of blowouts in the coastal dunes of The Netherlands. *Landscape Ecology*, *6*(1/2), 41–48. https://doi.org/10.1007/BF00157743
Klemas, V. (2011). Remote Sensing Techniques for Studying Coastal Ecosystems: An Overview. *Journal of Coastal Research*, *27*(1), 2–17. https://doi.org/10.2112/JCOASTRES-D-10-00103.1
KNMI. (2018). Daggegevens van het weer in Nederland. Retrieved 4 July 2018, from https://www.knmi.nl/nederland-nu/klimatologie/daggegevens
Koningsveld, M. V., Otten, C. J., & Mulder, J. P. M. (2007). Dunes: the Netherlands Soft But Secure Sea Defences. *Westerndredging.Org*, 167–184. Retrieved from https://www.westerndredging.org/phocadownload/ConferencePresentations/2007_WODA_Florida/Session2B-BeneficialUsesofDredging/2 - van Koningsveld, et al - Dunes, The Netherland's Soft but Secure Sea Defences.pdf
Landsberg, H., & Riley, N. A. (1943). Wind influences on the transportation of sand over a Michigan sand dune. In *Proc. 2nd Hydraulics Conf. Bulletin, vol. 27. Univ. Iowa Studies in Engineering* (pp. 342–352).
Loffler, M. A. M., Goessen, P., Hoogstrate, T., & van der Valk, B. (2016a). Dynamisch kustbeheer - Kustveiligheid en natuur profiteren van stuivend zand. *Water Matters*, *2*(December 2016).
Loffler, M. A. M., Goessen, P., Hoogstrate, T., & van der Valk, B. (2016b). Dynamisch kustbeheer - Kustveiligheid en natuur profiteren van stuivend zand. *Water Matters*, *2*(December 2016). Retrieved from https://www.h2owaternetwerk.nl/images/12artikelimages/H2O-Online_1612-05_Dynamisch_kustbeheer_Löffler_etal.pdf
Loffler, M. A. M., van der Spek, A. F. . J., & van Gelder-Maas, C. (2011). *Mogelijkheden voor dynamisch kustbeheer: een handreiking voor beheerders*.
Mangor, K. (2018). Definitions of coastal terms. Retrieved 25 July 2018, from http://www.coastalwiki.org/wiki/Definitions_of_coastal_terms#cite_note-2
MathWorks. (2018). Interpolate 2-D or 3-D scattered data with griddata. Retrieved 25 July 2018, from https://nl.mathworks.com/help/matlab/ref/griddata.html
Ministerie van Infrastructuur en Milieu. (2017). Meer zand voor Heemskerk | Rijkswaterstaat. Retrieved 25 June 2018, from https://www.rijkswaterstaat.nl/over-ons/nieuws/nieuwsarchief/p2017/04/meer-zand-voor-heemskerk.aspx
Ministerie van Infrastructuur en Milieu, & STOWA. (2013). Terschelling - Terschelling - Morfodynamiek Slufter - Voorbeelden - >Dynamisch Kustbeheer. Retrieved 25 June 2018, from http://www.dynamischkustbeheer.nl/content/content.asp?menu=10630000_000000
Ministerie van Verkeer en Waterstaat. (1990). *Eerste Kustnota; Kustverdediging na 1990*.

Ministerie van Verkeer en Waterstaat. (2000). *Derde Kustnota; Traditie, Trends en Toekomst.*
Ministerie van Verkeer en Waterstaat. (2016). *De staat van ons water*.
Mulder, J. P. M., Hommes, S., & Horstman, E. M. (2011a). Implementation of coastal erosion management in the Netherlands. *Ocean and Coastal Management*, *54*(12), 888–897. https://doi.org/10.1016/j.ocecoaman.2011.06.009
Mulder, J. P. M., Hommes, S., & Horstman, E. M. (2011b). Implementation of coastal erosion management in the Netherlands. *Ocean and Coastal Management*, *54*(12), 888–897. https://doi.org/10.1016/j.ocecoaman.2011.06.009
Mulder, J. P. M., Nederbragt, G., Steetzel, H. J., van Koningsveld, M., & Wang, Z. B. (2007). Different implementation scenarios for the large scale coastal policy of the Netherlands. In *Coastal Engineering 2006* (pp. 1705–1717). World Scientific Publishing Company. https://doi.org/doi:10.1142/9789812709554_0144
NASA. (2009). *Landsat 7 Science Data User's Handbook*. *NASA*. Greenbelt, Maryland. Retrieved from http://glovis.usgs.gov/%0Ahttp://edcsns17.cr.usgs.gov/EarthExplorer/%0Ahttp://www.landcover.org/index.shtml%0Ahttp://landsathandbook.gsfc.nasa.gov/handbook/handbook_toc.html
Nickling, W., & Davidson-Arnott, R. (1990). Aeolian Sediment Transport on Beaches and Coastal Sand dunes. In *Conference: Conference: Canadian Symposium on Coastal Sand Dunes, Canadian Coastal*. Guelph, Ontario, Canada, Ontario, Canada: University of Guelph.
NJSGC. (2016). *Dune Ecology : Secondary Dunes and Beyond* (Vol. 1). New Jersey.
Nordstrom, K. F., & Arens, S. M. (1998). The role of human actions in evolution and management of foredunes in The Netherlands and New Jersey, USA. *Journal of Coastal Conservation*, *4*(2), 169–180. https://doi.org/10.1007/BF02806509
Ozkan, K., Mert, A., & Gülsoy, S. (2010). Monitoring of Wetlands by Using Multitemporal Landsat Data ; A Case Study from Fethiye – Turkey. In *Survival and Sustainability* (pp. 785–793). Berlin, Heidelberg: Springer Berlin Heidelberg. https://doi.org/10.1007/978-3-540-95991-5
Pluis, J. L. A. (1992). Relationships between deflation and near surface wind velocity in a coastal dune blowout. *Earth Surface Processes and Landforms1*, *17*(7), 663–673.
Pluis, J. L. A., & Winder, B. De. (1989). Spatial patterns in algae colonization of dune blowouts. *CATENA*, *16*, 499–506.
PWN. (2018). PWN: Water en Natuur. Retrieved 25 June 2018, from https://www.pwn.nl/
Rijkswaterstaat, & Staatsbosbeheer. (2014). Jarkus-hoogtemetingen, Rijkswaterstaat, 1997. De groene en rode lijn ten noorden van Oosterend geeft de ligging van de primaire kering aan.
Ruessink, B. G., Arens, S. M., Kuipers, M., & Donker, J. J. A. (2018). Coastal dune dynamics in response to excavated foredune notches. *Aeolian Research*, *31*, 3–17. https://doi.org/10.1016/j.aeolia.2017.07.002
Sidhu, N., Pebesma, E., & Câmaraa, G. (2018). Using Google Earth Engine to detect land cover change: Singapore as a use case. *EUROPEAN JOURNAL OF REMOTE SENSING*, *51*(1), 486–500. https://doi.org/10.1080/22797254.2018.1451782
USGS. (2015). *Algorithm Description Document*.
USGS. (2016). *Landsat 8 (L8) Data Users Handbook*. *USGS* (Vol. 2.0). Sioux Falls, South Dakota. https://doi.org/http://www.webcitation.org/6mu9r7riR
USGS. (2017). *Landsat Collection 1 Level 1 Product Definition - Version 1*. Sioux Falls, South Dakota. Retrieved from https://landsat.usgs.gov/sites/default/files/documents/LSDS-1656_Landsat_Level-1_Product_Collection_Definition.pdf
USGS. (2018a). Landsat 5 History | Landsat Missions. Retrieved 27 June 2018, from https://landsat.usgs.gov/landsat-5-history
USGS. (2018b). Landsat 7 | Landsat Missions. Retrieved 16 March 2018, from https://landsat.usgs.gov/landsat-7
van Boxel, J. H., Jungerius, P. D., Kieffer, N., & Hampele, N. (1997). Ecological effects of reactivation of artificially stabilized blowouts in coastal dunes. *Journal of Coastal Conservation*, *3*, 57–62.
van der Meulen, F., Kooijman, A. M., Veer, M. A. C., & Boxel, J. H. van. (1996). *Effectgerichte maatregelen tegen verzuring en eutrofiering in open droge duinen. Eindrapportage fase 1*. Amsterdam.
Van der Valk, B., Reinders, J., van der Spek, A. J. F., & van Gelder-Maas, C. (2013). *Voorbeelden van dynamisch kustbeheer. Een inventarisatie van dynamisch kustbheerprojecten langs de*

Nederlandse kust.
van Koningsveld, M., & Mulder, J. P. M. (2004). Sustainable Coastal Policy Developments in the Netherlands. A systematic Approach Revealed. *Journal of Coastal Research*, *20*(2), 375–385.
Weier, J., & Herring, D. (2000, August 30). Measuring Vegetation (NDVI & EVI). Retrieved 15 March 2018, from https://earthobservatory.nasa.gov/Features/MeasuringVegetation/

Datasets

Google Earth
Google Earth, (2017). Heemskerk, the Netherlands. Viewed on 25-06-2018.
Google Earth, (2017). Terschelling, the Netherlands. Viewed on 16-06-2018.

Landsat 5
Image Collection ID: LANDSAT/LM5_L1T
Provider: USGS
Tags: Landsat, USGS, l5, lm5, mss, radiance
Last modified: 2017-10-31 20:21:33 UTC

Landsat 7
Image Collection ID: LANDSAT/LE7_L1T
Provider: USGS
Tags: Landsat, USGS, l7, le7, etm, radiance
Last modified: 2018-01-18 19:53:56 UTC

Landsat 8
Image Collection ID: LANDSAT/LC8_L1T
Provider: USGS
Tags: Landsat, USGS, l8, le8, etm, radiance
Last modified: 2018-03-21 12:33:01 UTC

LIDAR elevation data
Provider: Utrecht University, Department of Physical Geography
Locations: Heemskerk and Terschelling, the Netherlands
Resolution: 5x5, 2x2 and 1x1 (from 2006)

Appendix

Examples of change in dune morphology on Terschelling

Measurements from 1997 with the initial cuts in the foredune (top) and 2013 (bottom)

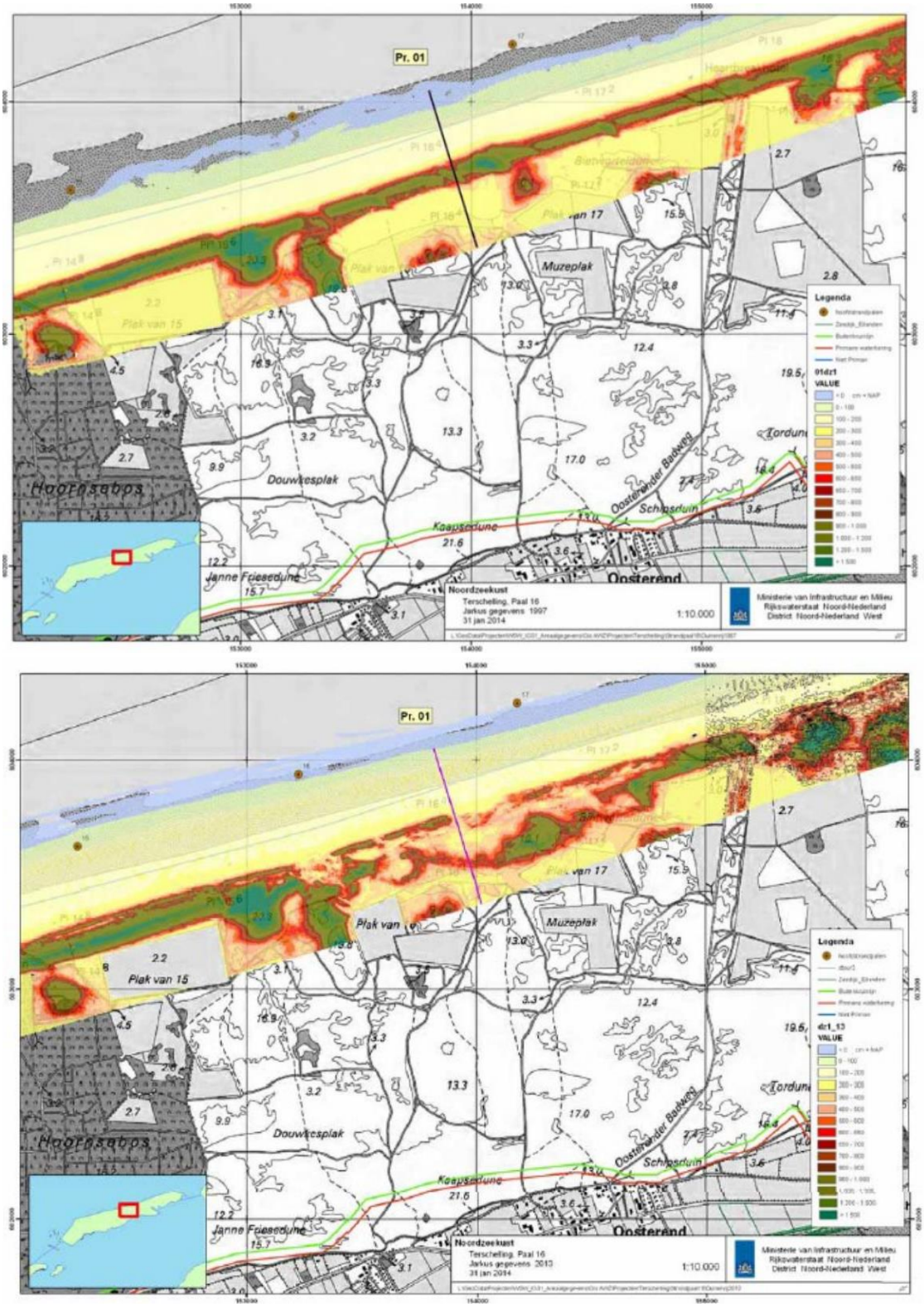

GEE initiation and data filtering

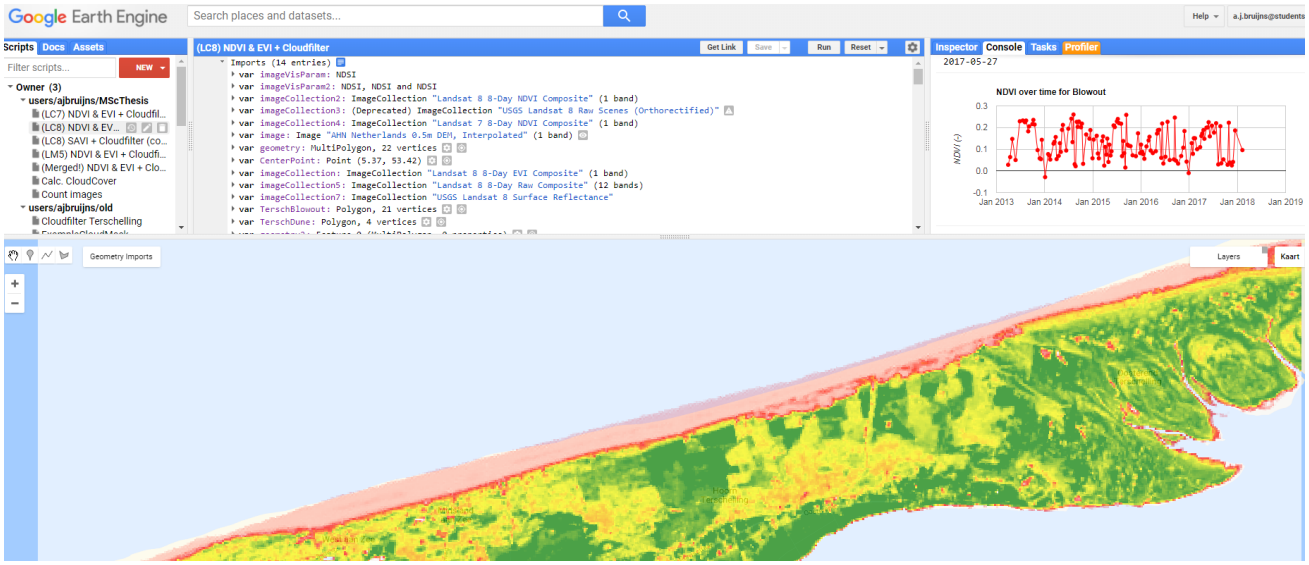

Figure 0-1 – GEE (https://code.earthengine.google.com/): the calculation of NDVI on Terschelling with JavaScript and visualising results with maps and charts (Google, 2018).

Step 1: Pre-processing data - Importing and filtering satellite imagery

Image collections of Landsat 5, 7 and 8 are imported into the script and can be filtered directly based on a start and an end date (Figure 3-17). In this case this will be from **1994-01-01 to 2018-02-01.** The end date is set different for the imagery of the LM5 mission, as these images are less accurate (paragraph 3.2.3). They will be excluded be importing them separately with an end date of **1998-01-01**, the start of the next (successful) mission Landsat 7. Therefore, Heemskerk will only include imagery from Landsat 7 and 8.

```
// Dates of intrest
  var start = ee.Date('1994-01-01');
    var startH = ee.Date('2004-01-01');
  var finish = ee. Date('2018-02-01');
  var finish_lm5 = ee. Date('1998-01-01');

    var LC7_Heemskerk = ee.ImageCollection("LANDSAT/LE07/C01/T1_SR")
  .filterBounds(Heemskerk)
  .filterDate(startH,finish)
    .map(maskClouds);

    var LC8_Heemskerk = ee.ImageCollection("LANDSAT/LC08/C01/T1_SR")
  .filterBounds(Heemskerk)
  .filterDate(startH,finish)
    .map(maskClouds);

  // Terschelling
      var LM5_Terschelling = ee.ImageCollection("LANDSAT/LT05/C01/T1_SR")
    .filterBounds(Terschelling)
    .filterDate(start,finish_lm5)
    .map(maskClouds);

  var LC7_Terschelling = ee.ImageCollection("LANDSAT/LE07/C01/T1_SR")
  .filterBounds(Terschelling)
  .filterDate(start,finish)
  .map(maskClouds);

  var LC8_Terschelling = ee.ImageCollection("LANDSAT/LC08/C01/T1_SR")
  .filterBounds(Terschelling)
  .filterDate(start,finish)
  .map(maskClouds);
```

Table 0-1 - Number of Landsat of images used.

	Heemskerk	Terschelling
Landsat 5	0	46
Landsat 7	299	279
Landsat 8	199	119

Figure 0-2 - Importing an image collection and filtering based on dates and cloud score.

The data is also filtered based on cloud cover by USGS (Figure 3-17). The clouded pixels where masked and removed from every image using an algorithm called CFMask (Foga et al., 2017; USGS, 2015). USGS filtered the data for clouds, cloud shadows and snow based on the entire Landsat imagery. These pixels are classified in the 'pixel_qa' band of every dataset. Each image will be checked for pixels classified as clouds and cloud shadows, these will be removed (set to NaN), while the rest of the pixels will be used in further calculations. This means that all images within the given time period and that fall within the set boundary will be used in further analysis, increasing the amount of data (Table 0-1). However, not all specified ROIs will contain data in each image and the number of pixels within them will vary per image. The cloud mask code is added to the appendix (page 65). The regions were defined by polygons drawn of the regions of interest; the blowout areas on Heemskerk and Terschelling.

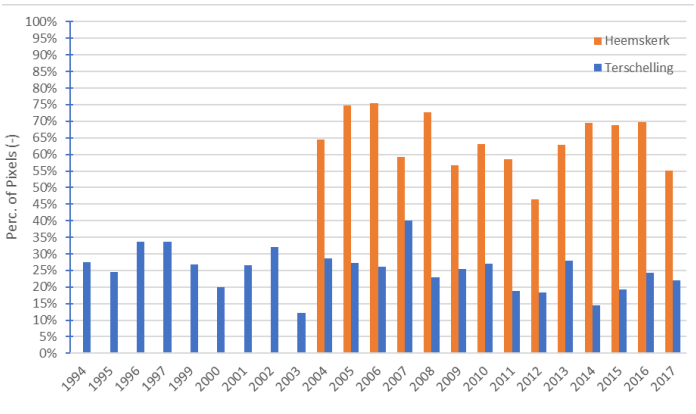

Figure 0-3 - The percentage of pixels, averaged per year, used after masking clouds and cloud shadows.

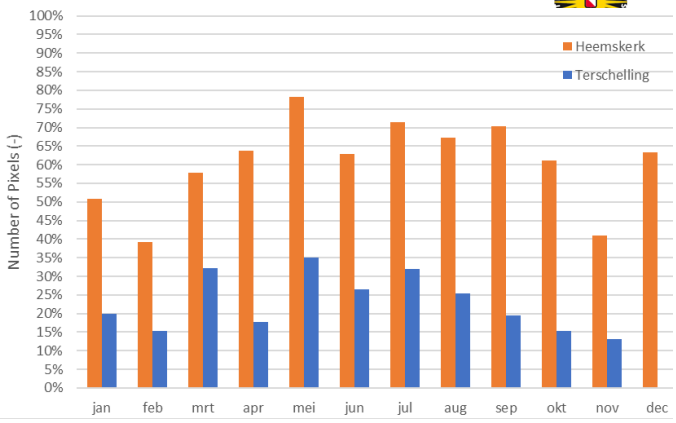

Figure 0-4 - Percentage of cover averaged per month

Figure 0-3 shows the percentage of pixels within the regions of Heemskerk and Terschelling that were left after masking clouds and cloud shadows. of images per cloud cover per season is added to the appendix for further information. The percentage of cover is considerably higher in Heemskerk, as it has a smaller area: $7{,}03*10^4$ m^2 vs $3{,}84*10^3$ m^2. For Terschelling 2003 was a really clouded year, there is not a lot of data present. The ROIs used for this analysis are added to the appendix (page 67). The cloud cover also varies within each year. Generally, there is more cover in spring and summer periods, as they are less cloudy periods. This has to be considered when analysing seasonality within the ROIs.

Step 2: Calculating NDVI

The second step in the GEE process is calculating the NDVI index for each image and both research locations. This is done by using the NDVI-equation (Equation 3-1) and de code displayed Figure 3-19. The band names differ for LM5 and LC7 (NIR is B4 and RED is B3) to those of LC8 (NIR is B5 and RED is B4).

```
//--set function for Landsat 5 bands
  var calcNDVI_LM5 = function(image) {
  var result = image.normalizedDifference(["B4","B3"]).rename("ndvi")
  return image.addBands(result);}

  //set funtion for Landsat 7 Bands
  var calcNDVI_LC7 = function(image) {
  var result = image.normalizedDifference(["B4","B3"]).rename("ndvi")
  return image.addBands(result);}

//set funtion for Landsat 8 Bands
  var calcNDVI_LC8 = function(image) {
  var result = image.normalizedDifference(["B5","B4"]).rename("ndvi")
  return image.addBands(result);}
```

Figure 0-5 - Calculation of NDVI in GEE and an example of the result: NDVI index for Terschelling for 13-05-2000

After calculations, a new band is added to each image, containing the NDVI index per pixel, resulting in images such as in Figure 3-19. The NDVI-bands of LM5, LC7 and LC8 were merged into one image collection to create one continuous dataset for the whole research period, which is needed for the time series analysis in step 3. All other bands (colours, NIR, etc.) were removed to decrease the size of the dataset for exportation of the images. The NDVI can be displayed in GEE separately (per satellite image) and as the merged collection.

Number of images per cloud cover/per season

Heemskerk

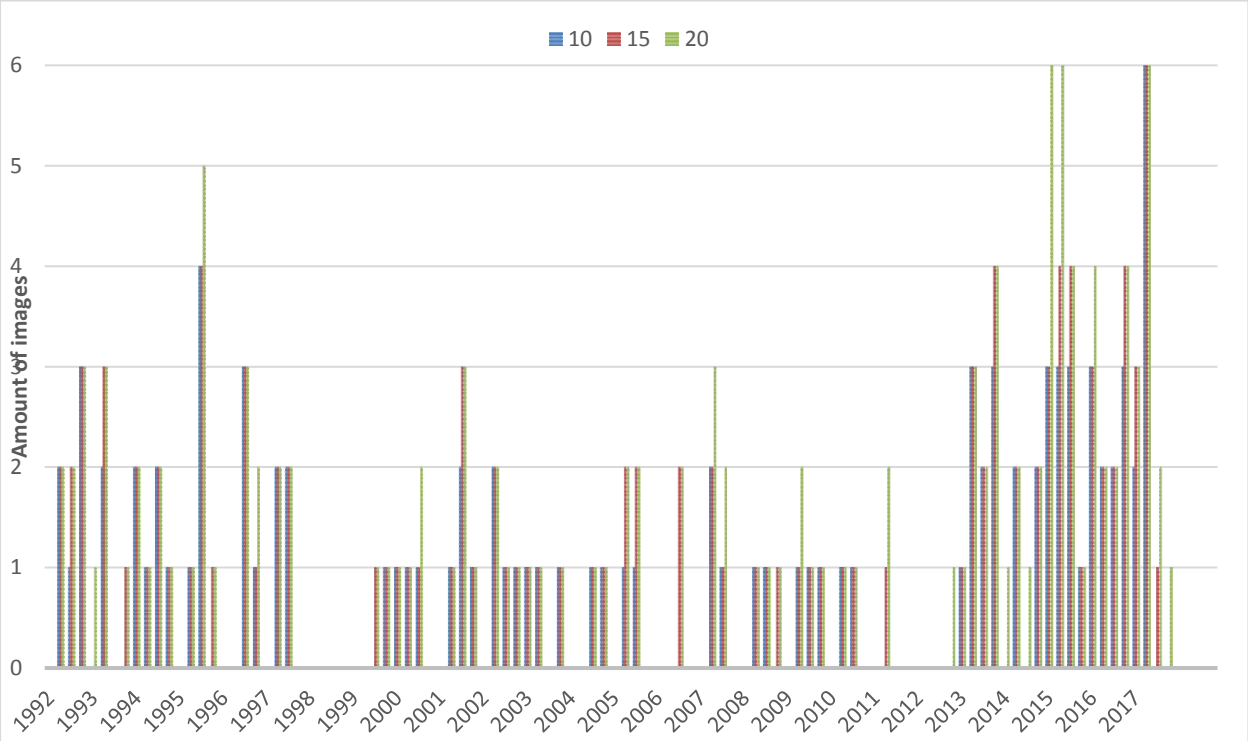

Terschelling

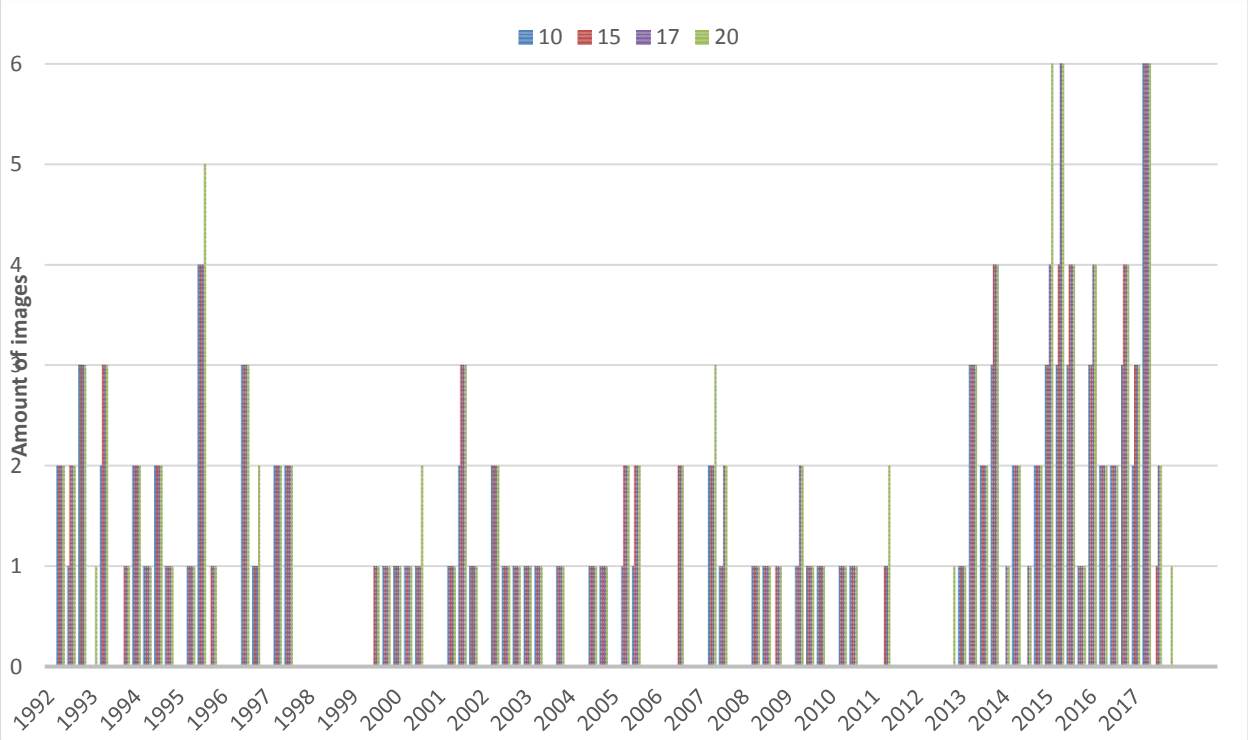

Google Earth Engine script

Mask clouded pixels

```
var getQABits = function(image, start, end, newName) {
    // Compute the bits we need to extract.
    var pattern = 0;
    for (var i = start; i <= end; i++) {
       pattern += Math.pow(2, i);
    }
    // Return a single band image of the extracted QA bits, giving the band
    // a new name.
    return image.select([0], [newName])
                  .bitwiseAnd(pattern)
                  .rightShift(start);
};

// A function to mask out cloudy pixels.
var cloud_shadows = function(image) {
  // Select the QA band.
  var QA = image.select(['pixel_qa']);
  // Get the internal_cloud_algorithm_flag bit.
  return getQABits(QA, 3,3, 'Cloud_shadows').eq(0);
  // Return an image masking out cloudy areas.
};

// A function to mask out cloudy pixels.
var clouds = function(image) {
  // Select the QA band.
  var QA = image.select(['pixel_qa']);
  // Get the internal_cloud_algorithm_flag bit.
  return getQABits(QA, 5,5, 'Cloud').eq(0);
  // Return an image masking out cloudy areas.
};

var maskClouds = function(image) {
  var cs = cloud_shadows(image);
  var c = clouds(image);
  image = image.updateMask(cs);
  return image.updateMask(c);
};
```

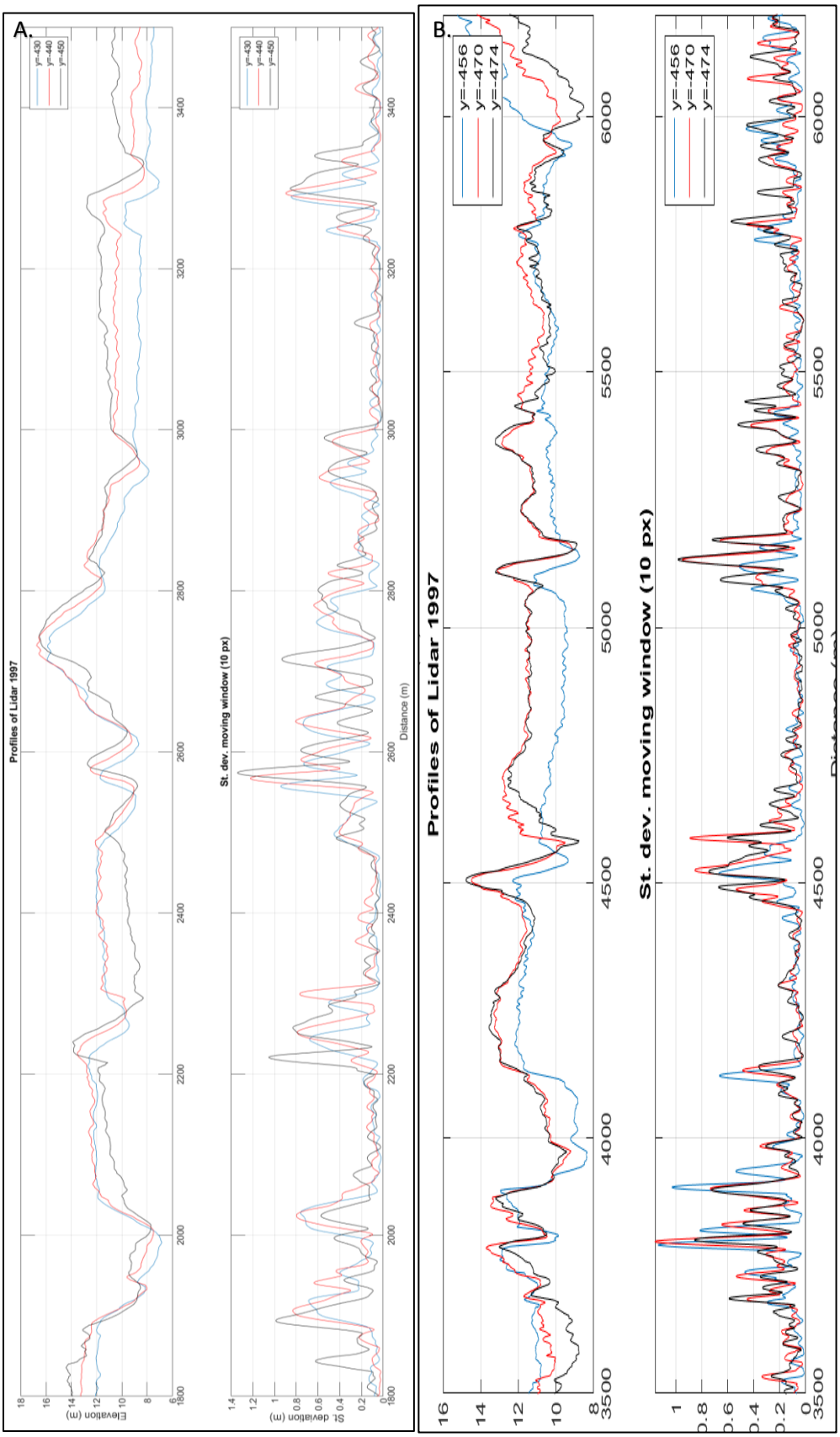

Figure 0-6 - Alongshore elevation profile of Terschelling at x= 1800m to x=3600m (A) and at x=3500m to x=6000m (B). Overview of exact locations is shown in Figure 3-13.

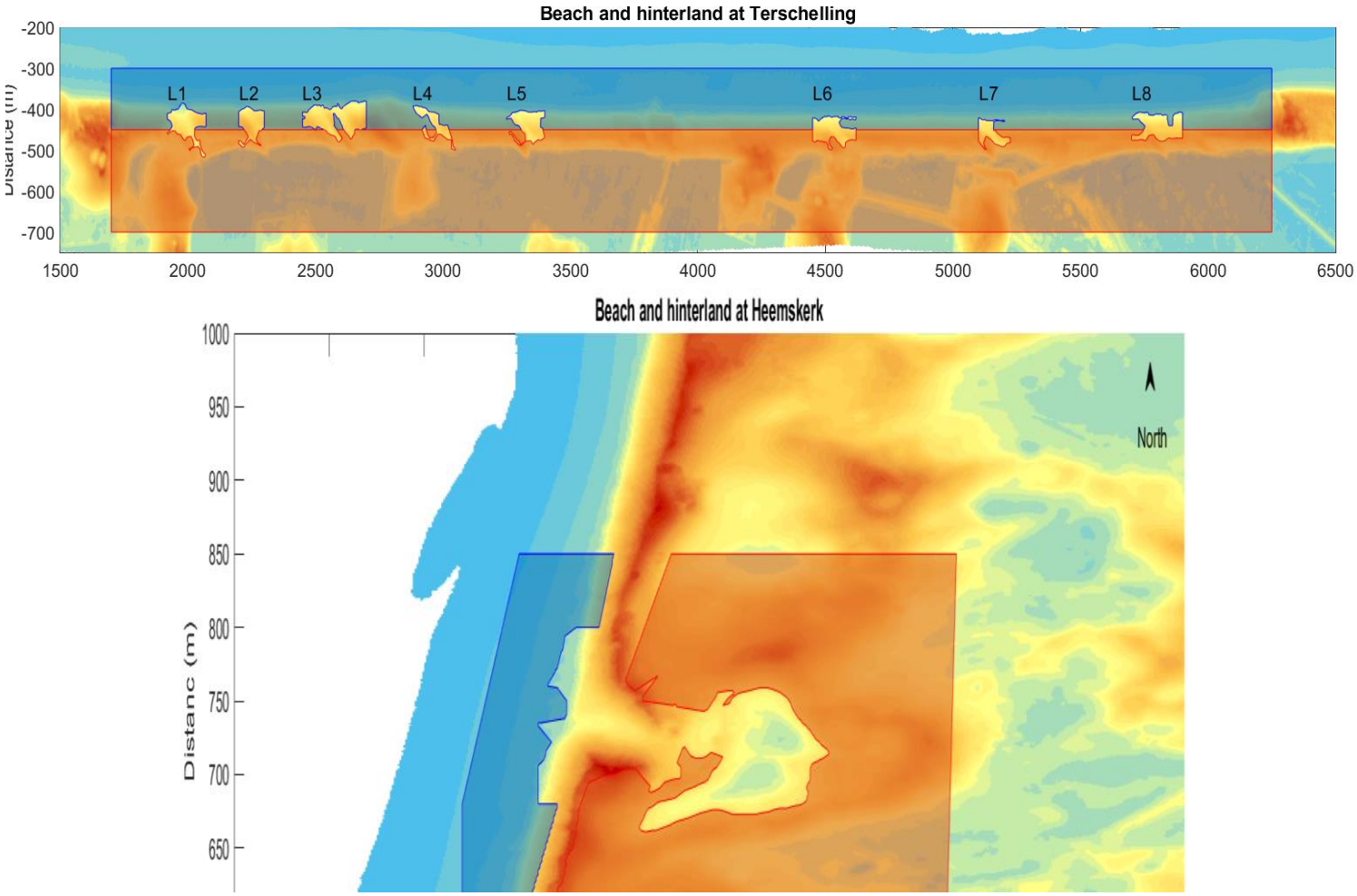

Figure 0-7 - Areas used for the volume analysis of beach(blue) and hinterland(red) at Terschelling (above) and Heemskerk (below), as determined from the 2007 Lidar elevation data.

Regions of interest/Geometries

Terschelling: Orange= reference dune, red=blowout left, green/blue is blowout right

Whole area

Heemskerk: White=whole area, blue= beach reference, cyan=blowout, red=lobe, orange= hinterland and green = reference dune

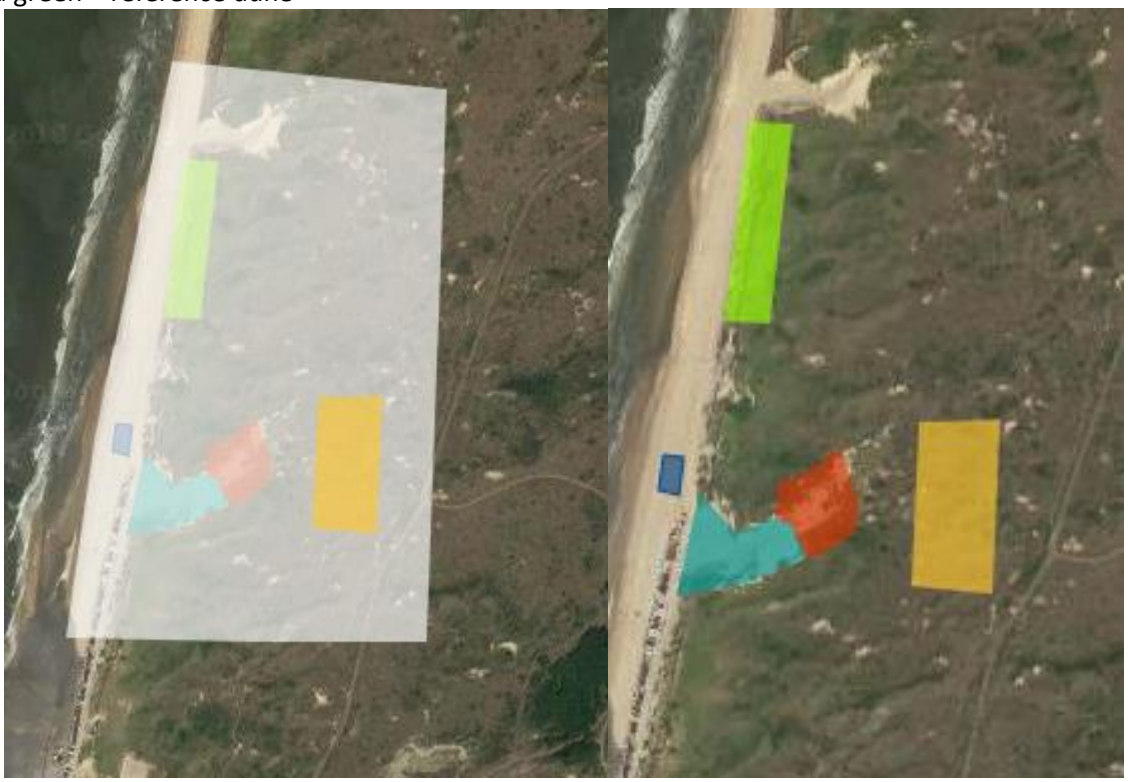

Annual LIDAR Elevation: Terschelling

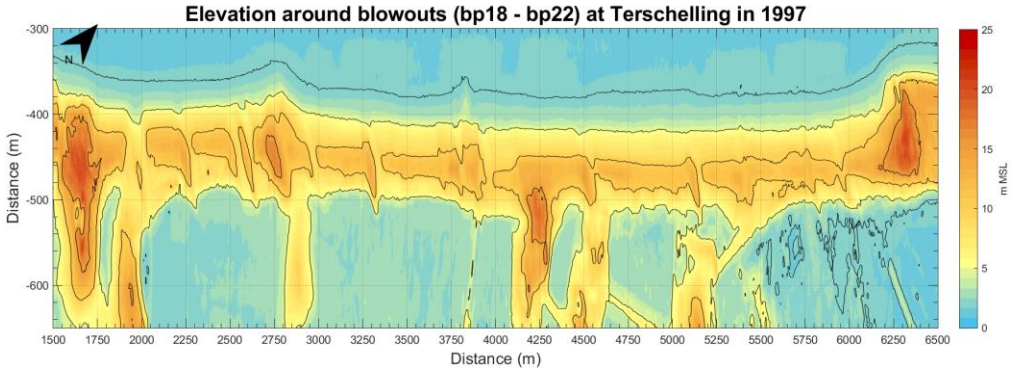

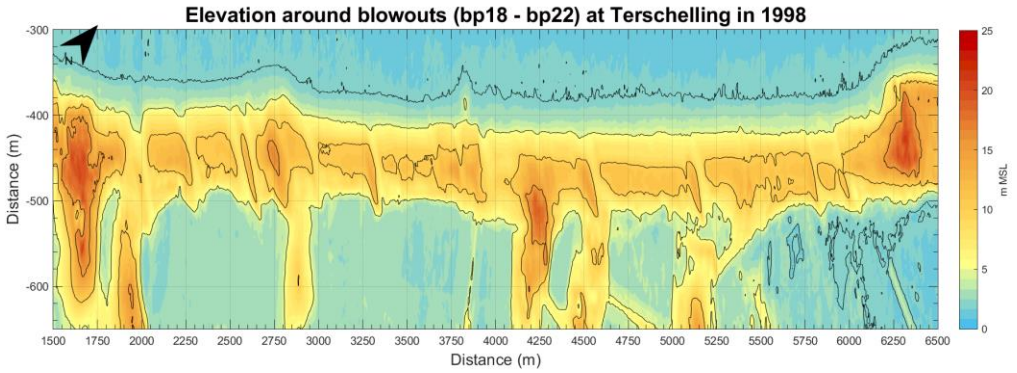

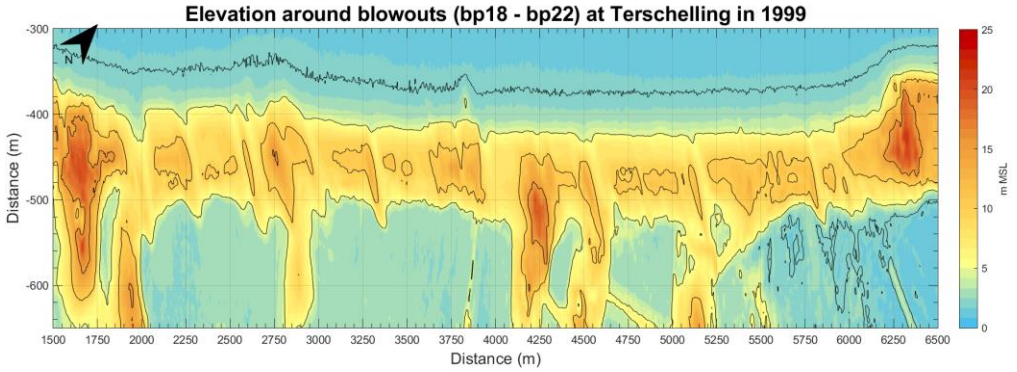

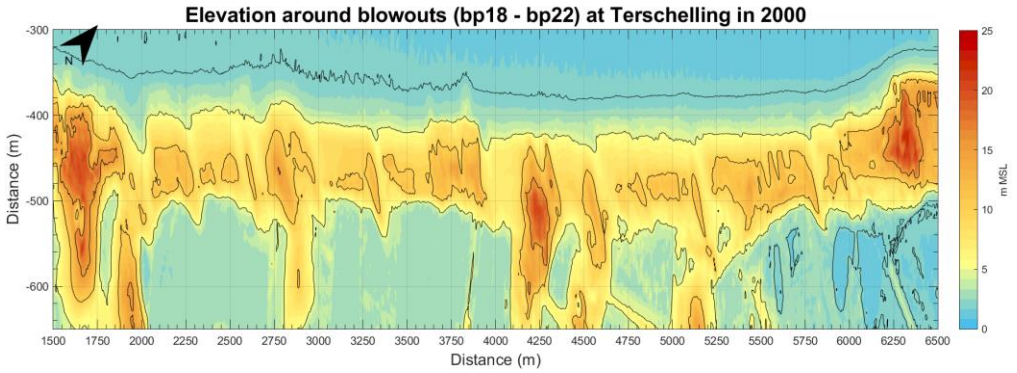

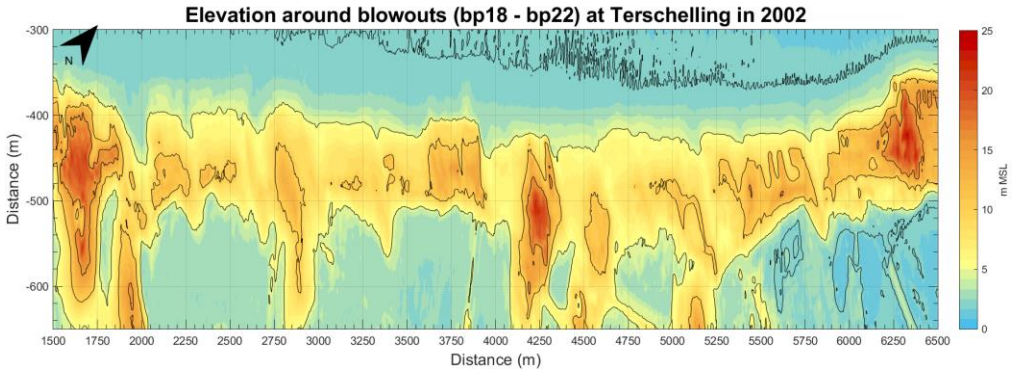
Elevation around blowouts (bp18 - bp22) at Terschelling in 2002
Distance (m)
-300
-400
-500
-600
1500 1750 2000 2250 2500 2750 3000 3250 3500 3750 4000 4250 4500 4750 5000 5250 5500 5750 6000 6250 6500
Distance (m)
N
m MSL
0 5 10 15 20 25

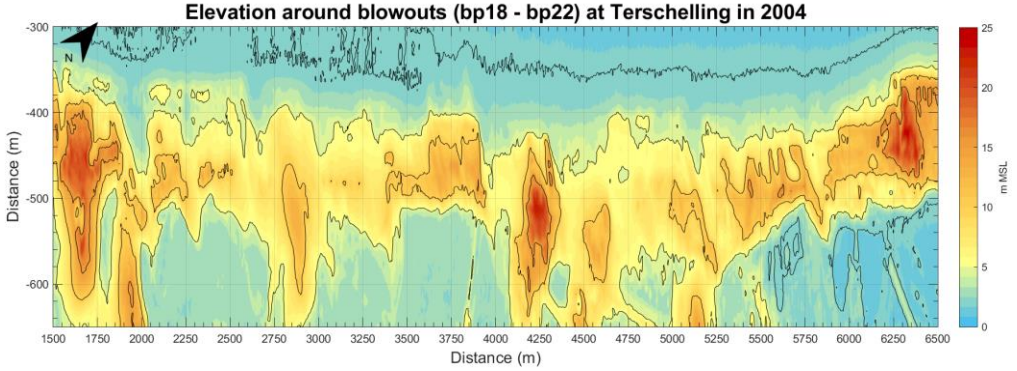
Elevation around blowouts (bp18 - bp22) at Terschelling in 2004
Distance (m)
-300
-400
-500
-600
1500 1750 2000 2250 2500 2750 3000 3250 3500 3750 4000 4250 4500 4750 5000 5250 5500 5750 6000 6250 6500
Distance (m)
N
m MSL
0 5 10 15 20 25

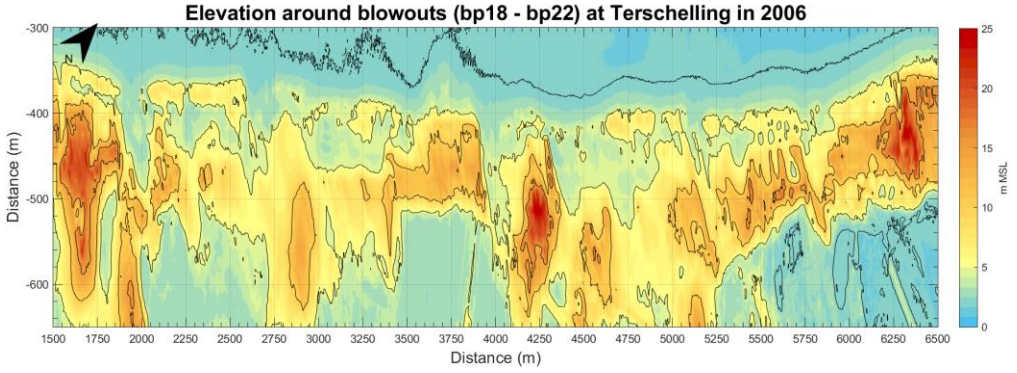
Elevation around blowouts (bp18 - bp22) at Terschelling in 2006
Distance (m)
-300
-400
-500
-600
1500 1750 2000 2250 2500 2750 3000 3250 3500 3750 4000 4250 4500 4750 5000 5250 5500 5750 6000 6250 6500
Distance (m)
N
m MSL
0 5 10 15 20 25

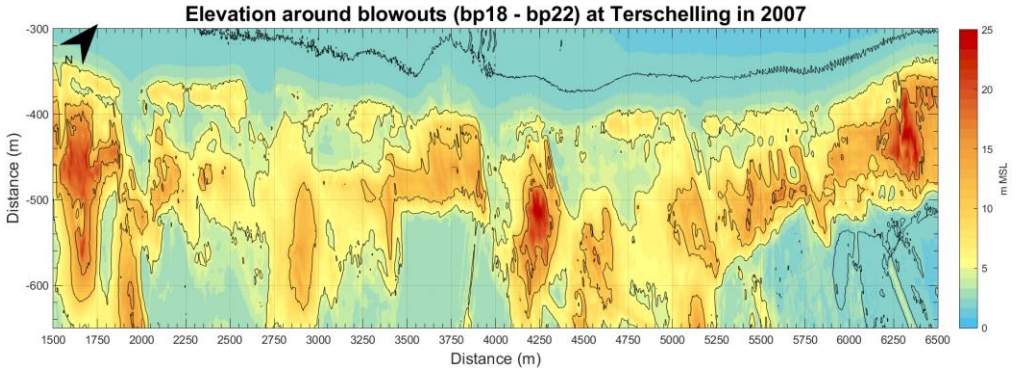
Elevation around blowouts (bp18 - bp22) at Terschelling in 2007
Distance (m)
-300
-400
-500
-600
1500 1750 2000 2250 2500 2750 3000 3250 3500 3750 4000 4250 4500 4750 5000 5250 5500 5750 6000 6250 6500
Distance (m)
N
m MSL
0 5 10 15 20 25

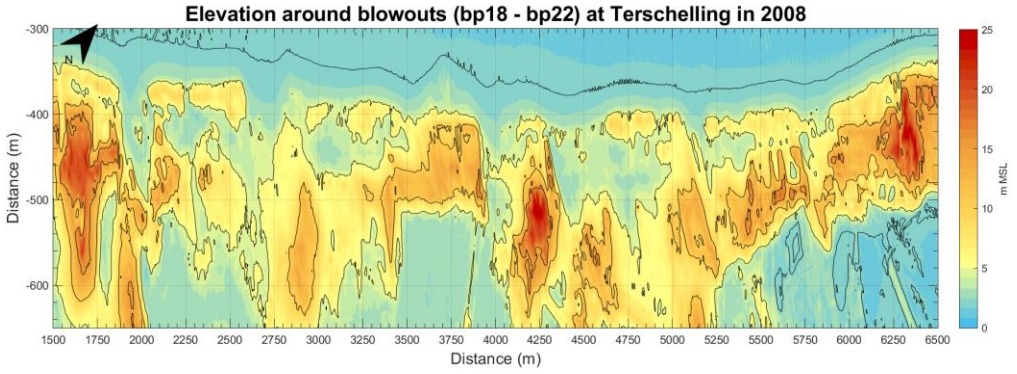
Elevation around blowouts (bp18 - bp22) at Terschelling in 2008
Distance (m)
-300
-400
-500
-600
1500 1750 2000 2250 2500 2750 3000 3250 3500 3750 4000 4250 4500 4750 5000 5250 5500 5750 6000 6250 6500
Distance (m)
N
m MSL
0 5 10 15 20 25

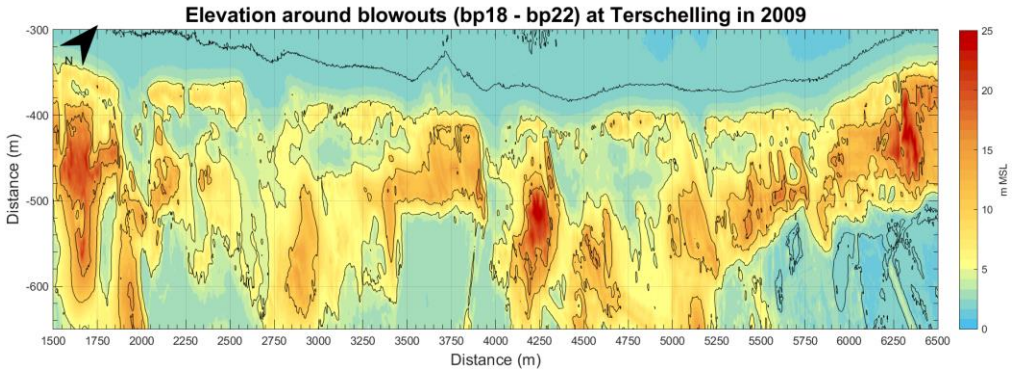
Elevation around blowouts (bp18 - bp22) at Terschelling in 2009
Distance (m)
-300
-400
-500
-600
1500 1750 2000 2250 2500 2750 3000 3250 3500 3750 4000 4250 4500 4750 5000 5250 5500 5750 6000 6250 6500
Distance (m)
m MSL
25
20
15
10
5
0

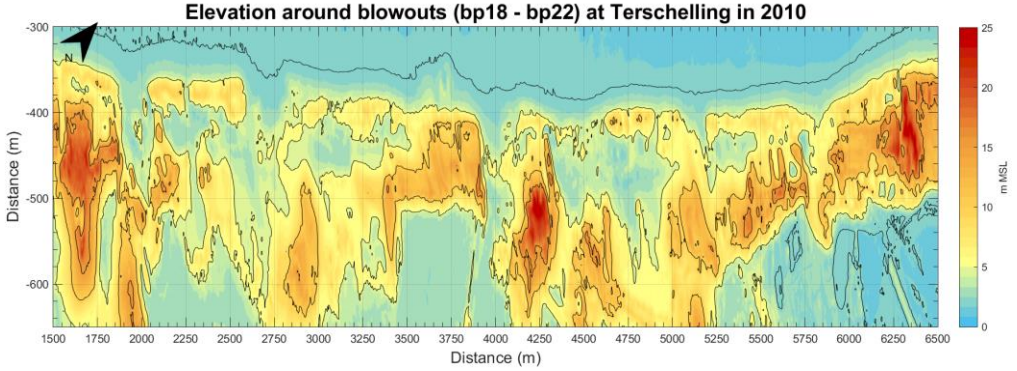
Elevation around blowouts (bp18 - bp22) at Terschelling in 2010
Distance (m)
-300
-400
-500
-600
1500 1750 2000 2250 2500 2750 3000 3250 3500 3750 4000 4250 4500 4750 5000 5250 5500 5750 6000 6250 6500
Distance (m)
m MSL
25
20
15
10
5
0

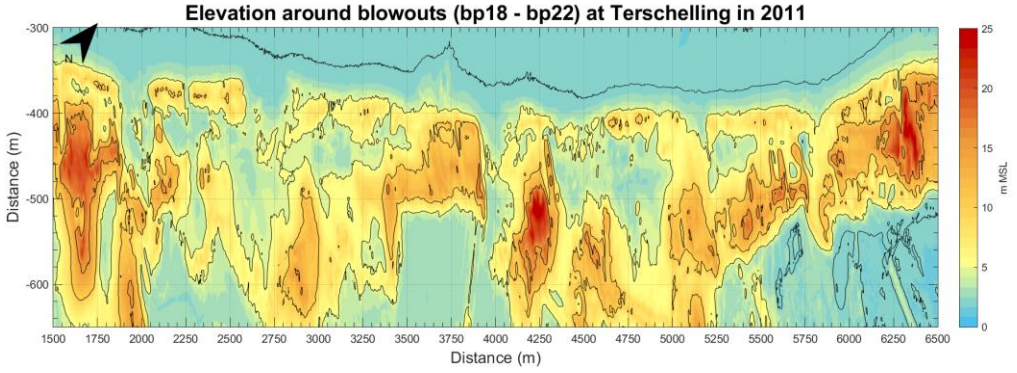
Elevation around blowouts (bp18 - bp22) at Terschelling in 2011
Distance (m)
-300
-400
-500
-600
1500 1750 2000 2250 2500 2750 3000 3250 3500 3750 4000 4250 4500 4750 5000 5250 5500 5750 6000 6250 6500
Distance (m)
m MSL
25
20
15
10
5
0

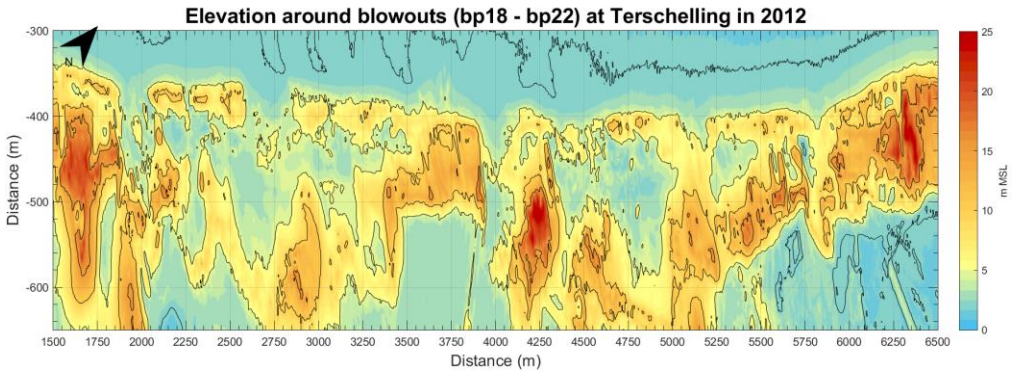
Elevation around blowouts (bp18 - bp22) at Terschelling in 2012
Distance (m)
-300
-400
-500
-600
1500 1750 2000 2250 2500 2750 3000 3250 3500 3750 4000 4250 4500 4750 5000 5250 5500 5750 6000 6250 6500
Distance (m)
m MSL
25
20
15
10
5
0

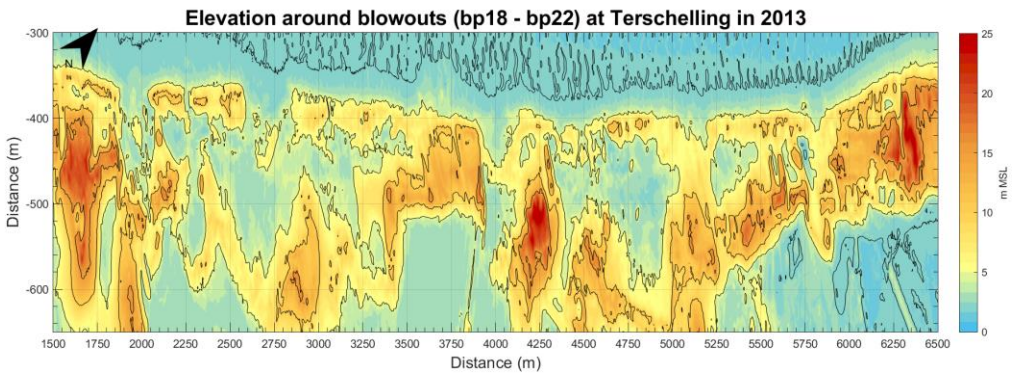
Elevation around blowouts (bp18 - bp22) at Terschelling in 2013
Distance (m)
-300
-400
-500
-600
1500 1750 2000 2250 2500 2750 3000 3250 3500 3750 4000 4250 4500 4750 5000 5250 5500 5750 6000 6250 6500
Distance (m)
m MSL
25
20
15
10
5
0

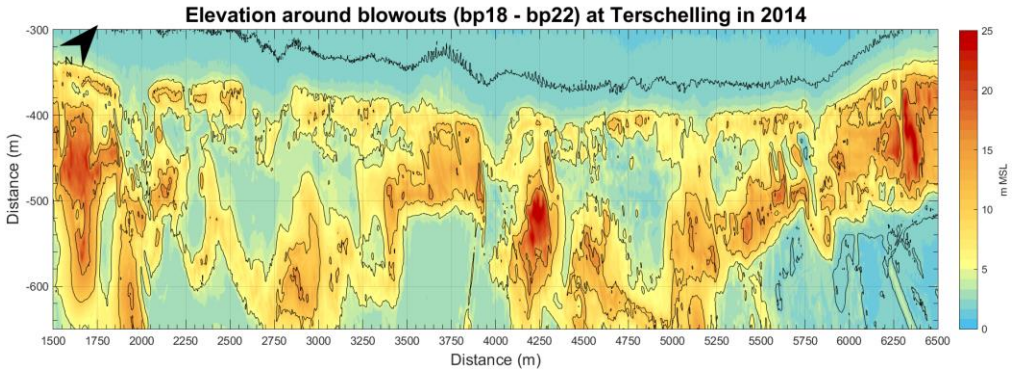
Elevation around blowouts (bp18 - bp22) at Terschelling in 2014
Distance (m)
-300
-400
-500
-600
1500 1750 2000 2250 2500 2750 3000 3250 3500 3750 4000 4250 4500 4750 5000 5250 5500 5750 6000 6250 6500
Distance (m)
m MSL
25
20
15
10
5
0

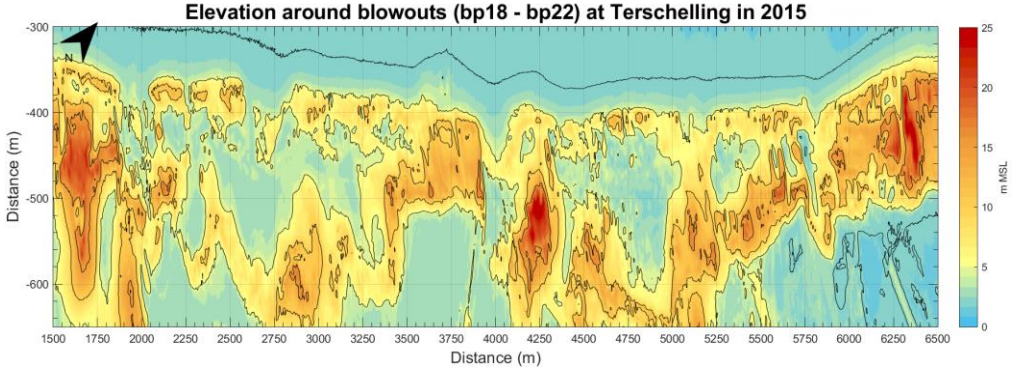
Elevation around blowouts (bp18 - bp22) at Terschelling in 2015
Distance (m)
-300
-400
-500
-600
1500 1750 2000 2250 2500 2750 3000 3250 3500 3750 4000 4250 4500 4750 5000 5250 5500 5750 6000 6250 6500
Distance (m)
m MSL
25
20
15
10
5
0

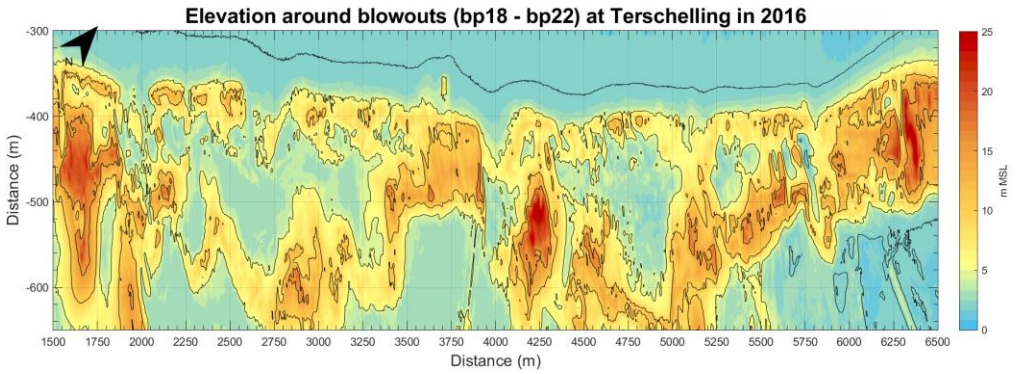
Elevation around blowouts (bp18 - bp22) at Terschelling in 2016
Distance (m)
-300
-400
-500
-600
1500 1750 2000 2250 2500 2750 3000 3250 3500 3750 4000 4250 4500 4750 5000 5250 5500 5750 6000 6250 6500
Distance (m)
m MSL
25
20
15
10
5
0

Annual change in elevation (LIDAR): Terschelling

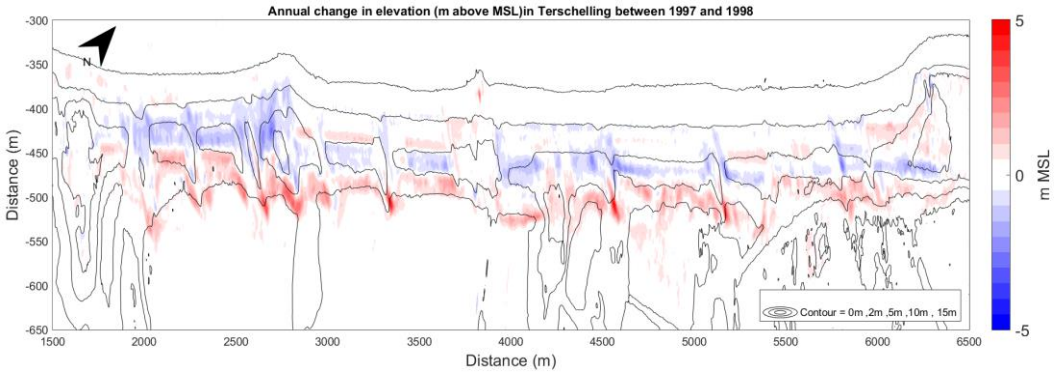

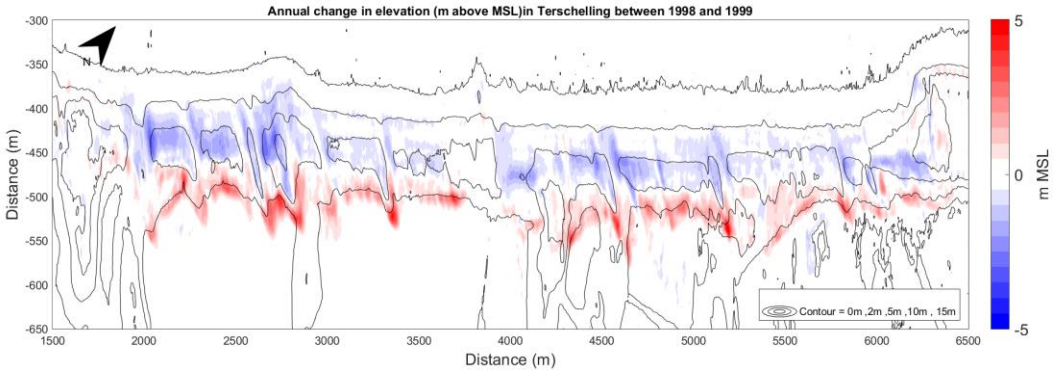

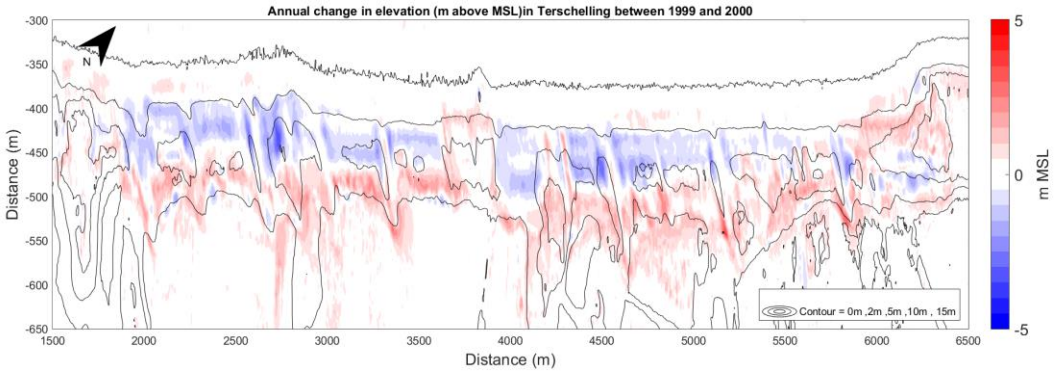

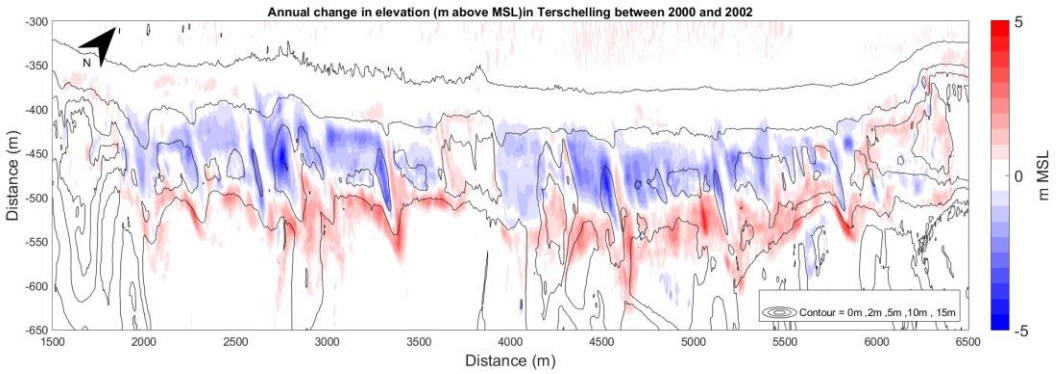

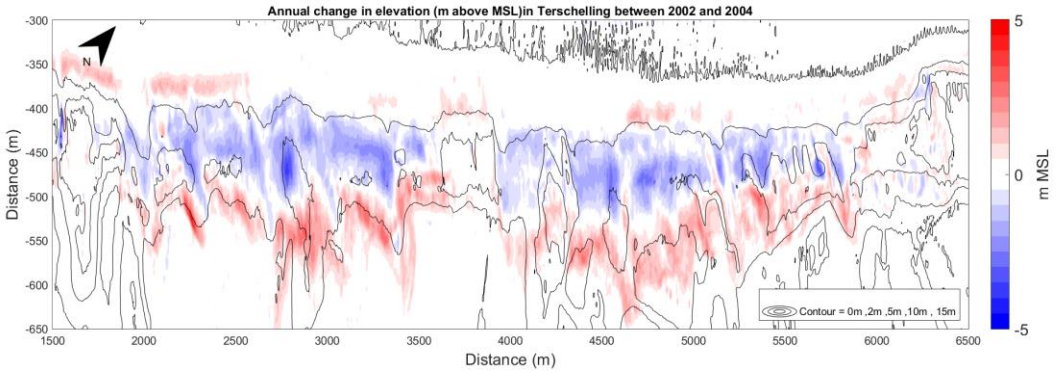

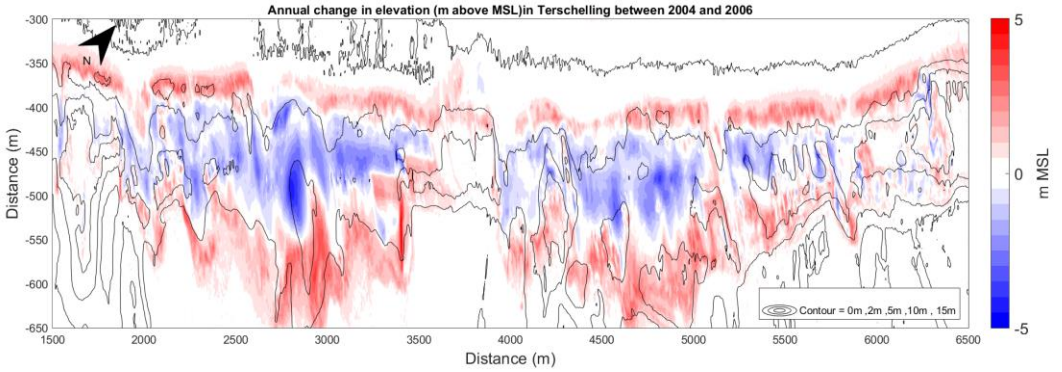
Annual change in elevation (m above MSL)in Terschelling between 2004 and 2006
Distance (m)
Distance (m)
m MSL
Contour = 0m ,2m ,5m ,10m , 15m
N

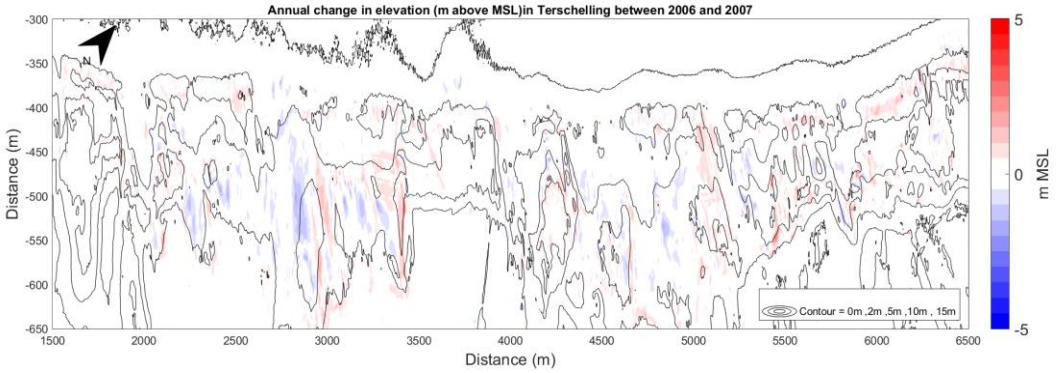
Annual change in elevation (m above MSL)in Terschelling between 2006 and 2007
Distance (m)
Distance (m)
m MSL
Contour = 0m ,2m ,5m ,10m , 15m
N

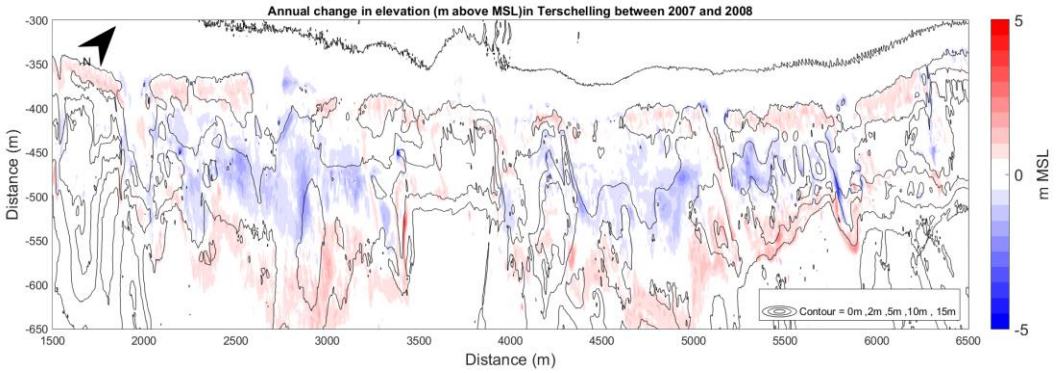
Annual change in elevation (m above MSL)in Terschelling between 2007 and 2008
Distance (m)
Distance (m)
m MSL
Contour = 0m ,2m ,5m ,10m , 15m
N

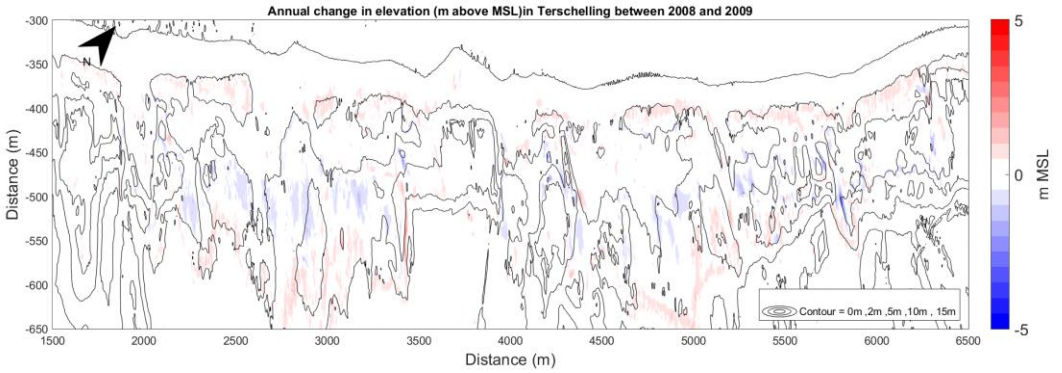
Annual change in elevation (m above MSL)in Terschelling between 2008 and 2009
Distance (m)
Distance (m)
m MSL
Contour = 0m ,2m ,5m ,10m , 15m
N

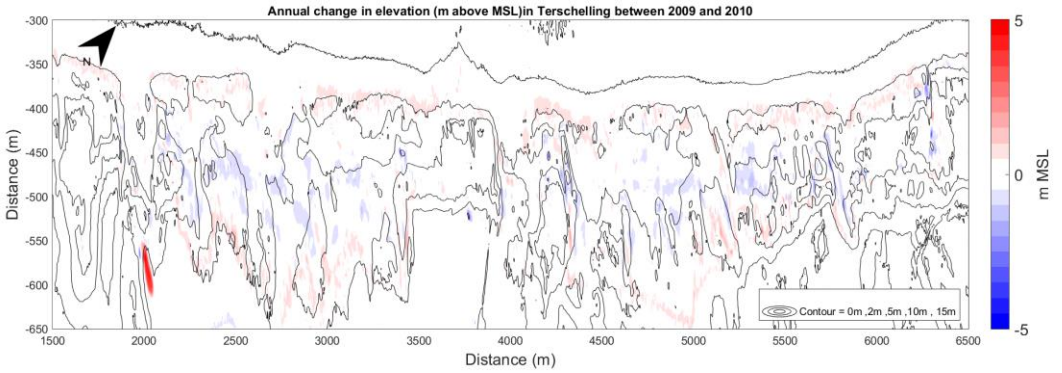
Annual change in elevation (m above MSL)in Terschelling between 2009 and 2010
Distance (m)
Distance (m)
m MSL
Contour = 0m ,2m ,5m ,10m , 15m
N

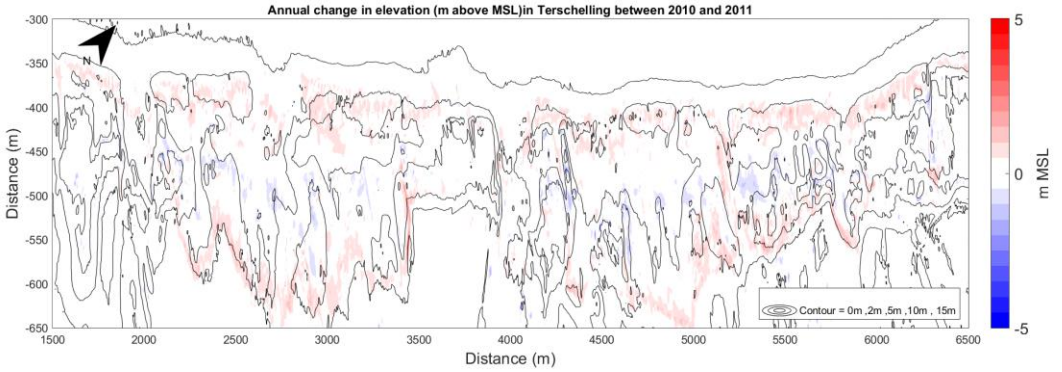
Annual change in elevation (m above MSL)in Terschelling between 2010 and 2011
Distance (m)
Distance (m)
m MSL
Contour = 0m ,2m ,5m ,10m , 15m
N

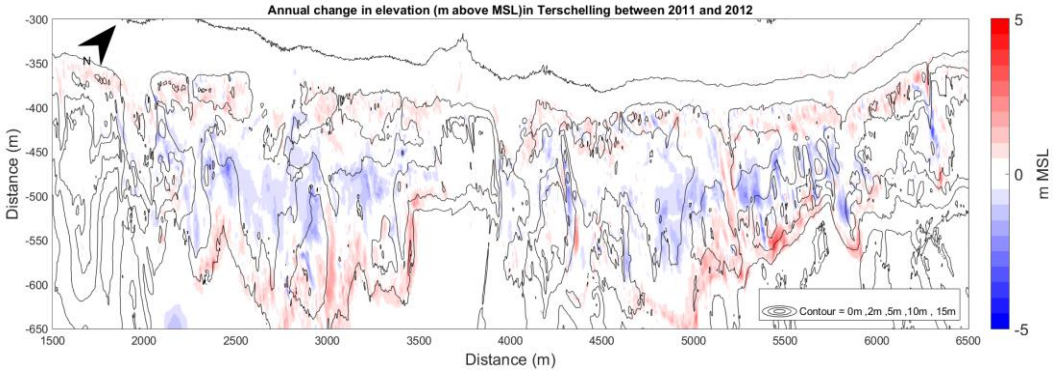
Annual change in elevation (m above MSL)in Terschelling between 2011 and 2012
Distance (m)
Distance (m)
m MSL
Contour = 0m ,2m ,5m ,10m , 15m
N

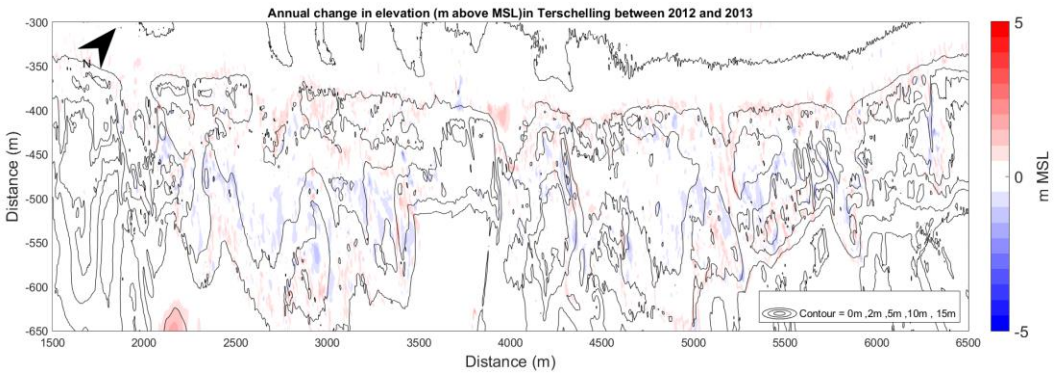
Annual change in elevation (m above MSL)in Terschelling between 2012 and 2013
Distance (m)
Distance (m)
m MSL
Contour = 0m ,2m ,5m ,10m , 15m
N

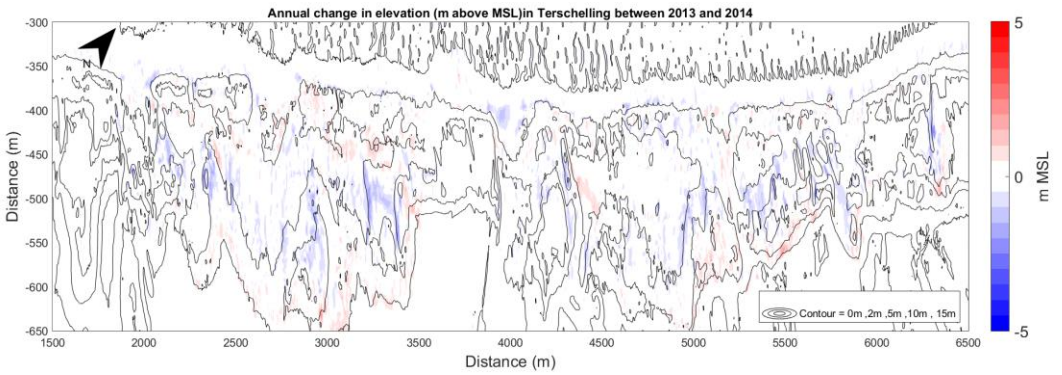
Annual change in elevation (m above MSL)in Terschelling between 2013 and 2014
Distance (m)
Distance (m)
m MSL
Contour = 0m ,2m ,5m ,10m , 15m
N

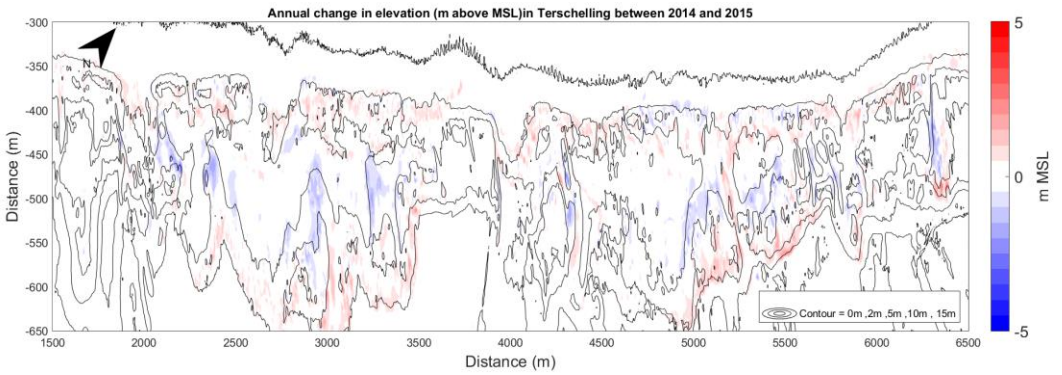
Annual change in elevation (m above MSL)in Terschelling between 2014 and 2015
Distance (m)
Distance (m)
m MSL
Contour = 0m ,2m ,5m ,10m , 15m
N

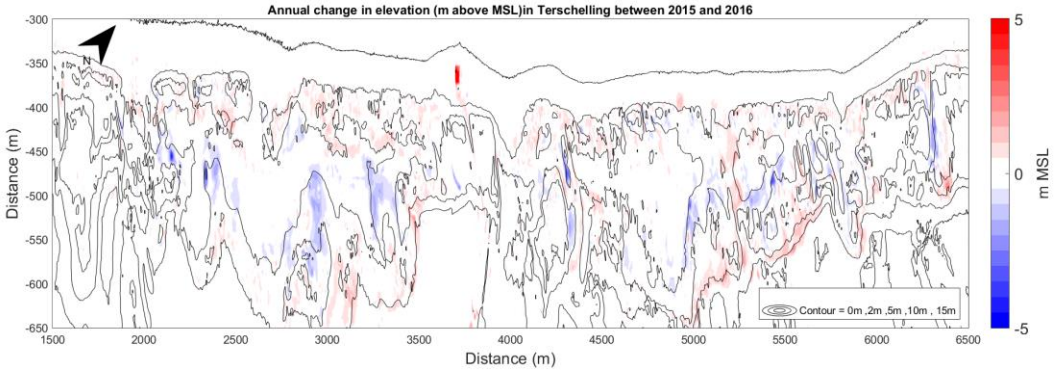
Annual change in elevation (m above MSL)in Terschelling between 2015 and 2016
Distance (m)
-300
-350
-400
-450
-500
-550
-600
-650
1500
2000
2500
3000
3500
4000
4500
5000
5500
6000
6500
Distance (m)
N
Contour = 0m ,2m ,5m ,10m , 15m
5
0
-5
m MSL

LIDAR: Change during 1997-2016 at Terschelling

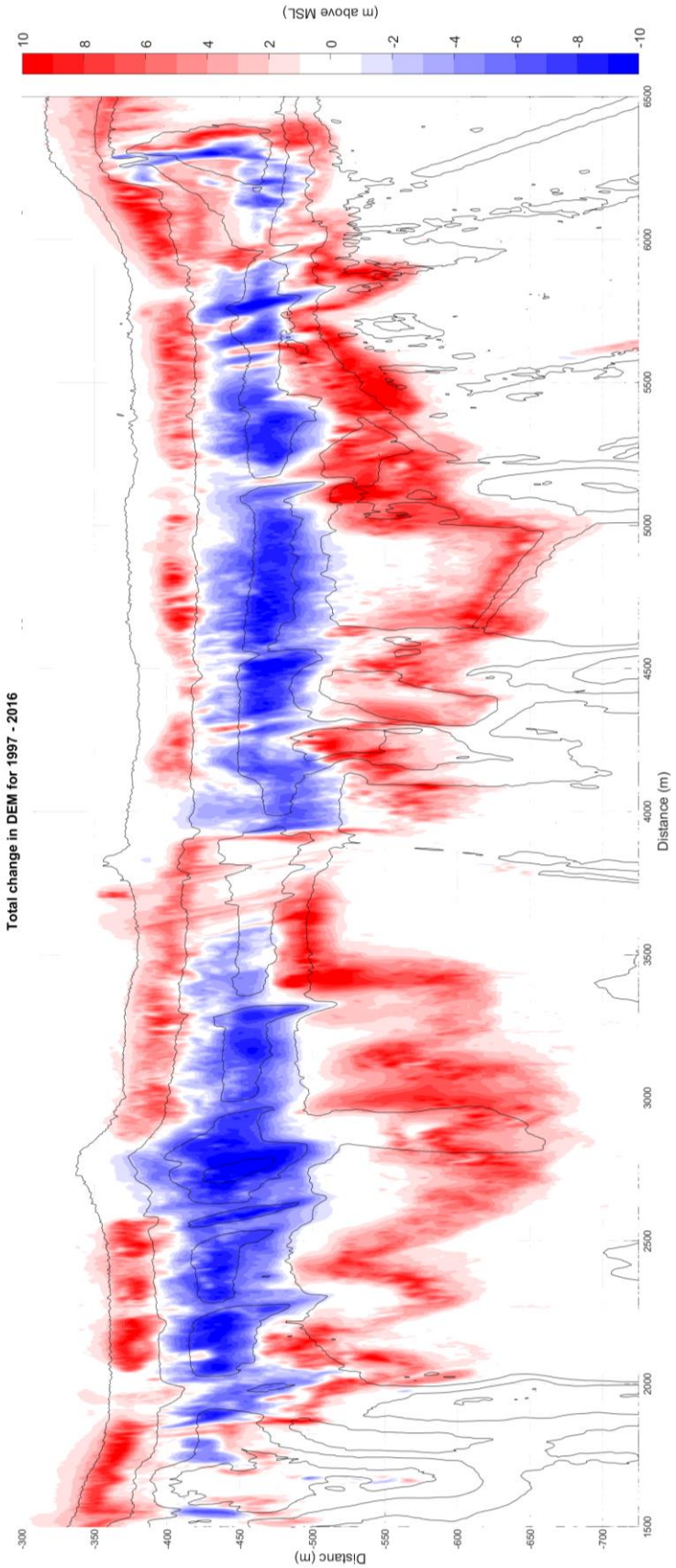

Locations of profiles and ROIs on Terschelling

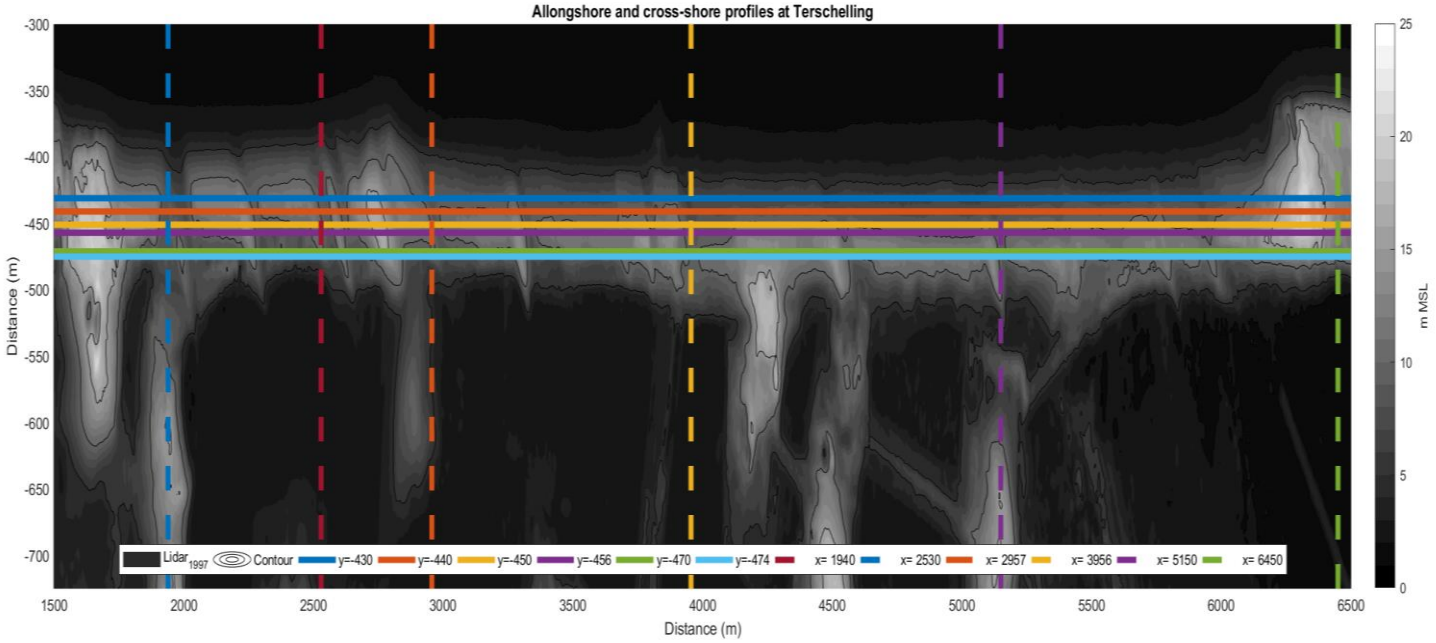

Figure 0-8 - Locations of cross-shore and alongshore profiles at Terschelling.

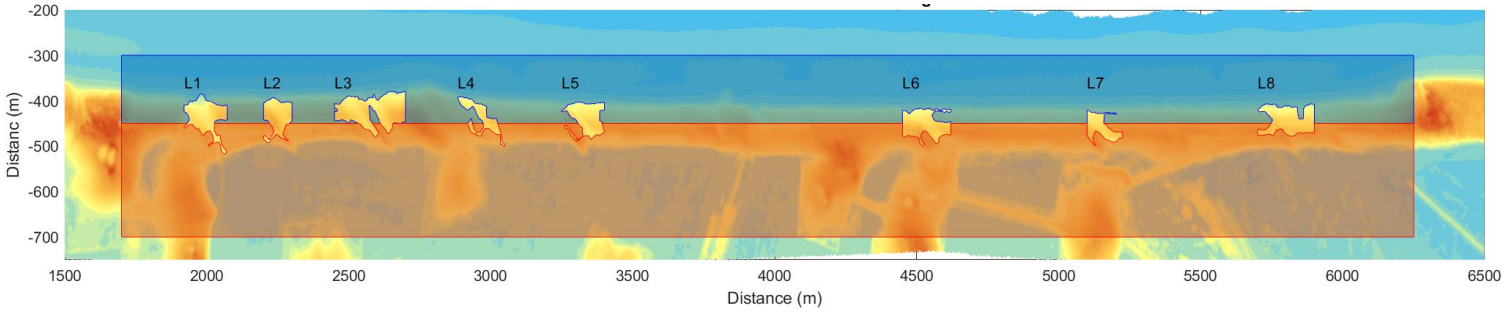

LIDAR of Heemskerk

Annual Elevation at Heemskerk

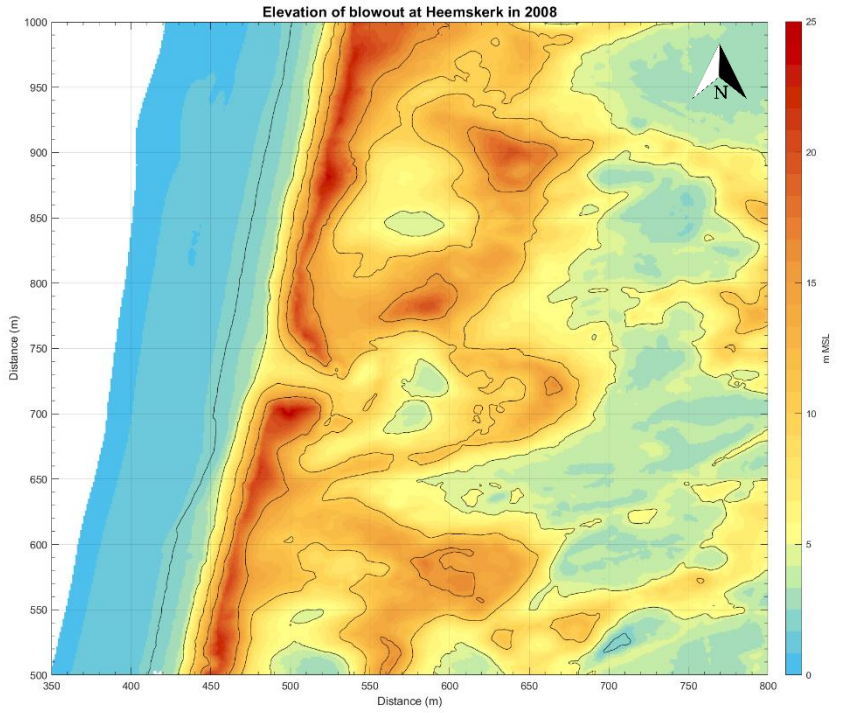

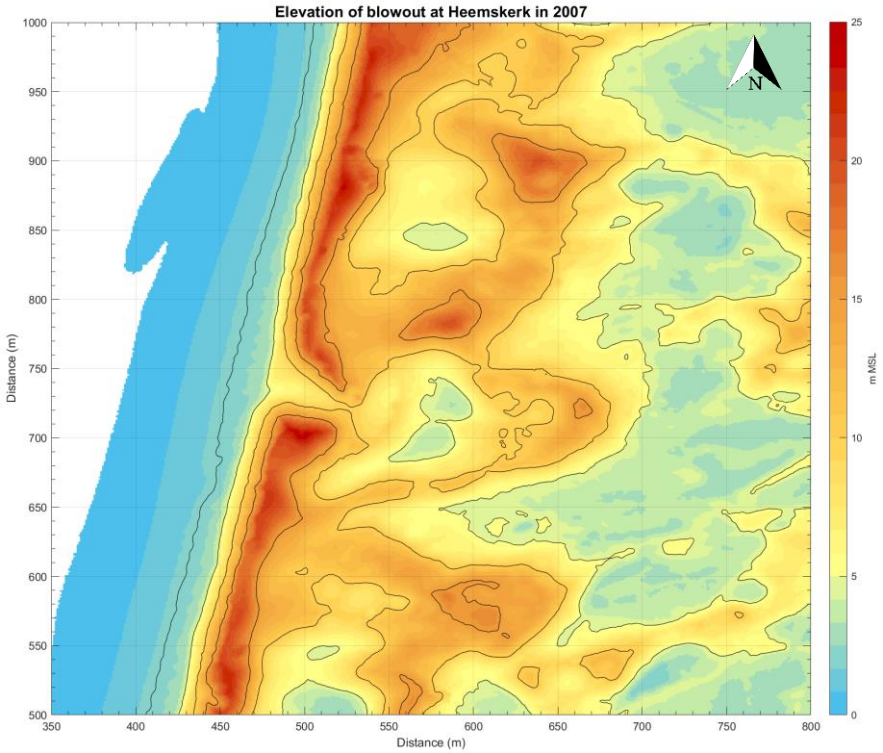

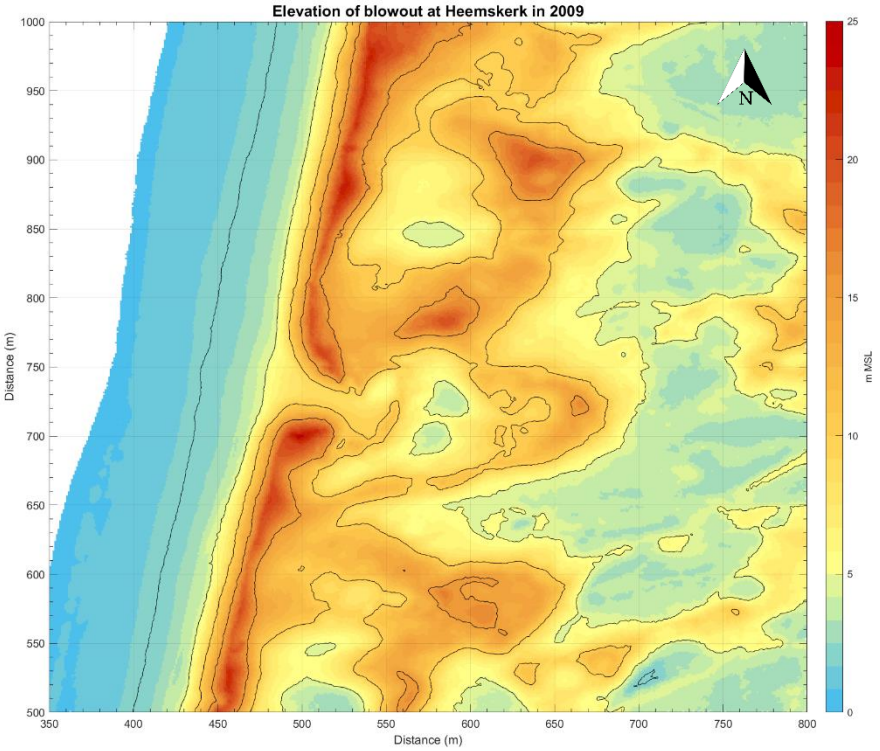
Elevation of blowout at Heemskerk in 2009
Distance (m)
Distance (m)
m MSL
N

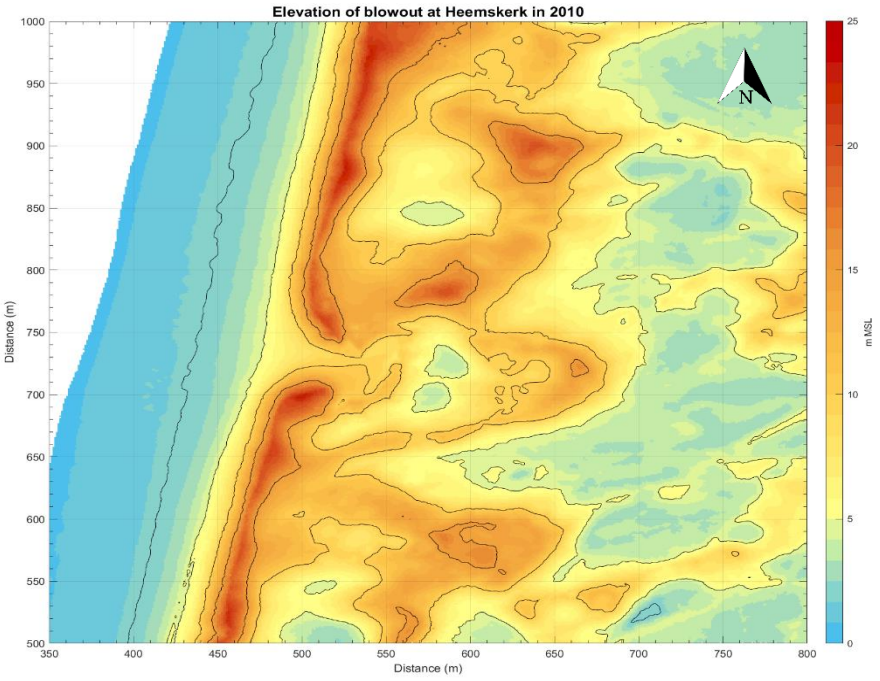
Elevation of blowout at Heemskerk in 2010
Distance (m)
Distance (m)
m MSL
N

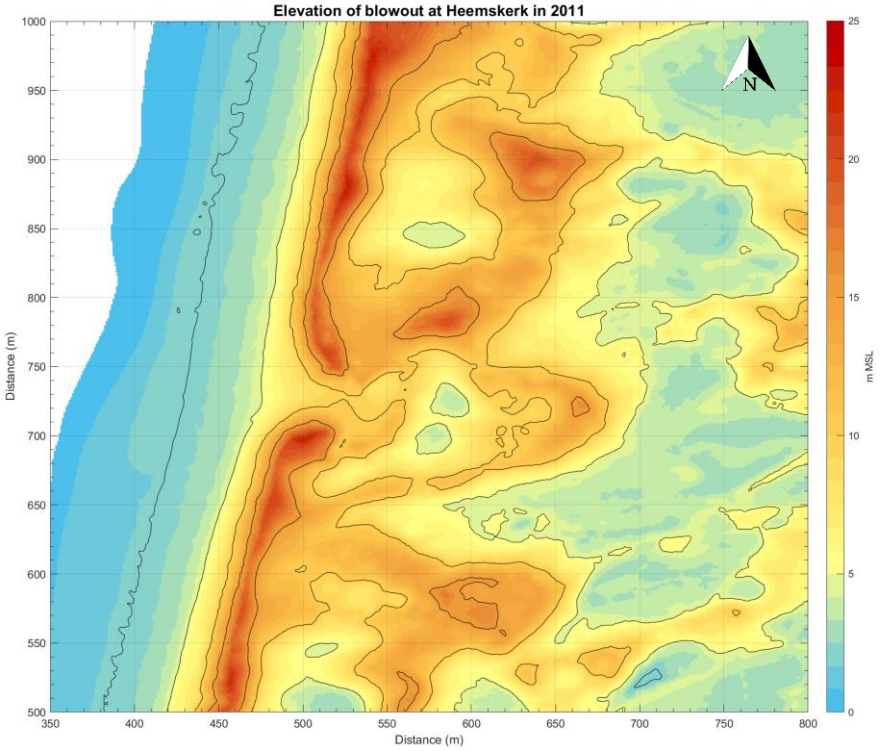
Elevation of blowout at Heemskerk in 2011
Distance (m)
Distance (m)
m MSL
N

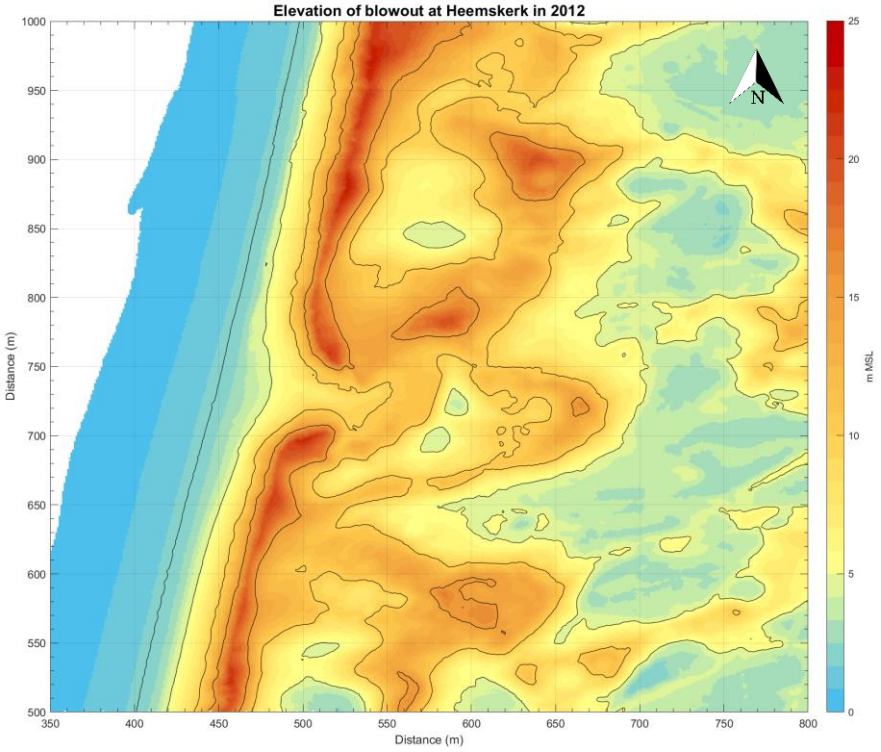
Elevation of blowout at Heemskerk in 2012
Distance (m)
Distance (m)
m MSL
N

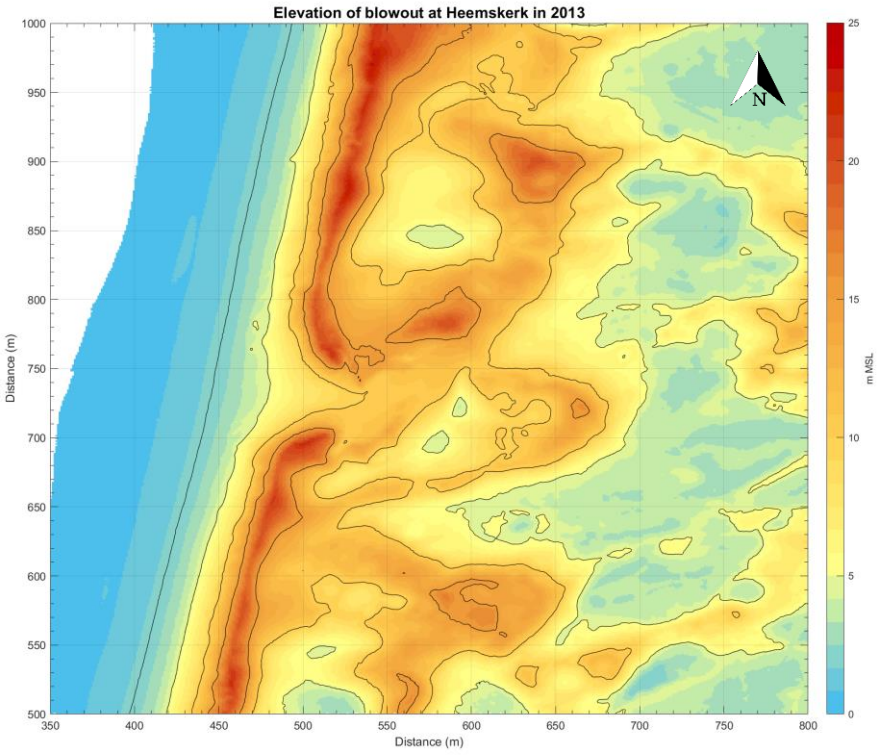
Elevation of blowout at Heemskerk in 2013
Distance (m)
Distance (m)
m MSL
N

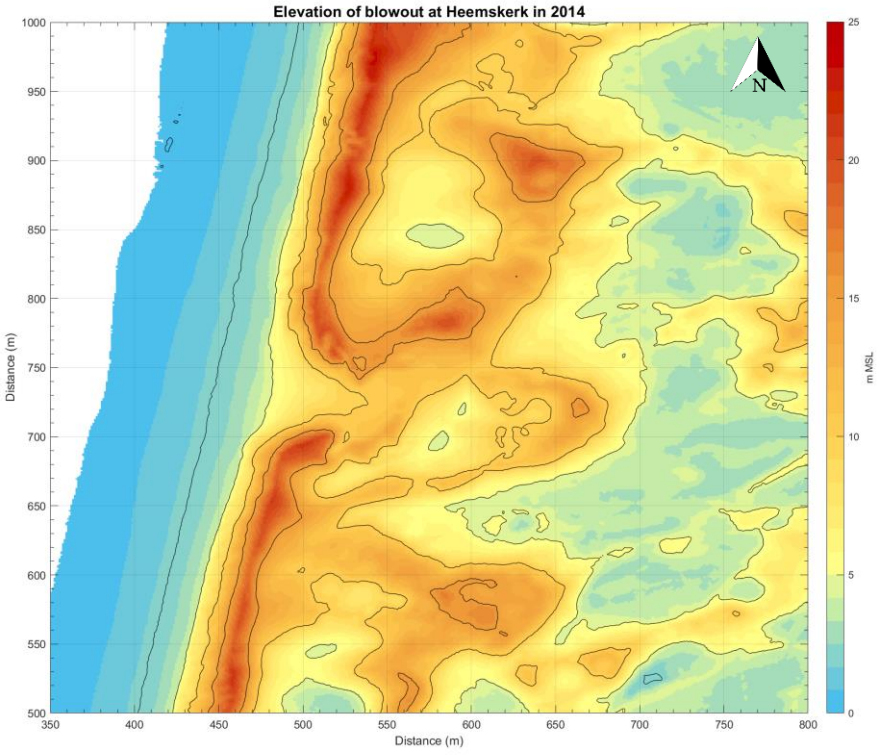
Elevation of blowout at Heemskerk in 2014
Distance (m)
Distance (m)
m MSL
N

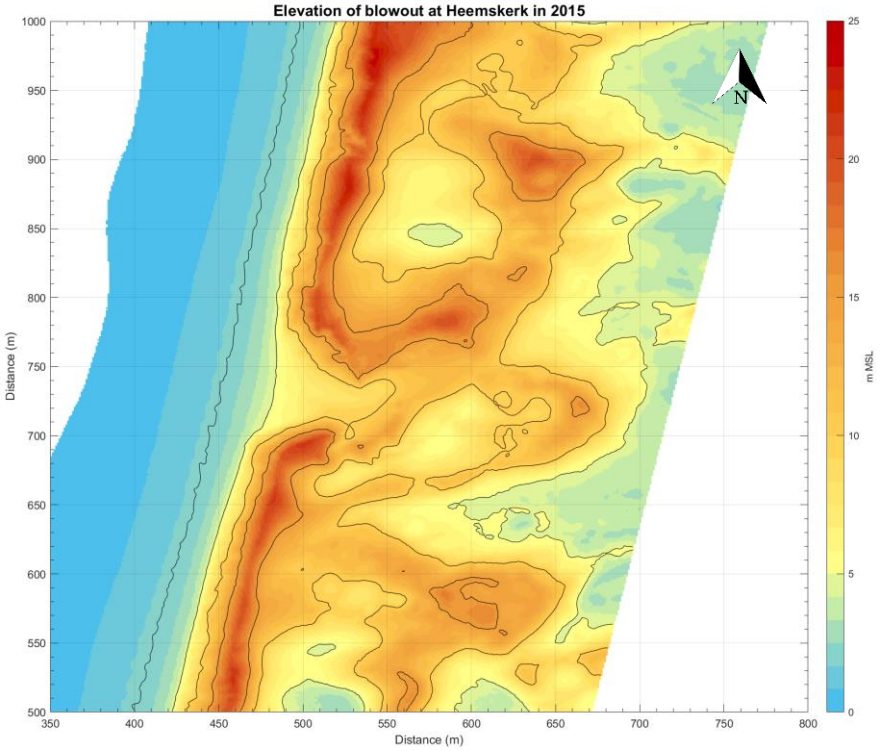
Elevation of blowout at Heemskerk in 2015
Distance (m)
Distance (m)
m MSL
N

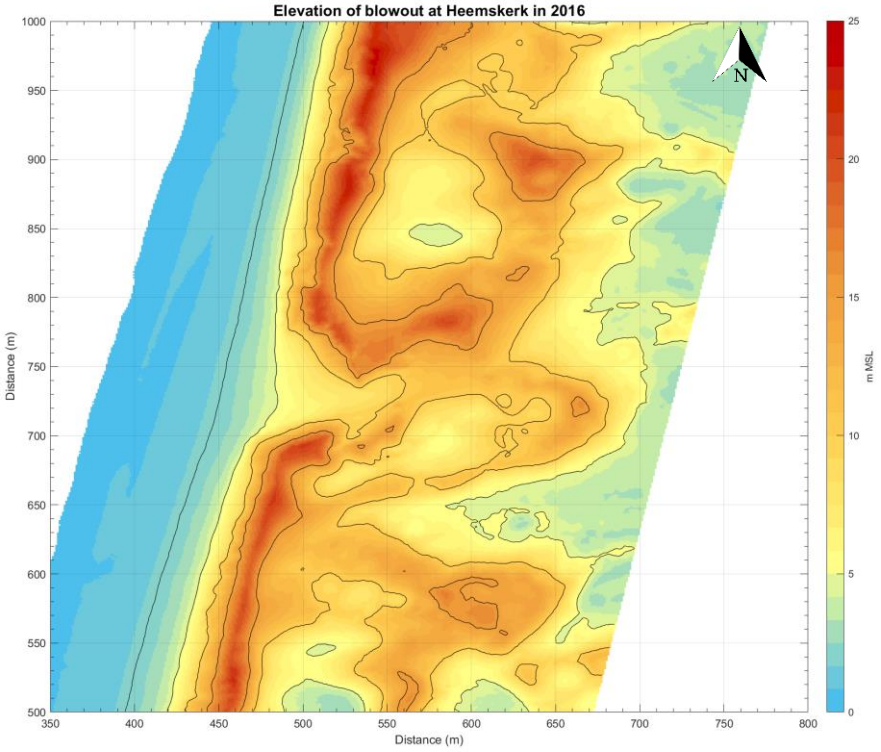
Elevation of blowout at Heemskerk in 2016
Distance (m)
Distance (m)
m MSL
N

Annual change in elevation at Heemskerk

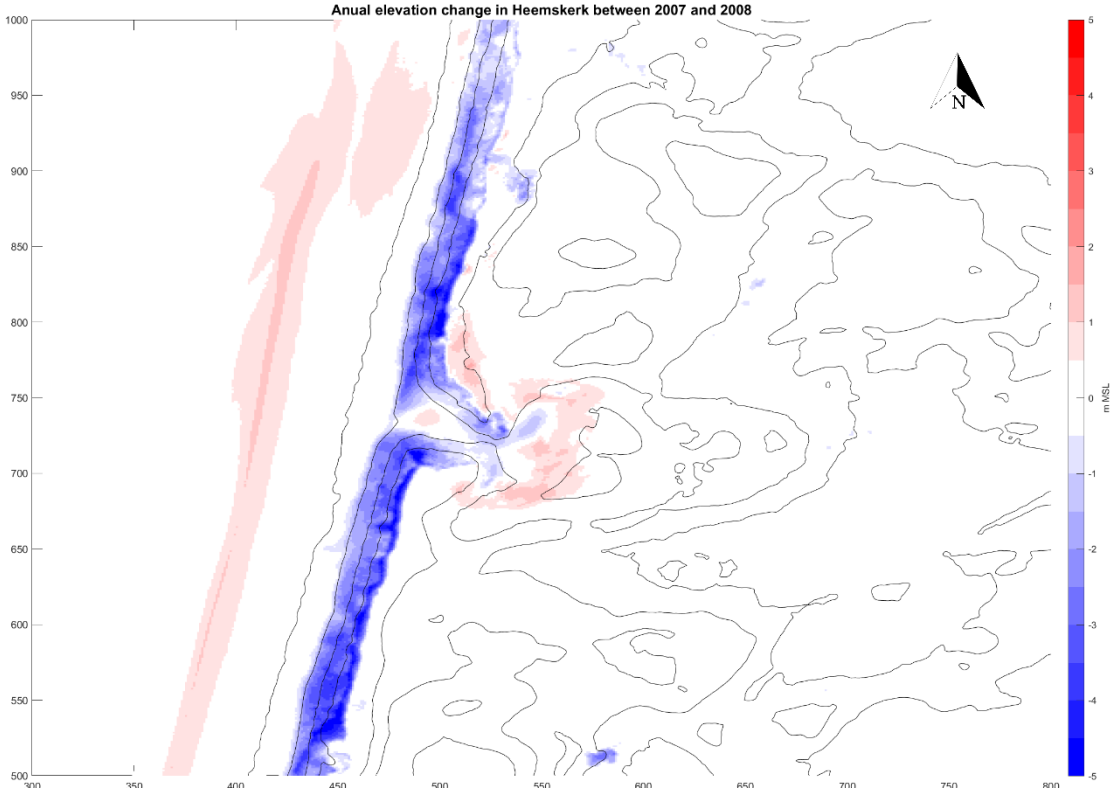

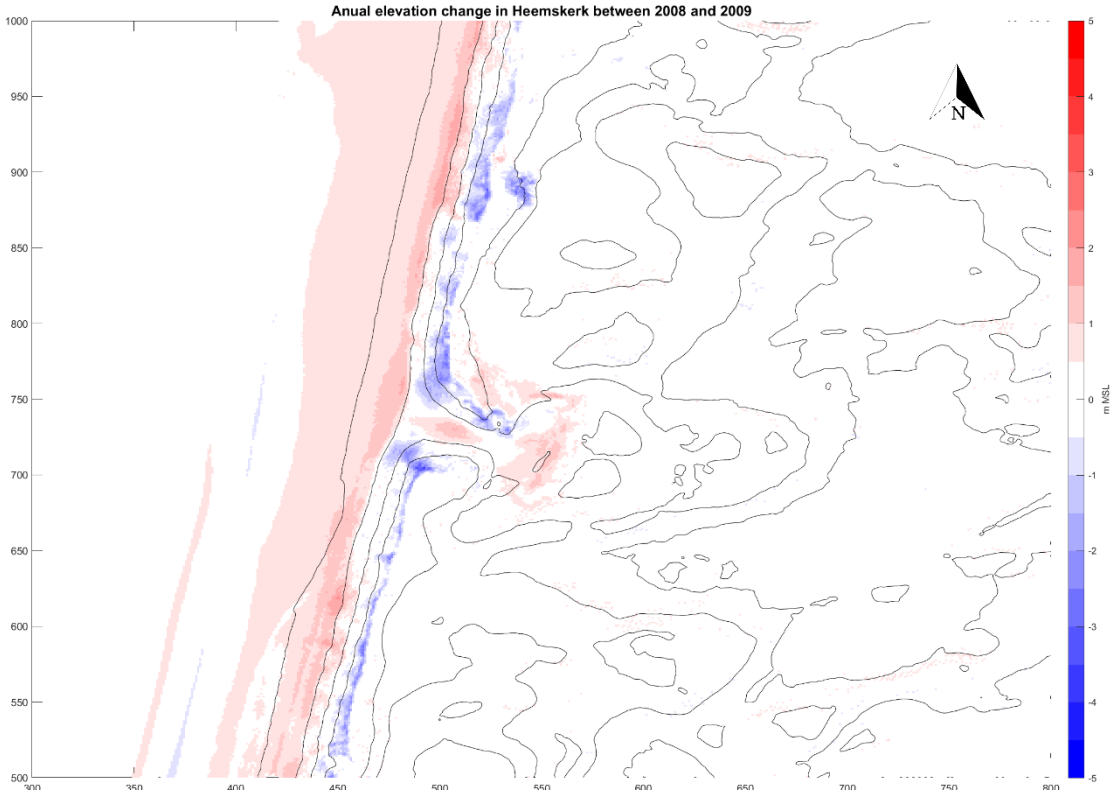

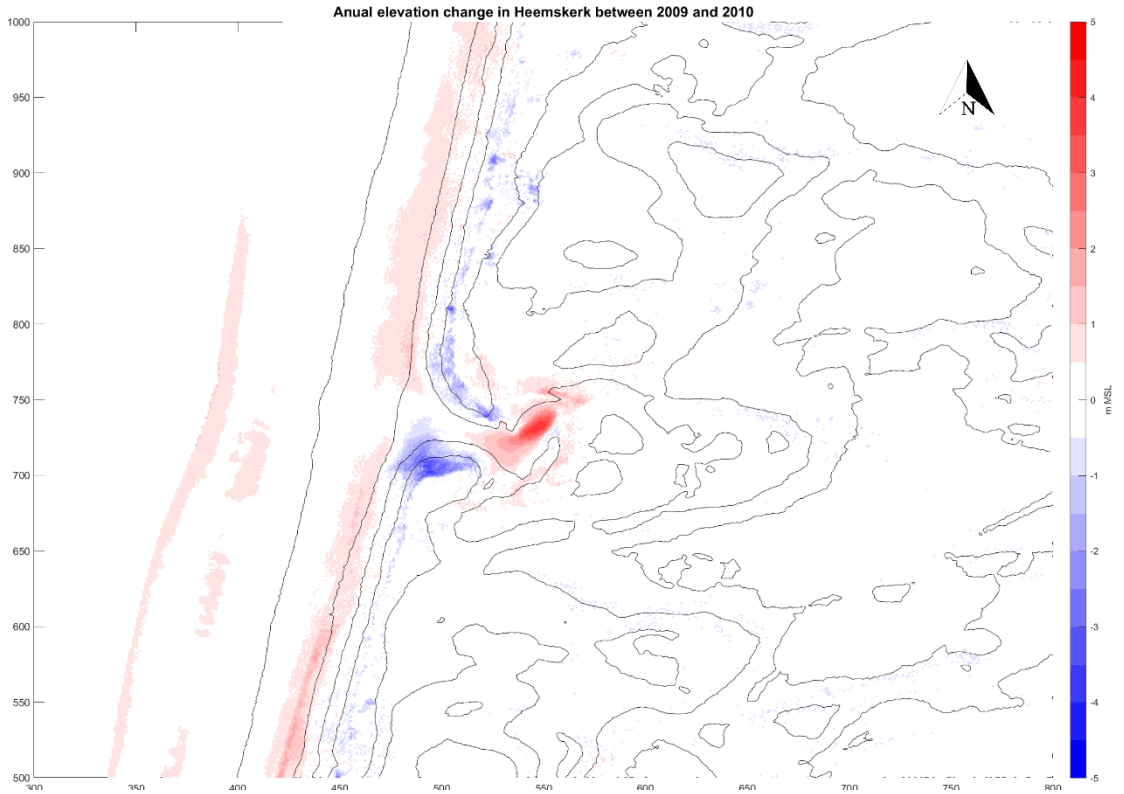
Anual elevation change in Heemskerk between 2009 and 2010
N
m MSL

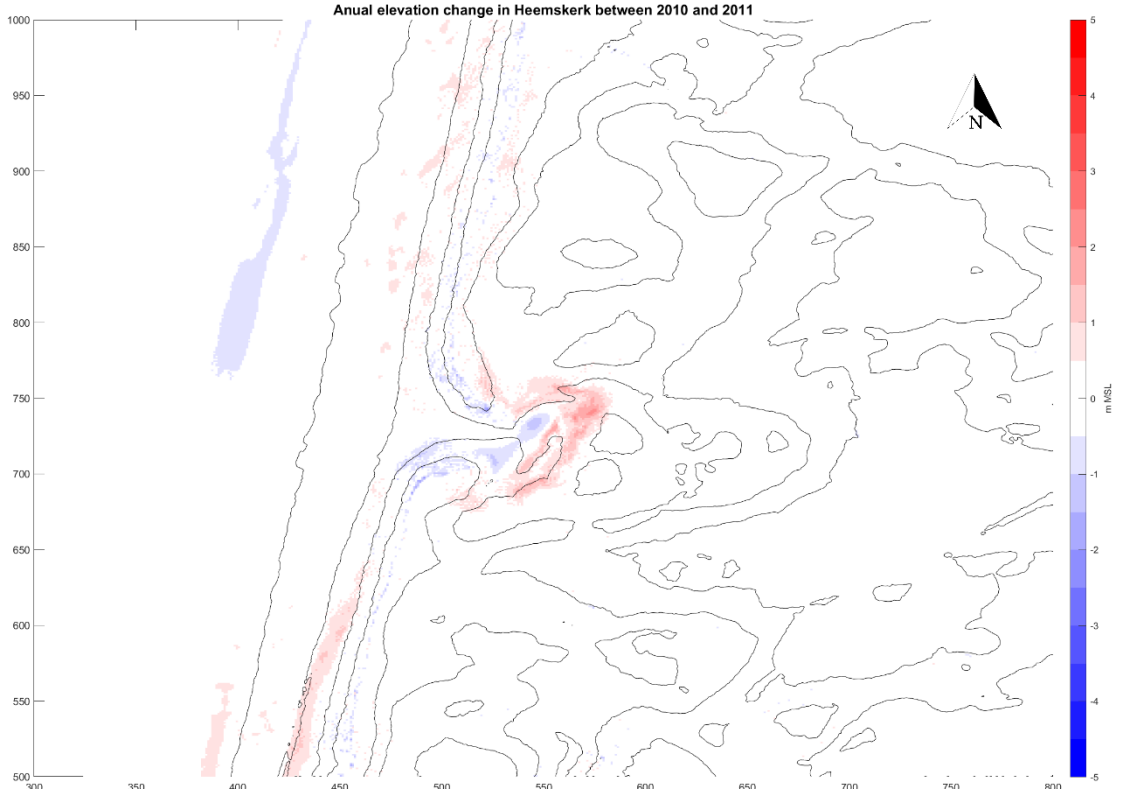
Anual elevation change in Heemskerk between 2010 and 2011
N
m MSL

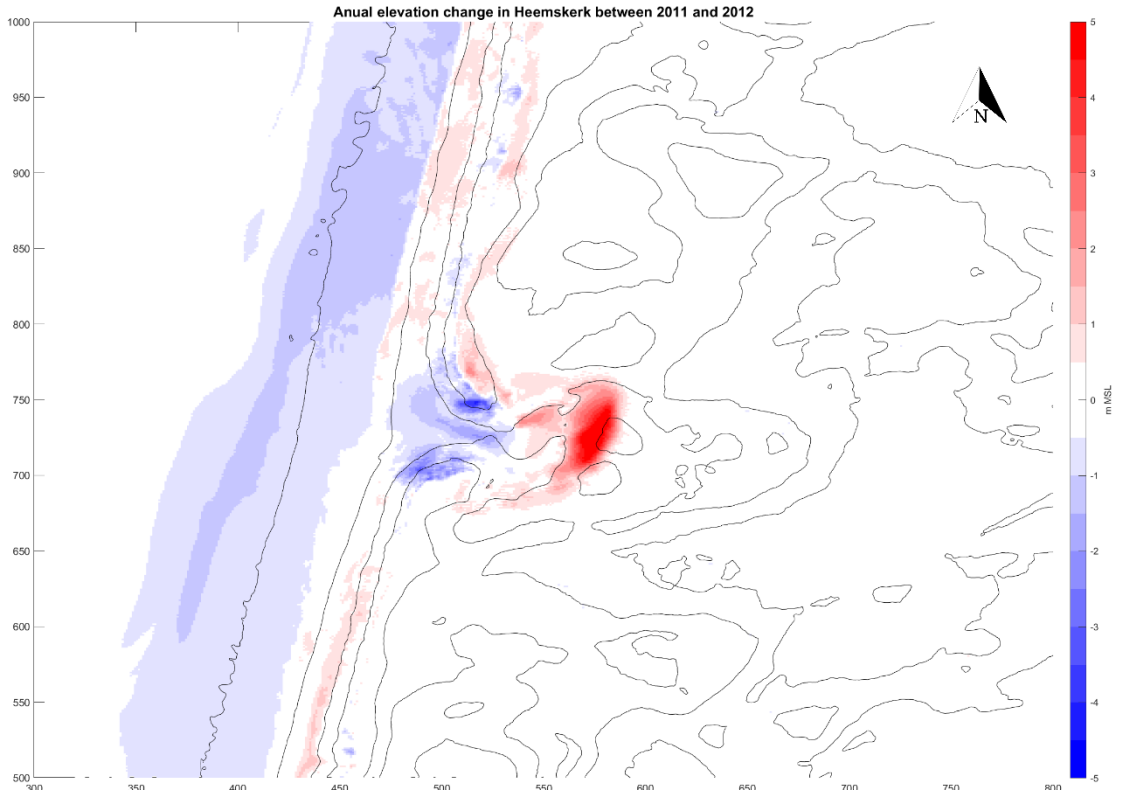
Anual elevation change in Heemskerk between 2011 and 2012
N
m MSL

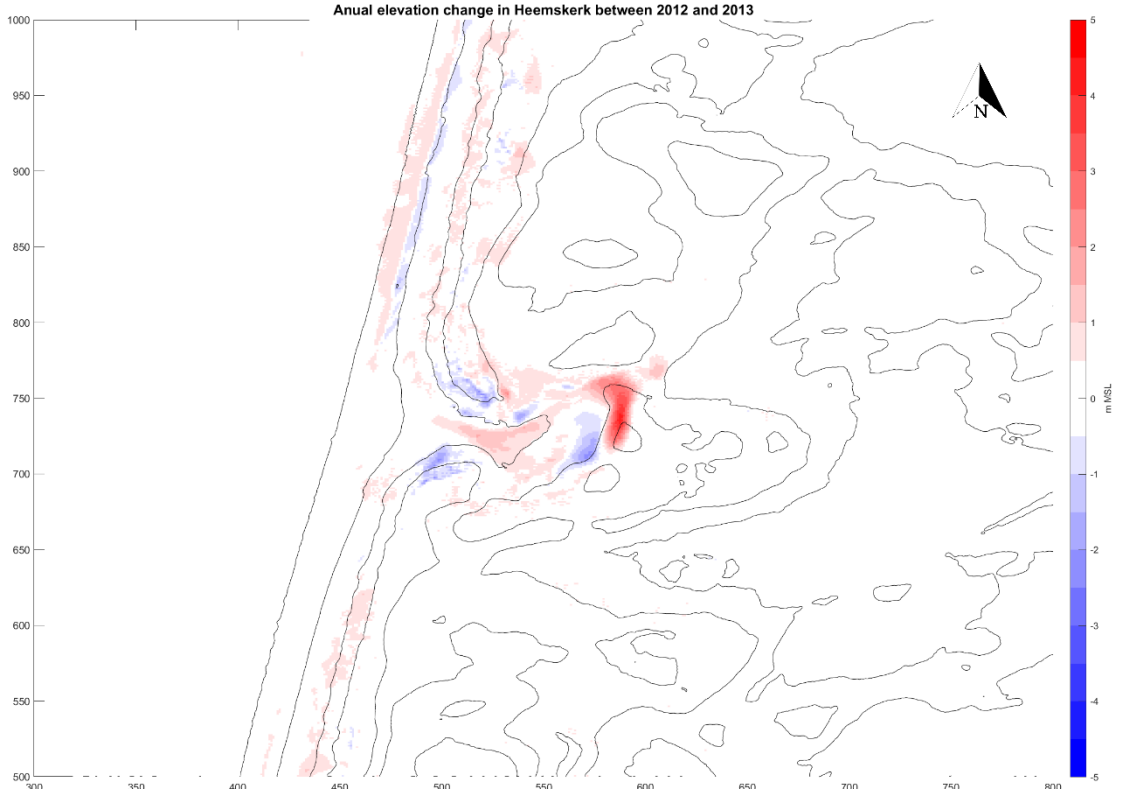
Anual elevation change in Heemskerk between 2012 and 2013
N
m MSL

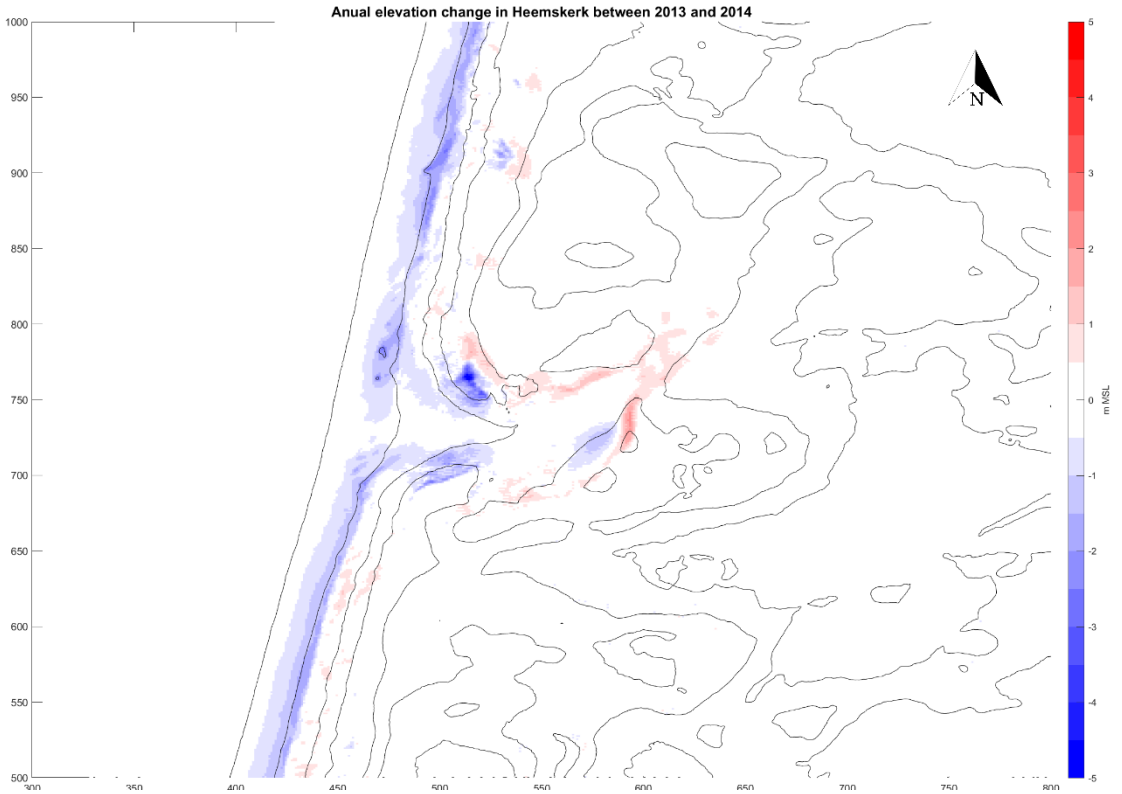
Anual elevation change in Heemskerk between 2013 and 2014
N
m MSL

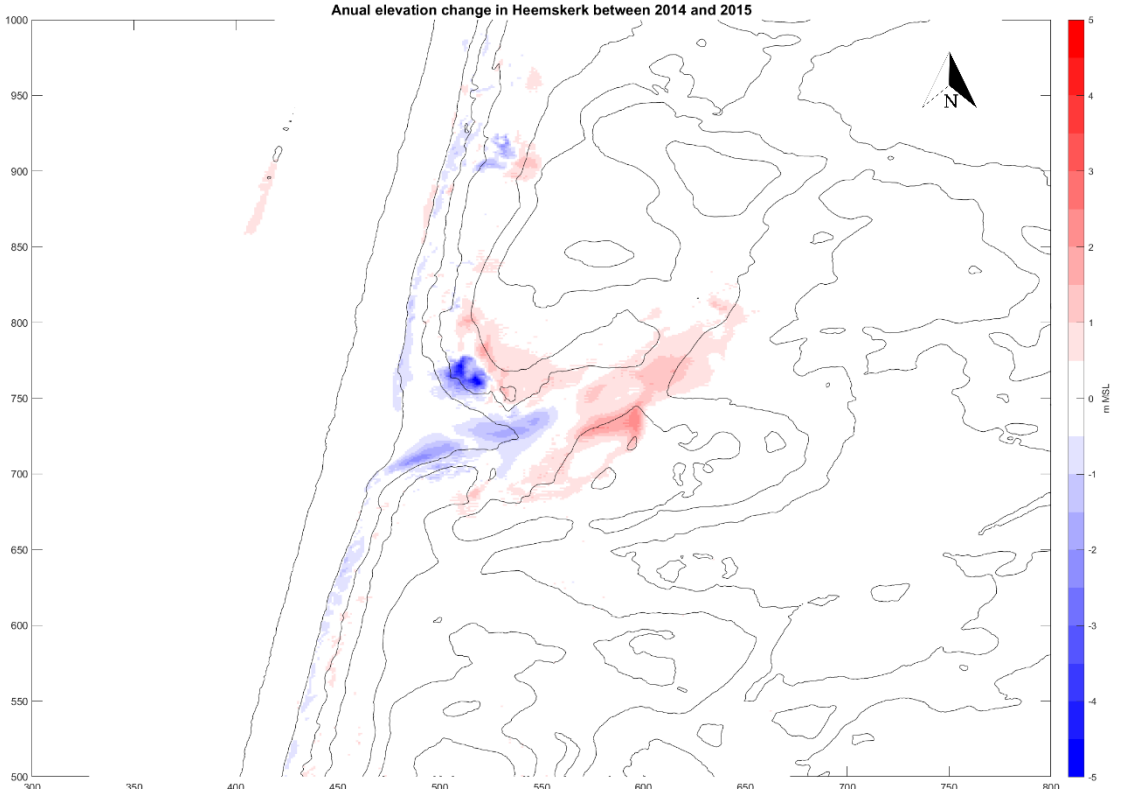
Anual elevation change in Heemskerk between 2014 and 2015
N
m MSL

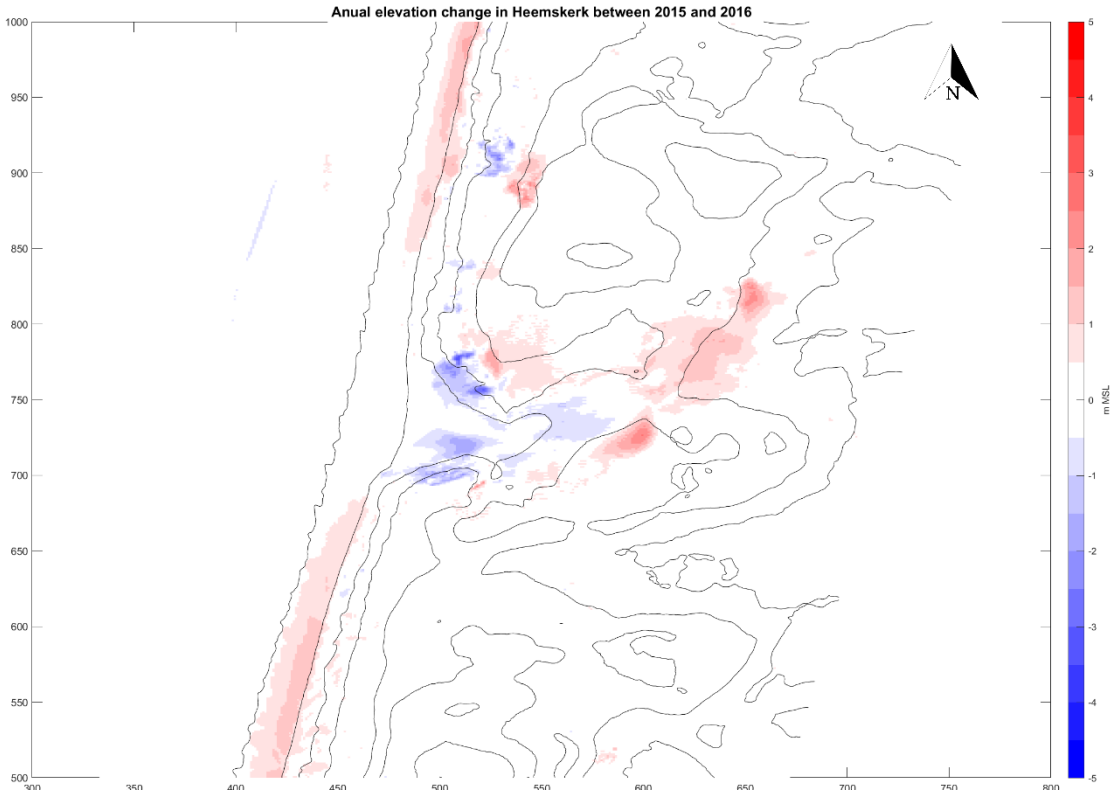
Anual elevation change in Heemskerk between 2015 and 2016
N
m WSL

Lidar: Change during 2006-2016 at Heemskerk

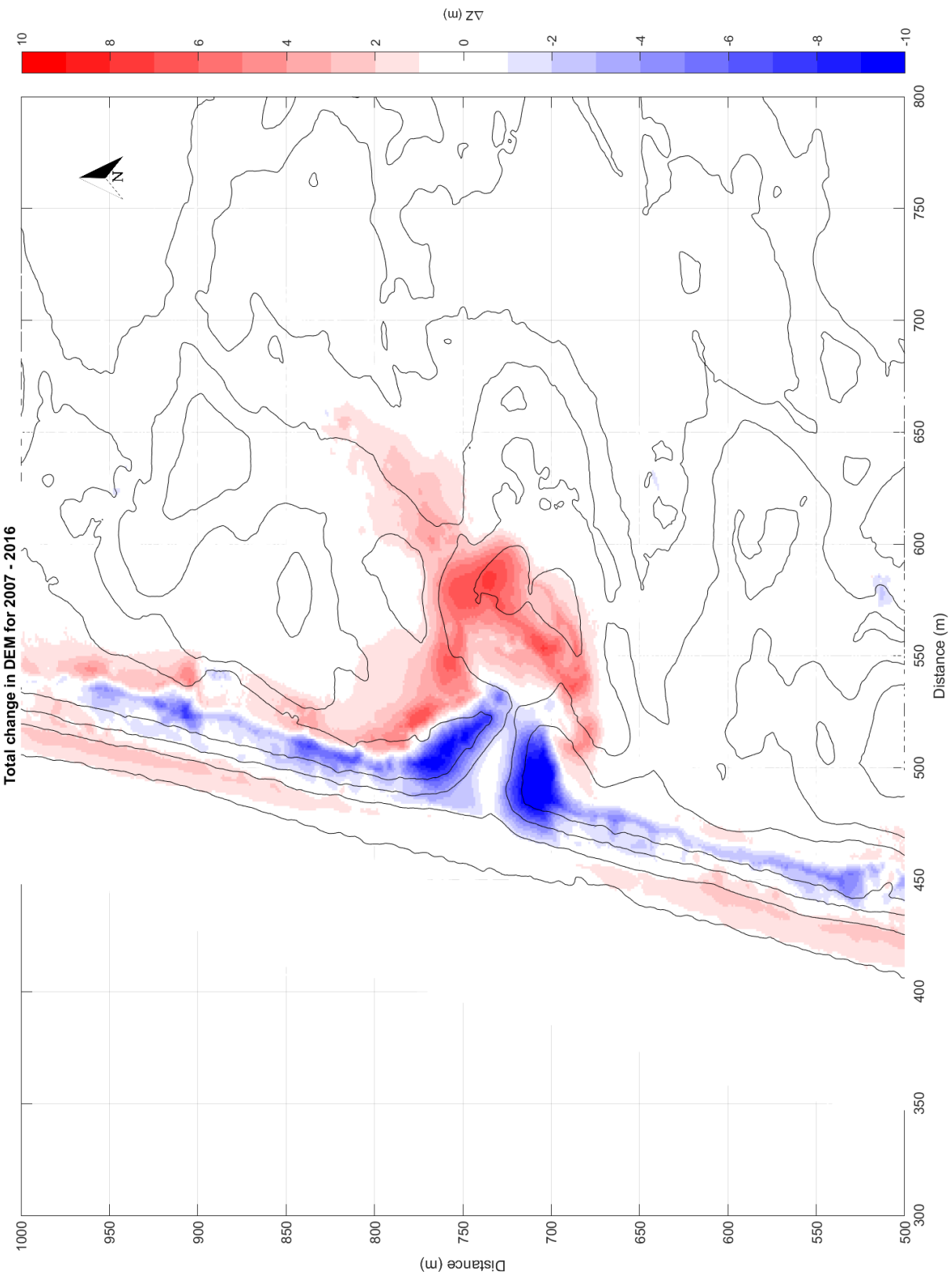

Locations of profiles at Heemskerk

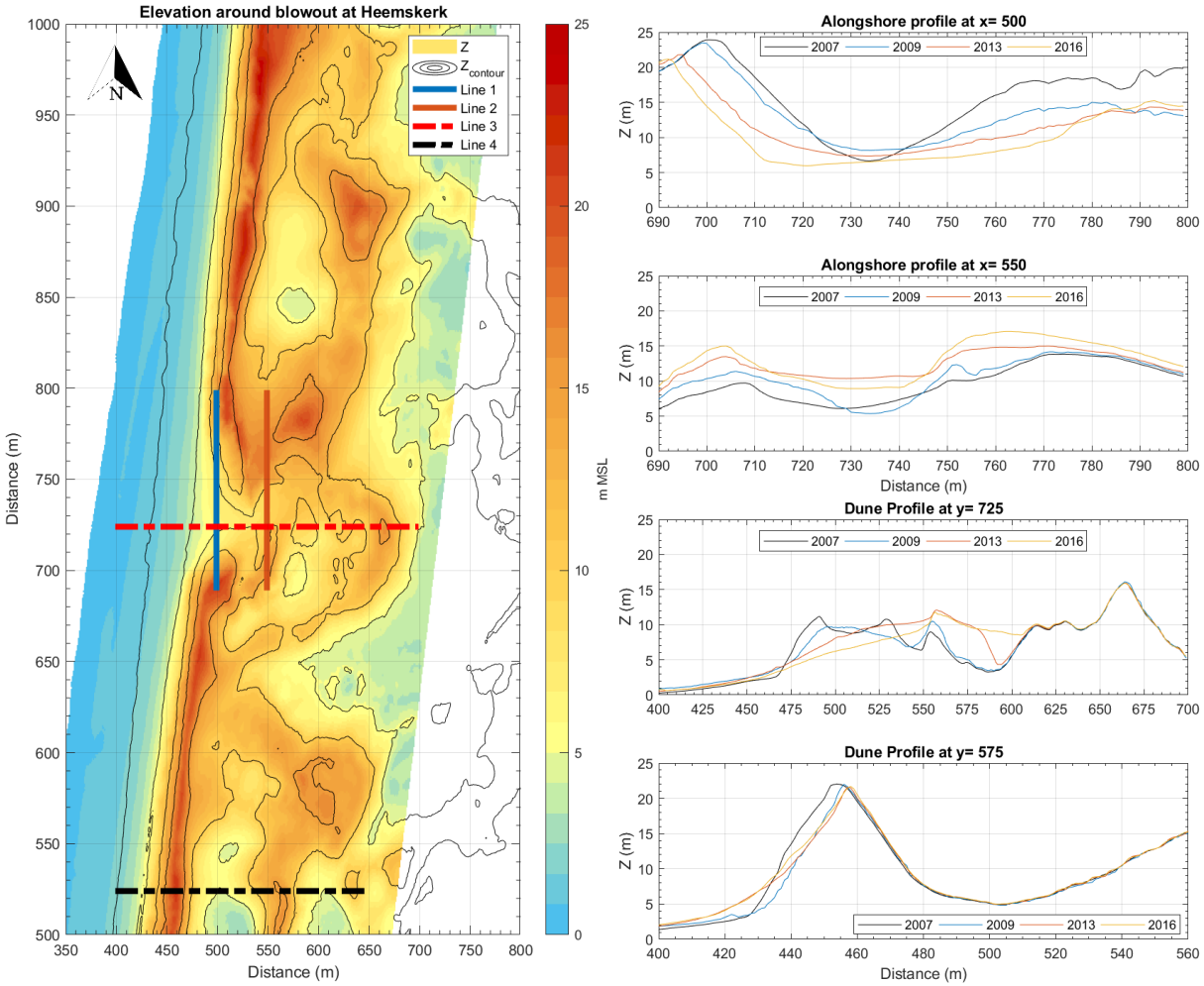

Volume regions at Heemskerk

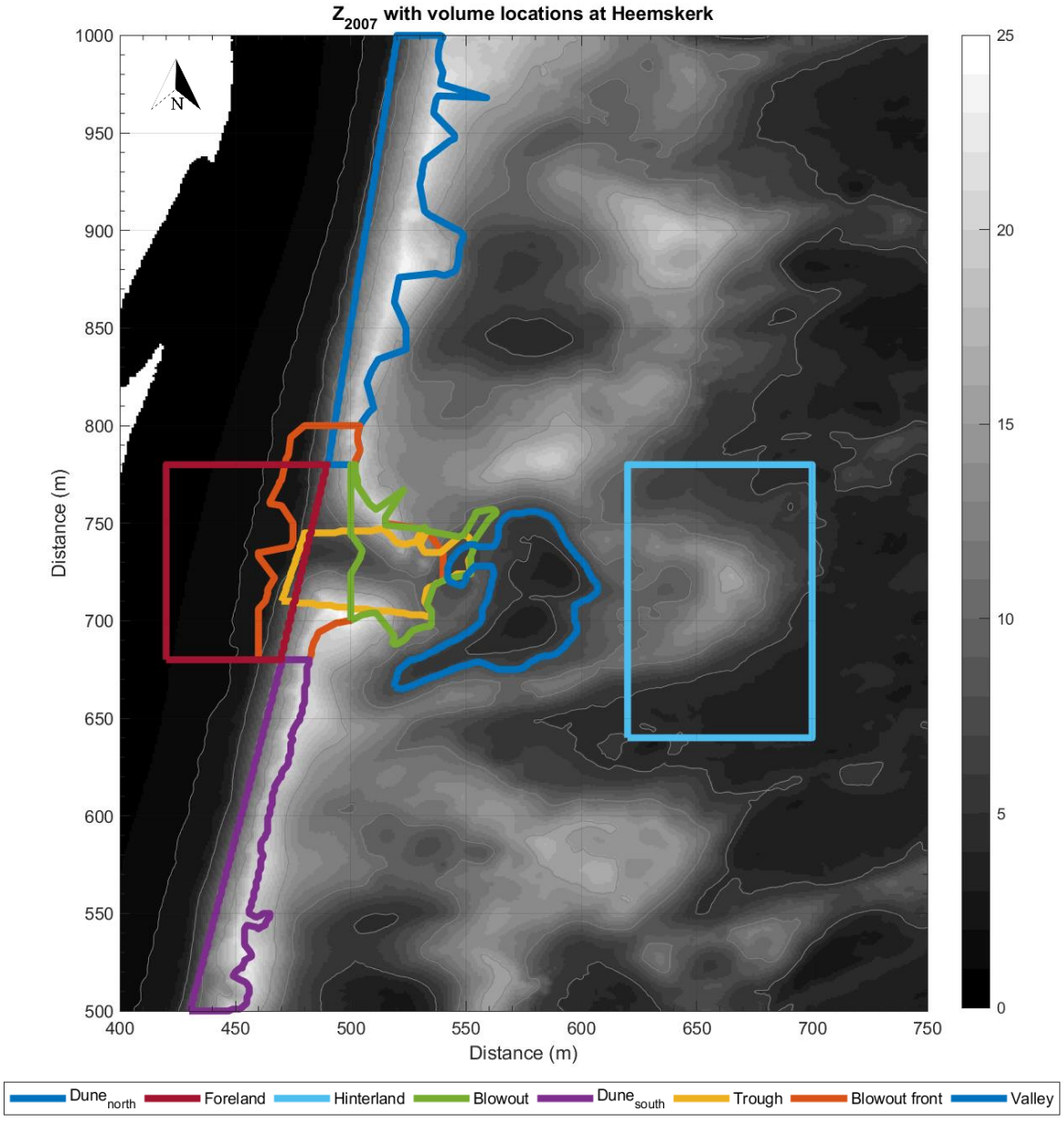

NDVI of Terschelling

Regions of Interest

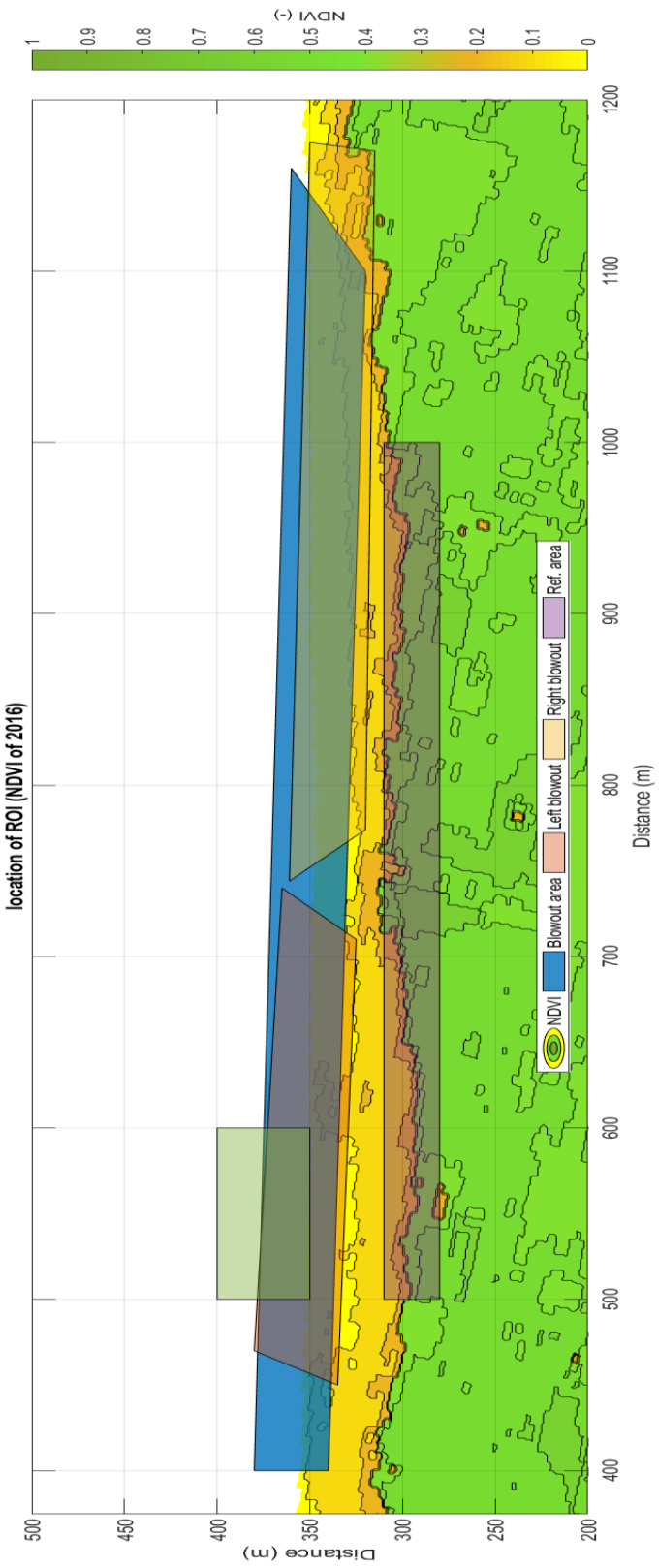

Annual average NDVI

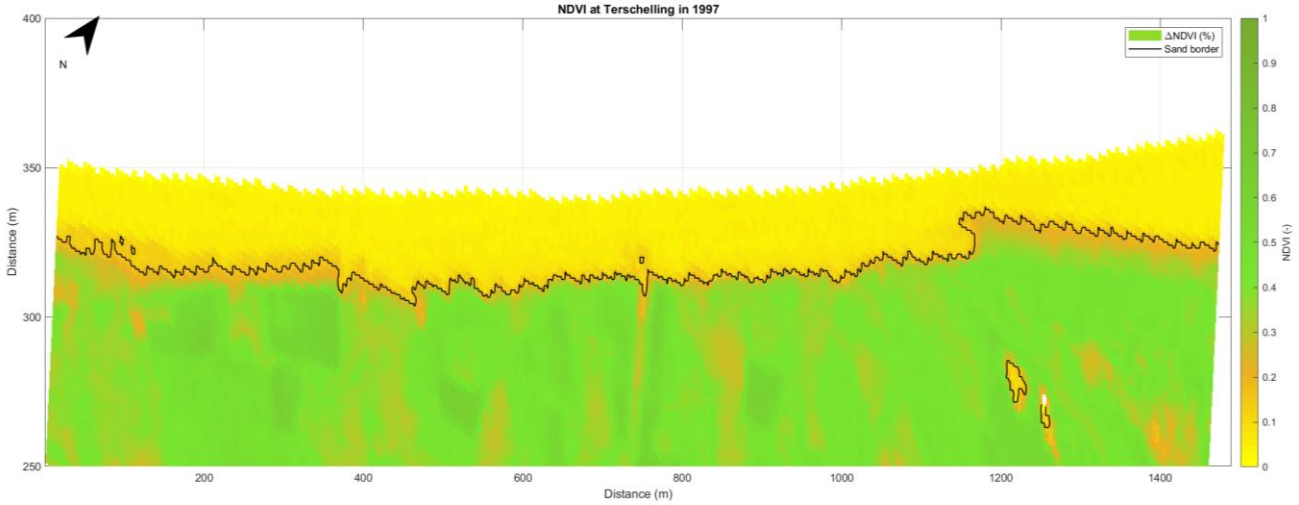

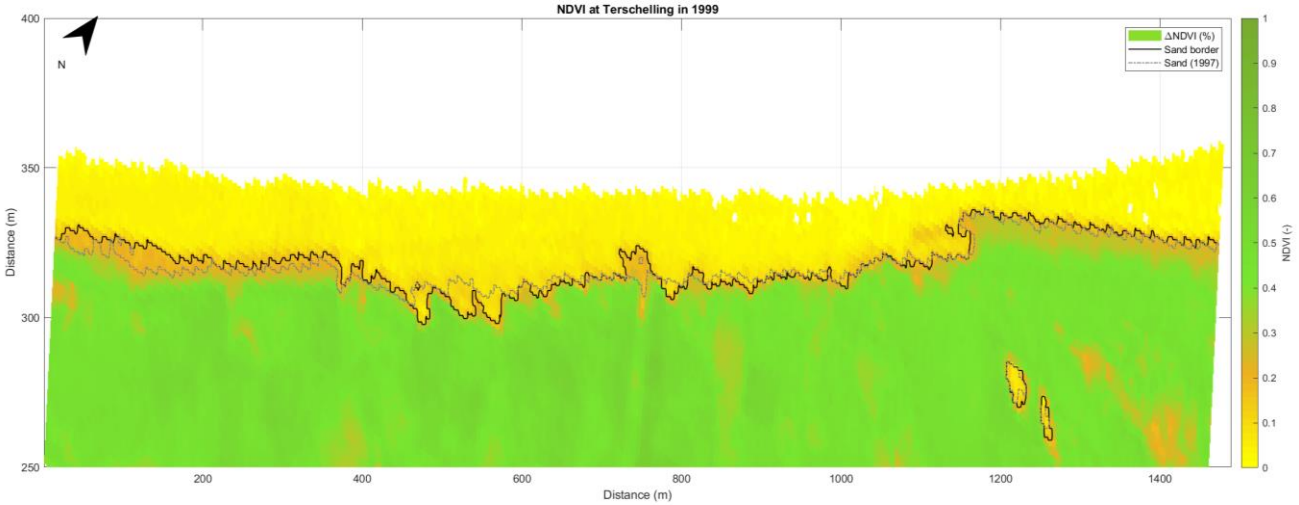

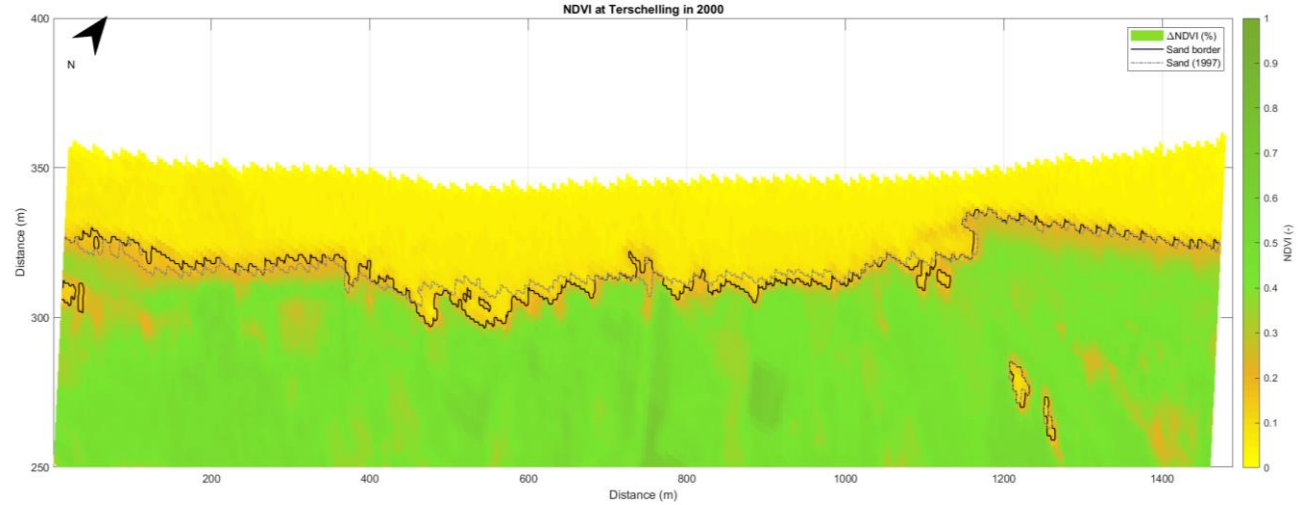

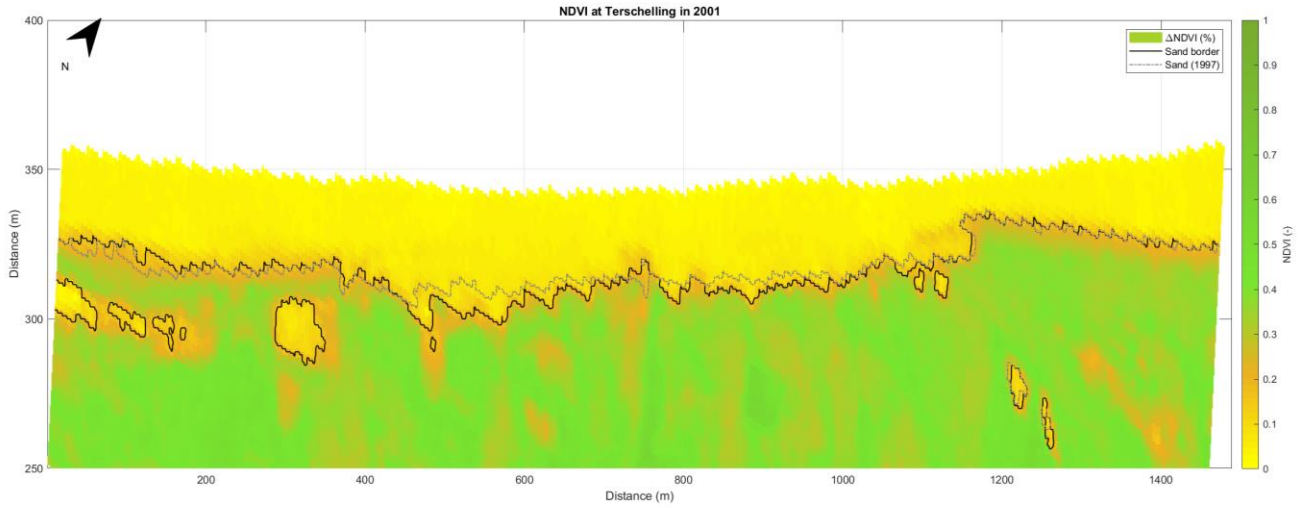
NDVI at Terschelling in 2001
N
ΔNDVI (%)
Sand border
Sand (1997)
Distance (m)
NDVI (-)

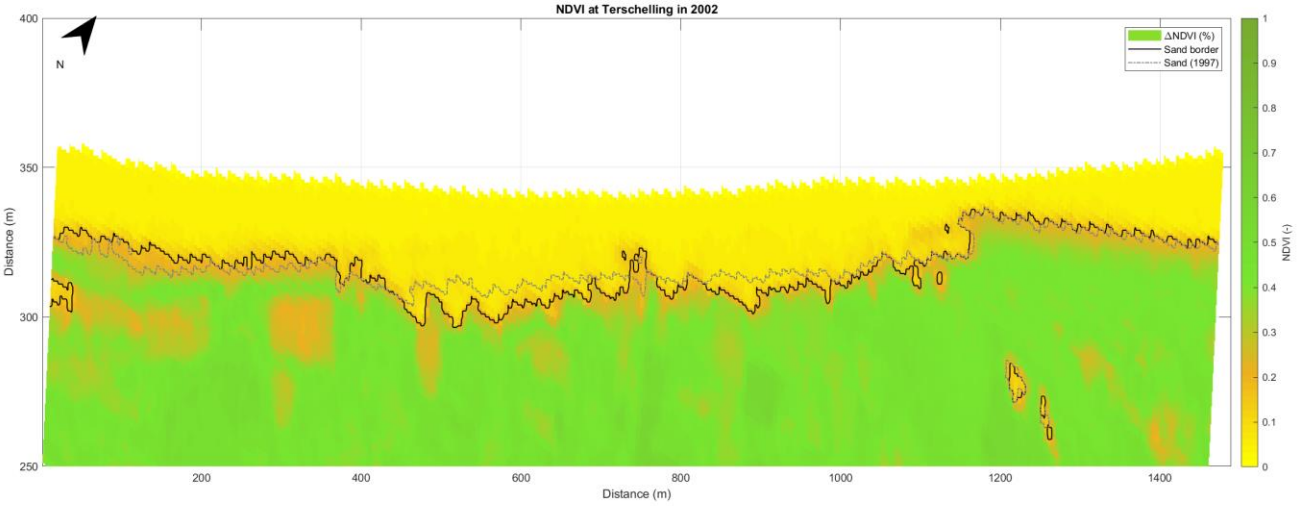
NDVI at Terschelling in 2002
N
ΔNDVI (%)
Sand border
Sand (1997)
Distance (m)
NDVI (-)

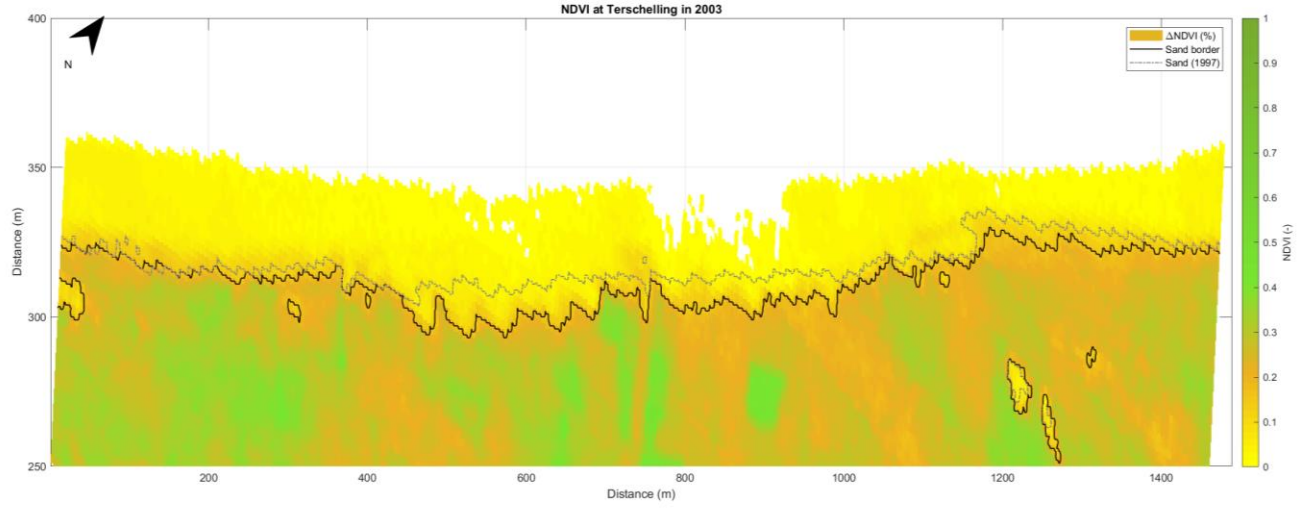
NDVI at Terschelling in 2003
N
ΔNDVI (%)
Sand border
Sand (1997)
Distance (m)
NDVI (-)

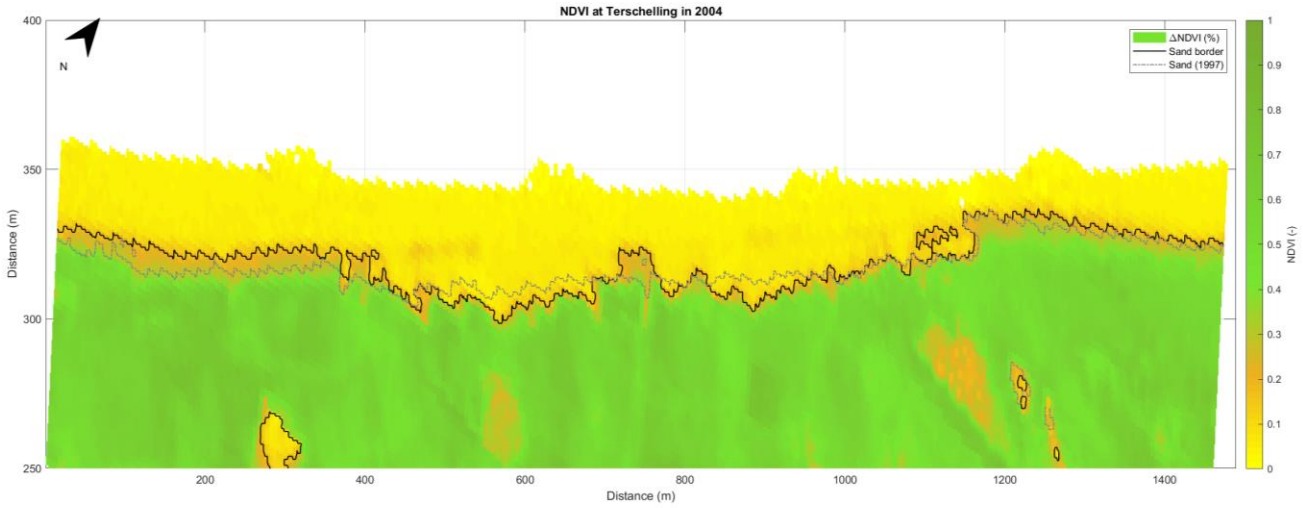
NDVI at Terschelling in 2004
N
ΔNDVI (%)
Sand border
Sand (1997)
Distance (m)
NDVI (-)

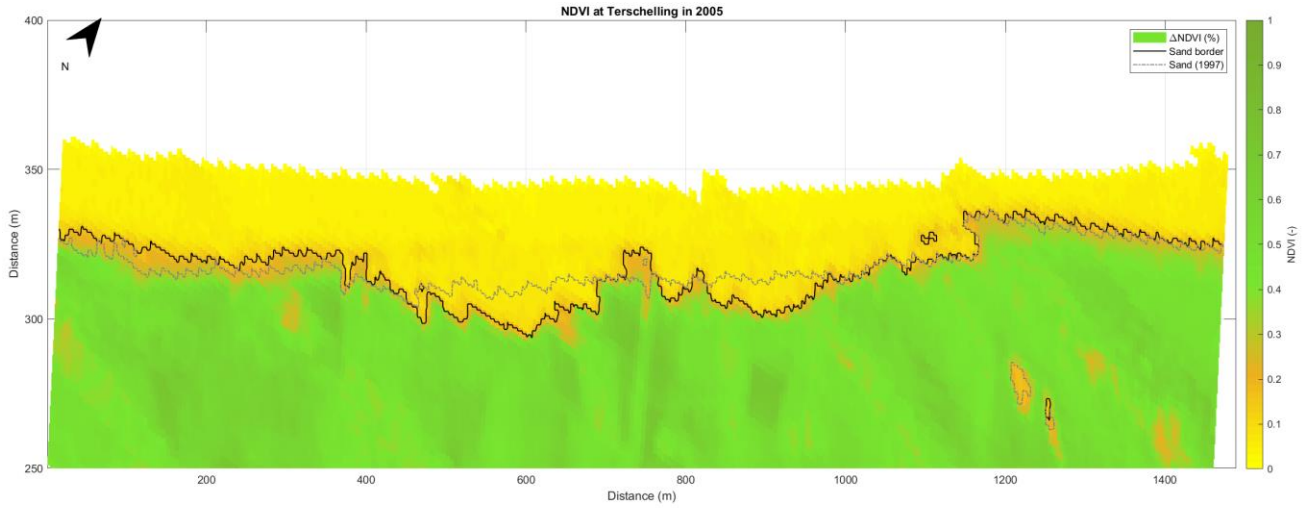
NDVI at Terschelling in 2005
N
ΔNDVI (%)
Sand border
Sand (1997)
Distance (m)
NDVI (-)

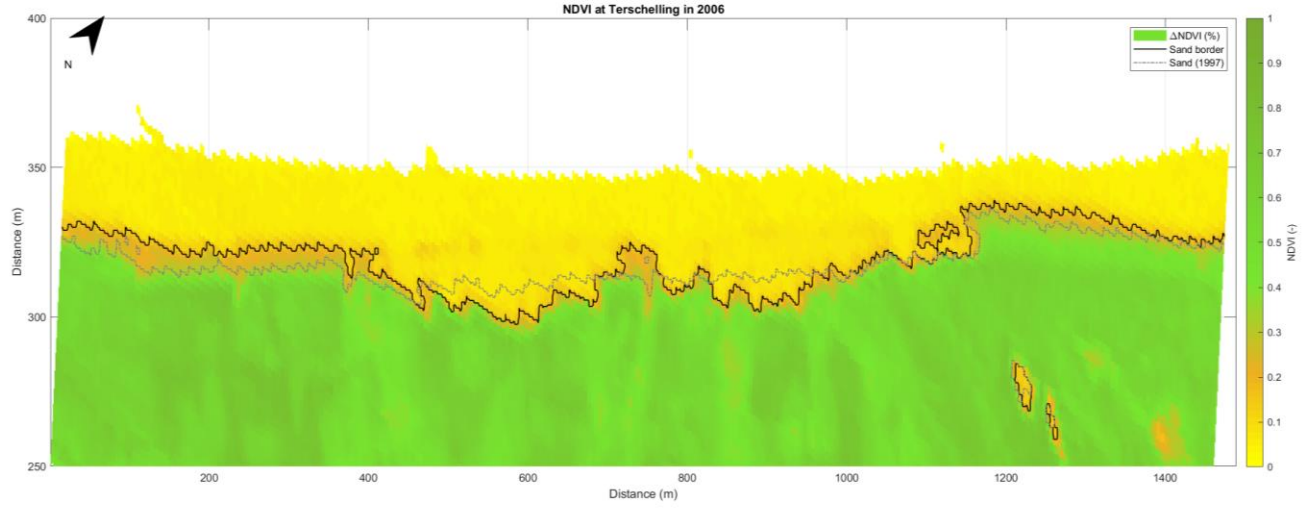
NDVI at Terschelling in 2006
N
ΔNDVI (%)
Sand border
Sand (1997)
Distance (m)
NDVI (-)

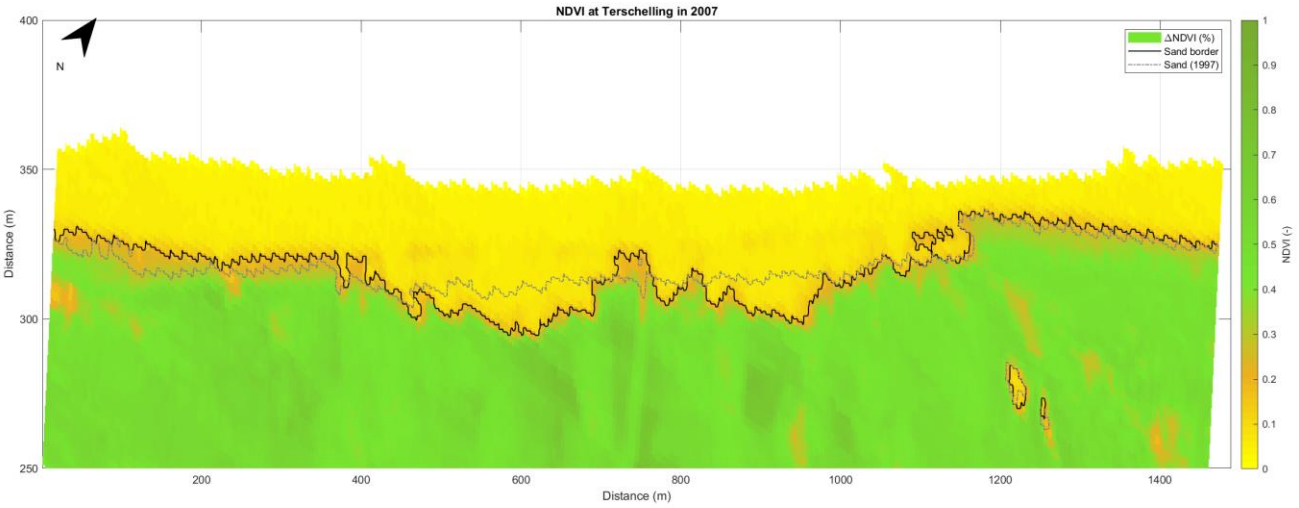
NDVI at Terschelling in 2007
N
ΔNDVI (%)
Sand border
Sand (1997)
Distance (m)
NDVI (-)
400
350
300
250
200
400
600
800
1000
1200
1400
0
0.1
0.2
0.3
0.4
0.5
0.6
0.7
0.8
0.9
1

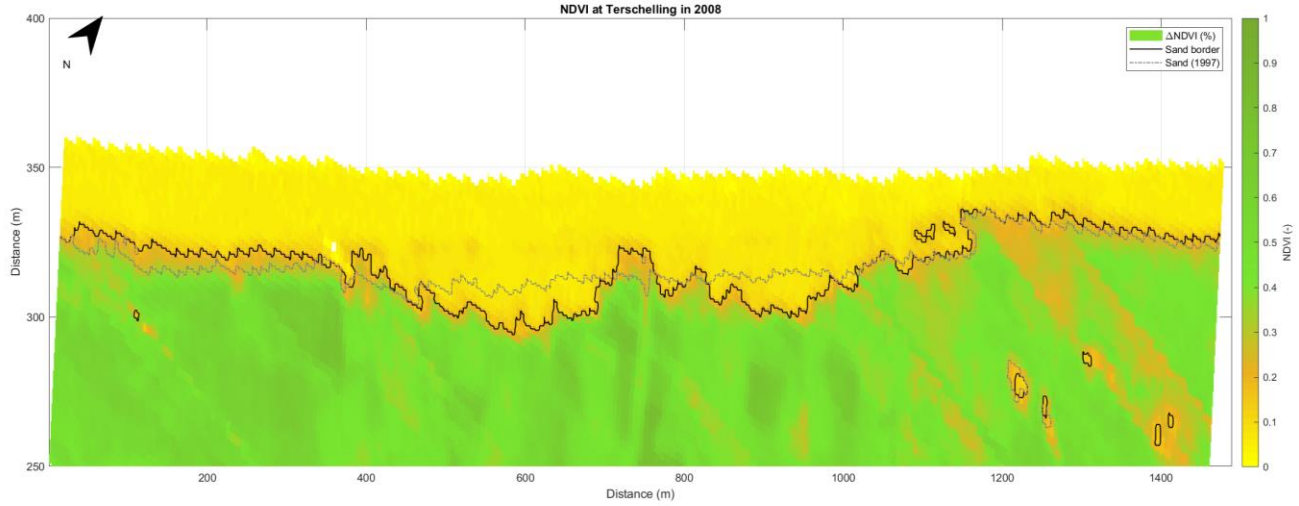
NDVI at Terschelling in 2008
N
ΔNDVI (%)
Sand border
Sand (1997)
Distance (m)
NDVI (-)
400
350
300
250
200
400
600
800
1000
1200
1400
0
0.1
0.2
0.3
0.4
0.5
0.6
0.7
0.8
0.9
1

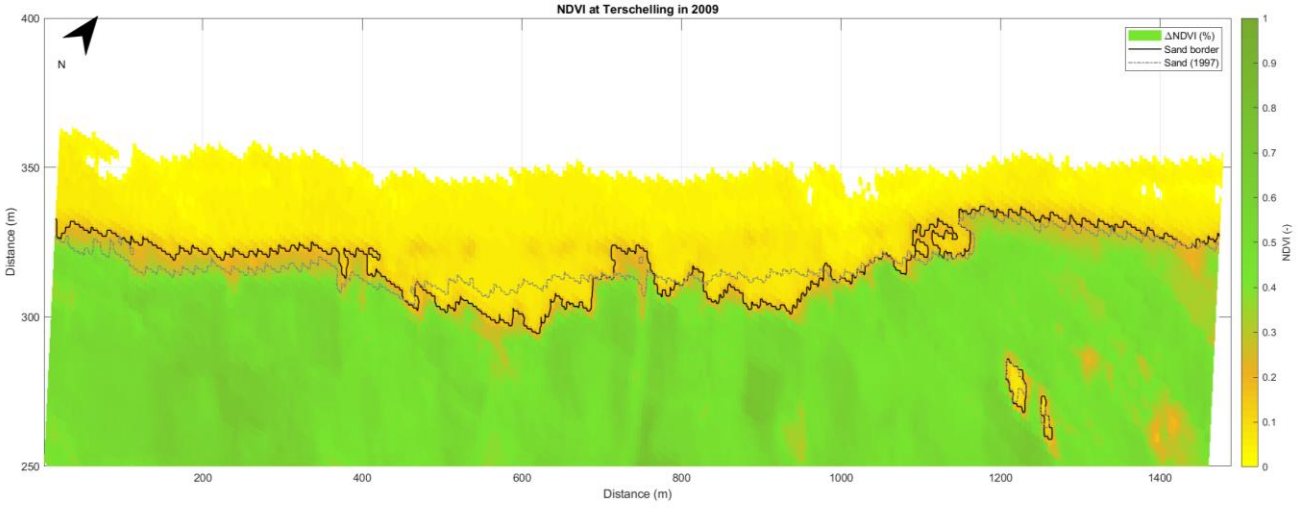
NDVI at Terschelling in 2009
N
ΔNDVI (%)
Sand border
Sand (1997)
Distance (m)
NDVI (-)
400
350
300
250
200
400
600
800
1000
1200
1400
0
0.1
0.2
0.3
0.4
0.5
0.6
0.7
0.8
0.9
1

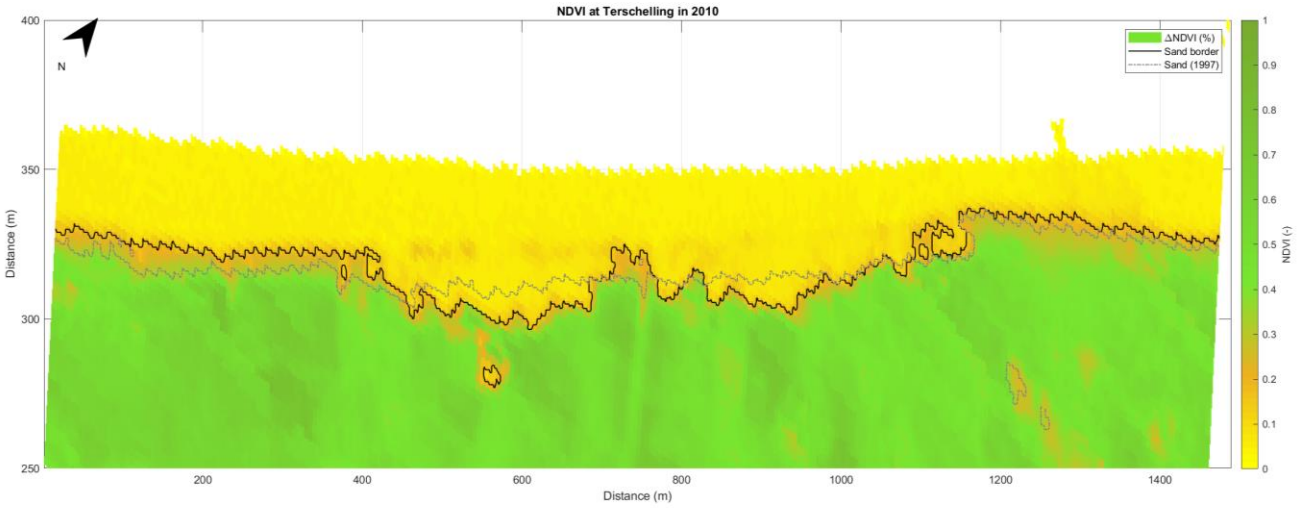
NDVI at Terschelling in 2010
N
ΔNDVI (%)
Sand border
Sand (1997)
Distance (m)
Distance (m)
NDVI (-)

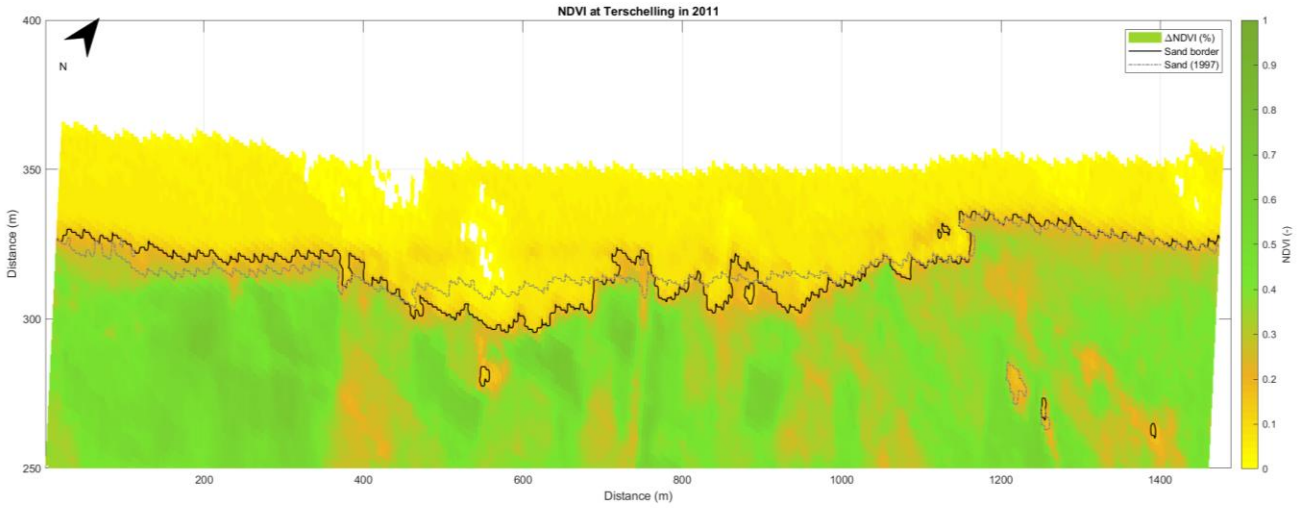
NDVI at Terschelling in 2011
N
ΔNDVI (%)
Sand border
Sand (1997)
Distance (m)
Distance (m)
NDVI (-)

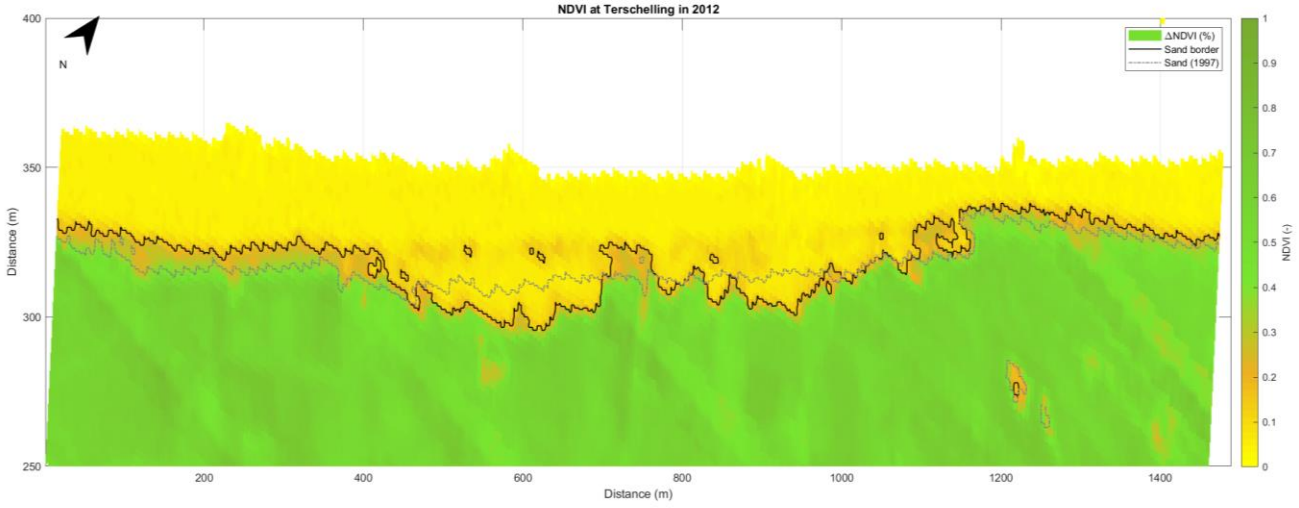
NDVI at Terschelling in 2012
N
ΔNDVI (%)
Sand border
Sand (1997)
Distance (m)
Distance (m)
NDVI (-)

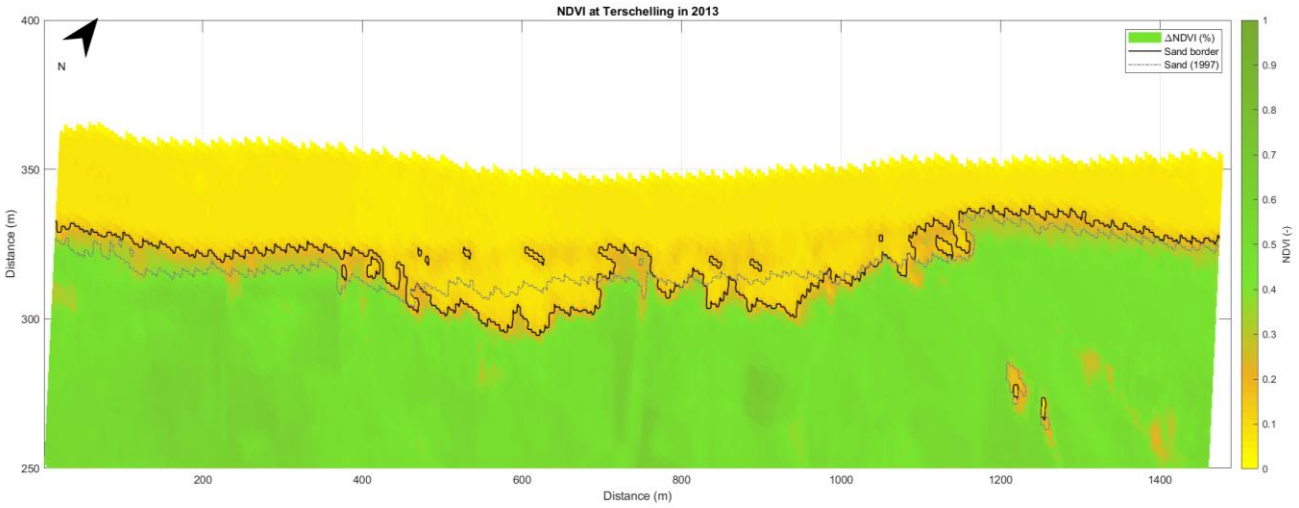
NDVI at Terschelling in 2013
N
ΔNDVI (%)
Sand border
Sand (1997)
Distance (m)
Distance (m)
NDVI (-)

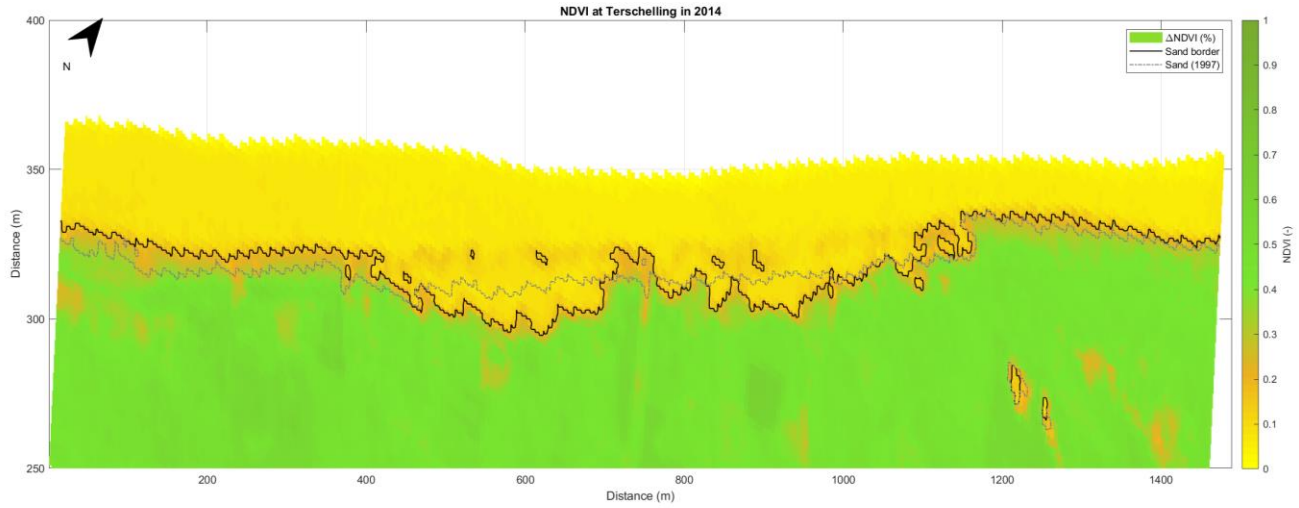
NDVI at Terschelling in 2014
N
ΔNDVI (%)
Sand border
Sand (1997)
Distance (m)
Distance (m)
NDVI (-)

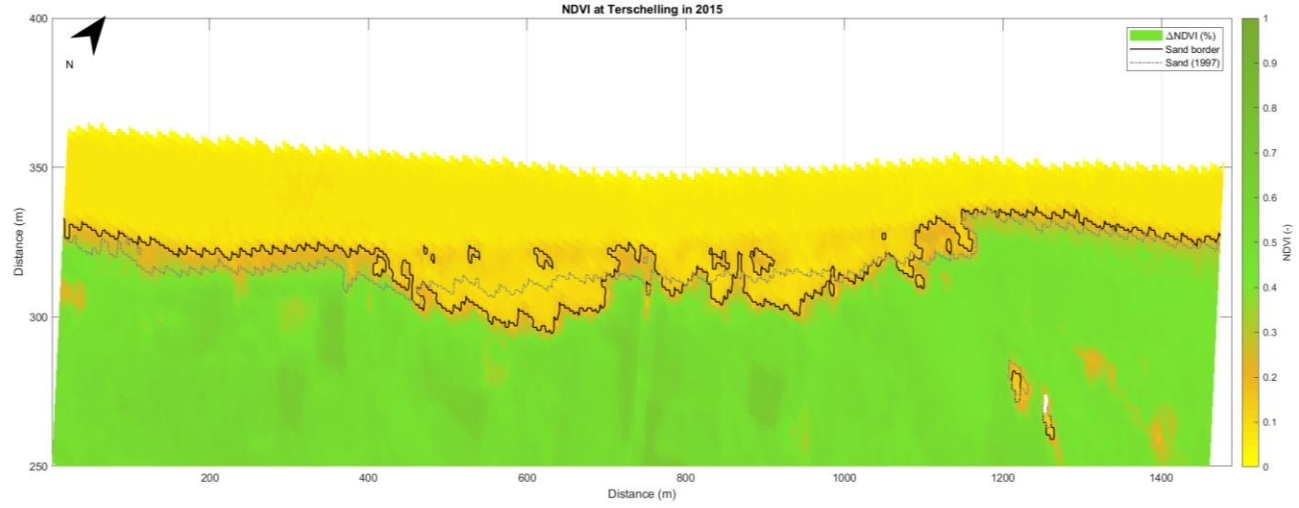
NDVI at Terschelling in 2015
N
ΔNDVI (%)
Sand border
Sand (1997)
Distance (m)
Distance (m)
NDVI (-)

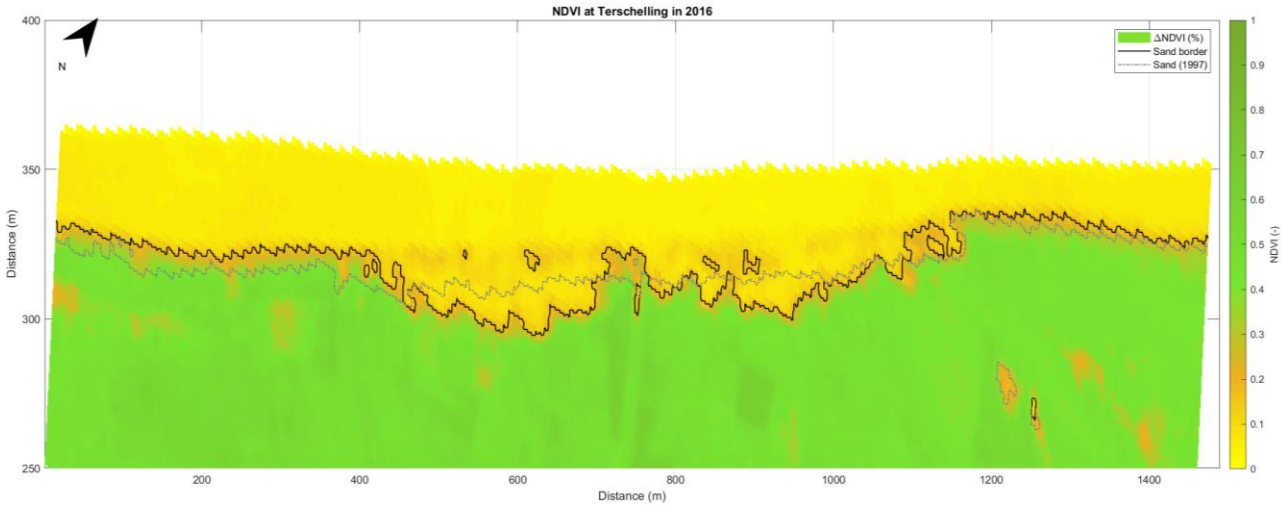
NDVI at Terschelling in 2016
N
ΔNDVI (%)
Sand border
Sand (1997)
Distance (m)
Distance (m)
NDVI (-)
400
350
300
250
200
400
600
800
1000
1200
1400
1
0.9
0.8
0.7
0.6
0.5
0.4
0.3
0.2
0.1
0

Annual change in NDVI

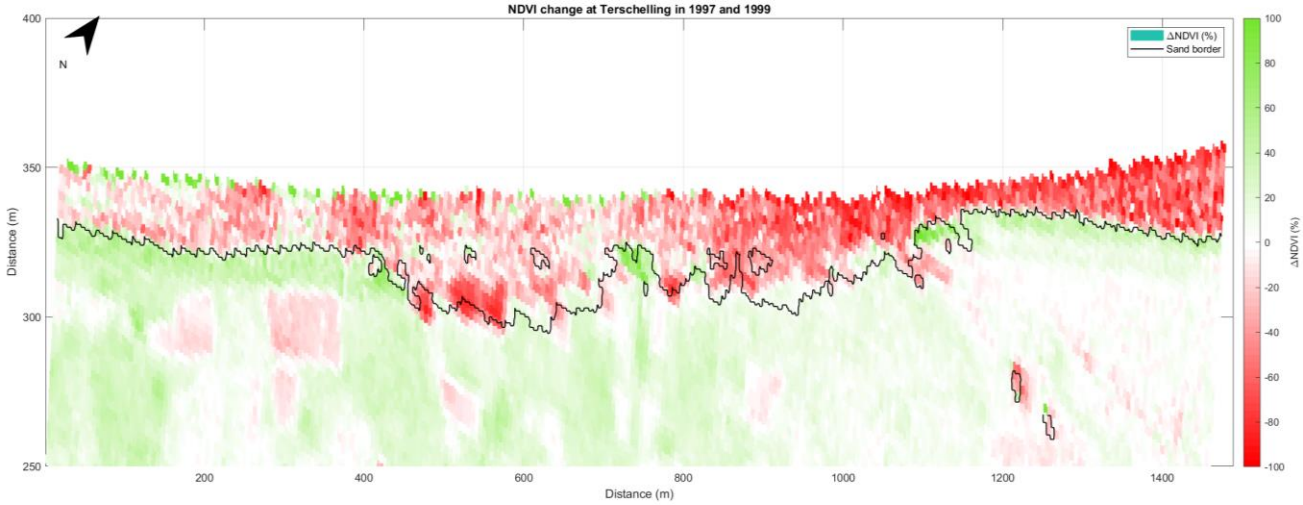

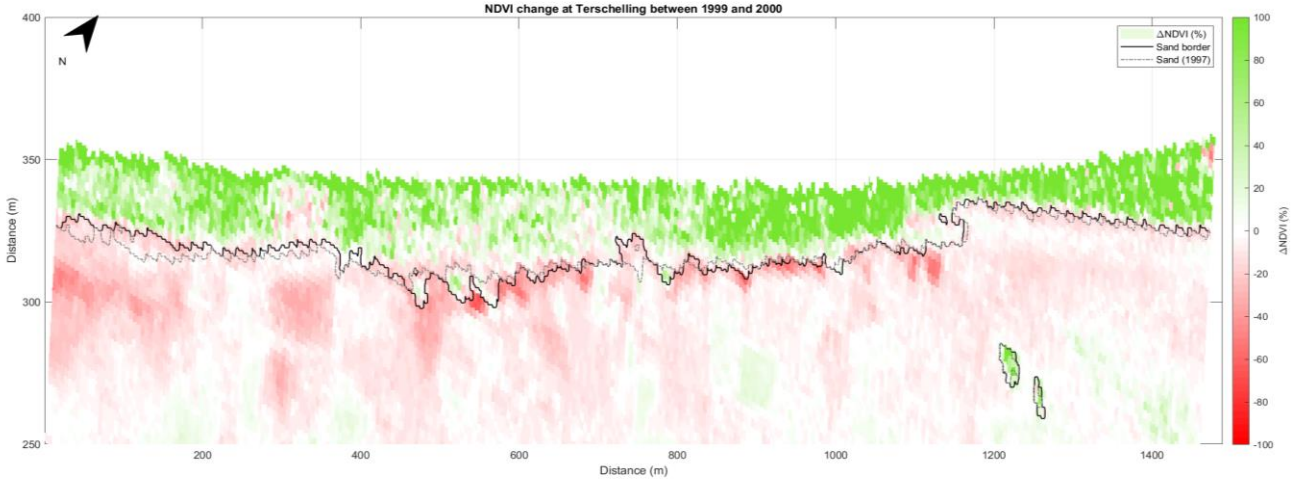

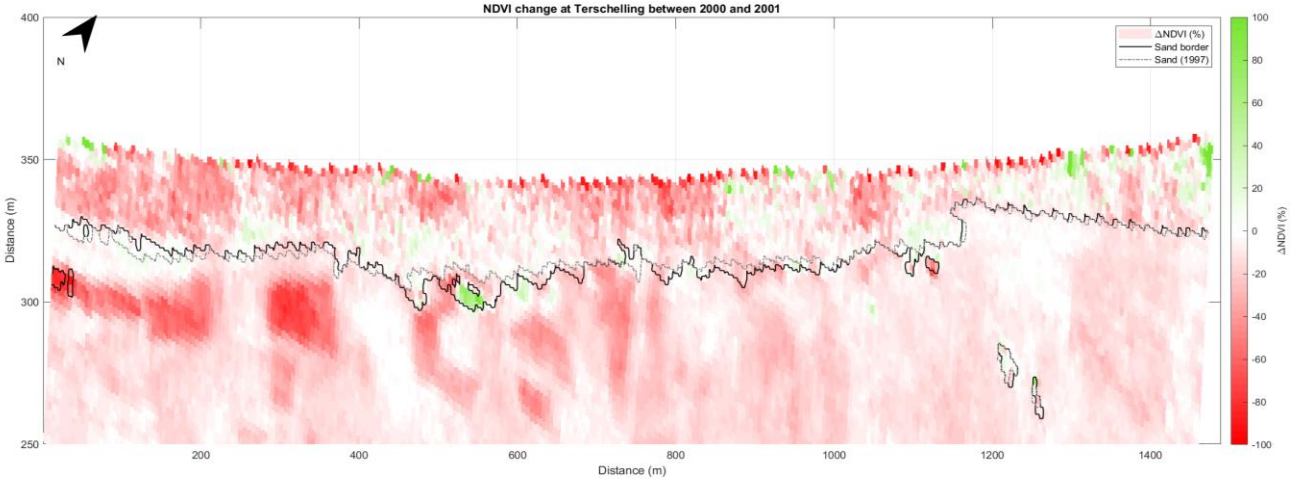

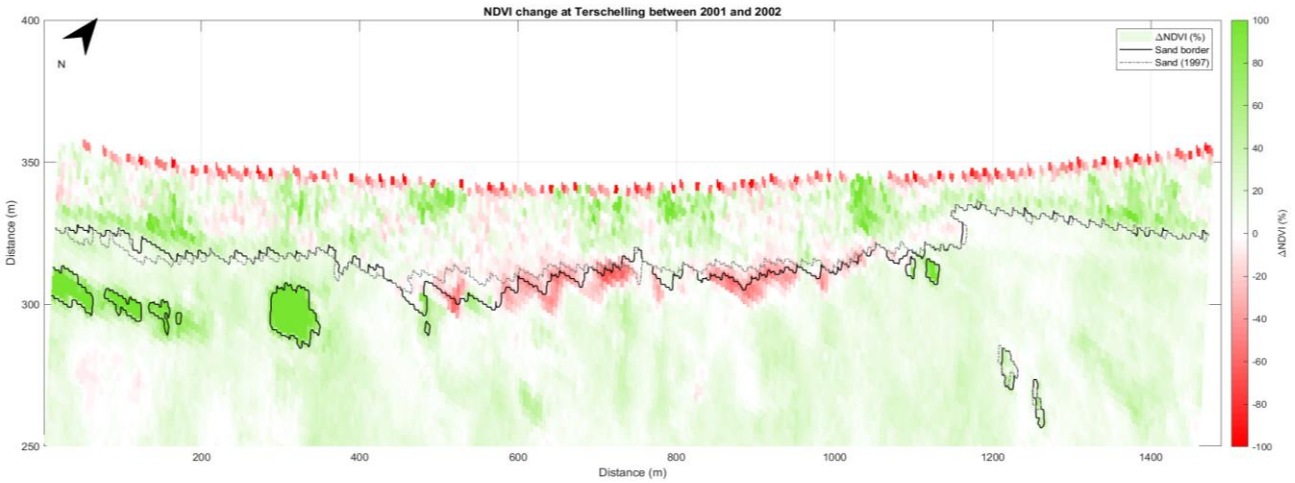
NDVI change at Terschelling between 2001 and 2002
N
ΔNDVI (%)
Sand border
Sand (1997)
Distance (m)
Distance (m)
ΔNDVI (%)

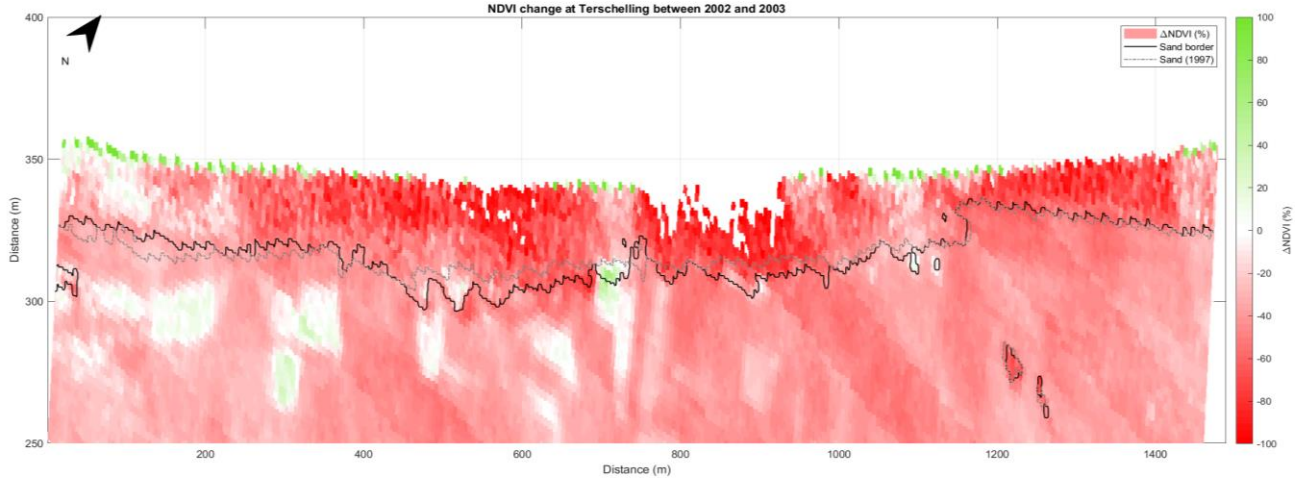
NDVI change at Terschelling between 2002 and 2003
N
ΔNDVI (%)
Sand border
Sand (1997)
Distance (m)
Distance (m)
ΔNDVI (%)

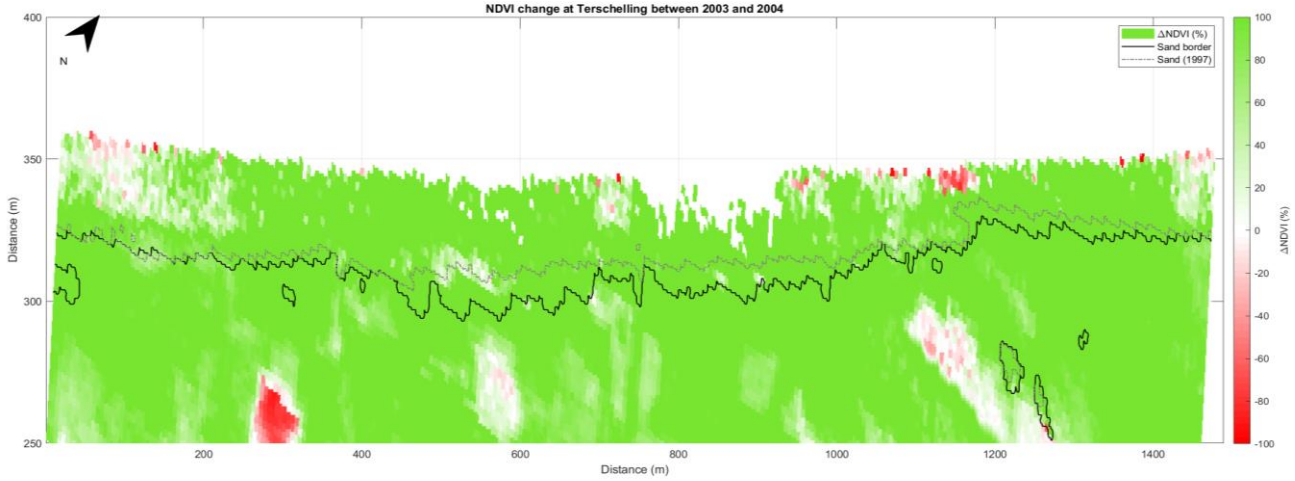
NDVI change at Terschelling between 2003 and 2004
N
ΔNDVI (%)
Sand border
Sand (1997)
Distance (m)
Distance (m)
ΔNDVI (%)

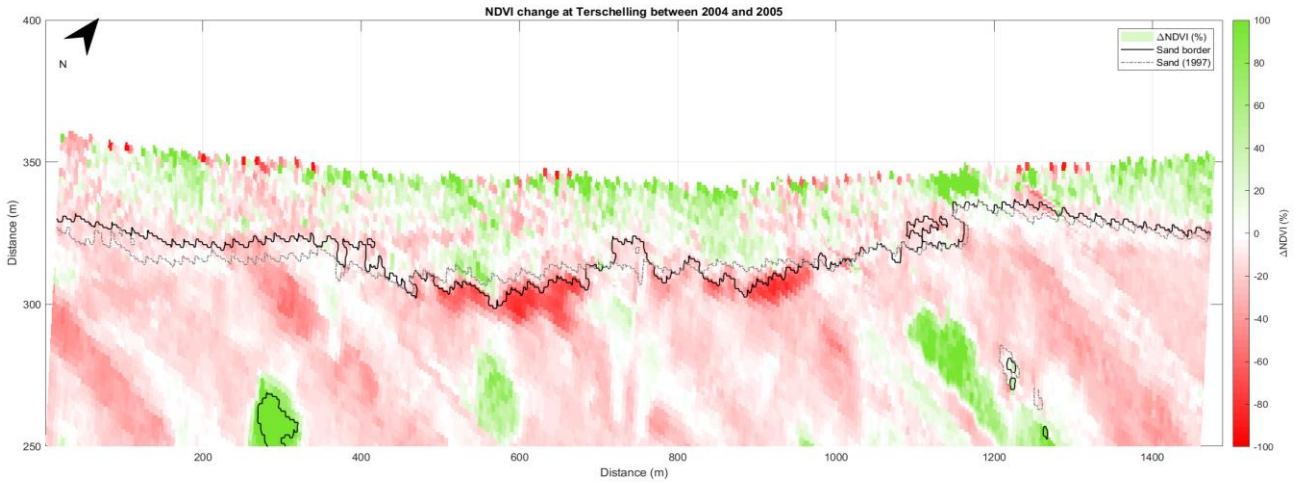
NDVI change at Terschelling between 2004 and 2005
N
ΔNDVI (%)
Sand border
Sand (1997)
Distance (m)
Distance (m)
ΔNDVI (%)

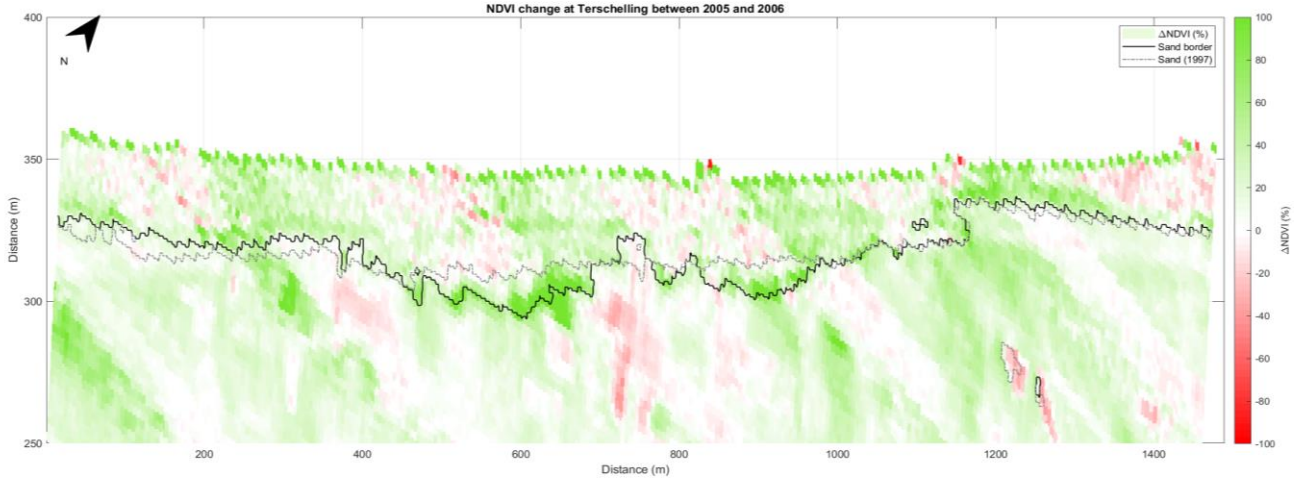
NDVI change at Terschelling between 2005 and 2006
N
ΔNDVI (%)
Sand border
Sand (1997)
Distance (m)
Distance (m)
ΔNDVI (%)

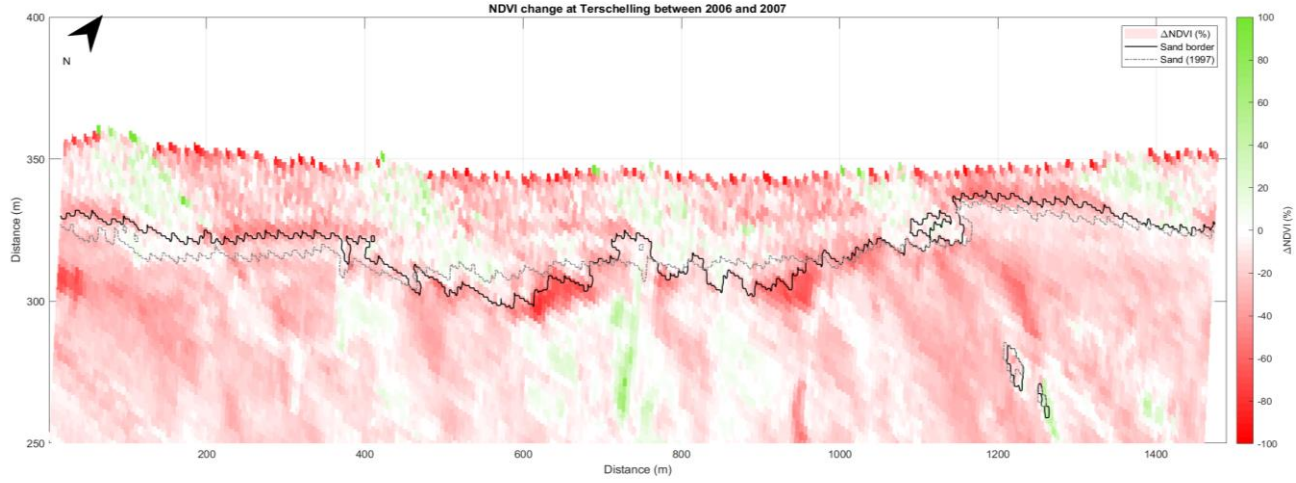
NDVI change at Terschelling between 2006 and 2007
N
ΔNDVI (%)
Sand border
Sand (1997)
Distance (m)
Distance (m)
ΔNDVI (%)

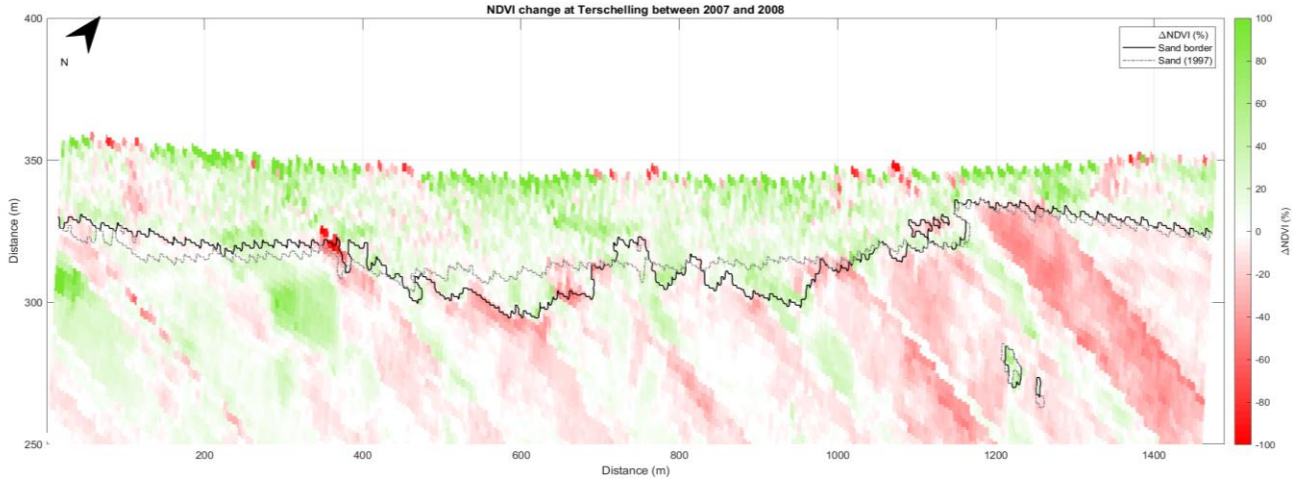
NDVI change at Terschelling between 2007 and 2008
N
ΔNDVI (%)
Sand border
Sand (1997)
Distance (m)
Distance (m)
ΔNDVI (%)

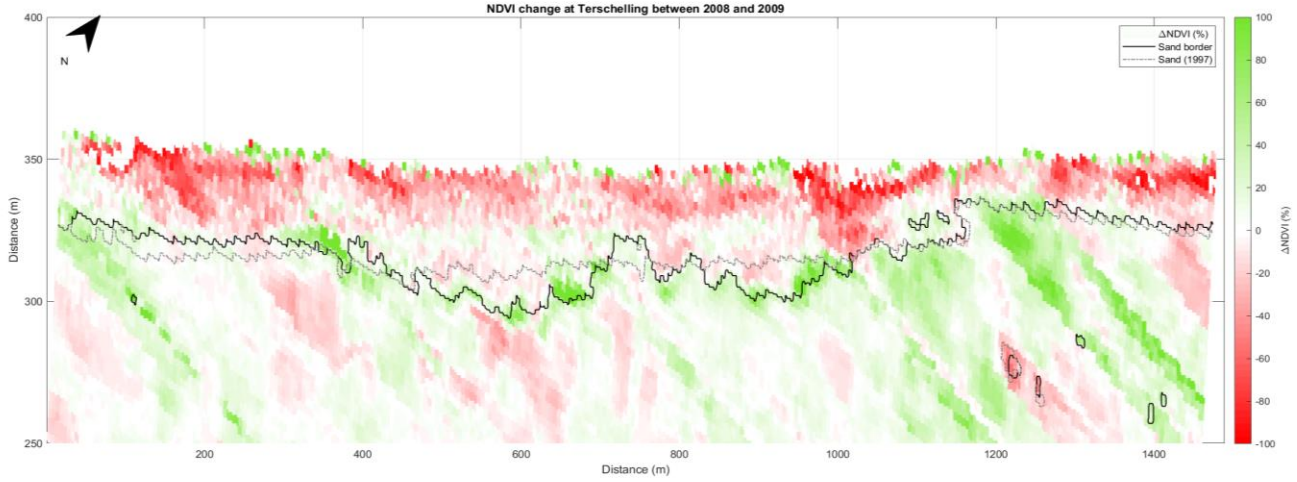
NDVI change at Terschelling between 2008 and 2009
N
ΔNDVI (%)
Sand border
Sand (1997)
Distance (m)
Distance (m)
ΔNDVI (%)

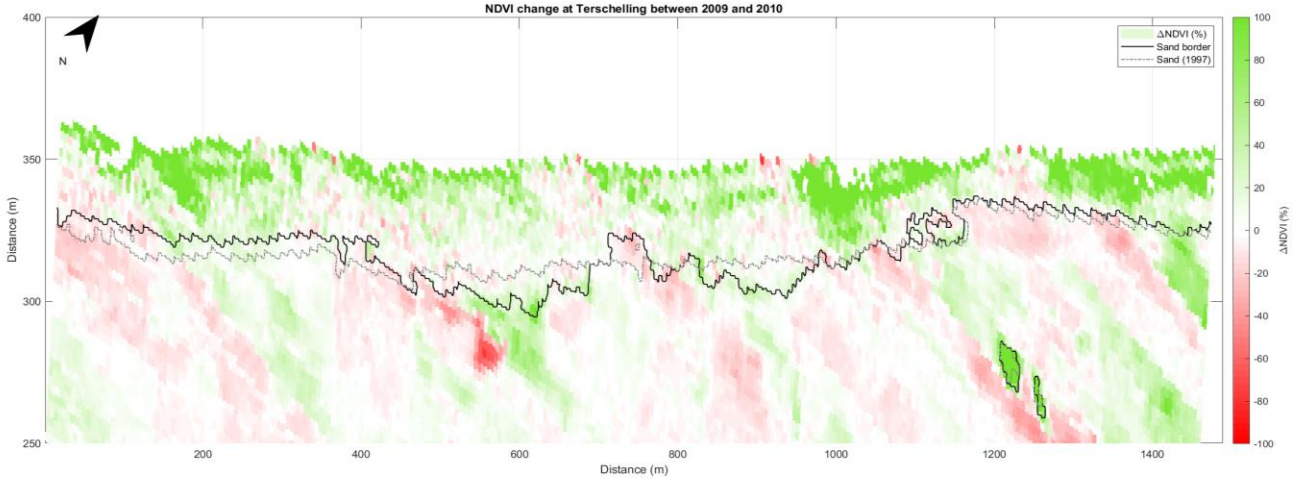
NDVI change at Terschelling between 2009 and 2010
N
ΔNDVI (%)
Sand border
Sand (1997)
Distance (m)
Distance (m)
ΔNDVI (%)

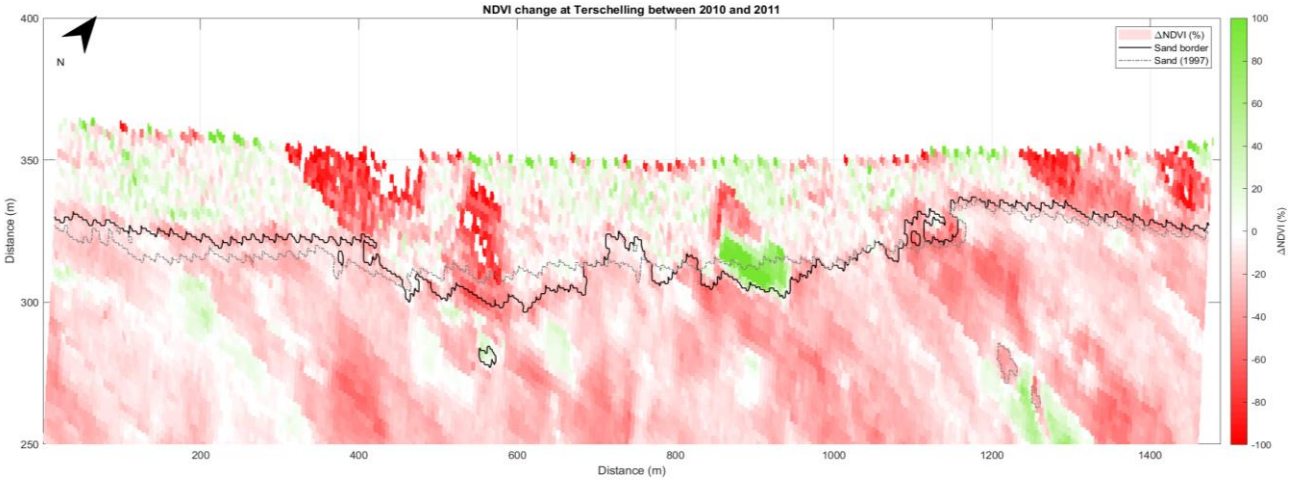
NDVI change at Terschelling between 2010 and 2011
N
ΔNDVI (%)
Sand border
Sand (1997)
Distance (m)
Distance (m)
ΔNDVI (%)

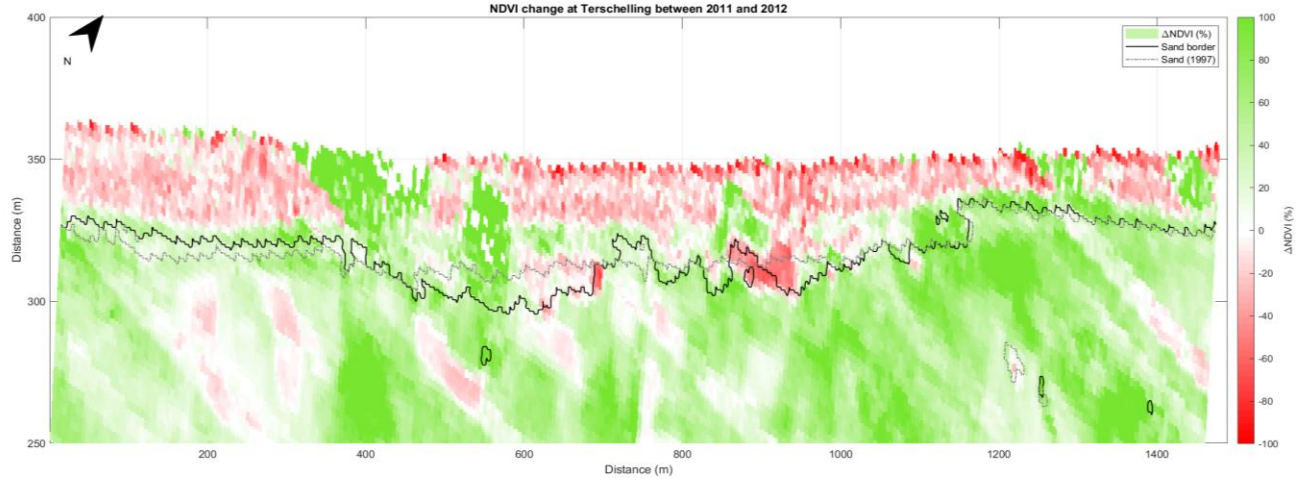
NDVI change at Terschelling between 2011 and 2012
N
ΔNDVI (%)
Sand border
Sand (1997)
Distance (m)
Distance (m)
ΔNDVI (%)

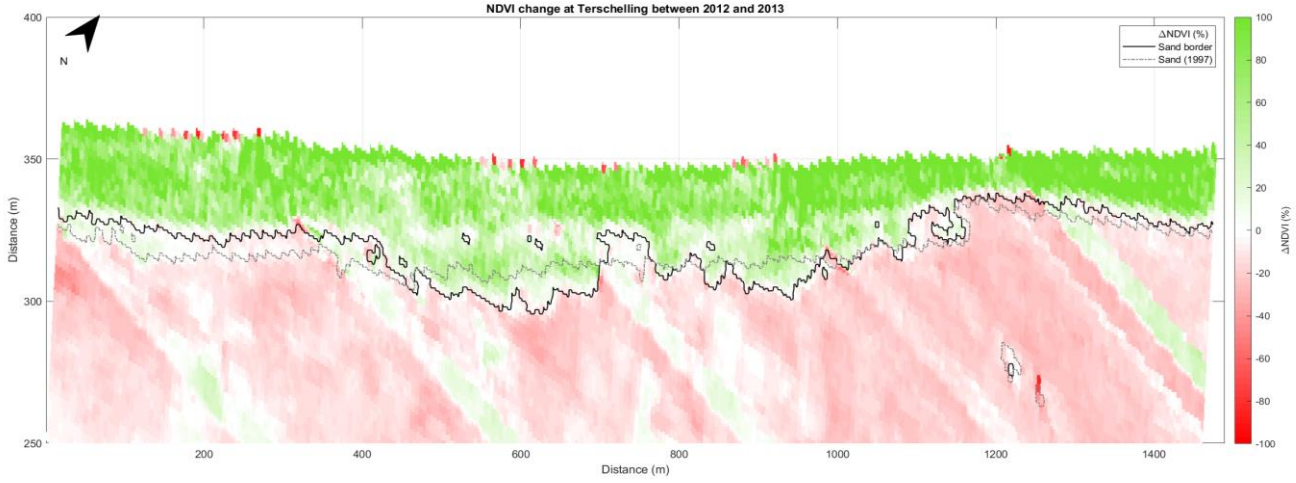
NDVI change at Terschelling between 2012 and 2013
N
ΔNDVI (%)
Sand border
Sand (1997)
Distance (m)
Distance (m)
ΔNDVI (%)

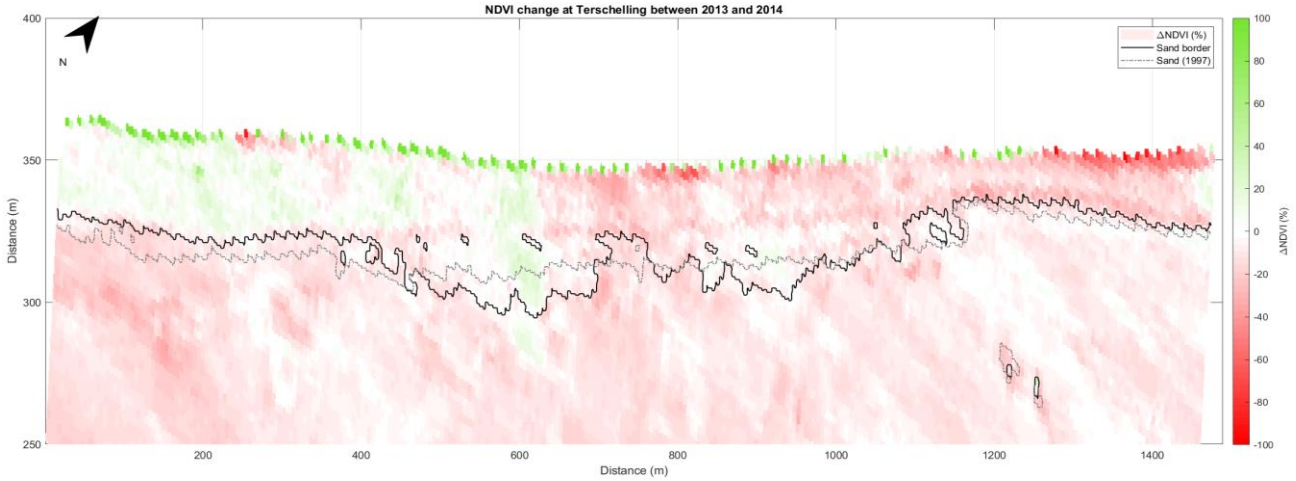
NDVI change at Terschelling between 2013 and 2014
N
ΔNDVI (%)
Sand border
Sand (1997)
Distance (m)
Distance (m)
ΔNDVI (%)

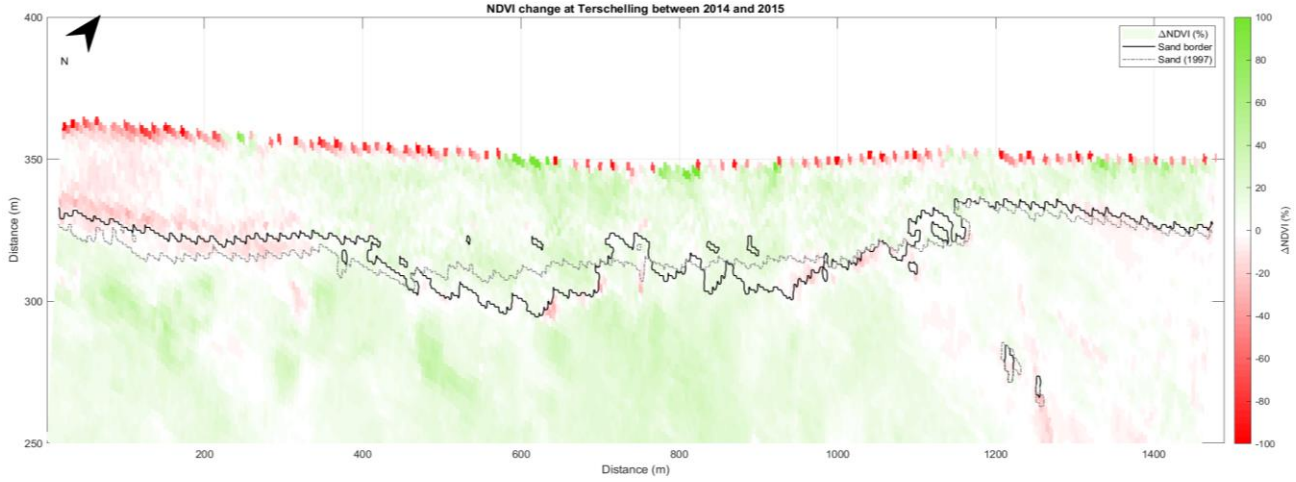
NDVI change at Terschelling between 2014 and 2015
N
ΔNDVI (%)
Sand border
Sand (1997)
Distance (m)
Distance (m)
ΔNDVI (%)

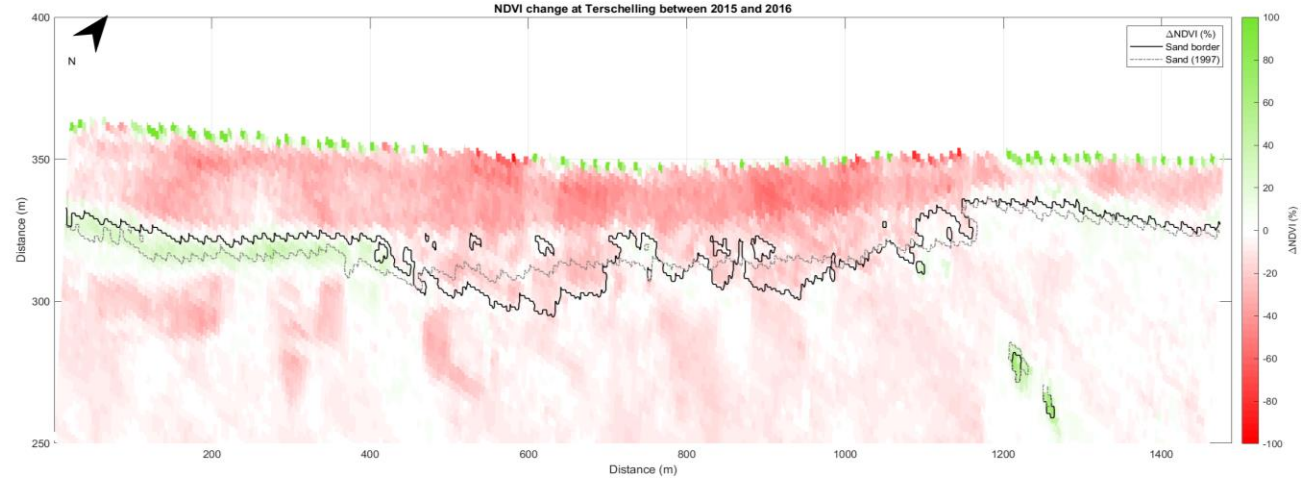
NDVI change at Terschelling between 2015 and 2016
N
ΔNDVI (%)
Sand border
Sand (1997)
Distance (m)
Distance (m)
ΔNDVI (%)

NDVI of Heemskerk

Regions of interest

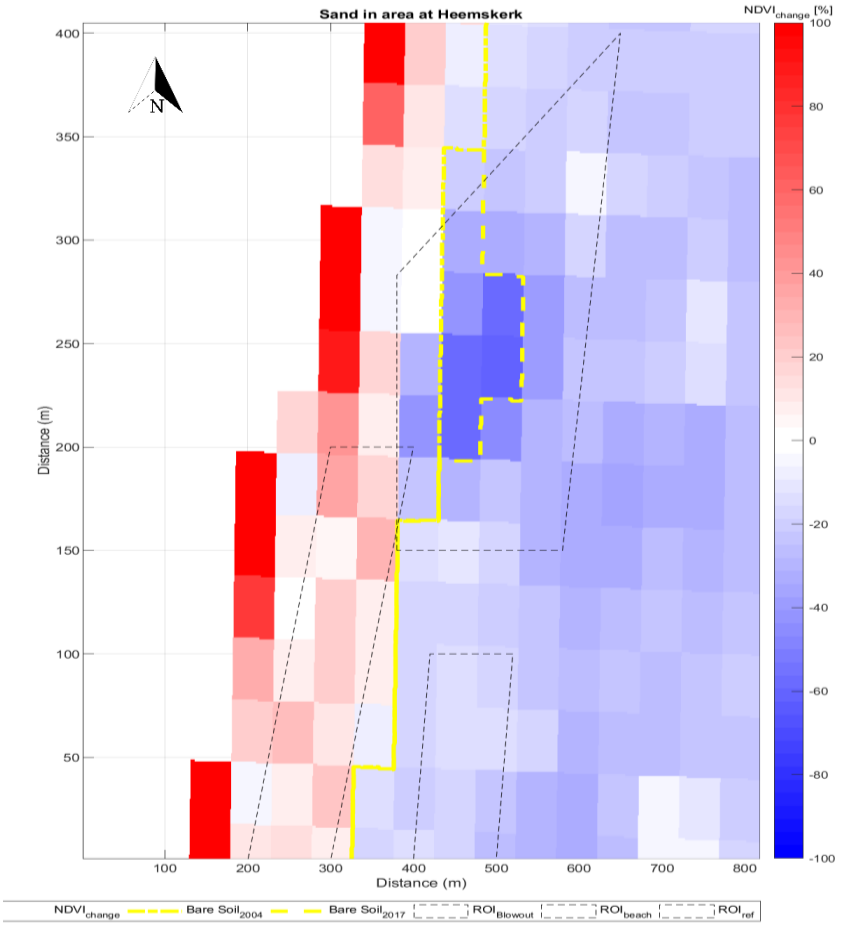

Landsat: Annual average NDVI

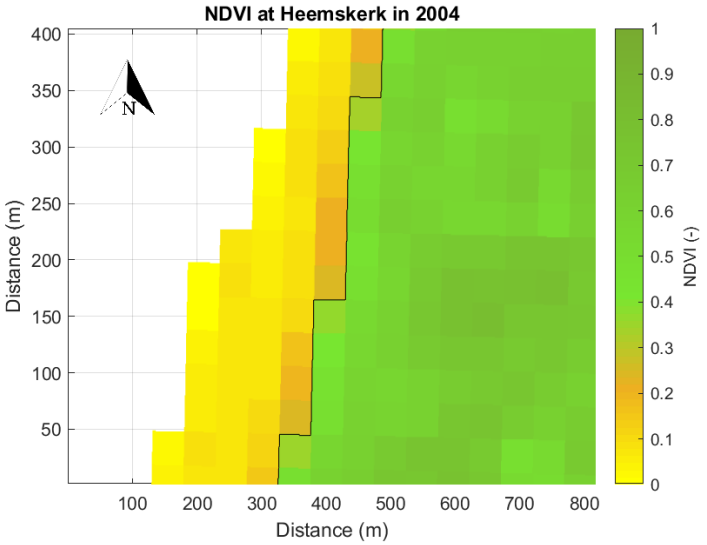

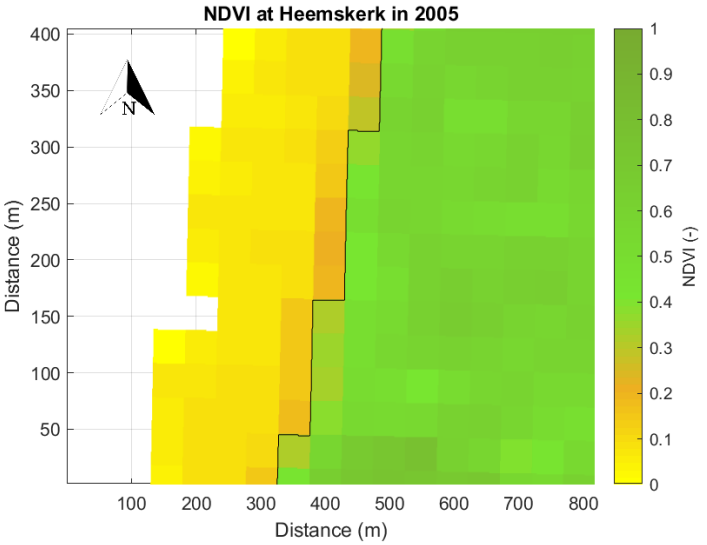

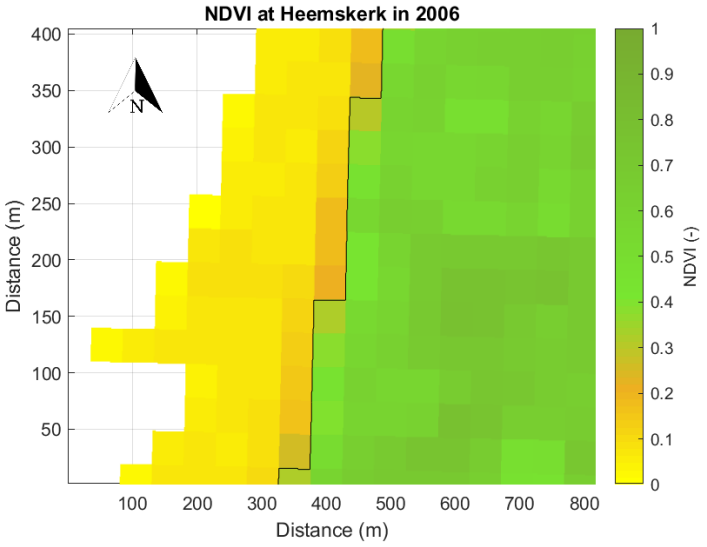

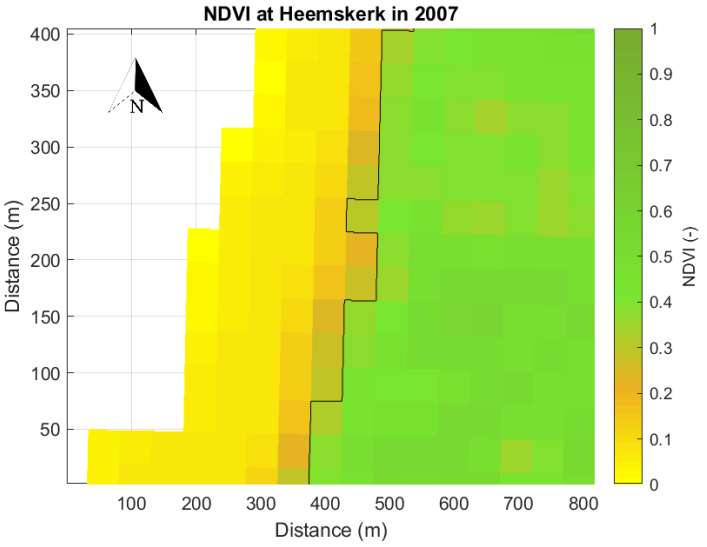

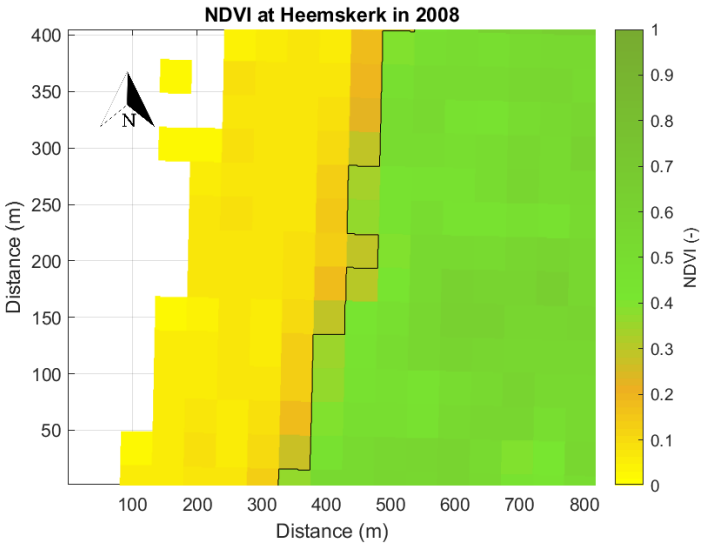

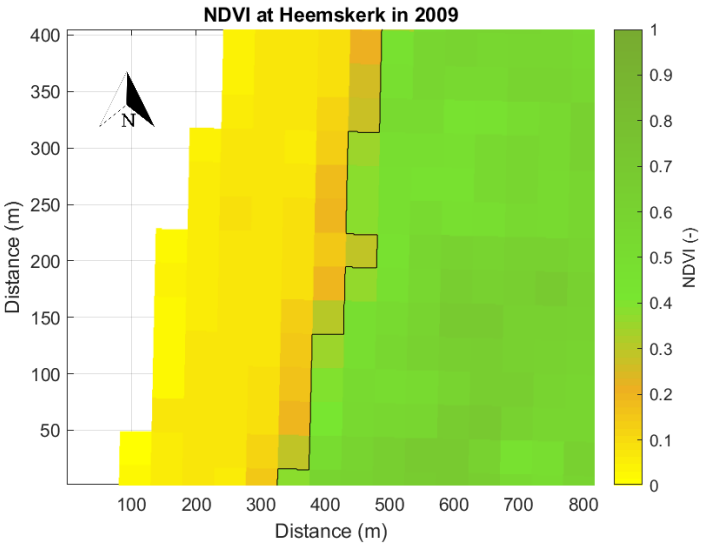

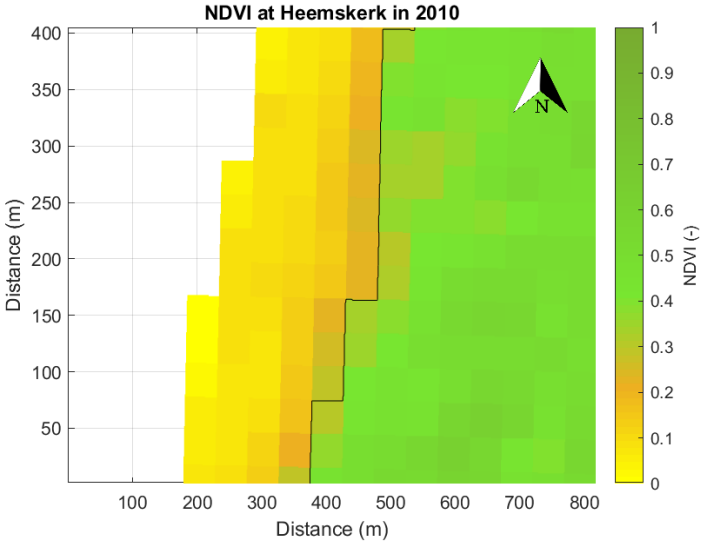
NDVI at Heemskerk in 2010
Distance (m)
Distance (m)
NDVI (-)
N

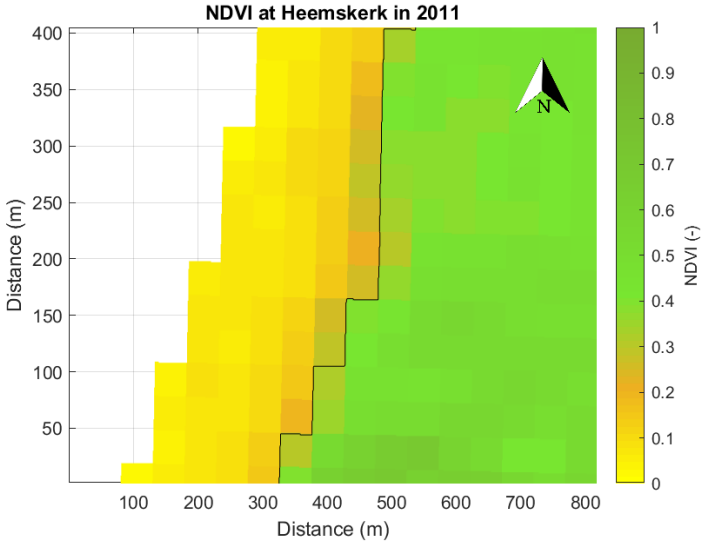
NDVI at Heemskerk in 2011
Distance (m)
Distance (m)
NDVI (-)
N

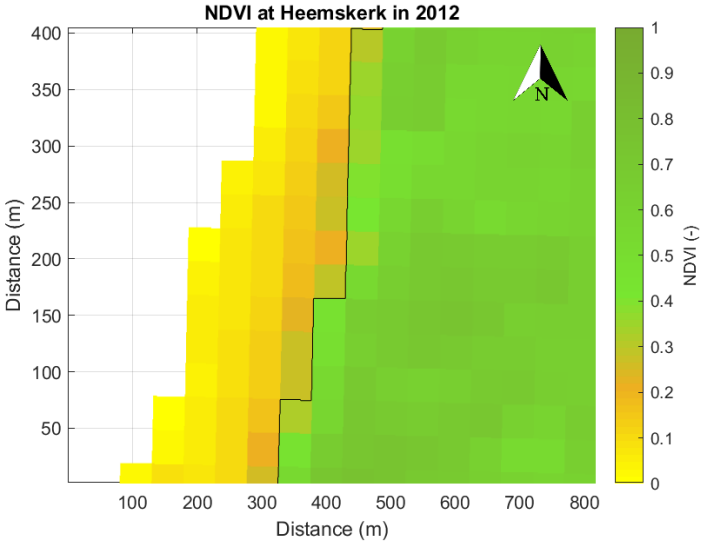
NDVI at Heemskerk in 2012
Distance (m)
Distance (m)
NDVI (-)
N

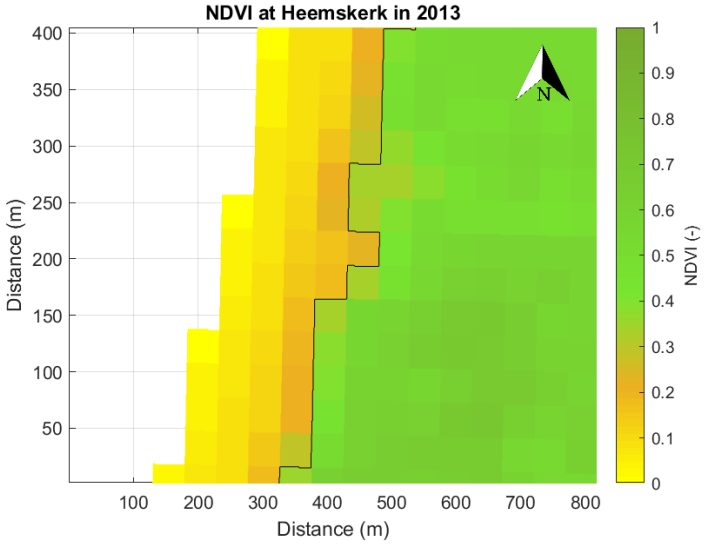
NDVI at Heemskerk in 2013
Distance (m)
Distance (m)
NDVI (-)
N

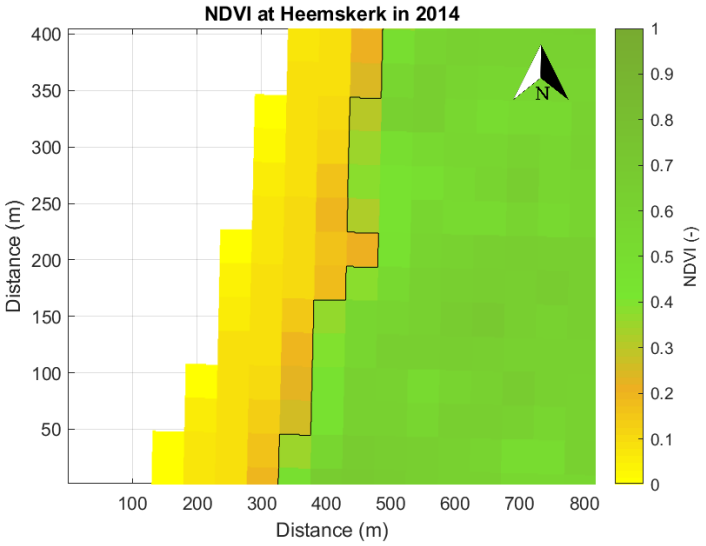
NDVI at Heemskerk in 2014
Distance (m)
Distance (m)
NDVI (-)
N

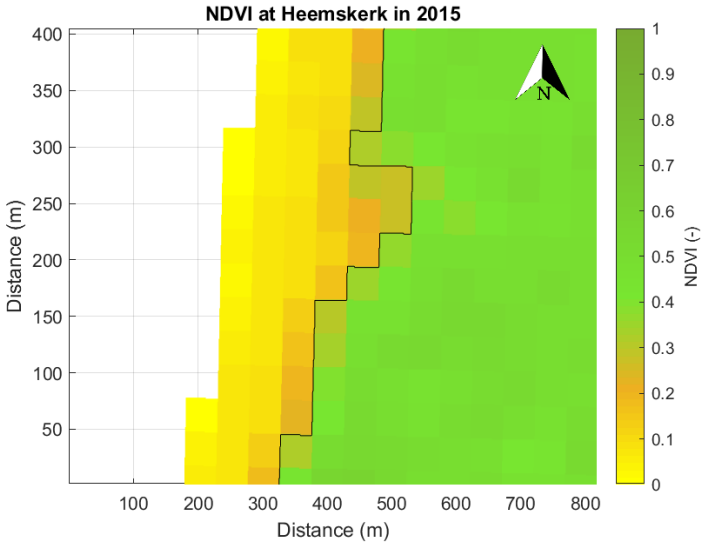
NDVI at Heemskerk in 2015
Distance (m)
Distance (m)
NDVI (-)
N

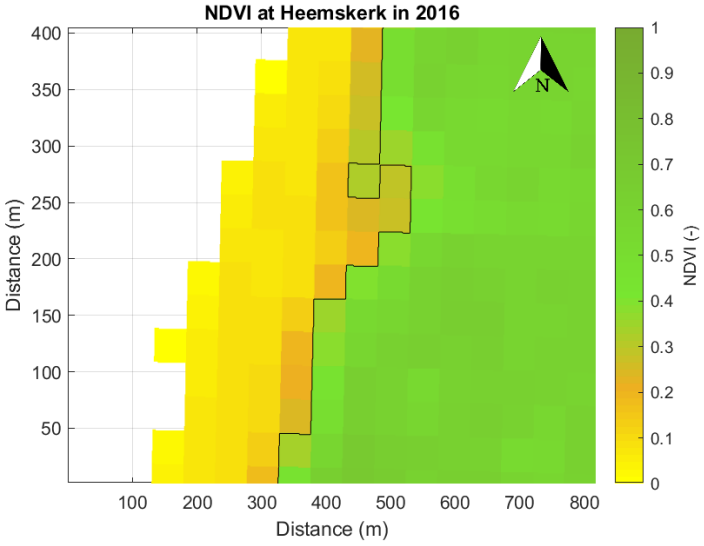

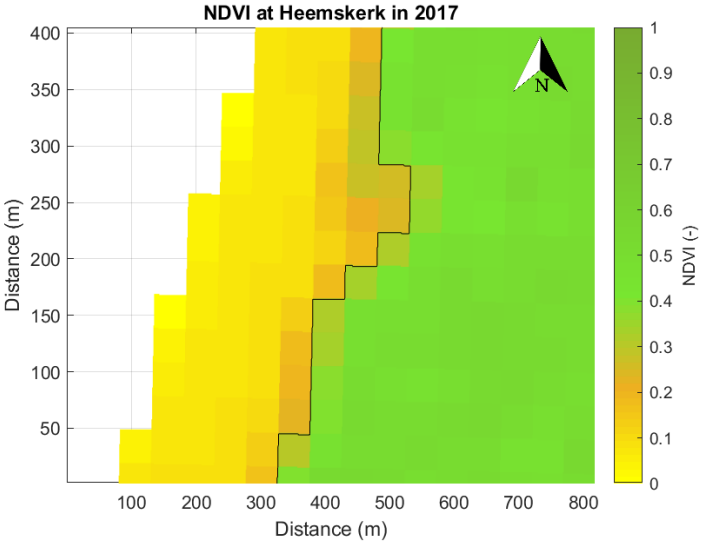

Landsat: annual change in NDVI

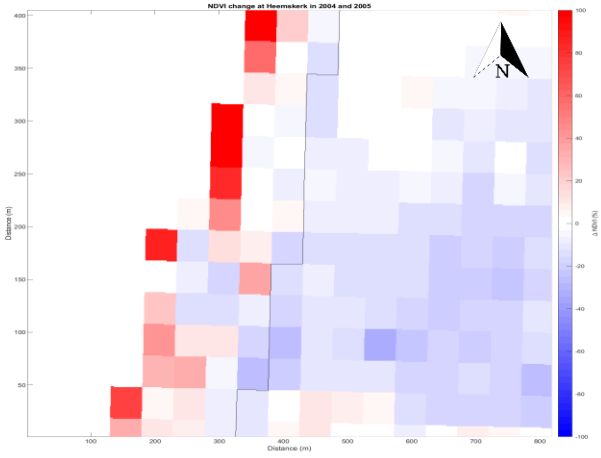

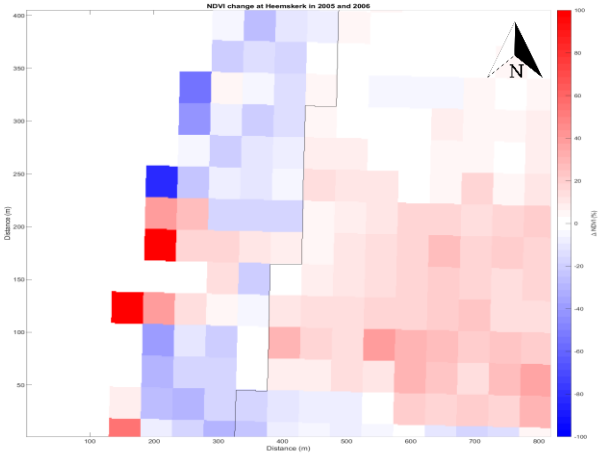

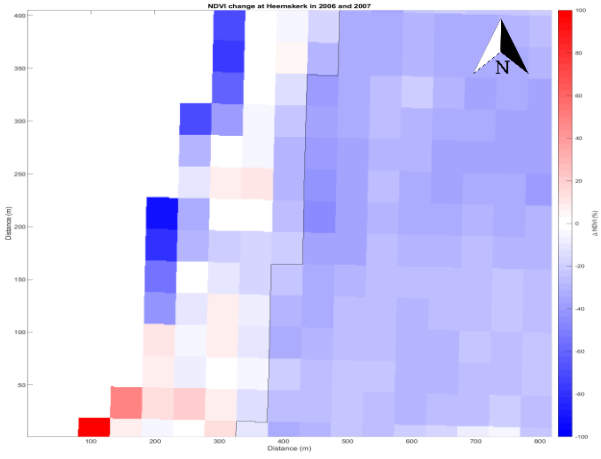

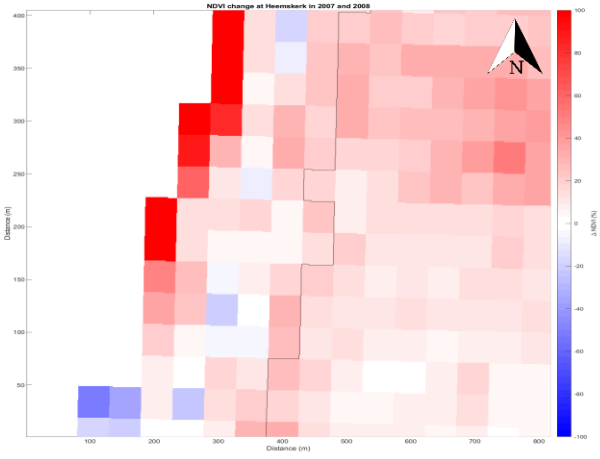

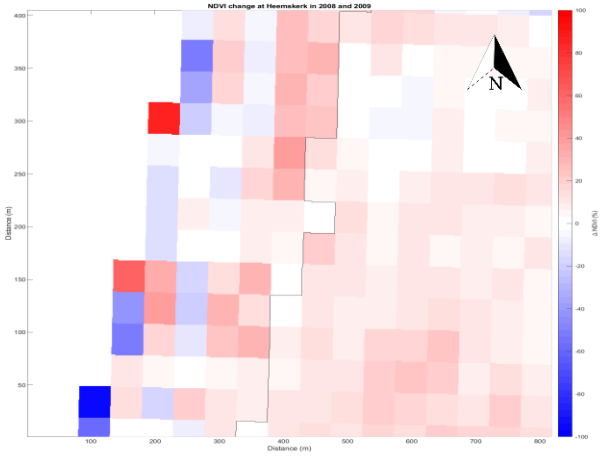
NDVI change at Heemskerk in 2008 and 2009
N
Distance (m)
Distance (m)
ΔNDVI (%)

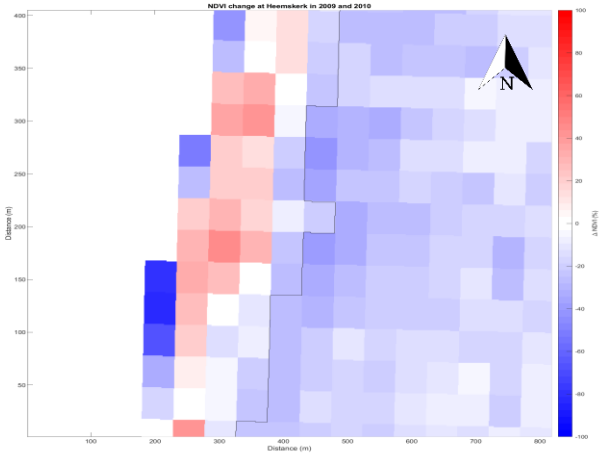
NDVI change at Heemskerk in 2009 and 2010
N
Distance (m)
Distance (m)
ΔNDVI (%)

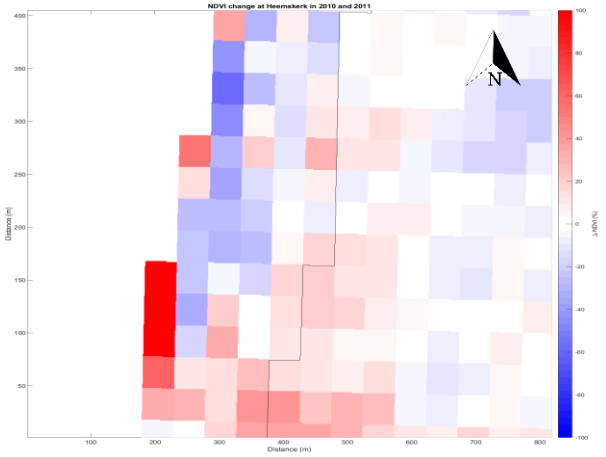
NDVI change at Heemskerk in 2010 and 2011
N
Distance (m)
Distance (m)
ΔNDVI (%)

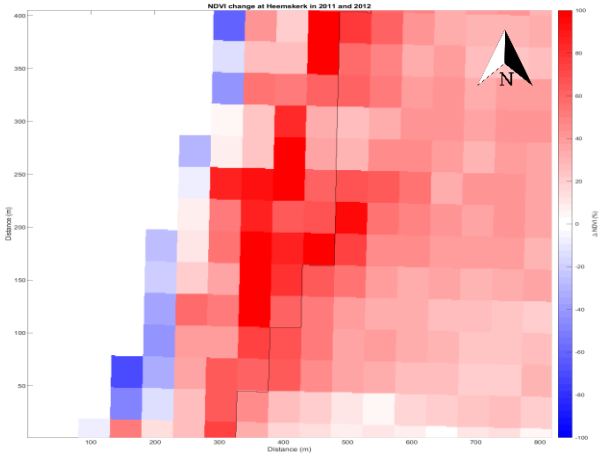
NDVI change at Heemskerk in 2011 and 2012
N
Distance (m)
Distance (m)
ΔNDVI (%)

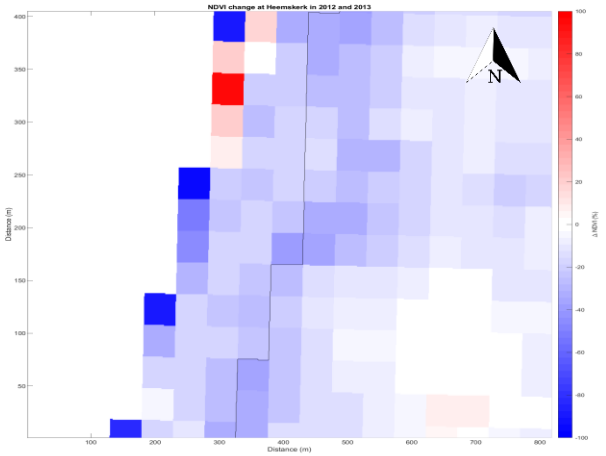
NDVI change at Heemskerk in 2012 and 2013
N
Distance (m)
Distance (m)
ΔNDVI (%)

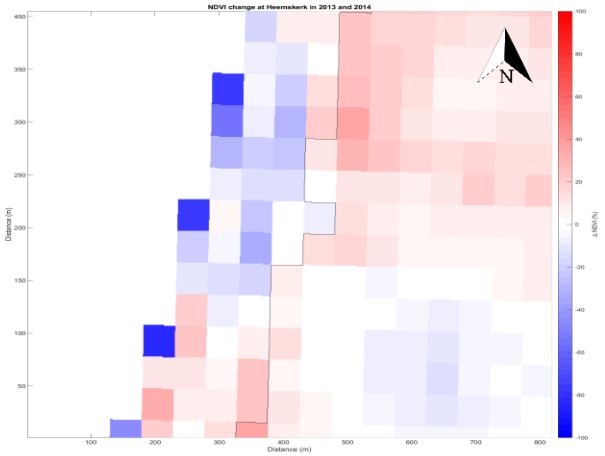
NDVI change at Heemskerk in 2013 and 2014
N
Distance (m)
Distance (m)
ΔNDVI (%)

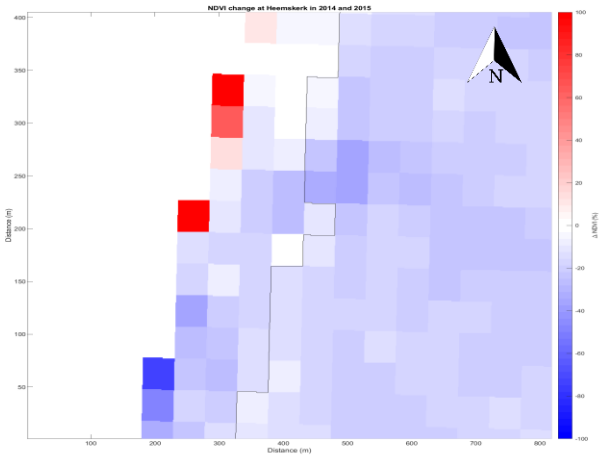
NDVI change at Heemskerk in 2014 and 2015
N
Distance (m)
Distance (m)
ΔNDVI (%)

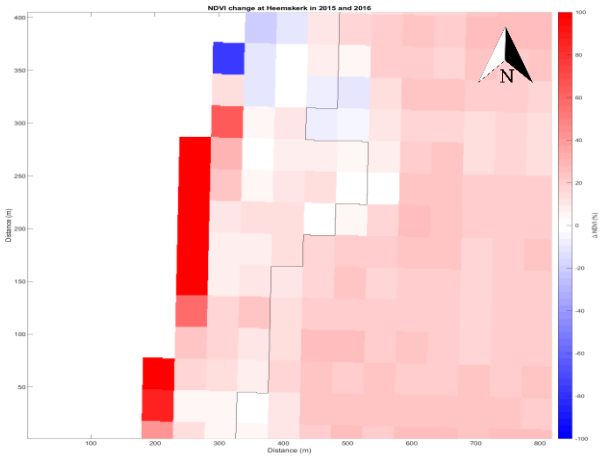
NDVI change at Heemskerk in 2015 and 2016
N
Distance (m)
Distance (m)
ΔNDVI (%)

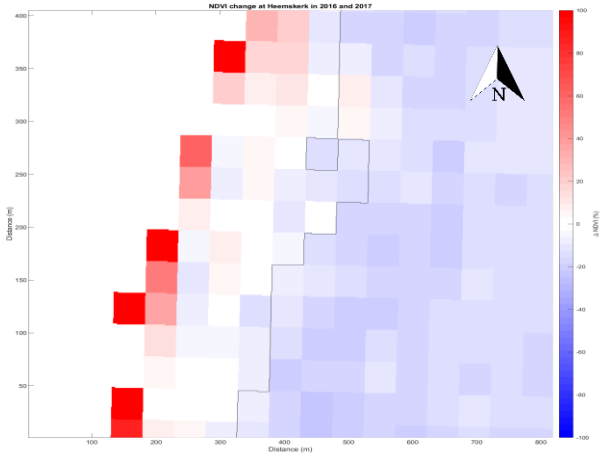
NDVI change at Heemskerk in 2016 and 2017
N
Distance (m)
Distance (m)
ΔNDVI (%)

Sentinel: Annual average NDVI

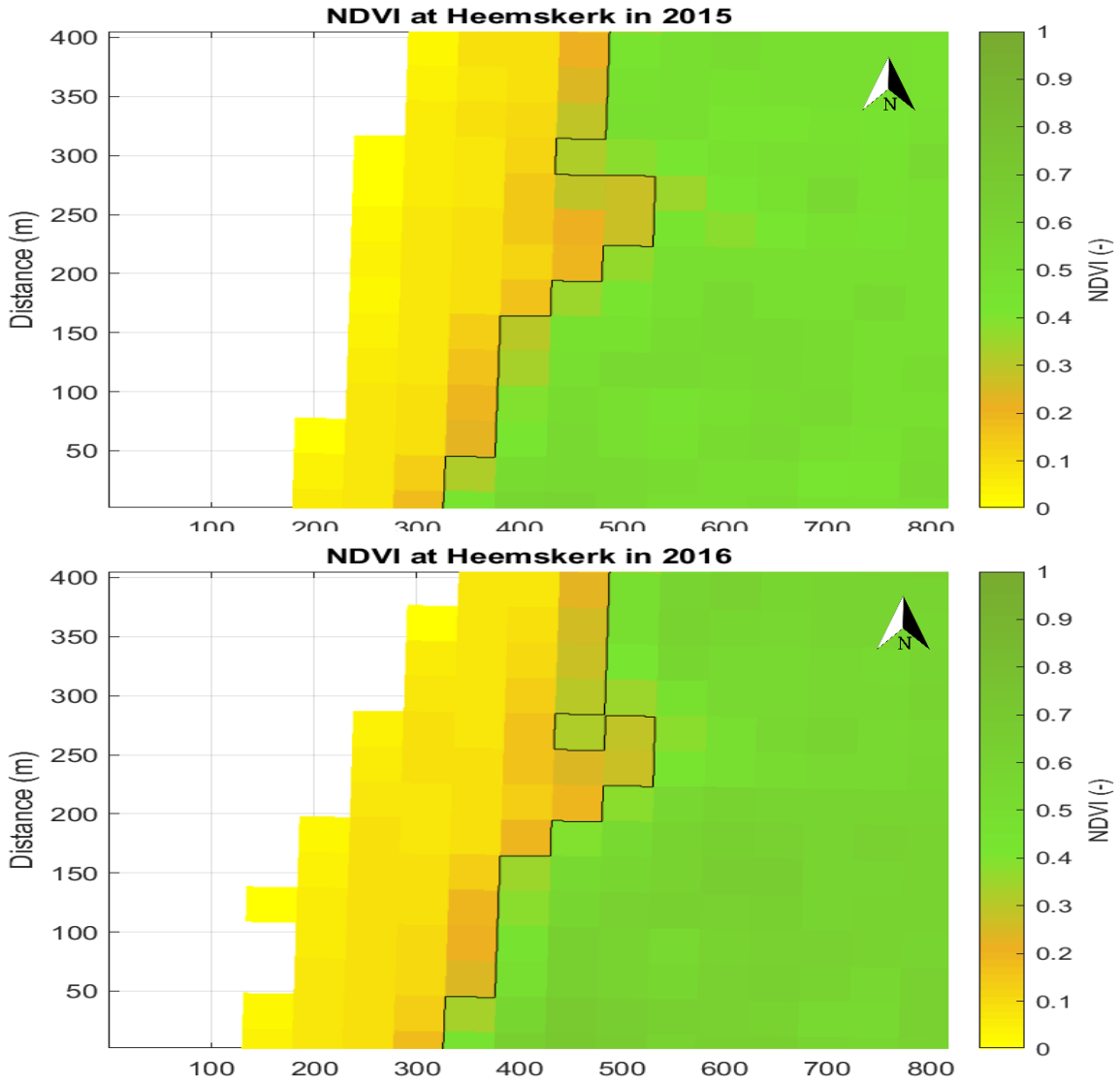

Sentinel: Annual change in NDVI